CRANFIELD UNIVERSITY

RAJEEV MOHAN BHATNAGAR

MODELLING AND DESIGN OF A DUAL CHANNEL MAGNETORHEOLOGICAL DAMPER

CRANFIELD DEFENCE AND SECURITY

DOCTOR OF PHILOSOPHY.

CRANFIELD UNIVERSITY

CRANFIELD DEFENCE AND SECURITY

DEPARTMENT OF ENGINEERING AND APPLIED SCIENCE

A thesis submitted for the degree of

DOCTOR OF PHILOSOPHY

Academic year 2011-2012

RAJEEV MOHAN BHATNAGAR

Modelling and Design of a Dual Channel Magnetorheological Damper

Supervisor(s): Dr Amer Hameed, Dr Dave J Purdy

Date of Submission: 20th June , 2011

Dedicated to my Spiritual masters and

Revered parents

Abstract

A limitation with the current analytical models for predicting the performance of a magnetorheological (MR) damper is that they fail to capture the hysteretic variation of force versus velocity variation correctly. This can significantly underestimate the damper force and overestimate the dynamic range of the device. In this work a transient analytical fluid dynamics model is developed by using a combination of Laplace and Weber transform and Duhamel's superposition of velocity boundary condition, to overcome these limitations. The solution of the system of nonlinear simultaneous equations, obtained by applying mass flow balance, velocity compatibility conditions and force equilibrium of Bingham plastic plug flow, gives the damper force. This method is shown to generate direct and inverse model of an MR device. The proposed model has been validated against a commercially available MR damper at low speed, to a range of test signals. The mean error using the above model has been shown to be 5% for all the test signals. This compares well with three conventional models which give; transient constant velocity model 35%, quasi static model 35% and phenomenological model 35%. The phenomenological model gives 10% mean error for a sinusoidal input signal.

The application of the proposed analytical model has been demonstrated by the design of a novel dual channel damper. The design of the electromechanical components has been shown to be np-hard problem and the optimisation using genetic algorithm has been applied to minimise the volume and electrical time constant. The performance of the dual channel damper has been simulated for various combinations of values of shear yield stress for two channels. Compared to the conventional single channel damper the novel design is shown to give 30% higher damper force, 50% improved dynamic range and limits the effect of transients to within 10% of the damper force. The dual channel damper is an effective solution to resist the onset of turbulent flow in the channels up to 20m/s piston velocity.

Acknowledgement

The idea of this thesis work took an intuitional form in course of author's work on high speed dampers during his stint at the Indian Ordnance factories. Therefore, the author wishes to express his most sincere gratitude to his spiritual masters as without their intuitional support this work would not have gained the present form. The author also wishes to acknowledge the inspirational guidance he continues to receive from his revered parents. The work on the design of magnetorheological fluid based damper design was started at the Indian Institute of Technology, Kanpur under Prof G Biswas and Prof. B Bhattacharya. Initial work led to a joint publication in the Journal of Mechanical Engineering science, Part C. The author acknowledges, with sincere gratitude, the supervision and guidance he received from both of them on modelling of pilot valve and taper groove based compounded dampers. I also express y sincere gratitude to Mr S K Roy who was my mentor in my early days in the Indian Ordnance factories and who was also helpful in initiating me into R&D work which ultimately led to this work on MR dampers.

This research work was resumed at Cranfield University with an objective to develop a design of a novel high speed damper. The work received a considerable funding and administrative support form from Prof John G Hetherington and therefore the author expresses his sincere gratitude towards him. The author acknowledges with sincere gratitude the guidance supervision he received from Dr Amer Hameed, Dr David J Purdy and Dr John T Economou. The administrative support rendered by Ms Ann O' Hea, Ms Paula Bentley, Ms Ros Gibson and staff of cash and accounts department is also acknowledged with sincere thanks. I also acknowledge with sincere thanks the help rendered to me in prompt services provided by the staff of library. I

would particularly like to acknowledge the support I received from Mrs Lynn Sedan, Mr Ian, Mrs Mandy Smith and Ms Rachel.

The suggestions given by the examiners Prof Kevin Knowles (Cranfield University), Dr Olutunde Oyadiji (University of Manchester) and Dr ND Sims (Sheffield University) are also acknowledged with sincere gratitude.

The experimental setup required the certain components to be manufactured form the workshop. I express my sincere thanks to all the personnel of the work shop who took pains to supply the components of the experimental setup in time by volunteering to work on weekends. I would like to convey my acknowledgement to Mr Mike Goodland, Mr Brian Uguid, Mr Karl Norris, Mr Paul Dicker, Mr Matthew Eatwell, Mr Tony Felon, Mr Chris Forward, Mr Mike Ireson, Mr Tony Low, Mr Barry Luffman, Mr Stacey Paget, Mr Bob Simpkins and Mr Adrian Ventress. I also acknowledge with thanks the help, support and suggestions I received from the officers and staff of Ordnance factory Kanpur, India, namely Mr M J Kurian, AGM, Mr Ravi Kant, AGM, Mr V S Sharma, Jt GM (retd.) Mr Shakti Roy, Mr A N Pandey, Mr Neeraj Kumar, Mr KK Rama Rao, Mr N P Shukla, Mr Borikar, Mr Nigam, Mr Mehdi, Mr Rehman and Mr A K Mishra.

The author acknowledges with sincere gratitude the support and encouragement he received from his wife Ragini Nutan, his children Rijul and Jessica and all his relatives.

R M Bhatnagar

Table of Contents

LIST OF TABLES

LIST OF FIGURES

Chapter 1

Chapter 2

Chapter 3

Chapter 4

Chapter 5

Annexure A

GLOSSARY

$\mathbf{A,A_0}$ Magnetic potential.

A_1 MR damper electromagnet core area

A_2 MR damper electromagnet cylinder wall area.

A_3 MR damper electromagnet cross section pole area.

A_{bw} Hysteretic parameter for Bouc Wen model.

A Orifice area at 'x' coordinate of the piston.

A_d Area of the annulus.

A_0 Area of orifice at the beginning of the damper stroke.

A_e Orifice area at the end of the damper stroke.

A_h Area of the damper piston without holes.

A_{shim} Surface area of the shim.

A_{holes} Holes covered by the shim valve.

$\overline{A}$ Area ratio

$\boldsymbol{a}$ Vector a

a_{grv} Area of orifice at the taper rod at the instant x of damper stroke.

a_o Total area of the orifice at the instant x of damper stroke and x_2 of pilot valve lift

$\dot{a}_o$ Time derivative of total orifice area at the instant x of damper stroke and x_2 of pilot valve lift.

a_h Area of the holes.

Bi Bingham number.

$\mathbf{B}$ magnetic flux density

$\boldsymbol{b}$ Vector b

b The circumference of the inner tube.

B_c Flux density through the core.

B_p Flux density through the pole.

B_w Flux density through the wall.

B_g Flux density through the gap.

C_d Coefficient of discharge of the orifice

C_{dgrv} Coefficient of discharge for taper rod orifice.

C_{dpv} Coefficient of discharge for pilot valve lift.

C_{v1}, C_{v2}, C_{x1} and

C_{x2} Coefficients of the polynomial, which contain the values of pressure and the input data for the expressions of the forces acting on the system such as the damper or the pilot valve.

C_{vdamp} The damping coefficient to account for viscosity effects in the equation.

C_{dshim} Coefficient of drag on the shim.

$\boldsymbol{c}$ Vector c

$\mathrm{c_e}$ The damping constant.

D Electric flux density.

D_t^{α} Fractional dimension differential operator.

D_p Diameter of the pole

d The gap between the two cylinders.

d_b Diameter of bleed hole.

d_s Diameter of holes covered by the shims.

d_{o} Outer diameter of the pilot valve.

d_p Diameter of the damper piston

d_r Diameter of the damper rod.

d_{piston} Diameter of the piston

$d_{piston\ min}$ Minimum piston diameter.

$d_{piston\ max}$ Maximum piston diameter.

d_{inner} Inner diameter of the outer bypass channel

$d_{inner\ min}$ Minimun Inner diameter of the outer bypass channel

$d_{inner\ max}$ Maximum Inner diameter of the outer bypass channel.

$\mathbf{E}$ Electric field intensity.

${}_1F_2$ Hypergeometric function.

$F(x)(t)$ Bouc Wen model Damper force of MR damper.

F_b Damper force at the spike.

F_{bnd} Non dimensional damper force at the spike.

$F(t)$ Time varying input load to the system.

F_i Pressure force in the i^{th} fluid domain.

F_{ij} j^{th} component of pressure force in i^{th} fluid domain.

F_{ijk} k^{th} sub-component of j^{th} component of pressure force in i^{th} fluid domain.

f force vector.

$\mathbf{f_i}$ force vector.

f_d Damper force .

$\boldsymbol{f_i}$,$\boldsymbol{f_{i+1}}$ i^{th} and $i+1^{th}$ function vectors for system of nonlinear simultaneous equations.

f_i Function evaluated at i^{th} step in Richardson' extrapolation or force vector in chapter 6.

f'_i Derivative of function evaluated at i^{th} step in Richardson' extrapolation

f_{trans} Damper force due to transient effects.

f_{qs} Damper force due to quasi static flow condition.

g Acceleration due to gravity or acceleration of the piston where specified.

g_p Annular flow gap for the piston flow channel.

g_o Annular flow gap for the bypass flow channel

$\mathcal{H}$ Hilbert space.

$\mathbf{H}$ Magnetic field intensity.

H_i i^{th} order Struve function.

H_g Magnetic field intensity through the flow gap for piston channel.

H_c Magnetic field intensity through the core of the piston.

H_p Magnetic field intensity through the pole.

H_w Magnetic field intensity through the cylinder wall

h_c coil height fro MR electromagnet.

h Time step.

i_{ac} Current through the actuator.

I_{ap} Applied current.

i,j,k Indices representing coordinate axis or fluid domain/sub domains or components / sub components of forces or iterative step in a numerical scheme.

i_c Excitation current for MR damper.

$\mathbf{J},\mathbf{J_0}$ Current density.

$\boldsymbol{J}$ Jacobean matrix for direct MR damper model.

J_j Jacobian for j^{th} subdomain.

$\mathbf{J}_r$ Jacobean matrix for reverse MR damper model.

J_i Bessel's function of first kind and i^{th} order.

κ constant of shear stress constitutive equation with dimensions compatible with fractional differential operator.

K, K_{ij} Stiffness matrix.

k Spring constant of restoring spring.

k_{shi} Stiffness of shim.

k_e Stiffness constant due gas spring.

L_{dmp} Length of the gap for flow of MR fluid.

l Length of the stroke of the damper.

l_z Length of annulus of MR fluid under magnetized field.

l_i Flow length for piston flow channel'

l_o Flow length for the outer-bypass flow channel

l_c Length of the core between the poles.

l_p Width of the pole

L_w Inductance of coil.

L_{spool} Inductance of spool

$\dot{m}$ Rate of displacement of mass of damper fluid the piston.

m_{shim} Mass of shim.

M_s Sprung mass of the system.

$N(\alpha_n)$ The Norm for the Weber transform.

n Number of holes covered by the shim.

n_h Index for normalised Bouc Wen model.

n_{hb} Index for shear rate in Herschel Bulkley equation.

n_p Number turns per layer in the coil.

n_s Number of spools in the coil.

n_l Number of layers of windings in one spool

ΔP_{max} Maximum pressure field pressure drop

ΔP_{max} Zero field pressure

ΔP Pressure drop across the length of gap for the flow of MR fluid.

ΔP_d Pressure drop across the orifice of shim valve.

$\mathscr{P}$ Dimensionless pressure gradient.

p Pressure.

p_1,p_2 Pressure at the inlet and outlet of the MR fluid flow annulus respectively.

p_x Gas pressure of the restoring spring at 'x' position of the damper piston.

p_i Initial gas pressure of the restoring spring.

q_e Electric space charge density.

q Orifice area.

q_1,q_2 scalars.

Q Effective area of the damper piston.

Q_f Flow rate of MR fluid through the gap.

Q_{max} Flow rate of MR fluid through the gap at maximum or zero field pressure drop.

r Coordinate in radial direction.

r_i radial coordinate at the i^{th} point.

$\mathbf{R}$ Real number space.

$\mathscr{R}$ Residual of the difference between the force(f_{trans}) due to transient effects and force (f_{qs})due to quasi static flow condition.

R Radius of MR damper.

R_e Reynolds number through the valve.

Re_a Operating Reynolds number through the valve.

Re_c Critical Reynolds number.

R_w Resistance of the coil.

R_{spool} Resistance of the one spool of the coil.

r_o radial coordinate at o^{th} point.

r_2 Slope of plastic region of hysteresis as percentage of slope of linear region.

$\mathscr{T}$ Dimensionless shear yield stress.

t_a Core radius of MR damper electromagnet.

t_b Flange height of MR damper electromagnet.

t_w Thickness of the cylinder wall

t Time.

T Time period

u scalar variable for complementary function of hysteretic limit cycle.

u_r component of velocity in r direction.

u_θ component of velocity in θ direction.

$u(z), u_z$ component of velocity in z direction.

u'_z component of velocity in z direction for a piston moving with constant velocity.

$\tilde{\bar{u}}_z(\alpha_n, s)$ Weber transform of the Laplace transform of the velocity in z direction.

u_p Piston velocity.

u_{po} Maximum piston velocity

$\mathscr{V}$ Dimensionless piston velocity.

v_r Relative velocity of the damper fluid relative to piston.

V_i Initial volume of gas of the restoring spring.

V_c volume of cylinder between the piston face and the cylinder face towards which the piston face is moving

w Deflection of shim.

w_c Coil width of MR damper electromagnet.

$w_n(t)$ Normalised hysteretic variable.

$\dot{\bar{w}}_n(t)$ Time derivative of hysteretic variable.

X_{max} Maximum input displacement of MR damper

$x(t)$ Displacement of the damper

x Coordinate of the damper piston along the direction of stroke.

x_{shim} Deflection of the shim.

$\mathbf{x}_i$ Solution vector at i^{th} iteration for nonlinear simultaneous equations for direct model.

$\mathbf{x}_i^r$ Solution vector at i^{th} iteration for nonlinear simultaneous equations for reverse model.

$\dot{x}$ Velocity of shim.

$\dot{x}_i$ Velocity along i^{th} coordinate.

$\ddot{X}$ Acceleration of the sprung mass.

$\ddot{x}_{shim}$ Acceleration of the shim.

$\ddot{x}_i$ Acceleration along i^{th} coordinates.

x_p Piston displacement.

x_{pmax} Maximum pilot valve lift.

z Z-coordinate

z_h Hysteretic variable

$\dot{z}_h$ Time derivative of hysteretic variable.

φ Solution of the Bessel's equation.

α Constant for MR fluid.

α_i Fraction of flow of MR fluid through the inner channel.

α_o Fraction of flow of MR fluid through the outer channel.

α_1 The geometrical constant for damper force.

α_n n^{th} zero of the Bessel's characteristic equation.

α_{ni} n^{th} zero of the Bessel's characteristic equation for fluid region between piston and plug flow.

α_{no} n^{th} zero of the Bessel's characteristic equation for fluid region between plug flow and outer cylinder wall.

β Hysteresis shape parameter.

$\bar{\delta}$ Width of plug flow region of MR fluid.

δ Slit width of pilot valve pocket.

γ Hysteresis shape parameter.

ι iota - $\sqrt{-1}$

λ Valve control ratio.

μ Coefficient of friction or scalar variable.

μ_{py} Post yield viscosity of MR fluid.

ξ Correction factor for viscosity.

ξ_1 Function of Bessel's function representing the part of the solution for velocity profile

ρ Density of damper fluid.

ρ_h Normalised parameter of Bouc Wen model.

Ω Magnetic computational domain.

Ω_i Fluid domain i.

Ω_{ij} Sub domain j of fluid domain i.

Ψ Weighted function.

$\varphi(\alpha_n,r)$ Kernel function for Weber transform.

φ_i Kernel function for Weber transform in the i^{th} fluid region.

$\varphi_{\sigma,n}^{+/-}(\mu)$ Complemetary functions for the solution of differential equation for hysteretic model.

$\varphi_{\sigma,n}(\mu)$ Solution of differential equation for hysteretic model.

$\psi_{\sigma,n}$ Inverse function of $\varphi_{\sigma,n}(\mu)$.

ϕ_B Magnetic flux through the core of the piston.

Φ_p Magnetic flux through the pole of the piston.

Φ_g Magnetic flux through the gap of the piston flow channel.

Φ_w Magnetic flux through the wall of the cylinder housing the piston.

v, v_0 The kinematic viscosity

τ Shear stress.

$\tau_{piston\ flow}$ Shear yield stress for the MR fluid flowing through the outer-bypass channel

$\tau_{outer\ bypass}$ Shear yield stress for the MR fluid flowing through the outer-bypass channel

τ_0 Yield shear stress.

$\tau_{0,j}$ Yield shear stress for j^{th} subdomain.

τ_1 Time variable.

$\theta(x)$ Hysteretic function.

θ Angular coordinate in cylindrical polar coordinate system.

ϑ Bulk modulus of MR fluid.

χ_i, χ_o Symbols representing the terms in the expression for the velocity profile.

γ_i, γ'_i Function component due to Duhamel superposition of sine velocity on solution of plug flow velocity profile for inner layer.

γ_o, γ'_o Function component due to Duhamel superposition of sine velocity on solution of plug flow velocity profile for outer layer.

CHAPTER 1

INTRODUCTION

1.1 Motivation:

In many engineering situation such as automobiles, bridges, gun etc. some form of energy dissipation is required to ensure their proper operation. This is because these structures are subjected to shock or oscillating load due to road shocks, seismic tremors, propulsive reaction etc. The common device used to dissipate the energy is termed as damper and in many situations the device converts the kinetic energy into heat, though it is also possible to convert it to potential energy such as electrical or mechanical or pressure energy. The damper is normally used with a spring which stores a part of the kinetic energy into potential energy. The design of hydraulic shock absorbers for the reduction of load transmitted to the structure, has dominated all the applications for almost a century. Over the period of the last hundred years the design of hydraulic dampers has evolved into different variants to suit the applications ranging from a door closure to the recoil system of an artillery gun. A hydraulic damper dissipates the kinetic energy input to the system by forcing the damper fluid through a narrow orifice. When fluid displaced by the damper piston flows through the narrow orifice it emerges in the form of a submerged high speed free jet. The turbulent mixing of the submerged free jet with the stagnation fluid results in the dissipation of the kinetic energy into heat energy. The pressure drop in the damper cylinder which causes the fluid to flow through the orifice, results in the damper force. This damper force results in a reduction of the force transmitted to the system. The schematic of a hydraulic damper is shown in Fig 1.

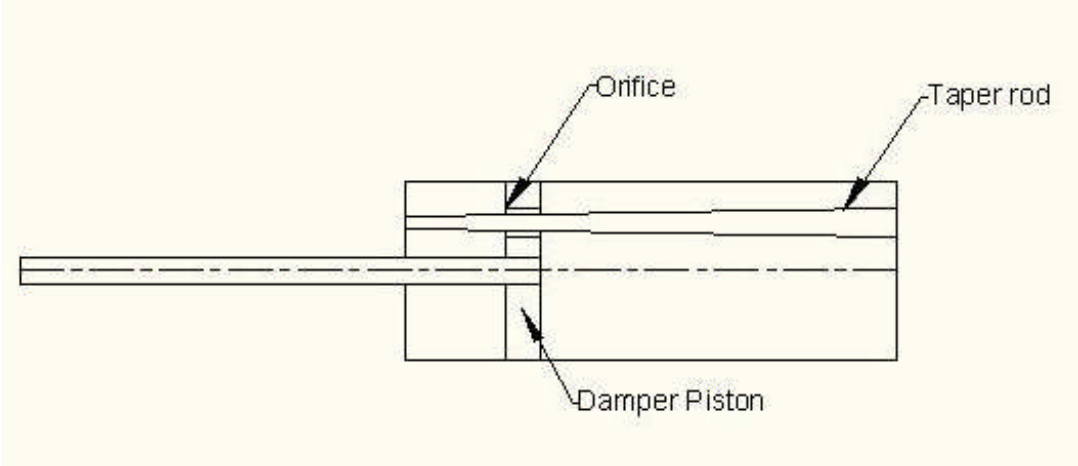

Fig1.1 Schematic of taper rod type damper.

If this damper is connected to a system with a spring and mass, as shown in Fig 1.2-1.4, and is subjected to impact load then such a system will accelerate due to the impact and then it will decelerate due to damper force. Due to the change in the velocity of the system, the rate of kinetic energy input to the damper varies. The rate of dissipation of the kinetic energy input to the damper depends upon the rate of flow of damper fluid through the orifice. The rate of flow of fluid through the orifice depends upon the size of the orifice and density of the damper fluid. If the orifice size is large the rate of dissipation of kinetic energy by the damper fluid will exceed the rate of kinetic energy input. This will result in a lower damper force. On the other hand if the orifice size is too small the rate of kinetic energy input will exceed the rate of dissipation of the kinetic energy. In such a case, there will be a higher pressure build up in the damper cylinder so as to increase the rate of flow of fluid through the orifice. This will result in an occurrence of pressure spike in the damper. To further understand the action of a hydraulic damper the modelling of a spring mass damper shown in Fig1.2-1.4 has been discussed. The Fig 1.2

illustrates the first case of a hydraulic damper which has a fixed orifice. In the second case the hydraulic damper has a small orifice during the initial part of the stroke, whilst in the later part it has a full orifice area. The change in orifice area is achieved by incorporating a restricting pin as shown in Fig 1.3. In the third case the orifice area is restricted during final part of the stroke of the damper (see Fig1.4). This provision is often made in the dampers to prevent the piston from dashing against the cylinder head. The practical example of the first type of damper can be of a passenger car damper. The action of shim valve type damper discussed in Appendix-I, is much similar to second case of hydraulic damper and is shown in Fig 1.3. The application of the third case of hydraulic damper can be a taper rod type damper which has been discussed in details in Appendix –I. The Appendix –I presents the survey and modelling techniques of hydraulic and ER/MR fluid based semi active damper in a taxonomical manner.

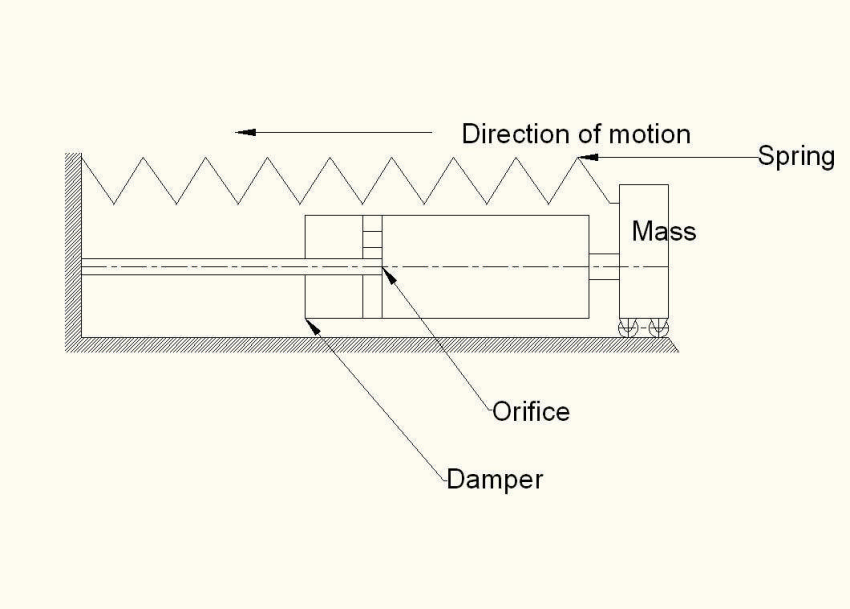

Fig 1.2 Spring, mass and damper system with a hydraulic damper with fixed area orifice (case1).

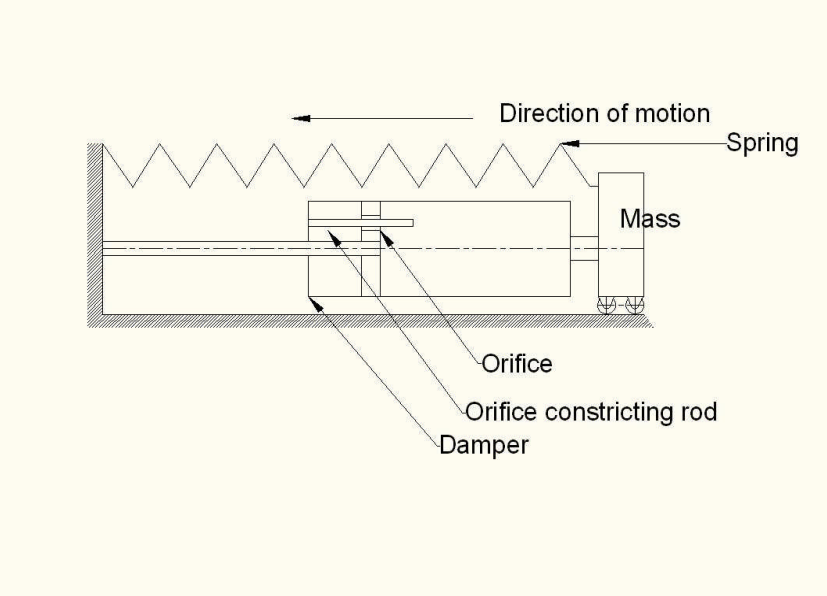

Fig 1.3 Spring, mass and damper system with hydraulic damper with an orifice area restricting rod for the initial part of the damper stroke (case2).

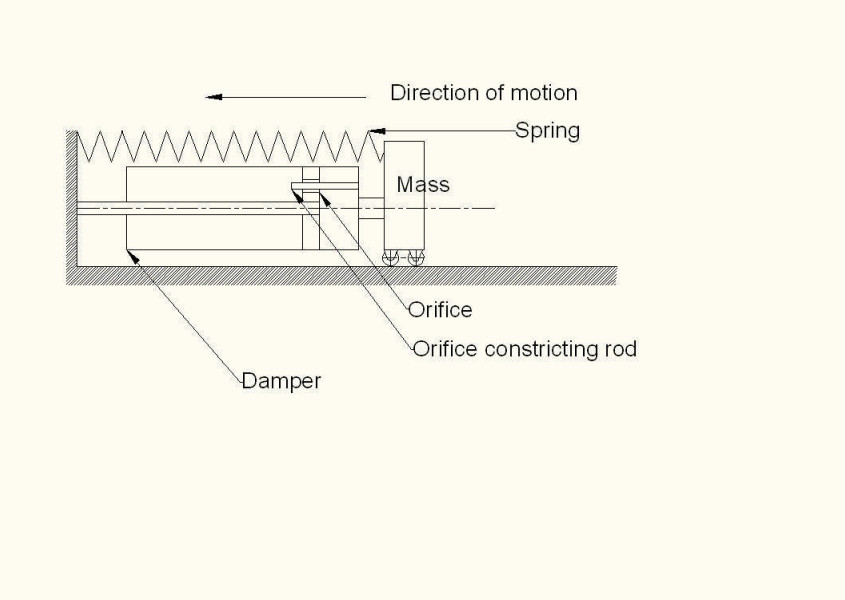

Fig 1.4 Spring, mass and damper system with hydraulic damper with an orifice area restricting rod for the end part of the damper stroke (case3).

These three cases can be modelled by a generalized SIMULINK model which is shown in Fig 1.5. The governing differential equation for the above three case is given as follows:

$$m\ddot{x} + F_d + kx = F(t) \qquad (1.1)$$

Where m is the mass of the system, F_d is the damper force, k is the spring constant, x is the displacement of the system and $F(t)$ is the impact force. For modelling purpose, the impact force of 8000N is applied for 10 m-seconds.

The damper force is given as follows (Hajihosseinloo et al (1989)):

$$F_d = \left(1 - \frac{C_d a_o}{A_p}\right)^2 \frac{\rho A_p^3 \dot{x}^2}{2(C_d a_o)^2} \qquad (1.2)$$

Where C_d is the coefficient of discharge, A_p is the piston area, a_o is the orifice area, ρ is the density of the fluid. The value of some of the variables is given in Fig 1.5.

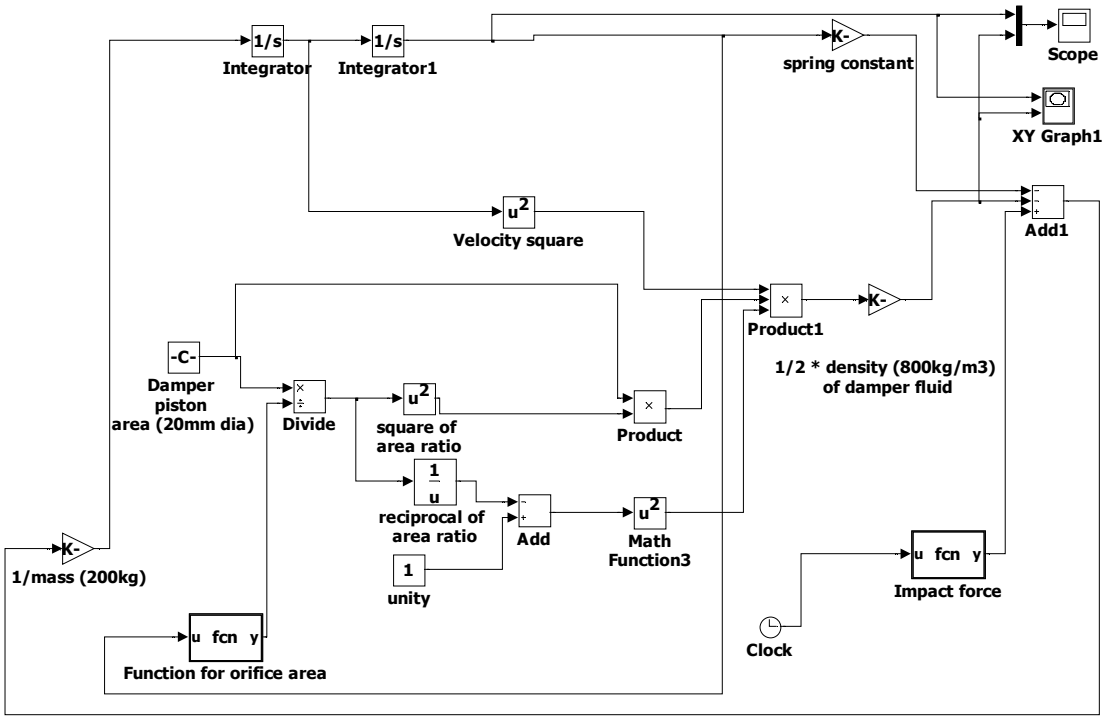

Fig 1.5 SIMULINK model of spring mass damper system for case 1,2 and 3.

The system output has been plotted as force versus displacement for case 1 is shown in Fig 1.6. From Fig 1.6, it can be seen that the damper force rises abruptly to a maximum value followed by a gradual reduction to a minimum value towards the end of the stroke and finally the damper force reduces to a zero value. In this case the damper force spike is not distinctly seen because the impact force is low.

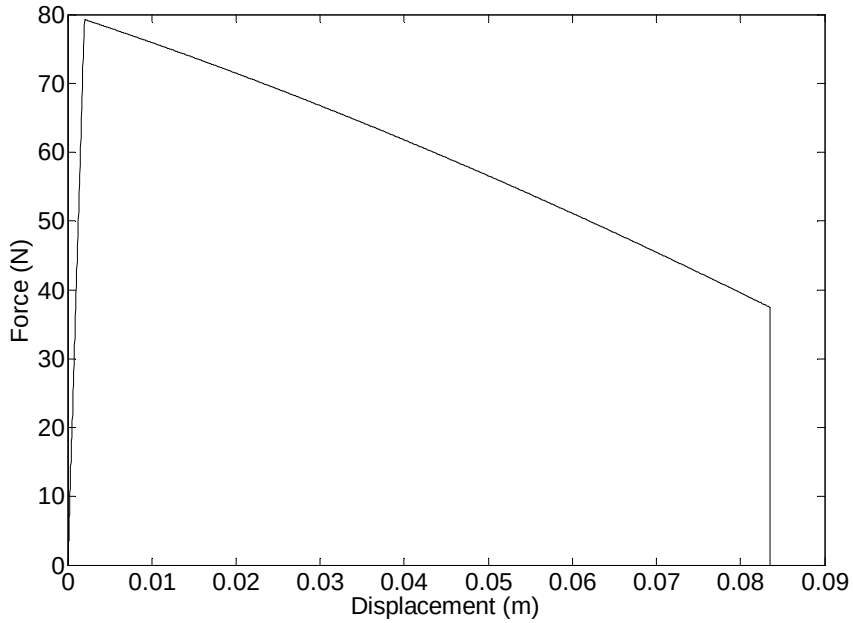

Fig 1.6 Variation of damper force with displacement for case 1 (Fig 1.2).

The simulation result for the case 2 demonstrate a distinct damper force spike as shown in Fig 1.7. This force spike occurs when the velocity of the system reaches the maximum value. This is because at the maximum velocity of the system the kinetic energy input to the damper exceeds the rate of dissipation. The damper piston accelerates the stagnation fluid leading to a sudden increase in the pressure drop across the orifice. The sudden increase in pressure drop leads to damper force spike. The valve type damper and taper grove and pilot valve type compounded dampers are the examples for this type of orifice area variation. The modelling of these type of dampers has been presented in Appendix-I and in Bhatnagar et al (2009).

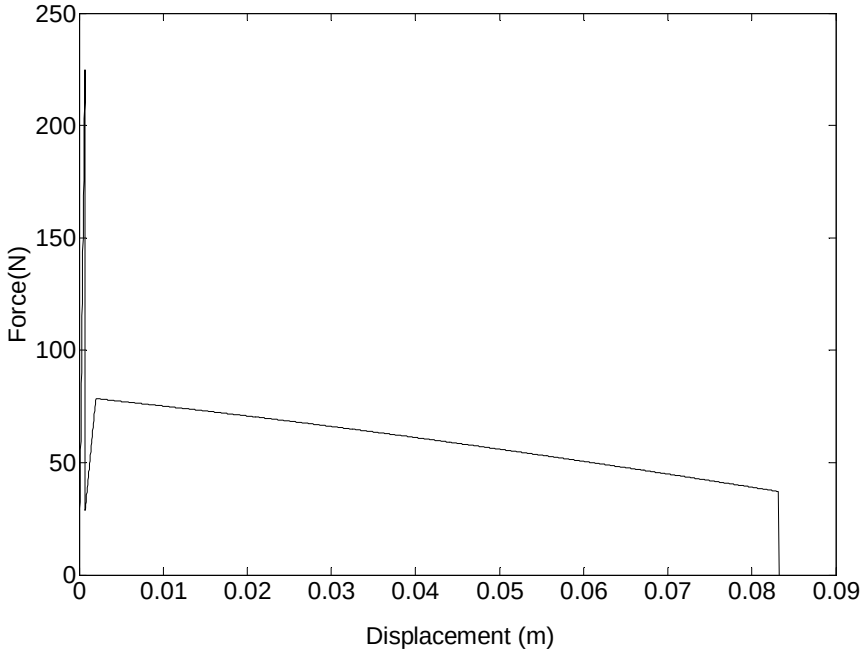

Fig 1.7 Variation of damper force with displacement for case 2 (Fig 1.3).

The damper force spike can also occur when the damper stroke during the concluding part of the damper stroke when the residual kinetic energy of the system is sufficiently high. In such a case the orifice area is suddenly reduced to prevent the piston from dashing against the cylinder head. This is the third case shown in Fig 1.4. The simulation results for the third case are shown in Fig 1.8. The variation of force versus displacement for the third case shows a damper force spike at the end of the stroke.

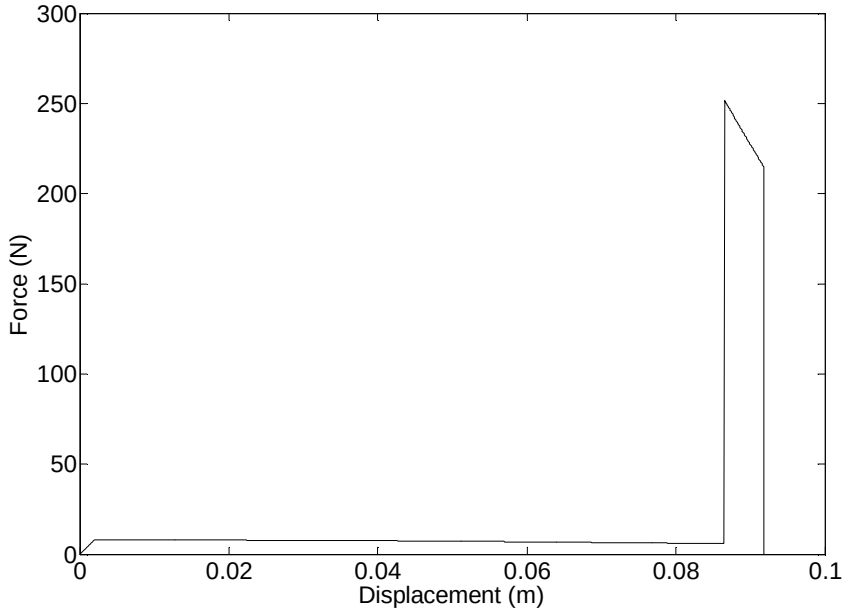

Fig 1.8 Variation of damper force with displacement for case 3 (Fig 1.4).

From the above discussion it can be gathered that if the velocity of the damper is constant, the orifice area is to be kept constant so as to maintain a constant damper force. However, as the damper stroke progresses the damper decelerates the system thereby reducing the velocity to zero at the end of the stroke. In case of a constant orifice area damper the damper force reduces with the reduction in the velocity of the spring mass damper system. However, for an ideal design the damper force is required to be kept constant throughout the damper stroke by the progressively reducing the damper orifice area. Whenever the load transmitted by the damper to the structure is a major contributor, the design of a structure is dependent upon the simultaneous minimisation of the transmitted force and the damper stroke. A very long damper stroke will result in the reduction in transmitted force but will also result in an increase in the size of linkages and components for the supporting or fixing the damper to the system. A damper with a

long stroke will itself require an enhanced rigidity for resisting the deflection due to the applied load. Thus, a long stroke damper will require a longer guiding support and so it will indirectly lead to an overall increase in the weight of the system. Therefore the damper stroke is required to be optimized for transmitting optimal force to the structure. However, the results of computational models (Hajihosseinloo et al (1989), Brown (1946), Bhatnagar et al (2009)) and experiments show that the variation of damping force with the damping stroke is not constant as is the aim of the design of hydraulic dampers. The approximate behaviour of such a damper can be attributed to the non-linearities of the governing differential equation and lack of adaptability inherent in the system-design. The control law for the variation of orifice area is based on inviscid flow analysis and as such in actual case an appearance of spike in curve for the variation of damper force versus stroke may be observed. In a manufactured product the geometric errors due to manufacturing tolerances and variation of coefficient of discharge due to inherent and environmental reasons contribute to the variation in the response.

The damper response that had been discussed so far in this section pertained to the systems subjected to the impact loading. The instances of high speed impact loading applications can be found in case of gun dampers, aircraft undercarriage dampers, collision beacons for the railway carriage etc. In this section the damper application for impulse load has been discussed in the beginning because the application of hydraulic damper started as a recoil system for artillery guns in 1862 (Hogg, (1971)). It is a specialised but a challenging of damper application. The hydraulic dampers find more extensive use in automotive suspensions, seismic isolation, vibration isolation of machines, vibration damping in machine tools and metal machining operations, etc. In these applications the excitation of the system is due to the cyclic load. If the

above mentioned spring mass and damper system is subjected to a base load as shown in Fig 1.9, the variation of transmissibility with excitation frequency depends upon the damping ratio.

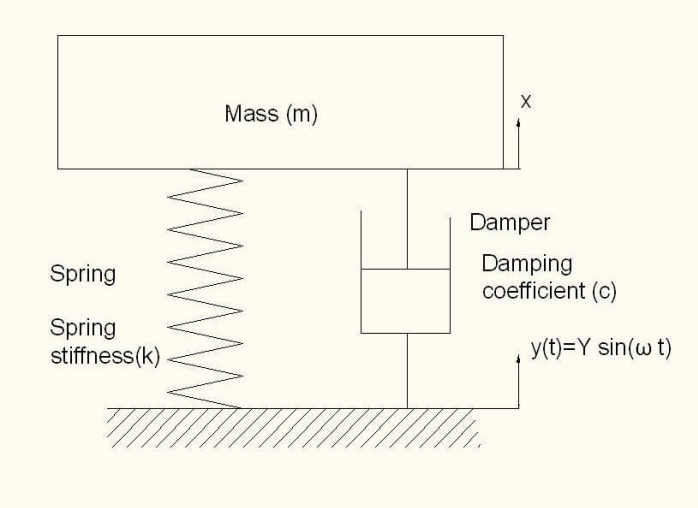

Fig 1.9 Schematic of a spring, mass and damper system with base excitation.

The governing equation of the system is given as follows:

$$m\ddot{x} + c\dot{x} + k\,x = c\,\dot{y} + ky \qquad (1.3)$$

Most of the symbols in the above equation have been defined previously except for the symbol *c* which is called as the damping coefficient. In the above equation *y* is the base excitation. If the Eq1.3 is reorganised in terms of the ratio of amplitude of vibration of mass to the amplitude of base excitation, the Eq 1.4 is obtained. This ratio is called as the displacement transmissibility and is given as follows:

$$\frac{|X|}{|Y|} = \sqrt{\frac{\left(1+(2\varsigma\ r)^2\right)}{\left(1-r^2\right)^2+(2\varsigma\ r)^2}} \qquad (1.4)$$

where

$$\omega_n = \sqrt{\frac{k}{m}}$$
$$r = \frac{\omega}{\omega_n} \qquad (1.5)$$
$$\varsigma = \frac{c}{2\sqrt{km}}$$

ω_n = natural frequency of vibration.

The variation of displacement transmissibility with frequency ratio at different damping ratios is shown in Fig 1.10. From the Fig 1.10 it can be seen that for low frequency ratio the transmissibility is low for high damping ratio. The transmissibility approaches infinity as the damping ratio approaches zero at the frequency ratio of 1. This is the condition for resonance. For high frequency ratio the transmissibility is low for low damping ratio. Since this case is much similar to a simple single wheel station suspension system therefore a damper is required to change the damping ratio at different frequencies of ground excitation. Such a variation of frequency on same road conditions can take place simply due to the change in the speed of the vehicle. A hydraulic damper with valve type orifice control can adapt to the variation of ground excitation frequencies in a limited way. In racing cars such requirements are met by using multi chamber dampers (Dixon, 1999). Due to the above limitations of the hydraulic damper there is a requirement to develop a damper which has a high degree of adaptability.

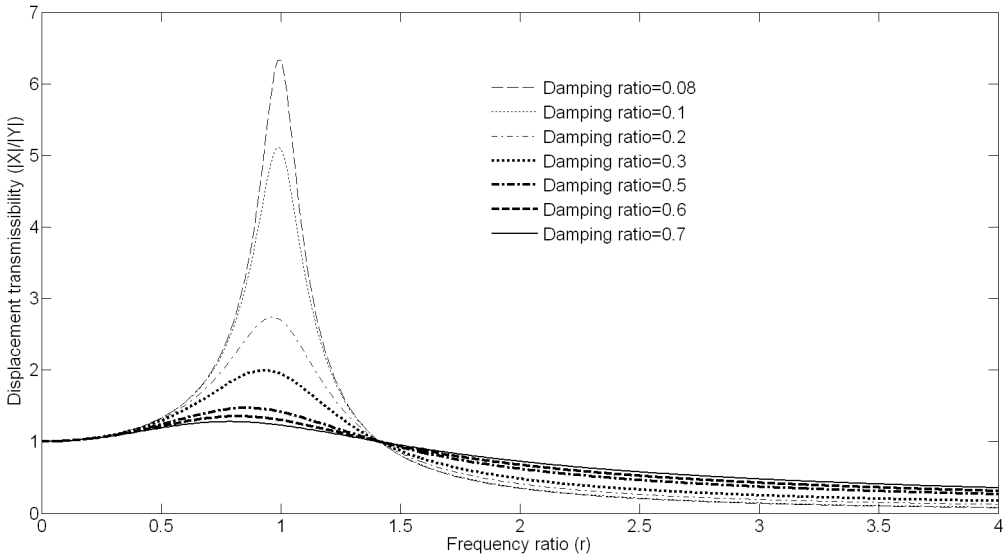

Fig 1.10 Variation of displacement transmissibility with frequency ratio at different damping ratios for a base excited spring mass damping system.

At this stage it will be relevant to mention that the damper force spike can also occur in the case of damper used in vibration isolation. From the previous simulations it was seen that the value of damper force spike can be considerably higher than the mean damper force. In such a case the force transmissibility can be quite high and the purpose of the damper to isolate input vibration can get defeated. On the other hand the damper force spike can lead to secondary excitation of the structure. This is also applicable to seismic damper application. The simulations for the impact load application correspond to the single stroke of the damper for vibration isolation applications. Therefore in the vibration isolation dampers the prevention of spike is also as important as the adjustability of the damping ratio to the frequency of the input vibration. In the vibration isolation damper applications the damping force is not aimed to remain constant

throughout as it may lead to high force transmissibility at low damper velocity. In such cases the damper force is aimed to be proportional to the damper velocity.

The presence of force spike in the dampers for impact application leads to the transmission of impact load to the structure. This can have detrimental effect on the fatigue life of the structure. In case of vibration isolation dampers the presence of spike lead to higher load transmissibility and may also lead to secondary vibrations of the structure. In case of damper with suspension applications this can lead to passenger discomfort or injuries. The hydraulic dampers have limited capability to attenuate the spikes and so the damper designs with high degree of adaptability hold a better promise.

The damper solutions with high degree of adaptability belong to two prime categories, which are active type and semi active type, Karnopp et al (1974) and Crosby et al (1973). An active type of damper has a servo mechanism which develops the counter force to the force input to the spring mass damper system such that the force transmitted to the structure is in the form of small reaction. An active type (Crolla (1988)) of damper system has an advantage that it can achieve nearly perfect vibration or force isolation for the structure to which it is connected. The disadvantages of an active system are complexity of control system, large power requirement for servo-power pack and are expensive. Due the complexity of control system there is also a problem of instability of the system leading to a rapid deterioration of performance of the system.

A semi-active damper is able to adaptively vary the damping coefficient in such a manner that the damper force can be varied as function of velocity or displacement depending upon the application. The force of a semi-active type damper can be adjusted so that the damping

coefficient can be kept at a value which minimises the transmissibility over the range of frequencies of the incident load. Since the damper responds to the sensor signal by modifying the fluid property so it is called a semi-active damper. The electro-rheological fluid based dampers (Fig 1.11) were the first to appear as smart fluid based semi-active dampers. Small electrorheological effects have long been known, but large scale practical applications were first studied by Winslow in 1947 (Dixon,1999).The electro-rheological fluids are the fluid which exhibit change in shear yield stress due to the application of voltage across the electrodes over which they flow (Alanoly and Sankar, (1987), Leitman and Reithmeier, (1993), Walter et al, (1992)). Since the voltages required for electro-rheological fluids are high so the requirement of high voltage power source and the insulation design led to reliability and design complexity drawbacks.

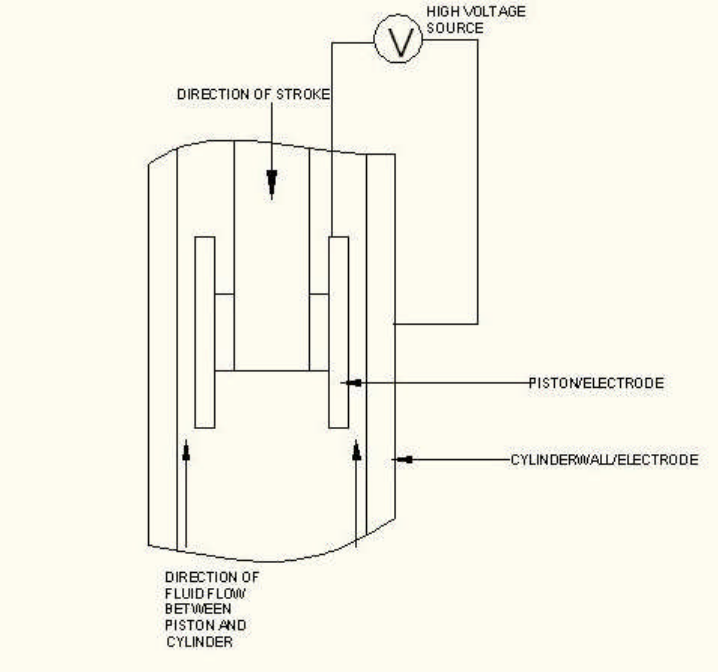

Fig1.11 Schematic of an electro-rheological damper.

The first important work on MR fluid based applications is attributed to Rainbow (1951), (Dixon,1999). For forty years from 1947 significant efforts were made on ER fluid based applications, largely neglecting MR fluid devices, but since 1990, when work on MR fluids increased, it has become apparent that MR devices may be much more practicable because of lower operating voltage, lower power requirement, higher shear yield stress achievable, broader operating temperature range, and greater tolerance of the liquid to contamination, particularly water. These advantages must be weighed against higher expenses and significant hazards in manufacture (Dixon, 1999). The magneto-rheological fluids undergo change in the shear yield stress due to the application of magnetic field. They have very short response time and require a low voltage current source such as 12V car battery.The schematic of an Mr damper is shown in Fig 1.12.

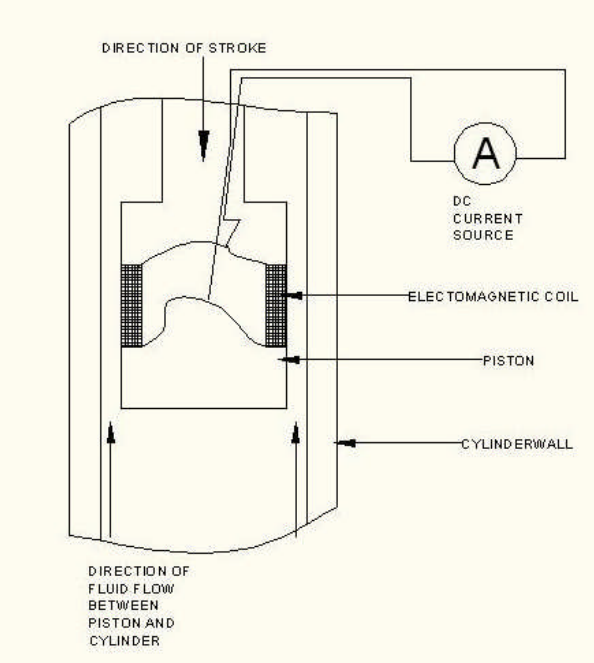

Fig 1.12 Schematic of a magneto-rheological damper.

The limitations of hydraulic dampers which have been further discussed in the survey of their design (ref Appendix-I), led to the motivation to investigate the innovative design of magnetorheological fluid based damper.

1.2 Aims:

With the motivation as outlined above the following aims have been set for the thesis:

(1) Development of a suitable direct and inverse analytical model for predicting the response of a magnetorheological fluid based damper.

(2) Investigation of an innovative design of magnetorheological damper which is capable of reducing the pressure spike.

1.3 Primary Outcomes:

The primary outcomes of the investigation of MR damper of existing design and proposed innovative design will be as follows:

(1) A direct and inverse analytical model for predicting the response of a damper taking into account the transient effects.

(2) Innovative design of a damper which is a magnetorheological fluid based semi active equivalent version of a compounded hydraulic damper.

(3) Improvement in response time of the electromagnetic actuators of magnetorheological damper by a suitable optimisation strategy.

1.4 Secondary Outcomes:

The secondary outcomes of this investigation will be as follows:

(1) Experimental validation of analytical model of magnetorheological damper by identification of the model of LORD Corporation make RD-8040-1 damper.

(2) Findings of the comparative study of the analytical model vis-à-vis hysteresis based phenomenological model.

(3) Design and optimization methodology for magnetorheological dampers.

1.5 **Contribution to knowledge**:

(1) Transient analytical model for magnetorheological fluid based devices.

(2) Extension of concept of compounding of dampers to the magnetorhological fluid based damper.

1.6 **Organisation of thesis**:

The work has been organised into eight chapters. The first chapter describes the motivation for this work, objectives, primary outcomes, secondary outcomes and the layout of the thesis. The second chapter presents the literature review pertaining to the modelling of dampers in respect of phenomenological model and analytical models and their limitations, the design of magnetorheological dampers and definition of problem. The third chapter deals with the transient analytical modelling of the damper, the solution method and the parametric study based on the simulation results of the model have been presented and discussed. The simulation results have been compared with the results of other papers. The fourth chapter deals with the experimental

validation of the model proposed in the chapter 3. The fifth chapter deals with the new design of MR damper based on dual channels for attenuation of flow transients. The chapter also introduces a new split flow scheme for simulating dual channel flow. The last section of the fifth chapter deals with the experimental validation of single and dual channel damper model for low and high speed. The design of fast response electromagnetic actuator through genetic algorithm based optimization has been discussed in the sixth chapter. The chapter also discusses the finite element simulation of the magnetization of flow paths. In the seventh chapter the primary and secondary outcomes of the investigation have been outlined along with the final conclusion. The chapter also discusses the future work in the areas of modelling and design of MR dampers.

Chapter 2

Literature Review

2.1 Introduction:

The investigation in pursuit of the objectives of the thesis requires a careful survey of the literature. This section has been divided into four sections. The first section deals with the overview of MR dampers. In the second section a review of modelling techniques has been presented. The review of the literature for dampers at high speed or impact load has been dealt with in the third section. The damper design which is required to be developed and investigated has to be optimised for achieving the desired performance and so the literature review pertaining to optimisation has been presented in the third section. The experimental validation of the new damper design has been derived based on survey of literature presented in the fourth section of this chapter.

2.2 Overview of Magnetorheological (MR) Dampers

The basic objective of this section is to present an overview and to derive the problem definition of this work. The magnetorheologocal damper from this section onwards will now be referred to as MR damper. The findings in the previous chapter led to the exploration of the solution in terms of smart fluid based dampers. Since MR dampers operate at low power current source therefore they have started finding application in areas such as vibration proof tables, mountain bike, seismic protection systems for civil structures and automobiles. The MR damper was commercially introduced by the Lord Corporation and the early model series was named as "Motion Master". These dampers were used in truck seat vibration isolation and prosthetic legs.

General Motors introduced these dampers for an exclusive model of Cadillac in 2003. All of the above applications are low speed applications as the peak velocity of the damper piston is not more than 2 m/s. However there is a recent interest in exploring the possibility of using MR dampers for high speed applications such as aircraft landing gears and artillery dampers.

2.2.1 Magnetorheological fluids

MR fluids are the slurry of hydrocarbon oils or silicone oils and micron size ferrite particles. The ferrite particles are coated with anticoagulant for preventing them from forming lumps due to coagulation. The coating of surfactant and anticoagulant also delays the sedimentation of the ferrite particles. When un-activated by the magnetic field they behave like ordinary slurry of ferrite particles. Therefore the viscous behaviour of an MR fluid in the absence of magnetic field is like an ordinary Newtonian fluid. However, when a magnetic field is applied in the direction perpendicular to the flow the ferrite particles align along the magnetic field to form columnar structures which offer resistance to the parent fluid as it flows over them. The parent fluid tries to shear off the chains of magnetised ferrite particles and because of this, the sheared off chains of ferrite particles flow in a plug like lump. As a result of this the MR fluids show a Bingham fluid like behaviour. The shear stress developed due to the flow of parent fluid over the ferrite particles chains, results in the breaking and reformation of ferrite particle chains. This results in an increase in apparent viscosity of fluids. The magnetic fluids can be divided into following three types:

(1) Magnetorheological fluid.

(2) Ferro fluids.

(3) Bi –disperse fluids.

Out of the above magnetic fluids the behaviour of magneto-rheological fluids has already been described above. Ferro-fluids are the suspensions of nano-ferrite particles in hydrocarbon oil. These fluids exhibit an increase in viscosity under steady magnetic field in the manner similar to MR fluids, with the difference that the increase in apparent viscosity is limited to twice the viscosity of parent fluids. This is because the ferro fluids contain nano size ferrite particles so they behave like colloids and the forces due to Brownian movement are stronger than the force of the magnetic field (Bossis et al (2002)). In case of MR fluids the increase in viscosity is 5-7 times that of parent fluid. The ferro-fluids have many other interesting properties such as they show a reduction in apparent viscosity as compared to the parent fluid when subjected to oscillatory magnetic field. The energy of the applied oscillatory magnetic field gets converted into the kinetic energy of the fluid, leading to an apparent decrease in the parent viscosity.

Bi-disperse fluids are the mixture of MR and Ferro fluids and they have faster response to magnetic field as compared to MR fluids and they have a longer sedimentation time for ferrite particles as compared to MR fluids (Bossis (2002), Ngatu and Wereley (2007)). The behaviour of all of the above types of fluids under the influence of steady magnetic field is the same. The formation of columnar structures of ferrite particles in magnetic fluids is as shown in Fig 2.1.

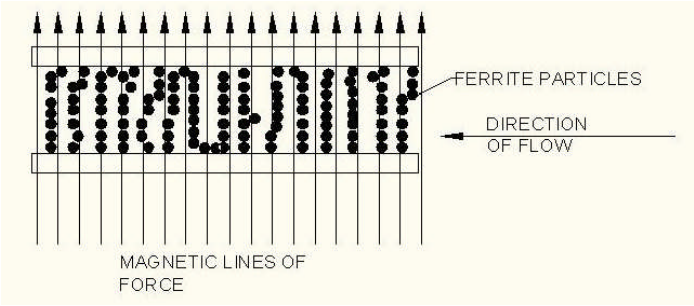

Fig 2.1 Behaviour of ferrite particles under the influence of magnetic field as the MR fluid flows between the two parallel plates.

MR fluids can be used in three modes of flow, (Stanway et al 1996, Boelter et al (1997), Dixon (1999) , Poynor (2001), Gregory et al (2007), Liao et al (2007),). In the valve mode the fluid flow is like a Poisueille flow. In this mode the resistance of the fluid flowing through the channel can be varied by varying the strength of the applied magnetic field. The channel in this case can be a gap between the two parallel plates or an annular gap between the two concentric cylinders, (see Fig 2.1).

In the shear mode one of the plate or cylinder is moving in the direction opposite to the flow. The MR fluid can be stationary or moving with some value of velocity. In latter case it is more appropriately called as the mixed mode operation of MR device (ref Fig 2.2).

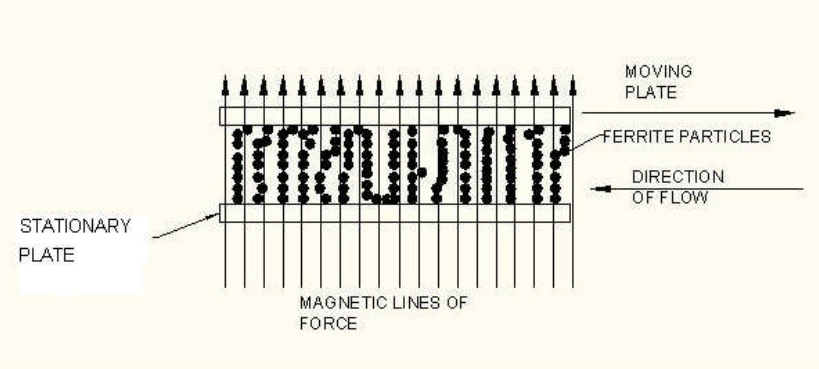

Fig 2.2 Shear mode operation of MR device.

In the rotary devices such as clutches and brakes pure shear mode type operation of MR fluid takes place. In the squeeze mode operation of an MR device one of the parallel plate moves perpendicular to the direction of flow as shown in Fig 2.3. Since the force required to squeeze

the magnetised force is quite large therefore the squeeze mode MR device is suitable for bearing applications.

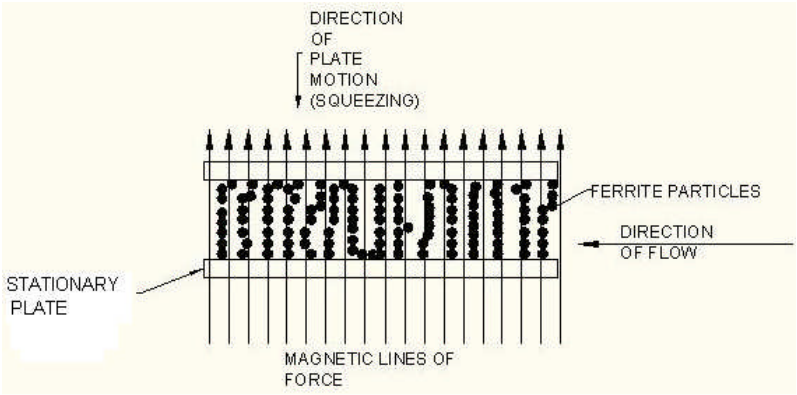

Fig 2.3 Squeeze mode operation of MR device.

2.2.2 MR devices

MR fluids can be used in various applications such as dampers, clutches, seals, bearing etc. In this work the application of MR devices shall be confined to the dampers as it is the theme of this investigation. Out of the application of above three modes the dampers use valve mode or shear mode operations. The simplest design of MR damper has a piston which has magnetic coils provided with suitable wiring arrangement for energisation. The damper is usually provided with an integral gas type restoring spring which similar in configuration to a hydraulic damper shown in Appendix –I, Fig A.13. If the damper has an integral restoring spring then it is called as twin tube damper. On the other hand if the restoring gas spring is separate then the MR dampers are usually mono-tube type construction (See Fig 2.4) (Dixon (1999), (2001), Boelter et al (1997), Gregory et al (2007), Liao et al (2007), Poynor (2001)). In this design the MR fluid flows between the cylindrical surface of the piston and the wall of the cylinder.

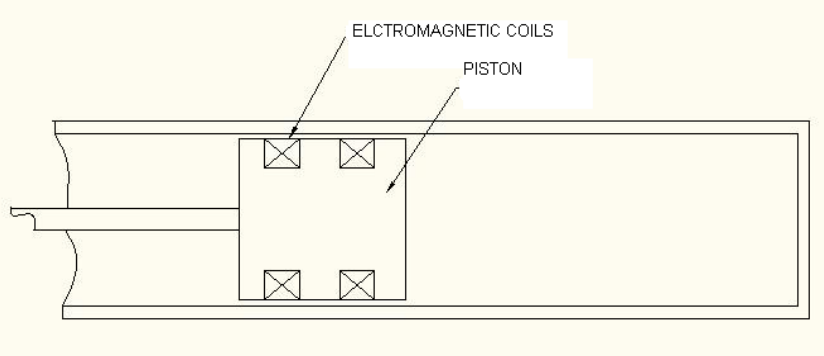

Fig 2.4 Schematic of a mono-tube damper

Thus, it is a flow and shear mode type damper or mixed mode type damper. In valve mode type dampers the MR fluids either flows through a hole in the piston which is surrounded by the coils or the piston forces the fluids through an annular gap which is surrounded by the coil as shown in Figs 2.5 and 2.6 (Dixon (1999), Kawashima et al (2001), Boelter et al (1997), Gregory et al (2007), Liao et al (2007), Poynor (2001)).

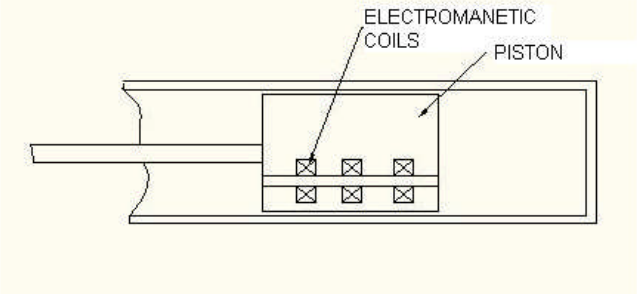

Fig 2.5 Schematic of a mono-tube valve mode type damper with flow passage embedded in the piston.

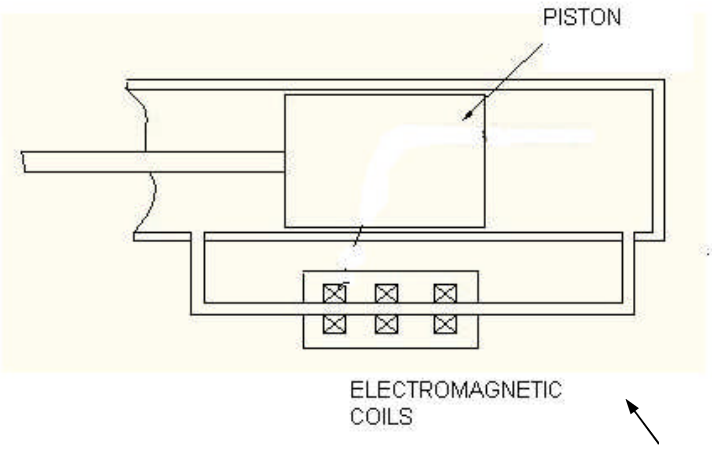

Fig 2.6 Schematic of a mono-tube valve mode type damper with bypass type flow passage.

The principle of valve mode type damper can also be used for valve application as described in Ai (2006). For enhancing the effectiveness of the valve the coils can be designed to be positioned in the annular gap so that the flow of MR fluid under the influence of magnetic field can be radial and annular. This design results in an increase in the fluid volume affected by the magnetic field. The MR fluids based valve can be modified into a more compact form and used to control the valve lift of the valve type damper described in the survey of conventional hydraulic type dampers to control the damper force spike. The schematic of such a design which, has been also referred to in Poynor (2001) is shown in Fig 2.7.

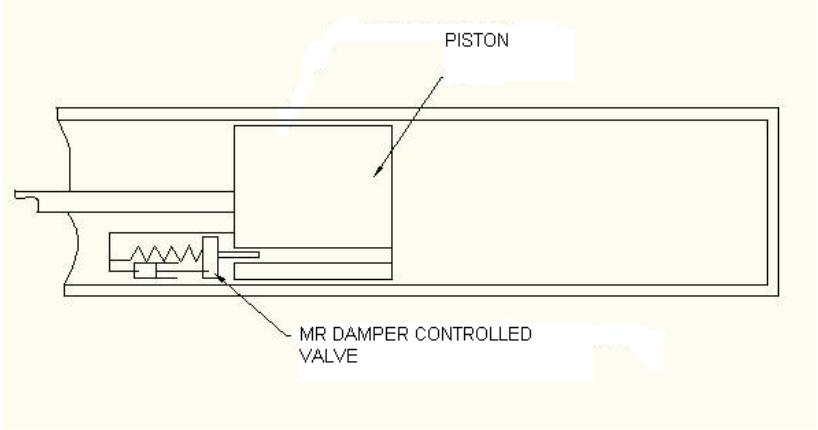

Fig 2.7 Schematic of a MR damper or valve controlled conventional valve type damper Poynor (2001).

A brief survey of all the damper designs based on study of literature such as (Dixon (1999), Boelter et al, (1997), Gregory et al (2007), Liao et al (2007), Poynor (2001)) shows that the MR dampers have been tested in speed range of 0-2m/s. However in recent times the work on MR dampers subjected to impact loading has started appearing (Wang and Li (2006), Lee and Wereley (1999), Norrsi and Ahmedian (2003), Facey et al (2005)). The study of publications on the MR dampers which were tested in the speeds in the range of 5-7 m/s show the presence of damping force spike (Wang et al (2006)). There are very few publications describing the performance of the damper behaviour at speeds above 8m/s second. This can be possibly because a large number of real life applications which require dampers to operate at speed up to 2m/s. The challenge in the development of high speed damper is the attenuation of transients which are non controllable components of the damper force. These transients appear as force spike in the force versus displacement curves for the hydraulic dampers in general and MR dampers in particular. The applications of dampers for aircraft landing gears (including UAVs)

operate at heavy loads and in the speed range of 5-7m/s (Batterbee et al (2007,1&2), Sims(2000), Peel and Bullough (1994)). The behaviour of MR dampers has been described by fluid dynamics model based on Herschel Bulkley model or Bingham plastic type non-Newtonian fluids (Kamath et al (1996)). Due to the formation and breakage of the chain ferrite particles in the MR fluids subjected to the magnetic field, MR fluids behave like Bingham fluids (nature of flow is similar to toothpaste). A generalized plot showing the variation of shear stress with the shear rate is shown in Fig 2.8. The fig 2.8 shows that the Bingham plastic behaves like a rigid body until the shear stress in the fluid is less than the initial shear stress. The yield shear stress is dependent on the strength of the magnetic field and this relationship makes the MR fluid a field controllable fluid. If the shear stress corresponding to the pressure gradient across the fluid channel exceeds the pre-yield shear stress, then the post yield shear stress is the sum of pre-yield shear stress and shear stress due to post yield viscosity.

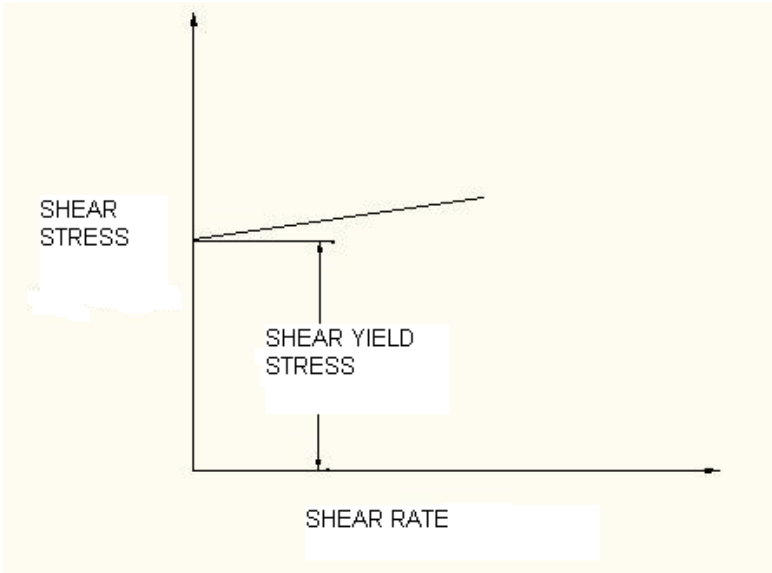

Fig 2.8 Herschel Bulkley model for Bingham plastics.

So far, the modeling of force of an MR damper has been done by three classes of models. The first class of models is called phenomenological models. Since the MR dampers exhibit a hysteretic behavior, MR damper models of the first type use the experimental data to fit a hysteresis curve to predict the damper force as a function of velocity. The details of such model have been outlined in Wereley et al (1999), Butz and Von Stryk (2002), Mohammad et al (2007) and Wang and Liao (2011). In this class, also lie the phase transition models based on Falk and Kanopka (1990), Lookman et al (2003) and Wang and Liao (2011). The phase transition model for MR dampers was developed on the basis of phase transition theory which was proposed for the investigation of crystallographic phase transition in shape memory alloys (Wang and Liao (2011)). However, in Wang and Liao (2011) it is given that although the physics involved in the MR fluids is taken into account to some extent in this model but it is still a phenomenological model. The second class of models is called as sigmoid function models Wang et al (2003). In these models the force velocity relationship is obtained by fitting the sigmoid function to the experimental data. In the third class of models called as the equivalent models, the variation of force with velocity is expressed in terms of equivalent springs, variable viscous damping and friction element (Oh and Onoda (2002)). The third class of models are based on the quasi steady solution of the Navier Stokes equations using either Bingham plastic model or Herschel Bulkley model for deriving the equations for the velocity profile of MR fluid flowing through the channel, Phillips (1969), Kamath et al (1996), Lee and Wereley (1999), Norrsi and Ahmedian (2005), Facey and Rosenfeld (2005), Chooi and Oyadiji (2008), Wang and Gordaninejad (2007), Li (2000). In this work the quasi steady model will be discussed in details as present work is going to be an extension of this model.

2.3 Fluid dynamical models for MR dampers

The fluid dynamical models published so far are based on Bingham plastic model or Herschel Bulkley model. The Herschel Bulkley model is the more generalized model for describing the shear stress in the MR fluid flow and is given by the following equation:

$$\tau = \tau_0 sign\left(\frac{du_x}{dx}\right) + K\left\{\left(\frac{du_x}{dx}\right) sign\left(\frac{du_x}{dx}\right)\right\}^{n_{hb}} sign\left(\frac{du_x}{dx}\right) \qquad (2.1)$$

where τ is the total shear stress, τ_0 is the yield shear stress, K is the consistency index, n_{hb} is the index for shear rate in Herschel Bulkley equation and du/dx is the shear rate (Wereley and Li (1998)). Depending upon the choice of flow behaviour, the index n_{hb}, can be used to account for post yield shear thinning or shear thickening in the following manner:

(1) $n_{hb}>1$ shear thickening.

(2) $n_{hb}<1$ shear thinning.

(3) $n_{hb}=1$ Bingham fluid behaviour.

In the case of shear thinning the post yield viscosity decreases with the increase in the shear rate. The shear thickening fluids show an increase in the post yield viscosity with the increase in the shear rate.

These models are based on following assumptions:

(1) Flow through the channel is plug flow in the pre yield region and laminar flow in the post yield region.

(2) The flow is fully developed.

(3) The operating Reynolds number is less than the critical Reynolds number.

(4) Inertia effect has been neglected in the governing differential equation.

In Wereley and Li (1998), the model for flow through the annulus of MR damper has been approximated by considering the parallel plate flow Philips (1969). The parallel plate approximate considerably simplifies the solution and enables the fluid behaviour to be obtained as a closed form solution. This is because the equation of mass balance for the parallel plate model is a function of pressure gradient and so the solution of a system of nonlinear equation gets decoupled. The velocity profile obtained for the flow of MR fluid under the influence of magnetic field has three regions. The central region is a region of plug flow and the region on the either side of the plug flow region have laminar flow velocity profile (see Fig 2.9). The shear stress in the region of plug flow is less than or equal to the shear yield stress and as such this region has constant velocity, along the direction of flow. Here it is mentioned that in the absence of magnetic field there will be no plug flow region and the velocity profile will be identical to the velocity profile for flow of a Newtonian fluid flowing through the channel.The interface between the two regions has velocity and shear stress compatibility boundary conditions and the boundary conditions for the regions in contact with the walls are no slip boundary conditions. The governing differential equation is given as follows:

$$\rho \frac{\partial u_x}{\partial t} = -\frac{\partial p}{\partial x} + \frac{\partial \tau}{\partial x} \qquad (2.2)$$

Since the model presented in (Wereley and Li (1998)) is a quasi steady model therefore the time derivate of velocity has been neglected.

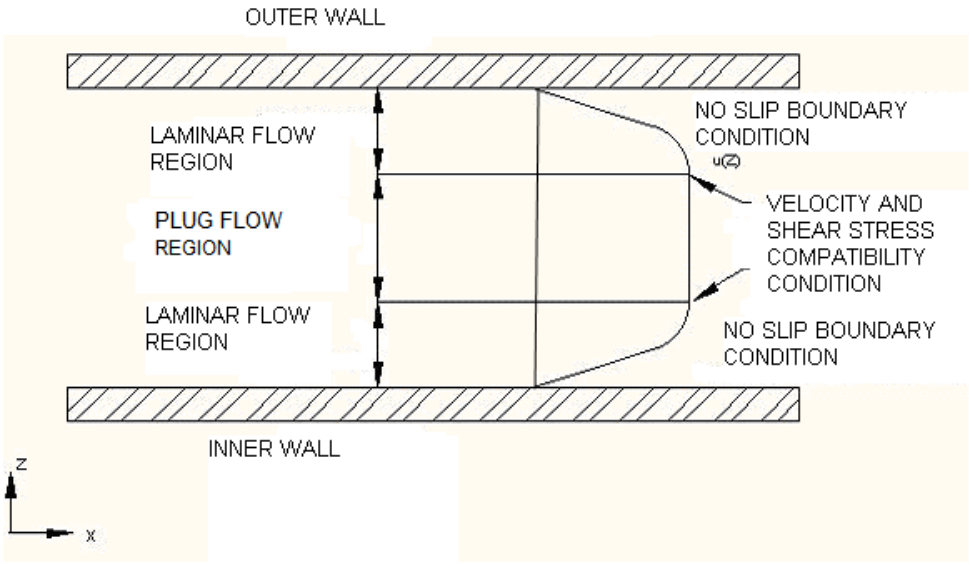

Fig 2.9 Typical velocity profile of MR fluid flow through an annular fluid path in the presence of axial linear pressure gradient and under the influence of magnetic field perpendicular to the flow path.

The governing differential equation given above can be integrated to obtain the expression of velocity in term of pressure gradient and the radii of the damper. The flow rate in (Werely and Li (1998)) has been obtained using parallel plate model. The expression for flow rate is given as:

$$\left|Q_f\right| = \frac{bd^3\Delta P}{12\mu_{py}L}\left(1-\bar{\delta}\right)^2\left(1+\frac{\bar{\delta}}{2}\right) \qquad (2.3)$$

where Q_f is the flow rate of MR fluid through the annular gap between the two concentric cylinders, d is the gap between the two cylinders, ΔP is the pressure drop across the gap for the flow of MR fluid, L is the length of the gap, v_0 is the kinematic viscosity and $\bar{\delta}$ is the width of plug flow region. Since the flow rate can be determined from the velocity of the piston of MR damper therefore the above expression of flow rate of MR fluid has two unknowns as pressure

drop and plug width. These unknowns have been reported to be determined by following three approaches:

(1) Solve the quintic equation ,due to Philips (1969), given as follows:

$$3(\mathscr{P}-2\mathscr{T})^2\left(\mathscr{P}^3-(1+3\mathscr{T}-\mathscr{V})\mathscr{P}^2+4\mathscr{T}^3\right)+\mathscr{T}\mathscr{V}^2\mathscr{P}^2=0 \quad |\mathscr{V}|<\frac{3(\mathscr{P}-2\mathscr{T})^2}{\mathscr{P}} \tag{2.4}$$

In the above equation the dimensionless velocity V of the piston is given as:

$$\mathscr{V}=-\frac{b\,d\,v_0}{2Q_f} \tag{2.5}$$

The dimensionless pressure gradient P and shear stress T are defined as follows:

$$\mathscr{P}=-\frac{bd^3}{12A_h v_0 \mu_{py}}\frac{\Delta P}{L} \tag{2.6}$$

$$\mathscr{T}=\frac{bd^2}{12A_h v_0 \mu_{py}}\tau_0 \tag{2.7}$$

The pressure gradient and the width of plug region can be calculated by combining Eq (2.27) and the quintic equation.

(2) The second approach is to use Ergun equation mentioned in Chase and Dachavijit (2008) for MR fluids. This equation has been used for modelling ER fluid flow through porous media and as such use of this equation may either be not relevant or application of such equation may introduce complexities in the solution. In view of this reason the Ergun equation has not been discussed in this work.

(3) In the third approach the governing differential equation for parallel plate flow of MR fluid is integrated to obtain the expression of velocity of flow of MR fluid in the annular gap for laminar regions using the boundary condition mentioned in the Fig 2.12. The expression for velocity profiles are used to obtain the expressions of flow rate in each region of flow and the sum of these flow rate is equated to the rate of fluid displaced by the piston to get the following equation:

$$\alpha_2 Bi^2 + \alpha_1 Bi + \alpha_0 = 0 \tag{2.8}$$

The symbols in the above equation are defined as follows:

$$\alpha_0 = \frac{3}{2}\delta^3$$

$$\alpha_1 = -3\left[1+2\frac{A_h}{A_d}\right]\left(1-\bar{\delta}\right)^2\bar{\delta} \tag{2.9}$$

$$\alpha_2 = \left(1-\bar{\delta}\right)^4\left(1+\frac{\bar{\delta}}{2}\right)$$

The Bingham number Bi is a function of the non dimensional plug thickness and the area coefficient A_h/A_d:

$$Bi = 6\bar{\delta}\left(\frac{1}{2}+\frac{A_h}{A_d}\right)\left[\frac{1+\sqrt{1-\frac{\bar{\delta}}{6}\left(1+\frac{\bar{\delta}}{2}\right)\left(\frac{1}{2}+\frac{A_h}{A_d}\right)^{-2}}}{2\left(1-\bar{\delta}\right)^2\left(1+\frac{\bar{\delta}}{2}\right)}\right] \tag{2.10}$$

The exact analytical solution for electrorheological fluid flow for cylindrical domain has been given in Kamath et al (1996) and Chooi and Oyadiji (2008), and can be applied for MR fluid flow as well. The equation for zero velocity gradient across the plug thickness and the equation of conservation of volumetric flux result in a system of simultaneous non-linear algebraic equation. This system of equation has been described to be solved by secant iteration method. The solution will be described in details in the following chapters as it forms the basis of this work. The comparison of parallel plate solution and quasi steady state solution for MR fluid has been described in Chooi and Oyadiji (2008). In Chooi and Oyadiji (2008) the system of equation has been solved using SIMULINK routine. The model described in the this paper has been claimed to agree well with the experimental results and is able to include the hysteretic effect in the force velocity curve and this likely to be because of the inclusion of wall shear stress on the damper piston. The effect of this force due to wall shear stress has been apparently neglected in most of the works referred above. This work also compares the results of annular flow model with the parallel plate model and it has been shown that there is a small error in the parallel plate model. Similar model has been reported in Cesmeci and Tehsin (2010), with a difference that it records the limitation of the analytical model as its inability to predict hysteretic behaviour and the use of phenomenological model has been resorted to. The inability of the model to capture the hysteretic behaviour is likely to be due to the neglecting of wall shear stress force on the piston and use of incorrect volume flow rate displaced by the piston. In an earlier work by Wang and Gardaninejad (2007), the analytical model using Herschel-Bulkley flow

model for shear stress and parallel plate model for flow rate has been claimed to capture the hysteresis behaviour with good accuracy. The other method to model the hysteretic behaviour is somewhat empirical and has been described by Hong et al (2005). In this model the inertia effects on the fluid have been attempted to be included by an 'inertance' term and the fluid compressibility has been accounted for in the manner similar to Wang and Gardaninejad (2007).

From the above discussion it is gathered that the solution of MR fluid flow is a complex problem even if the Bingham plastic model is used and the complexities are further increased, if the shear thinning or thickening are taken into account. To obtain the solution with shear thickening effect using Herschel Bulkley model the parallel plate approximation has been used in Wereley (2008) . The study of the (Chooi and Oyadiji (2008), Wereley and Li (1998), Wereley (2008) and Cesmesi and Tehsin (2010)) shows that the region of laminar flow is quite small as compared with the plug flow region and as such the error induced in flow rate expression using Bingham model and annular flow will be less than the error induced in the solution using shear thickening and parallel plate model. This is because error due to the neglecting of the wall curvature is more significant in dampers with smaller diameters than the neglecting of the shear thickening effect. It therefore leads to the conclusion that Bingham model for MR fluid in cylindrical domain is the best approach for predicting the force developed by MR damper. The quasi static model given in the above mentioned literature is based on important assumptions that the flow through the MR channel is plug flow with laminar flow between the channel wall and plug flow and negligible inertia effects. The models have been experimentally validated at speeds less than 1m/s. For high speed applications such as aircraft landing gear in the works published by Batterbee et al (2007,1&2), Sims(2000) and Peel and Bullough (1994) and in gun damper in Ahmedian and Poynor (2001), the correlation with experimental data was not found to

be good . In the experimental data presented in Ahmedian and Poynor (2001) there are a number spike seen for the experimental firing of gun installed with an MR damper. These works have indicated the need for a model which can account for higher order inertia and fluid inertia. In these works also quasi static model has been presented and it has been mentioned that for modelling of MR dampers at high speed the inertia forces need to be included.

It also gathered from the above review that the error due to quasi static solution will be sufficiently significant for MR dampers piston velocity and so there is a need to develop a transient model for predicting the force in MR dampers. Based on the above review this investigation will aim at development of flow model for MR damper using Bingham plastic model and using governing differential equation for cylindrical domain. The pressure drop predicted by the analytical model shall be validated by the experimental methods. This is because the quasi static models and the phenomenological models are not able to explain the hysteretic variation of force versus velocity. Since the variation of force with velocity and displacement are dependent upon the fluid flow the development of suitable fluid mechanical model is a necessary requirement to correctly model the force response of an MR damper.

2.4 Survey of MR damper designs for high speed applications

The general design used for low speed application has already been presented in the introductory chapter and as such this section shall discuss the design of the MR dampers used for high speed applications and which are more appropriately referred in the publications as impact MR dampers. The design of MR damper for high impulsive loads requires the damper to develop a large controllable force in short time. The damper must also have a high dynamic range (*D*)

which is defined as the ratio of total damper force to the uncontrollable force and is given as follows (Dug et al (2002))

$$D = \frac{F_\eta + F_f + F_\tau}{F_\eta + F_f} \tag{2.11}$$

If the parallel plate model is used then these forces appearing the above equation are defined as follows:

$$F_\eta = \left(1 + \frac{bdv_0}{2Q}\right)\frac{12\eta_{py}QLA_p}{wd^3} \tag{2.12}$$

$$F_\tau = c\frac{\tau_0 LA_p}{d} sgn(v_0) \tag{2.13}$$

$$c \approx 2.07 + 1/(1 + 0.4\mathcal{T}) \tag{2.14}$$

$$F_\tau = \left(2.07 + \frac{12Q\eta_{py}}{12Q\eta + 0.4bd^2\tau_0}\right)\frac{\tau_0 LA_p}{d} sgn(v_0) \tag{2.15}$$

where, $F_{\eta,}$ is the force due to post yield viscosity, F_f is the friction force, F_τ is the force due to shear yield stress, b is the width of plate equal to the perimeter of the cylinder, L is the length of flow path, Q is the fluid flow rate, A_p is the area of the piston of MR damper , η_{py} is the post yield viscosity, τ_0 is the yield shear stress, v_0 is the velocity of the piston, $\mathcal{T}$ is the non dimensional shear yield stress and c is a constant dependent upon the non dimensional shear yield stress. The expressions for dynamic range shall change due to model proposed in this work. The design of damper presented in (Mao et al (2007)) is as shown below:

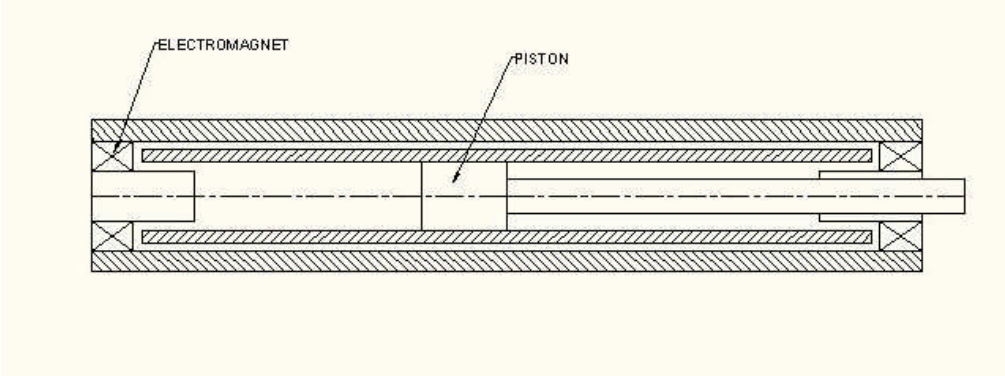

Fig 2.10 Schematic of bi-fold valve type MR damper (Mao et al,(2007)).

The study of this design reveals that it has been derived by relocation of the coils from the piston to the radial and annular passage at either end of the damper for the MR fluid flow. The design is an attempt to maximize the volume of MR fluid under the influence of magnetic field and thus achieve compactness in the design. The relocation of magnetic coils from the piston to the cylinder ends simplifies the design of connections to electromagnetic coils by eliminating the need for a wire tunnel in the piston rod. Similar design has been proposed in Gordaninejad et al (2004), (see Fig 2.11) wherein the flow passage has been designed in the piston. While the design may have complexities in electrical connection to the coil and the piston assembly itself, the advantage of this configuration is that the core of the electromagnet can be sufficiently thick so as to remain unsaturated over a wide range of current. In both of the designs the fluid flows through the radial and annular path, so the analytical model will be complex and so a phenomenological model will be required to be developed for direct and reverse modelling of the damper for determining the control policies. The designs of dampers referred above have been reported to be tested up to the maximum speed of 2m/s. As such this is may not be suitable

for high speed applications. An inner bypass type MR damper with a combination of an electromagnet and permanent magnet has been reported by Zhang et al (2007).

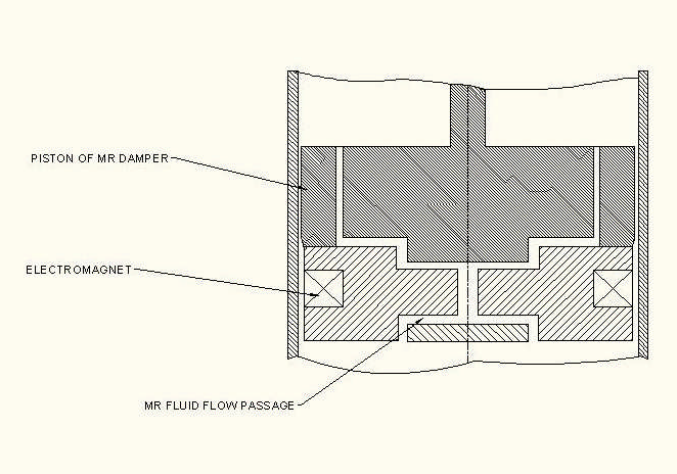

Fig 2.11 Schematic of a novel geometry of flow and mixed mode type MR damper Gordaninejad et al (2004).

The survey of the damper designs leads to the following conclusions:

(1) The bi-fold valve design of MR damper and internal bypass design in (Mao et al (2007)) can give good dynamic range. The response time of these dampers can be improved by the optimization of electro-magnetics.

(2) The above designs can give a high value of controllable force because of increase in the volume of magnetisable flow passage for MR fluid. All of the above designs are likely to give damper force spike at high impact velocities. This is because the above damper designs with control laws and analytical model require a suitable design feature to relieve the spike.

2.5 Design methodology and optimisation of damper

A high speed damper will require an effective actuator design and controller to respond to the control input based on the feedback of the damper force from the sensor. Since the MR fluids have very high density therefore at high speed the damper force spike is likely to be high if the actuator current is not estimated correctly and if the actuator response time is more than 25% of the time of occurrence of spike. In addition of above the validity of laminar flow assumption needs to be evaluated with respect to critical Reynolds number. This will require the development of a new conceptual design of an MR damper for high speed applications.

The conceptual design of and MR damper also includes a suitable optimisation strategy for achieving the best performance of MR damper design. The earliest work on optimisation of MR damper has been outlined in Gavin et al, (2001). In this paper an objective function which is a weighted sum of time constant and the power consumption has been proposed. The linear inequality constraints set consist of wire diameter, time constant, flux density, damper force at specified velocities and constraints on the geometry of the damper.

Rosenfield et al (2004), have presented a comparative study on the volume constrained optimization of MR and ER valve and dampers. In this work generalised candidate geometry of the MR valve has been chosen with the parameters as shown in Fig 2.12.

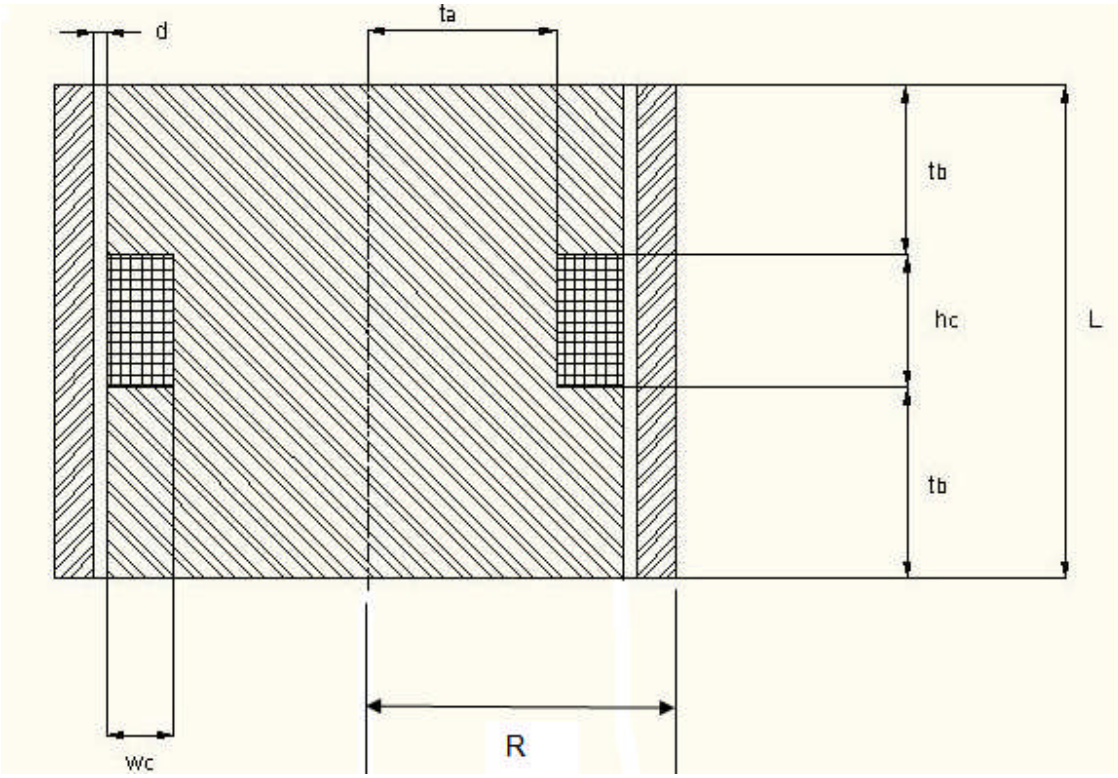

Fig 2.12 Generalised geometry for MR damper electromagnet (Rosenfield et.al,(2004)).

The generalised geometry has been defined by the following dimensions: radius of damper *R*, length of flow gap *L*, d gap between the two cylinders or the flow gap, bobbin core radius t_a, flange height t_b, gap width w_c and coil height h_c. The critical areas are defined as A_1 MR damper electromagnet core area, A_2 MR damper electromagnet cylinder wall cross section area, A_3 MR damper electromagnet cross section pole area. These areas are defined by the following equations:

$$A_1 = \pi t_a^2 \tag{2.16}$$

$$A_2 = \pi [\, R^2 - (t_a + w_c + d)^2 \,] \tag{2.17}$$

$$A_3 = 2\pi t_a t_b \qquad (2.18)$$

If (2.16) is equated to (2.17) and terms are rearranged in quadratic form for positive value of t_a then following equation is obtained:

$$t_a = \frac{1}{2}\left[-(w_c + d) + \sqrt{2R^2 - (w_c + d)^2}\right] \qquad (2.19)$$

The above conditions are imposed to obtained uniform cross sectional area and to ensure that the core does not saturate. Similarly if (2.16) is equated to (2.18) then the following equation is obtained:

$$t_b = \frac{1}{2} t_a \qquad (2.20)$$

The length of active coil and coil height are given by the following relations:

$$L_A = 2t_b \qquad (2.21)$$

$$h_c = L - 2t_b \qquad (2.22)$$

The paper by Rosenfield et.al (2004, optimises these parameters using the power density as the objective function. The power density is given by the following expression:

$$Power\,density = \frac{I_{ap}^2 R_w}{A_d L_A} \qquad (2.23)$$

I_{ap} is the applied current, R_w is the resistance of the coil and A_d is the cross sectional area of the flow annulus. The effect of variation of power density has been studied for variation of non dimensional plug thickness, damping coefficient for different number of wraps of coils. The

paper also presented the effect of variation of power densities for variation of plug thickness and damping coefficients for silicon steel and Hyperco alloy. Following the similar approach Batterbee et al (2007) present the modelling and performance prediction of optimal MR damper based aircraft landing gear (Batterbee (2007)). The proposed optimization strategy is based on the study of effect of variation of power required to generate maximum yield stress, time constant of the coil, the valve's control ratio (defined below) and Reynolds number through the valve:

$$\lambda = \frac{\Delta P_{max}(Q_{max,}\tau_{y\,max})}{\Delta P_0(Q_{max,}\tau_y = 0)} \qquad (\lambda > 1) \tag{2.24}$$

$$R_e = \frac{\rho Q}{\mu_{py} b} \tag{2.25}$$

In the above equation, ΔP_{max} is the maximum field pressure drop and ΔP_0 is the zero field pressure drop. Where ΔP_{max} is the maximum pressure field pressure drop and $\Delta Pmax$ is the zero field pressure drops. In Batterbee, (2007) the FEM based electromagnetic simulation is used to obtain the magnetic field developed by the electromagnet and that the core and MR fluid does not reach saturation limit.

Nguyen et al (2009) have proposed a new objective function which is the weighted sum of dynamic range, yield force and time constant of electromagnetic coil with the constraint that the sum of three weights is unity. The dynamic range and the yield force are based on the parallel plate approximation for the analytical model.

The review of the above literature on design methodology and optimal design strategy leads to the conclusion that the optimisation strategy can be further improved to achieve the

above objective by a suitable combination of performance parameters and the novel design of the damper which is based on improved analytical flow model.

2.6 Chapter Summary:

The literature review describes the various phenomenological model used for modelling the performance of a MR damper. The next section describes the analytical model and the need for a new for improved model prediction of damper performance. The literature review of optimization of MR damper design leads to the conclusion that new optimal strategy can be developed which improves the performance of MR damper.

Chapter 3

Modeling of Magnetorheological fluid based dampers at low speed

3.1 Introduction:

This chapter presents the transient model for the flow of MR fluid in an MR damper. The flow model is used to predict the damper force. The literature review in the previous chapter describes the quasi static model for predicting the MR damper force. The quasi steady solution of the Navier Stokes equations using either Bingham plastic model or Herschel Bulkley model for deriving the equations for the velocity of MR fluid flowing through the channel have been published by Phillips (1969), Kamath et al (1996), Lee and Wereley (1999), Norrsi and Ahmedian (2005), Facey and Rosenfeld (2005), Chooi and Oyadiji (2008), Wang and Gordaninejad (2007), Li (2000) etc. The equation of the velocity is used to obtain the equation for the conservation of volumetric flux and the equation for equilibrium of forces acting on the MR fluid flowing through the channel. Bingham plastic fluids are non Newtonian fluids that behave like a rigid body when the shear stress in the fluid channel is less than the yield stress and they flow with a constant shear rate when the shear stress exceeds the yield shear stress (Kamath et al (1996), Lee and Wereley (1999), Li (2000), Norrsi and Ahmedian (2005), Facey and Rosenfeld (2005), Wang and Gordaninejad (2007) and Chooi and Oyadiji (2008)). The equations for the shear stress in the fluid are given as (Stanway et al (1996), Wang and Gordaninejad (2007)):

$$\tau = (\tau_0 + k|\dot{\gamma}|^{n-1}\dot{\gamma})sign(\dot{\gamma}) \qquad |\tau| > \tau_0$$

$$\dot{\gamma} = 0 \qquad |\tau| \leq \tau_0$$

(3.1)

where τ is the shear stress; $\dot{\gamma}$ is the shear rate; and *k* and *n* are the fluid index parameters; τ_0 is the yield shear stress and is the function of applied magnetic field for MR fluids. The quasi steady MR fluid flow model based on Bingham plastic model was applied by Kamath et al (1996) and Chooi and Oyadiji (2008). However they reported that the model is not able to capture the hysteretic variation of force with the velocity of the damper. The Herschel Bulkley model was applied by Lee and Wereley (1999), Wang and Gordaninejad (2007) and Li (2000). In Eq 3.1 the yield shear stress is a function of magnetic field which is applied perpendicular to the flow path of the MR fluid. It was reported by Sims et al (2000), Batterbee et al (2007) and Wang and Gordaninejad (2007) that the hysteresis in the MR damper is due to the following primary reasons:

(1) Compressibility of the MR fluid. This is particularly important when a small amount of air is trapped in the fluid.
(2) Seal friction.

The inability of the fluid mechanical models for MR dampers to satisfactorily predict the force versus velocity relationship, has led researchers to prefer phenomenological models to quasi steady model (Chooi and Oyadiji (2008) and Cesmeci and Tehsin (2010), Ehrgott and Masri (1992), Gavin et al (1996) and Chang and Roschke (1998)).

The quasi steady flow model described in Chooi and Oyadiji (2008) , Cesmeci and Tehsin (2010), Ehrgott and Masri (1992), Gavin et al (1996) and Chang and Roschke (1998),

neglect the transient effects in modelling MR fluid flow through the channel. In an MR damper the magnetized flow channel can be of the following three types:

(1) Embedded in the piston.

(2) Annular gap between the piston and cylinder.

(3) Bypass duct which is surrounded by the electromagnetic coil.

The size and application of MR damper determines the choice of the design of channel from amongst above three types. For these three configurations the transient effects for the flow of MR fluid in an MR damper can be primarily due to the following reasons:

(1) Transients due to starting or stopping or change in the direction of fluid flow in a MR damper.

(2) If the MR fluid flow channel is either embedded in the piston or the channel is in the form of an annular gap between the piston and the cylinder, then there will be an additional transient effect in a MR damper due to the body force acting on the MR fluid due to the acceleration or deceleration of the piston.

For the design of MR dampers in which the MR fluid flow channels are either embedded in the piston or they are in the form of annular gaps between the piston and the cylinder, there will be a transient effect in the MR damper due to the time dependent variation of the velocity boundary condition. In all of the quasi steady models , Cesmeci and Tehsin (2010), Chooi and Oyadiji (2008), Choi et al (2002), Chang and Roschke (1998), Gavin et al (1996) and Ehrgott and Masri (1992), the velocity of the piston has been assumed to be constant during a given time step.

Therefore this work aims to present a transient model which includes all the above three transient effects so that the force versus velocity variation of MR damper can be satisfactorily predicted. The following sections deal with the modelling of magnetorheological fluid based

dampers using an analytical solution of the Navier Stokes equations. The work describes the model of an MR damper in which the flow channel is an annular gap between the piston and the cylinder. The generalised transient model proposed in this section considers the flow of MR fluid as a pressure driven Poiseuille flow superposed with Couette flow. The model can be used to analyse any of the above three types of channels of an MR damper with the modifications of boundary conditions. The technique used in this paper can also be used to analyse the unsteady flow of Newtonian fluids in a pipe due to sudden starting and stopping of flow (Das and Arakeri (1998)). In future the proposed approach can be used for developing fractional calculus based MR fluid models which may be more accurate. Many complex fluids such as polymer solutions, blood, paints and certain oil cannot be described by Newtonian constitutive equations with sufficient accuracy and so the fractional calculus has been found to be quite flexible in describing the viscoelastic behaviour, Fetecau et al (2005, 2006). The hydrodynamic motion of viscoelastic fluids has been studied using fractional calculus, to obtain closed form solutions, by a number of researchers such as Fetecau et al (2005, 2006), Hayat et al (2004-2006), Bagley (1983), Friedrich (1991), and Wang et al (2009). In the paper by Wang et al (2009), the unsteady axial Couette flow of fractional second grade fluid and fractional Maxwell fluid flow between two infinite cylinders has been presented.

3.2 Formulation of transient MR fluid flow model:

In this work the flow of MR fluid through the annulus between the piston and the cylinder can be considered to be a pressure driven Poiseuille flow superposed with the Couette flow. This is because the flow of MR fluid through the annulus is due the combined effect of the pressure gradient across the channel and the velocity of the piston. Thus, it is a case of a mixed mode damper. The computational domain and the enlarged view of the velocity profile for the flow of Mr fluid through the channel are given in Fig 3.1 and 3.2. The velocity profile of the MR fluid

flow through the annulus between the piston and the cylinder wall can be considered to be a plug flow between the inner and outer layers of laminar flow.

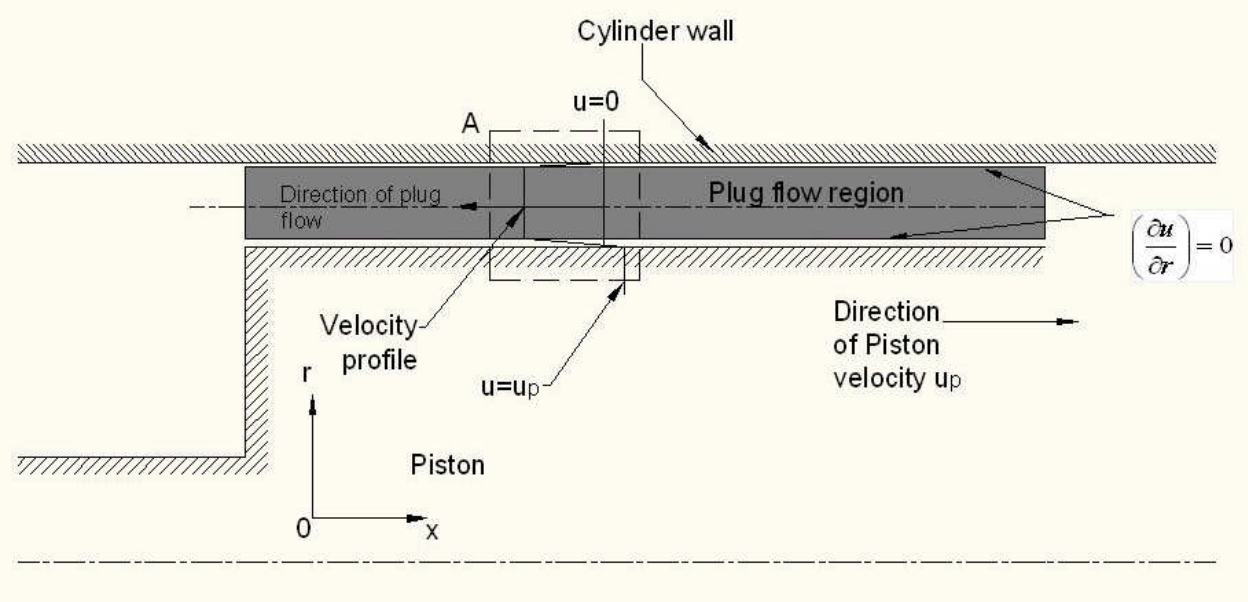

Fig 3.1 Axi-symmetric fluid domain and velocity profile for the flow of MR fluid.

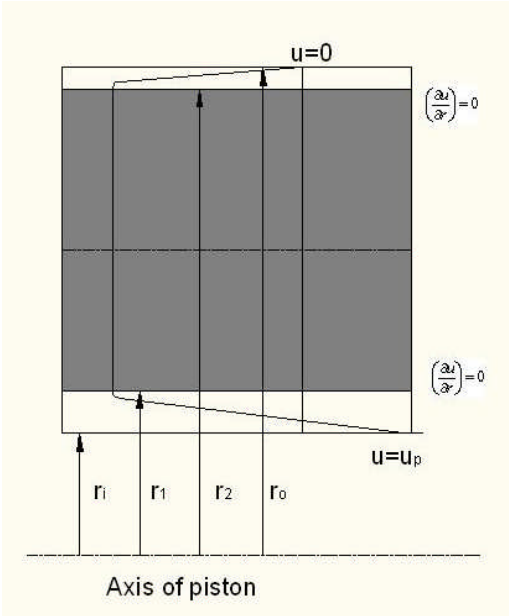

Fig 3.2 Enlarged view of frame A of Fig 1 showing the assumed velocity profile and plug flow region with the definition of radial coordinates.

The region of velocity profile, where the shear stress is equal to yield shear stress of the MR fluid, is a plug flow region. The regions where the shear stress exceeds the yield shear stress there is a laminar flow, Fig 3.1.

Before proceeding to the formulation it is necessary to outline the underlying assumptions with justifications for the applicability of the model. The assumptions for the model are as follows:

(1) The MR fluid that flows through the annulus is equal to the fluid displaced by the piston. The fluid displaced by the piston lies between the piston face and the cylinder head of the damper cylinder. In a case where the MR fluid lies between the damper piston and the floating piston of the gas spring, there is a possibility of flow of fluid through annulus due to velocity of the piston under negligible pressure gradient. This will be the case of a boundary driven flow. However, this case is kept out of the purview of this work.

(2) The operating Reynolds number (Re_a) is less than the critical Reynolds Number. The turbulent flow has been taken into account by using correction factors for the range of operation Reynolds number in Mao et al (2005). In this work the validity of the plug flow assumption is assessed based on the publications by Garg and Rouleau (1972), Frigaard et al (1994) and Nouar and Frigaard (2001). From these papers and the paper of Hedstrom (1952) it is gathered that the effect of yield stress is negligible for the turbulent flow of Bingham fluids. For a field controllable MR dampers the flow of MR fluid as a plug flow is necessary for maximising the controllability of the damper. The correction for the turbulent flow as suggested in Mao et al (2005) may require some careful considerations because the turbulent flow modelling of MR fluid

will require the interaction of magnetic field with the turbulent flow vortices, to be taken into account. In this paper it is considered that the operating Reynolds number is less than the critical Reynolds number. The critical Reynolds number is a function of Bingham number. The Bingham number is defined as follows:

$$Bi = \frac{\tau_{py} d}{\mu_{py} \overline{A} u_p} \qquad \text{(Mao et al (2005))} \qquad (3.2)$$

$$\overline{A} = \frac{r_i^2}{(r_o^2 - r_i^2)} \qquad (3.3)$$

where $\overline{A}$ is the ratio of piston area to the area of the annulus, u_p is the velocity of the piston, d is the width of the annulus, μ_{py} is the post yield viscosity and other symbols are defined in Fig 3.1 and 3.2. Similarly the operating Reynolds number is defined as follows:

$$\mathrm{Re}_a = \frac{2\rho \overline{A} u_p d}{\mu_{py}} \qquad (3.4)$$

In Eq(3.4) ρ is the density of MR fluid. The critical Reynolds number is given by the following correlations (Nouar and Frigaard (2001)):

$$\mathrm{Re}_c \approx \begin{cases} 1050Bi & Bi \le 0.4047 \\ 1701.39Bi^{0.538} & 0.4047 < Bi < 27.13 \\ 676Bi & 27.126 < Bi < 100 \end{cases} \qquad (3.5)$$

In this work the maximum width of the annulus has been taken as 1mm. This is because the operating Reynolds number tends to exceed the critical Reynolds number for more than 1mm width of the annulus. If the diameter of the piston is varied between 50 mm to 200 mm the corresponding area ratio will vary from

12.5 to 50 for 1mm width of the annulus. This can be considered as an acceptable range for all the applications described in the previous chapter. If the density of the MR fluid is taken as 3000 kg/m^3 and the post yield viscosity is taken as 0.18 Pa-s the variation of critical and operating Reynolds numbers with the piston speed are given in Fig 3.3.

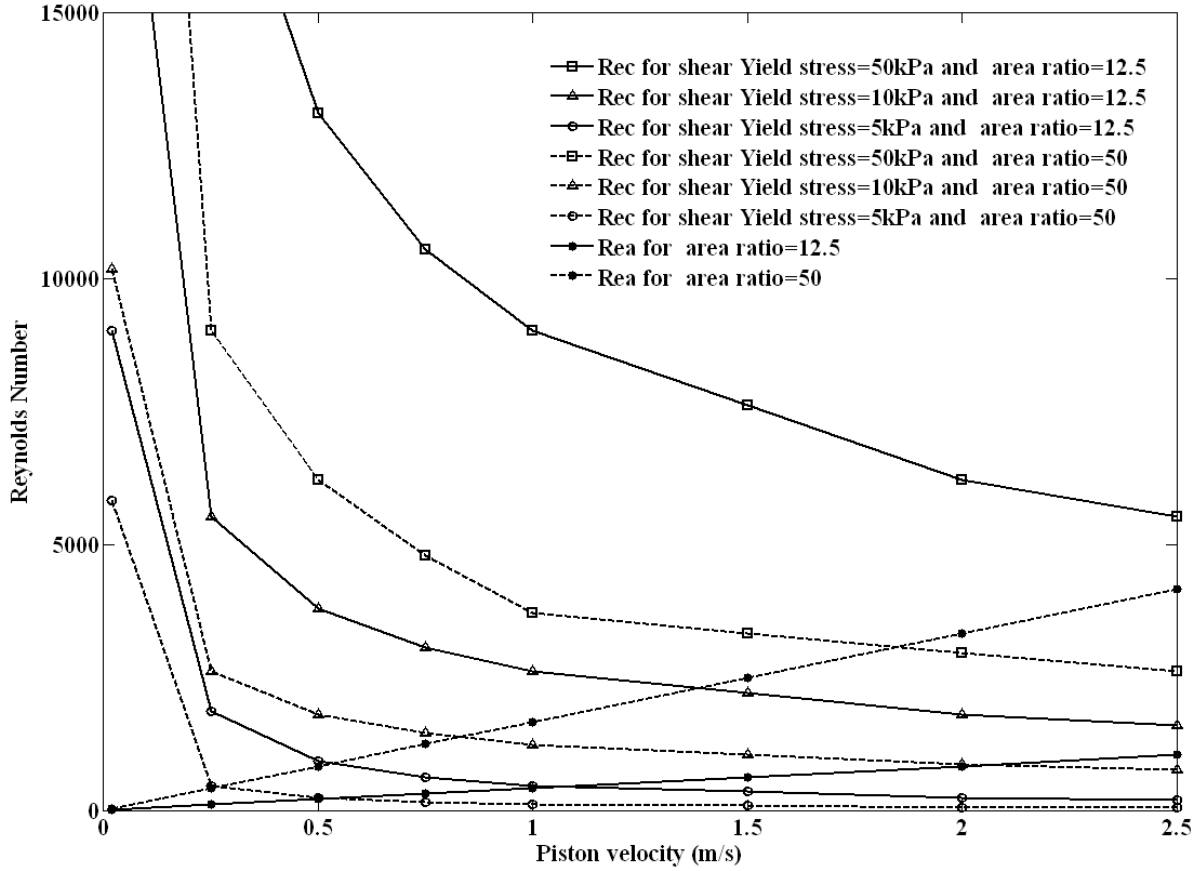

Fig 3.3 Variation of critical and operating Reynolds number for the flow of MR fluid through the annulus for MR dampers with area ratio of 12.5 and 50 respectively for the values of yield shear stress between 5 kPa to 50 kPa.

In the Fig 3.3 above, the values of yield shear stress have been taken as 50 to 5 kPa. This has been done to compare the operating Reynolds number with the

critical Reynolds number corresponding to the maximum and minimum values of yield shear stress for MR fluids. The value of shear stress of 5 kPa has been included as this corresponds to the maximum value of yield shear stress for ER fluids (Carlson et al (1996) and Carlson and Jolly (2000)). From the above figure it is observed that the critical Reynolds number reduces rapidly with the increase in the area ratio and the decrease in yield shear stress. At the area ratio of 50 the operating Reynolds number crosses the critical value at the piston velocity of 0.25 m/s for the yield shear stress of 5 kPa. On the other hand if the area ratio is 12.5 the operating Reynolds number just reaches the critical value at the piston velocity of 1m/s. For the area ratio of 50 there is a piston speed limitation for all the values of yield shear stress from 5 to 50 kPa. From the Fig 3.3 it is also deduced that the variation of critical Reynolds number, with velocity and area ratio, imposes limitation on the operational speed and size of ER dampers. This is because the yield shear stress of ER fluids varies between 1 to 5 kPa (Carlson et al (1996) and Carlson and Jolly (2000)). In the end, it is mentioned that the critical Reynolds numbers for the piston velocities less than 0.25 m/s, are much higher than the operating Reynolds numbers and so the flow through the annulus is plug flow.

(3) The ratio of flow path length to the piston diameter is at least equal to 0.8. This is necessary to ensure that the entrance length for the development of plug flow through the channel is small as compared to the flow path length. Thus the flow can be considered to be fully developed throughout the channel. If the entrance length for the development of flow is to be taken into account then the flow path length can be corrected by subtracting the entrance length. This will result

in a reduction in damper pressure proportional to the corrected flow path length. The correlations for the entrance length are given in Novak and Gajdeczko (1983) and Poole and Chhabra (2010). Since these correlations are based on theoretical models and the experimental verification has not been given therefore this assumption has been briefly discussed here and the attempt to incorporate the correction of pressure gradient for the entrance length effects has not been made.

(4) The effect of shear thinning is neglected. This is because of two reasons. The first reason is that the pressure gradient is a stronger function of yield shear stress as compared to the post yield viscosity at low shear rates. Secondly the effect of shear thinning can be finally accounted for by using a suitable correction factor for pressure gradient. Therefore, the constitutive model used in this work is given as follows:

$$\begin{aligned} \tau_{rx} &= (\tau_0 + \mu_{py}\dot{\gamma})sign(\dot{\gamma}) \qquad |\tau| > \tau_0 \\ \dot{\gamma} &= 0 \qquad\qquad\qquad\qquad\quad |\tau| \le \tau_0 \end{aligned} \tag{3.6}$$

(5) The yield shear stress of the MR fluid is constant during the given time step.

(6) The relationship between the yield shear stress and the magnetic field is given as follow:

$$\tau_{py} = 45000B^{1.5} \qquad \text{(Jiang et al (2011))} \tag{3.7}$$

In the above equation B is the applied magnetic field in T. Although the model presented in this work is valid for all the values of yield shear stress, the results for the simulation are given for yield shear stress between 10-40 kPa. Wherever

a different function for the yield shears stress will be used the equation for relating yield shear stress with the applied magnetic field will be given.

(7) The body force arising due to the acceleration or deceleration of the fluid domain due to the force acting on the piston, has been assumed derivable from the potential and so it will be combined with the pressure gradient in the governing differential equation (Lipscomb and Denn (1984)).

(8) The governing differential equation will be applied to the sheared domain only. This is the underlying assumption for all the quasi static models (Kamath et al (1996), Lee and Wereley (1999), Li (2000), Norrsi and Ahmedian (2005), Facey and Rosenfeld (2005), Wang and Gordaninejad (2007) and Chooi and Oyadiji (2008)). It is because of this assumption that the governing differential equation is linear. If the pre-yield domain is included in the formulation the governing differential equation will become non linear and it cannot be solved in the way it has been solved for quasi static model. Therefore the boundary conditions that will be applied will correspond to the boundary coordinates within the sheared sub-domain only. In Wang and Gordninejad (2007) the constant for the solution of the differential equation has been obtained by using the coordinate of the plug flow domain. This has not been done in this work so as to maintain the validity of linear differential equation. In this work the sheared sub-domain boundary is at '$\delta r \rightarrow 0$' distance from the plug flow boundary. This is also the basis for the analytical solution for the Navier Stokes equation for the Maxwell fractional grade fluids by Xu and Tan (2001), Friedrich (1991), Fetecau et al (2005, 2006), Hayat et al (2004-2006), Bagley (1983) and Wang et al (2009). In Xu and Tan (2001) this assumption is applied

to use the Duhamel's superposition principle for the transient boundary conditions.

The continuity and Navier Stokes equations are given as follows (Kleinstreuer (1997)):

Continuity equation:

$$\frac{1}{r}\frac{\partial(ru_r)}{\partial r}+\frac{1}{r}\frac{\partial(u_\theta)}{\partial \theta}+\frac{\partial(u_x)}{\partial x}=0 \tag{3.8}$$

r- component of the incompressible Navier Stokes equation:

$$\rho\left(\frac{\partial u_r}{\partial t}+u_r\frac{\partial u_r}{\partial r}+\frac{u_\theta}{r}\frac{\partial u_r}{\partial \theta}-\frac{u_\theta^2}{r}+u_x\frac{\partial u_r}{\partial x}\right)=-\frac{\partial p}{\partial r}+\rho a_r$$
$$+\left[\frac{1}{r}\frac{\partial}{\partial r}(r\tau_{rr})+\frac{1}{r}\left(\frac{\partial \tau_{r\theta}}{\partial \theta}\right)+\frac{\partial \tau_{xr}}{\partial x}-\frac{\tau_{\theta\theta}}{r}\right] \tag{3.9}$$

θ- component of the incompressible Navier Stokes equation:

$$\rho\left(\frac{\partial u_\theta}{\partial t}+u_r\frac{\partial u_\theta}{\partial r}+\frac{u_\theta}{r}\frac{\partial u_\theta}{\partial \theta}+\frac{u_r u_\theta}{r}+u_x\frac{\partial u_\theta}{\partial x}\right)=-\frac{\partial p}{r\partial \theta}+\rho\, a_\theta$$
$$+\left[\frac{1}{r^2}\frac{\partial(r^2\tau_{r\theta})}{\partial r}+\frac{1}{r}\frac{\partial(\tau_{\theta\theta})}{\partial \theta}+\frac{\partial(\tau_{x\theta})}{\partial x}-\frac{\tau_{\theta r}-\tau_{r\theta}}{r}\right] \tag{3.10}$$

x- component of the incompressible Navier Stokes equation:

$$\rho\left(\frac{\partial u_x}{\partial t}+u_r\frac{\partial u_x}{\partial r}+\frac{u_\theta}{r}\frac{\partial u_x}{\partial \theta}+\frac{u_r u_\theta}{r}+u_x\frac{\partial u_x}{\partial x}\right)=-\frac{\partial p}{\partial x}+\rho a_x$$
$$+\left[\frac{1}{r}\frac{\partial(r\tau_{rx})}{\partial r}+\frac{1}{r}\frac{\partial \tau_{\theta x}}{\partial \theta}+\frac{\partial \tau_{xx}}{\partial x}\right] \tag{3.11}$$

In the above Navier Stokes equations *u* is the velocity and subscript associated with the velocity denotes the direction of the velocity. Similarly τ is the shear stress and the first letter in the

subscript denotes the direction of the normal to the plane on which the shear stress is acting and the second letter in the subscript denotes the direction of stress. The symbol a is the acceleration of the domain and the subscript denotes the direction of acceleration, p is the pressure, ρ is the density and t is time. Since the component of velocity in the radial and θ direction, τ_{rr} , $\tau_{r\theta}$, $\tau_{\theta\theta}$, $\tau_{x\theta}$, $\tau_{\theta x}$, τ_{xx} , a_r , a_θ and the derivatives of pressure with respect to r and θ are zero therefore Eq 3.9 and 3.10 are identically satisfied. The Navier Stokes equation in the x direction can be modified in the following manner:

$$\rho\left(\frac{\partial u_x}{\partial t}+\overbrace{u_r\frac{\partial u_x}{\partial r}}^{=0\,\because\,u_r=0}+\overbrace{\frac{u_\theta}{r}\frac{\partial u_x}{\partial\theta}}^{=0\,\because u_\theta=0}+\overbrace{\frac{u_r u_\theta}{r}}^{=0\,\because\,u_r=u_\theta=0}+\overbrace{u_x\frac{\partial u_x}{\partial x}}^{=0\,\because\,\frac{\partial u_x}{\partial x}=0}\right)=-\overbrace{\left(\frac{\partial p}{\partial x}+\overbrace{\rho a_x}^{body\ force\ due\ to\ piston\ \ acceleration}\right)}^{refer\ assumption\ (7)}$$

$$+\left[\frac{1}{r}\frac{\partial(r\tau_{rx})}{\partial r}+\overbrace{\frac{1}{r}\frac{\partial\tau_{\theta x}}{\partial\theta}}^{=0}+\overbrace{\frac{\partial\tau_{xx}}{\partial x}}^{=0}\right]$$

(3.12)

Therefore, the governing differential equation for the computational domain is shown in Fig 3.1 and 3.2 is given as follows:

$$\rho\left(\frac{\partial u_x}{\partial t}\right)=-\left(\frac{\partial p}{\partial x}+\rho a_p\right)+\left[\frac{1}{r}\frac{\partial}{\partial r}(r\tau_{rx})\right]$$

(3.13)

In the above equation p is the pressure, a_p is the acceleration of the piston and all the other symbols have been defined previously. In order to obtain the analytical solution of the governing differential equation with the above mentioned boundary conditions, the partial

differential equation is required to be converted into an ordinary differential equation using Laplace transform.

The Laplace transform and its inverse are defined as follows:

$$\bar{u}_z(r,s) = \mathscr{L}(u_z(r,t),s) = \int_0^{\infty} u_z(r,t)e^{-st}dt, \tag{3.14}$$

$$u_z(r,t) = \mathscr{L}^{-1}(\bar{u}_z(r,s),t) = \frac{1}{2\pi\iota}\int_{\sigma-\iota\infty}^{\sigma+\iota\infty} \bar{u}_z(r,s)e^{-st}ds \tag{3.15}$$

If the constitutive Eq (3.6) is substituted in the governing differential Eq (3.12) and the Laplace transform is applied, the Eq (3.12) gets transformed to the following form:

$$\frac{\partial^2 \bar{u}_z}{\partial r^2} + \frac{1}{r}\frac{\partial \bar{u}_z}{\partial r} - \frac{s}{\nu}\bar{u}_z = \frac{1}{s}\left(-\frac{1}{\mu_{py}}\left(\frac{\partial p}{\partial x} + \rho a_p\right) + \frac{\tau_0}{r\mu_{py}}\right) \tag{3.16}$$

The above equation is a non-homogenous Bessel's differential equation and the solution of the above differential equation is obtained using Weber transform (Xu and Tan (2001), and Tan et al (2003)). The Weber transform and its inverse for the velocity are defined as follows:

$$\tilde{\bar{u}}_x(\alpha_n, s) = \int_{r_i}^{r_1} r\,\bar{u}_x(r,s)\varphi(\alpha_n, r)\,dr \tag{3.17}$$

$$\bar{u}_x(r,s) = \sum_{n=0}^{\infty} \tilde{\bar{u}}_x(\alpha_n, s)\frac{\varphi(\alpha_n, r)}{N(\alpha_n)} \tag{3.18}$$

Where φ is the kernel function and N is the normalization function. The kernel and normalisation functions are defined depending on the boundary conditions in the following manner, Ozisik (1980) (see Fig 3.2 for the definition of radial coordinates):

In the Fig 3.2 above r_i is the inner radius of the annular gap and is equal to the damper piston diameter, r_1 is the radius of the inner boundary of the plug flow region of the velocity profile, r_2 is the radius of the outer boundary of the plug flow region of the velocity profile and r_o is the outer radius of the annular gap and is equal to the bore of the cylinder.

Boundary conditions:

Set (1)

$u_x = u_p$ at $r=r_i$ and

$\frac{\partial u_x}{\partial r} = 0$ at $r = r_1$

$$\varphi(\alpha_n, r) = J_0(\alpha_n r) Y_0'(\alpha_n r_1) - J_0'(\alpha_n r_1) Y_0(\alpha_n r) \tag{3.19}$$

$$\frac{1}{N(\alpha_n)} = \frac{\pi^2}{2} \frac{\alpha_n^2 J_0^2(\alpha_n r_i)}{\left[J_0^2(\alpha_n r_i) - J_0^2(\alpha_n r_1)\right]} \tag{3.20}$$

The characteristic equation is given as follows:

$$J_0(\alpha_n r_i) Y_0'(\alpha_n r_1) - J_0'(\alpha_n r_1) Y_0(\alpha_n r_i) = 0 \tag{3.21}$$

Set (2)

$\frac{\partial u_x}{\partial r} = 0$ at $r = r_2$

$u_x=0$ at $r=r_o$ and

$$\varphi(\alpha_n, r) = J_0(\alpha_n r) Y_0(\alpha_n r_o) - J_0(\alpha_n r_o) Y_0(\alpha_n r) \tag{3.22}$$

$$\frac{1}{N(\alpha_n)} = \frac{\pi^2}{2} \frac{\alpha_n^2 J'^2_0(\alpha_n r_o)}{\left[J'^2_0(\alpha_n r_o) - J_0^2(\alpha_n r_2) \right]} \tag{3.23}$$

$$J'_0(\alpha_n r_2) Y_0(\alpha_n r_o) - J_0(\alpha_n r_o) Y'_0(\alpha_n r_2) = 0 \tag{3.24}$$

The solution of above mentioned equation is obtained in terms of zero[th] order Bessel's functions and as such the Weber transform will use the zero[th] order Bessel's functions for the kernel function. The Weber transform for the Eq 3.16 together with the boundary conditions Eq 3.19-3.21 for the region between r_i and r_1 gives the following equation:

$$\tilde{\bar{u}}_x = \frac{-2}{\pi} \frac{\nu}{s\left(s + \nu \alpha_{n_i}^2\right)} \frac{J'_0(\alpha_{ni} r_1)}{J_0\left(\alpha_{ni} r_i\right)} - \frac{\nu}{\alpha_{n_i}} \frac{1}{s\left(s + \nu \alpha_{n_i}^2\right)} \left(\frac{\partial p}{\partial x} + \rho a_p \right) \frac{1}{\mu} \xi_1 + \frac{\nu}{s\left(s + \nu \alpha_{n_i}^2\right)} \tau_{py} \frac{1}{\mu} \chi \tag{3.25}$$

The inverse Weber transform followed by inverse Laplace transform gives the following solution:

$$u_x = \sum_{n=1}^{\infty} \left(\begin{array}{l} \dfrac{\pi u_p e^{-\nu \alpha_n^2 t}}{\alpha_{n_i}} \cdot \dfrac{J'_0(\alpha_{n_i} r_1) J_0(\alpha_{n_i} r_i)}{\left(J_0^2(\alpha_{n_i} r_i) - J'^2_0(\alpha_{n_i} r_1) \right)} \varphi_1 - \dfrac{\pi^2}{2} \left(\dfrac{\partial p}{\partial x} + \rho a_p \right) \dfrac{e^{-\nu \alpha_{n_0}^2 t}}{\alpha_{n_i} \mu} \dfrac{J_0^2(\alpha_{n_i} r_{i)}}{\left(J_0^2(\alpha_{n_i} r_i) - J'^2_o(\alpha_{n_i} r_1) \right)} \varphi_1 \xi_1 \\ \\ + \dfrac{\pi^2}{2} \dfrac{\tau_{py} e^{-\nu \alpha_{n_i}^2 t}}{\alpha_{n_i} \mu} \dfrac{J_0^2(\alpha_{ni} r_{i)}}{\left(J_0^2(\alpha_{n_i} r_i) - J'^2_o(\alpha_{n_i} r_1) \right)} \varphi_1 \chi_i \end{array} \right)$$
$$+ u_p - \frac{\tau_{py}}{\mu} \left(r - r_i - r_1 \ln\left(\frac{r}{r_i} \right) \right) + \frac{1}{4\mu} \left(\frac{\partial p}{\partial x} + \rho a_p \right) \left(r^2 - r_i^2 - 2 r_1^2 \ln\left(\frac{r}{r_i} \right) \right) \tag{3.26}$$

The symbols in the above equation are defined as follows:

$$\varphi_1 = \left(J_0(\alpha_{n_i} r) Y_0'(\alpha_{n_i} r_1) - J_0'(\alpha_{n_i} r_1) Y_0(\alpha_{n_i} r)\right) \tag{3.27}$$

$$\xi_1 = \left\{\left(r_1 J_1(\alpha_{n_i} r_1) - r_i J_1(r_i \alpha_{n_i})\right) Y_0'(\alpha_{n_i} r_1) - \left(r_1 Y_1(\alpha_{n_i} r_1) - r_i Y_1(r_i \alpha_{n_i})\right) J_0'(\alpha_{n_i} r_1)\right\} \tag{3.28}$$

$$\chi_i = \left\{ \begin{array}{l} \left(r_1 \, {}_1F_2\left(\frac{1}{2}; 1, \frac{3}{2}; -\frac{1}{4}\alpha_{n_i}^2 r_1^2\right) - r_i \, {}_1F_2\left(\frac{1}{2}; 1, \frac{3}{2}; -\frac{1}{4}\alpha_{n_i}^2 r_i^2\right)\right) Y_0'(\alpha_{n_i} r_1) - \\ \left(\frac{\pi}{2} r_1 \left(H_{-1}(\alpha_{n_i} r_1) Y_0(\alpha_{n_i} r_1) + H_0(\alpha_{n_i} r_1) Y_1(\alpha_{n_i} r_1)\right) \right. \\ \left. - \frac{\pi}{2} r_i \left(H_{-1}(\alpha_{n_i} r_i) Y_0(\alpha_{n_i} r_i) + H_0(\alpha_{n_i} r_i) Y_1(\alpha_{n_i} r_i)\right) \right) J_0'(\alpha_0 r_1) \end{array} \right\}$$

(3.29)

Using similar procedure, the solution for the fluid region between the plug flow boundary and the outer wall i.e. $r_2 \le r \le r_o$, is given as follows:

$$u_x = \sum_{n=1}^{\infty} \left(\begin{array}{l} -\frac{\pi^2}{2}\left(\frac{\partial p}{\partial x} + \rho a_p\right) \frac{e^{-\nu \alpha_{n_o}^2 t}}{\alpha_{n_o} \mu} \frac{J_0'^2(\alpha_{n_o} r_2)}{\left(J_0'^2(\alpha_{n_o} r_2) - J_o^2(\alpha_{n_o} r_o)\right)} \varphi_2 \xi_2 \\ \\ +\frac{\pi^2}{2} \frac{\tau_{py} e^{-\nu \alpha_{n_o}^2 t}}{\alpha_{n_o} \mu} \frac{J_0'^2(\alpha_{n_o} r_2)}{\left(J_0'^2(\alpha_{n_o} r_2) - J_o^2(\alpha_{n_o} r_o)\right)} \varphi_2 \chi_o \end{array} \right)$$
$$- \frac{\tau_{py}}{\mu}\left(r - r_o - r_2 \ln\left(\frac{r}{r_o}\right)\right) + \frac{1}{4\mu}\left(\frac{\partial p}{\partial x} + \rho a_p\right)\left(r^2 - r_o^2 - 2 r_2^2 \ln\left(\frac{r}{r_o}\right)\right)$$

(3.30)

$$\varphi_2 = \left(J_0(\alpha_{n_o} r) Y_0(\alpha_{n_o} r_o) - J_0(\alpha_{n_o} r_o) Y_0(\alpha_{n_o} r)\right) \tag{3.31}$$

$$\xi_2 = \left\{\left(r_o J_1(\alpha_{n_o} r_o) - r_2 J_1(r_2 \alpha_{n_o})\right) Y_0(\alpha_{n_o} r_o) - \left(r_o Y_1(\alpha_{n_o} r_o) - r_2 Y_1(r_2 \alpha_{n_o})\right) J_0(\alpha_{n_o} r_o)\right\}$$

(3.32)

$$\chi_o = \left\{ \begin{array}{l} \left(r_o \ {}_1F_2\left(\frac{1}{2}; 1, \frac{3}{2}; -\frac{1}{4}\alpha_{no}^2 r_o^2\right) - r_2 \ {}_1F_2\left(\frac{1}{2}; 1, \frac{3}{2}; -\frac{1}{4}\alpha_{n_o}^2 r_2^2\right)\right) Y_0(\alpha_{no} r_o) - \\ \left(\begin{array}{l} \frac{\pi}{2} r_o \left(H_{-1}(\alpha_{n_o} r_o) Y_0(\alpha_{n_o} r_o) + H_0(\alpha_{n_o} r_o) Y_1(\alpha_{n_o} r_o)\right) \\ -\frac{\pi}{2} r_2 \left(H_{-1}(\alpha_{n_o} r_2) Y_0(\alpha_{n_o} r_2) + H_0(\alpha_{n_o} r_2) Y_1(\alpha_{no} r_2)\right) \end{array} \right) J_0(\alpha_o r_o) \end{array} \right\}$$

(3.33)

In the above equations the ${}_1F_2$ is the hypergeometic function, H_0 and H_{-1} are the Struve functions and all other terms and symbols have been defined previously. The above solution is true for steady state wall boundary condition for the piston velocity.

In case of an accelerating or decelerating piston, the piston velocity varies with time. The variation of piston velocity with time can be taken into account by superposition of the function for the variation of piston velocity using Duhamel's principle (Xu et al (2001)). The Duhamel's superposition principle (Xu et al (2001)) is applicable because the governing differential equations are linear.

$$u_x = \int_0^t u_x(r, \tau_1) f'(t - \tau_1).d\tau_1 + f(0) u_x(r, t) \qquad (3.34)$$

In the above equation f is the time function for the time varying boundary condition and the τ_1 is the variable for time for the given time step. To show the application of Duhamel's superposition principle the following velocity function is used:

$$u_p = u_{p0} \sin(\omega(t + t_0)) \qquad (3.35)$$

where u_p is the piston velocity, u_{p0} is the peak piston velocity, ω is the angular velocity, t is the time for the given time step and t_0 is the time from the beginning of the damper stoke to beginning of the given time step. From the Eq (3.34) it can be seen that the *f(0)* is the initial condition at the beginning of the time step, (Ozisik (1980, pp 199-200)).

Using the above velocity function Eq 3.26 will have following modified form

$$u_x = \sum_{n_i=1}^{\infty} \gamma_i \left(\begin{array}{l} \dfrac{\pi u_p e^{-\nu \alpha_{n_i}^2 t}}{\alpha_{n_i}} \cdot \dfrac{J_0'(\alpha_{n_i} r_1) J_0(\alpha_{n_i} r_i)}{\left(J_0^2(\alpha_{n_i} r_i) - J_0'^2(\alpha_{n_i} r_1)\right)} \varphi_1 - \dfrac{\pi^2}{2}\left(\dfrac{\partial p}{\partial x} + \rho a_p\right) \dfrac{e^{-\nu \alpha_{n_i}^2 t}}{\alpha_{n_i} \mu} \dfrac{J_0^2(\alpha_{n_i} r_{i)}}{\left(J_0^2(\alpha_{n_i} r_i) - J_o'^2(\alpha_{n_i} r_1)\right)} \varphi_1 \xi_1 \\ \\ + \dfrac{\pi^2}{2} \dfrac{\tau_{py} e^{-\nu \alpha_{n_i}^2 t}}{\alpha_{n_i} \mu} \dfrac{J_0^2(\alpha_{ni} r_{i)}}{\left(J_0^2(\alpha_{n_i} r_i) - J_o'^2(\alpha_{n_i} r_1)\right)} \varphi_1 \chi_i \end{array} \right)$$
$$+ \left(u_{p0} - \frac{\tau_{py}}{\mu}\left(r - r_i - r_1 \ln\left(\frac{r}{r_i}\right)\right) + \frac{1}{4\mu}\left(\frac{\partial p}{\partial x} + \rho a_p\right)\left(r^2 - r_i^2 - 2 r_1^2 \ln\left(\frac{r}{r_i}\right)\right)\right) \gamma_i' \qquad (3.36)$$

Where,

$$\gamma_i = \left(\frac{\omega}{\left(1 + \dfrac{\omega^2}{\left(\nu \alpha_{n_i}^2\right)^2}\right)\left(\nu \alpha_{n_i}^2\right)} \right) (-\cos(\omega t + \omega t_0) + \cos(\omega t_0)) - \left(\frac{\omega^2}{1 + \left(\dfrac{\omega}{\nu \alpha_{n_i}^2}\right)^2} \right) \frac{1}{\left(\nu \alpha_{n_i}^2\right)} (\sin(\omega t + \omega t_0) - \sin(\omega t_0)) \qquad (3.37)$$

$$\gamma_i' = (\sin(\omega t + \omega t_0) - \sin(\omega t_0)) \qquad (3.38)$$

In a practical situation the Duhamel's superposition cannot be applied directly, because the velocity function may not be known. However this situation can be dealt by using a Fourier series based extrapolation of the velocity function. This procedure will require the solution of the equation of motion for the spring mass damper system using the damper force predicted by the constant piston velocity solution. This is followed by the correction of force using the

constant velocity solution and Duhamel's superposition of velocity function obtained by applying Fourier series representation to the velocity time history of the previous time steps. The set of nonlinear equation obtained after applying Duhamel's superposition principle, are required to be solved in the same manner as outlined in section 3.3 to obtain the solution vector consisting plug flow boundary radial coordinates and pressure gradient for each time step. The pressure gradient can be used to obtain the damper force. This damper force is used in the equation of motion for calculating the corrected piston velocity. The above steps are iterated till the solution converges for a given time step. The equations outlined above are complex and the simplification has not been suggested due to following reasons:

(1) The body forces and the transients during the starting and stopping of an MR damper are likely to be significant and therefore the application of above model is justified.
(2) The solution developed in this section should form the basis for modelling the MR dampers for high speed applications.
(3) The use of symbolic math toolbox makes the above complexity affordable.

3.3 Solution for the transient MR fluid flow model:

The solution of Navier Stokes equations obtained in the previous section pertains to the variation of velocity in the regions between the wall and the plug flow boundaries. As such in the equations for the velocity profile there are three unknowns which are required to be determined to obtain the velocity profile for the region of MR fluid which is flowing under the influence of magnetic field. These three unknowns are r_1, r_2 and the pressure gradient for a known value of piston velocity. The piston velocity will be given as an input from the solution of spring mass damper system model for any given iterative step. From Fig 3.1& 3.2 it can be seen that the plug flows with a uniform velocity. This implies that the velocity of plug at its inner boundary r_1 is equal to the velocity of the plug at its outer boundary r_2. Therefore, using

Eq 3.26 and 3.30 the equation for the condition of zero velocity gradient across the plug is given as:

$$f_1 = u_x\big|_{r=r_1} - u_x\big|_{r=r_o} = 0 \tag{3.38}$$

The second equation is obtained by considering the conservation of volumetric flux. Therefore, the second equation is given as follows:

$$f_2 = \underbrace{\int_{r_i}^{r_1} 2\pi\, r\, u_x dr}_{(1)} + \underbrace{\pi(r_2^2 - r_1^2)u_x\big|_{r=r_1}}_{(2)} + \underbrace{\int_{r_2}^{r_o} 2\pi\, r\, u_x dr}_{(3)} - \pi r_i^2 u_p = 0 \tag{3.39}$$

The first term in the above equation represents the flow rate in the flow domain between the radius r_i to r_1 , the second term represents the flow rate through the plug flow region, the third term represents the flow through the fluid domain between r_2 and r_o and the last term is the rate of fluid displaced by the piston. If the compressibility of MR fluid is taken into account the Eq3.39 gets modified into following form (Sims et al (1999), Sims et al (2000), Batterbee et al (2007), Wang and Gordaninejad (2007)):

$$f_2 = \underbrace{\int_{r_i}^{r_1} 2\pi\, r\, u_x dr}_{(1)} + \underbrace{\pi(r_2^2 - r_1^2)u_x\big|_{r=r_1}}_{(2)} + \underbrace{\int_{r_2}^{r_o} 2\pi\, r\, u_x dr}_{(3)} - (\pi r_i^2 u_p - \dot{q}) = 0 \tag{3.40}$$

$$\dot{q} = \frac{l\dfrac{d}{dt}\left(\dfrac{dp}{dx}\right)}{\dfrac{\beta}{\pi\, r_i^2}\left(\dfrac{1}{(L_1 - x_p)} + \dfrac{1}{(L_2 + x_p)}\right)} \tag{3.41}$$

For a sufficiently small time step the above equation can be written in the following finite difference form:

$$\dot{q} = \frac{l\left(\left(\frac{dp}{dx}\right)_i - \left(\frac{dp}{dx}\right)_{i-1}\right)}{\frac{\beta\,\Delta t}{\pi\, r_i^2}\left(\frac{1}{(L_1 - x_p)} + \frac{1}{(L_2 + x_p)}\right)} \qquad (3.42)$$

where $\dot{q}$ is the rate of change of volume with time due to compressibility, β is the Bulk modulus, $\left(\frac{dp}{dx}\right)$ is the pressure gradient, l is the length of flow path, i is the current time step, *(i-1)* is the previous time step, Δt is the time step, x_p is the piston stroke, L_1 is the chamber length of the damper in front of the piston at the beginning of the stroke and L_2 is the chamber length of the damper on the rear side of the piston at the beginning of the stroke(ref Fig 3.4).

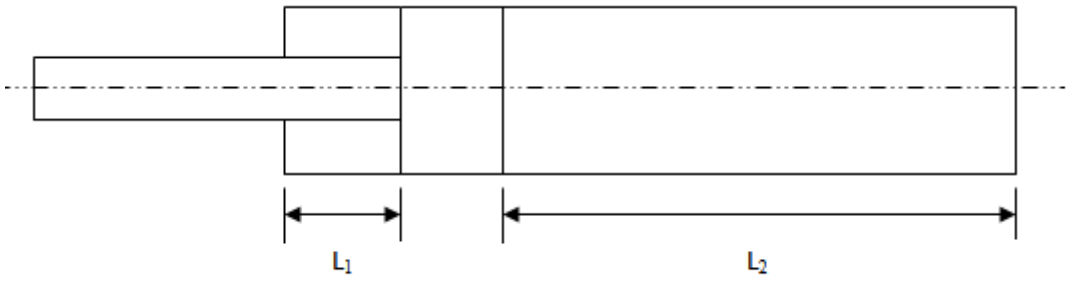

Fig 3.4 Schematic of MR damper showing initial chamber length L_1 and L_2.

The third equation is obtained by considering the equilibrium of forces in the plug flow region. Since the flow of the MR fluid is a transient flow, so there will be an inertia force acting in the plug flow region due to the change in velocity with time. Here, it is mentioned that Fig 3.5 is not a free body diagram and as such the inertia force has been shown for the visualisation purpose.

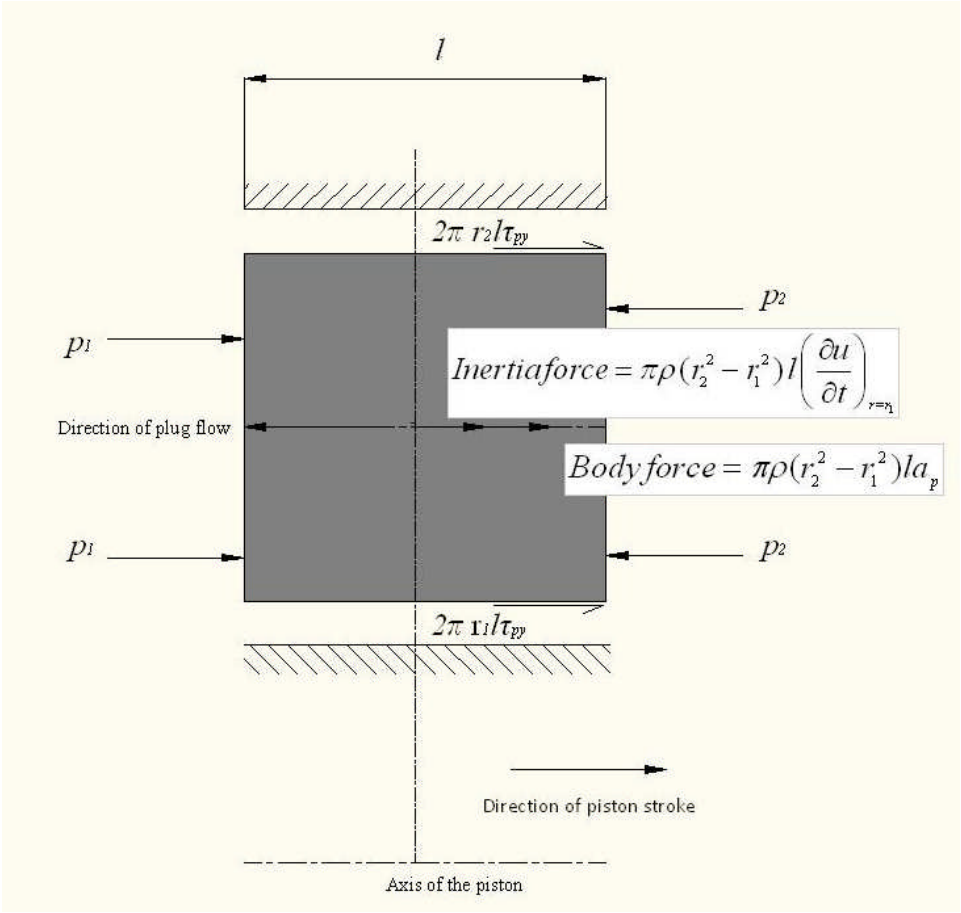

Fig 3.5 Equilibrium of forces in the plug flow region.

Therefore the equation for the equilibrium of forces is given as follows:

$$f_3 = 2\tau_{py} - \left(\frac{\partial p}{\partial x} - \rho a_p\right)(r_2 - r_1) + (r_2 - r_1)\rho \frac{\partial u_x}{\partial t}\bigg|_{r=r_1} = 0 \qquad (3.43)$$

In the above equation the first term is the force per unit area due to shear stress τ_0, the second term is the force per unit area due to the pressure gradient and the body force and the third term is the inertia force per unit area. In the quasi static flow models, given in Chooi and Oyadiji (2008) and Cesmeci and Tehsin (2010), Ehrgott et al (1992), Gavin et al (1996,) and Chang et al (1998), the inertia term is not included in the equilibrium equation. This model

considers that the change in velocity of the MR damper will result in an inertia force on the plug flow. The Eq 3.38-3.40 form a system of simultaneous nonlinear algebraic equations which have can be solved by Newton Raphson method.

For ensuring the convergence of the above algorithm the problem was transformed into a minimisation problem such that each equation achieves a minimum value close to zero under the following constraints:

$$\begin{aligned} &r_i < r_1, \\ &r_i \le r_1 \le (r_o + r_i)/2.0, \\ &(r_o + r_i)/2.0 \le r_2 \le r_o \end{aligned} \qquad (3.44)$$

The trials for the above methods were done using MATLAB toolbox as well as indigenously developed codes for Newton Raphson method, secant method and Broyden method. The trial evaluation led to the conclusion that Newton Raphson method gives the best performance in terms of stability and speed of convergence (see Dahlquist (1974, ch 6-12), for definition of accuracy). In this problem the roots of the characteristic equation for both the regions of the laminar velocity profile are also required to be determined for each iterative step. For finding the zeros of Bessel's characteristic equations the Descartes' method is used to detect the change in sign of the equation followed by Newton Raphson's method.

The Newton Raphson's method for the system of nonlinear equation is given by the following equation:

$$\mathbf{x_{i+1}} = \mathbf{x_i} + \mathbf{J^{-1}f_i} \qquad (3.45)$$

where, $\boldsymbol{f_i}$ is the function vector which has components represented by Eq 3.38, 3.40 and 3.43, $\boldsymbol{J}$ is the Jacobean matrix described below and $\boldsymbol{x}_i$ is the solution vector consisting of r_1,r_2 and $\frac{\partial p}{\partial x}$ as described below:

$$\mathbf{J} = \begin{bmatrix} \frac{\partial f_1}{\partial r_1} & \frac{\partial f_1}{\partial r_2} & \frac{\partial f_1}{\partial\left(\frac{\partial p}{\partial x}\right)} \\ \frac{\partial f_2}{\partial r_1} & \frac{\partial f_2}{\partial r_2} & \frac{\partial f_2}{\partial\left(\frac{\partial p}{\partial x}\right)} \\ \frac{\partial f_3}{\partial r_1} & \frac{\partial f_3}{\partial r_2} & \frac{\partial f_3}{\partial\left(\frac{\partial p}{\partial x}\right)} \end{bmatrix},$$

$$\mathbf{x_i} = \begin{pmatrix} r_1 \\ r_2 \\ \frac{\partial p}{\partial x} \end{pmatrix}_i$$

The algorithm for obtaining the solution vector is given as follows:

(1) Set an initial value of $\boldsymbol{x}_i$ which is compliant with the constraints Eq 3.44.

(2) Calculate at least the first 20 the roots of the following characteristic equations:

$$\varphi_1\big|_{r=r_1} = 0 \qquad (3.46)$$

$$\varphi_2\big|_{r=r_2} = 0 \qquad (3.47)$$

(3) Calculate $\boldsymbol{x}_{i+1.}$

(4) If all the elements of the function vector at $\boldsymbol{f}_{i+1}$ are less than the convergence criteria then $\boldsymbol{x}_{i+1}$ is the solution vector and the iteration is stopped.

(5) Else, set $x_i = x_{i+1}$ and repeat the steps 1-5 till the convergence is achieved.

The model described above is the direct model of a MR damper which is used to simulate the pressure developed in a MR damper. However for developing the control policies the objective is to calculate the current that should give the targeted value of pressure in the MR damper. This can be achieved by the reverse model. In the reverse model the yield shear stress is calculated for the targeted value of the pressure gradient. The reverse model is described as follows:

$$\mathbf{x}_{\mathbf{i+1}}^{\mathbf{r}} = \mathbf{x}_{\mathbf{i}}^{\mathbf{r}} + \mathbf{J}_{\mathbf{r}}^{-\mathbf{1}}\mathbf{f} \tag{3.48}$$

Where,

$$\mathbf{J}_r = \begin{bmatrix} \frac{\partial f_1}{\partial r_1} & \frac{\partial f_1}{\partial r_2} & \frac{\partial f_1}{\partial \tau_{py}} \\ \frac{\partial f_2}{\partial r_1} & \frac{\partial f_2}{\partial r_2} & \frac{\partial f_2}{\partial \tau_{py}} \\ \frac{\partial f_3}{\partial r_1} & \frac{\partial f_3}{\partial r_2} & \frac{\partial f_3}{\partial \tau_{py}} \end{bmatrix}, \tag{3.49}$$

$$\mathbf{x}_{\mathbf{i}}^{\mathbf{r}} = \begin{pmatrix} r_1 \\ r_2 \\ \tau_{py} \end{pmatrix}_i \tag{3.50}$$

The solution algorithm is the same as given above for the direct model.

3.4 Model simulation based parametric study

The results of the simulation based on the formulation described above have been presented in the form of a parametric study for the constant piston velocity boundary condition. This has been done for comparing the results of transient model with steady boundary condition with the results of quasi static model (Kamath et al (1996), Lee and Wereley (1999), Norrsi and Ahmedian (2005), Facey and

Rosenfeld (2005), Weng and Oyadiji (2008), Wang and Gordaninejad (2007) and Li (2000)), for the variation of pressure gradient with the velocity. In this section the acceleration of the piston has been considered zero in Eq 3.43. For the transient model simulation for this section, the piston was assumed to start with a given constant velocity and the pressure gradient variation with time is compared with the pressure gradient for the quasi static model. This parametric study is presented to achieve the following objectives:

(1) To establish the stability of the solution over the operating range of yield shear stress developed in MR fluid due to applied magnetic field.
(2) Study of transient effects in MR fluid for the velocity range from 0-1m/s.
(3) To determine the effect of variation of parameters such as velocity, yield shear stress and transients on hysteretic behaviour of the MR damper.

During the operation of an MR damper the velocity of the damper piston varies with time. Therefore in order to apply the quasi static model to predict the variation of damper force with time the researchers such as Kamath et al,(1996), Chooi and Oyadiji,(2008), and Cesmeci and Tehsin,(2010), have considered the piston velocity to be constant during a given time step. In this section the damper piston is considered to start suddenly at a given velocity and variation of pressure gradient with time due to transient effect has been presented for velocities in the 0-1m/s. The range of yield shear stress for the MR fluid has been taken as 10-40 kPa. This model can be called as the constant velocity transient model. The variation for pressure gradient for piston speeds 0.025-0.25m/s have been shown in Fig 3.6-3.7. The Fig 3.7 is the enlarged view of the boxed portion of Fig 3.6. The two figures show that the transient effects are significant at low speeds. The fluctuations of pressure gradient with time are more significant if the time scale is of the order of μ-seconds. If the piston velocity is considered in the range of 0.5-1m/s the transient effect start becoming

very significant when the time scale is of the order of 10 μ-seconds. This can be seen in the Fig 3.8-3.9. The above two sets of figures have the following common observations:

(1) The overshoots of the transient are high at low piston velocity. The overshoots also increase with the in the yield shear stress. This is because the thickness of the plug is higher for low piston velocity. Since the thicker plug has higher inertia therefore the over shoot are higher at lower piston velocities.

(2) The time decay of pressure gradient transient increases with the increase in yield shear stress of MR fluids.

(3) The time of decay of transients increase with the increase in piston.

In this work the transient effects in terms of the variation of pressure gradient with time have been shown. However, it s pertinent to mention that the transient effect also causes changes in the plug thickness of the MR fluid flowing through the channel, till the steady state is reached. It is due to the above reason that some of the results may not be in agreement with the above mentioned observations. Here the results for the variation of the thickness of the plug of MR fluid with time have not been presented as they may be difficult to verify experimentally. During the experiments on the MR damper the measurement of force is usually taken at a sampling rate which is of the order of 5 kHz, as such the transient effect must be taken into account for predicting the force of the damper. Therefore, in order to give an overview of the effect of fluid transients on the pressure gradient, the results of variation of pressure gradient with velocity corresponding to the time at the instance 0.1 m-seconds and the variation of pressure gradient with velocity due to quasi static model have been presented (Fig 3.10). From Fig 3.6 and 3.8 it can be seen that the fluid transients can be significant at the time scale of 0.1m-seconds for some combinations of piston speed and yield shear stress of an MR fluid.

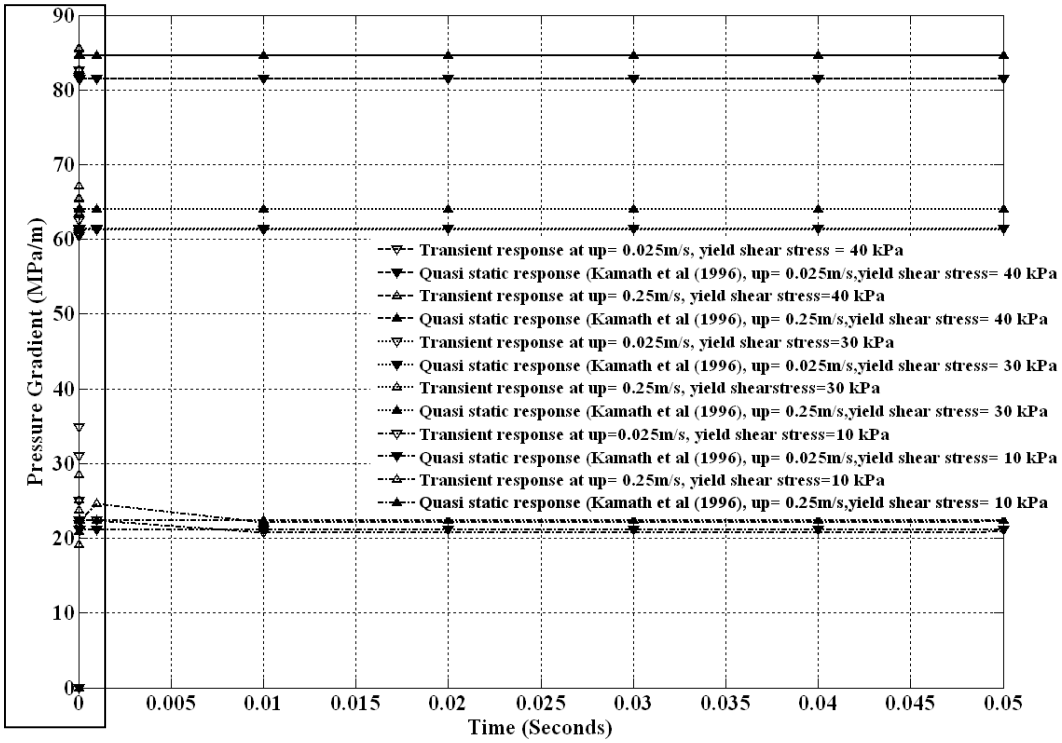

A

Fig 3.6 Variation of pressure gradient with time for piston velocities 0.025-0.25m/s and yield shear stress 10-40 kPa.

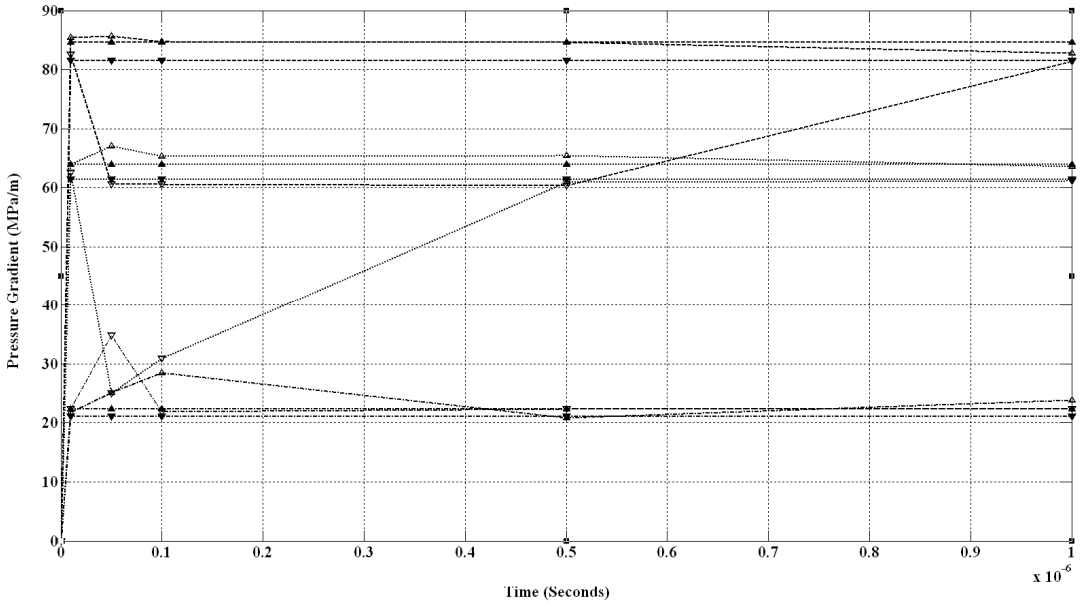

Fig 3.7 Enlarged view of box A showing transient effects at µ-seconds time scale.

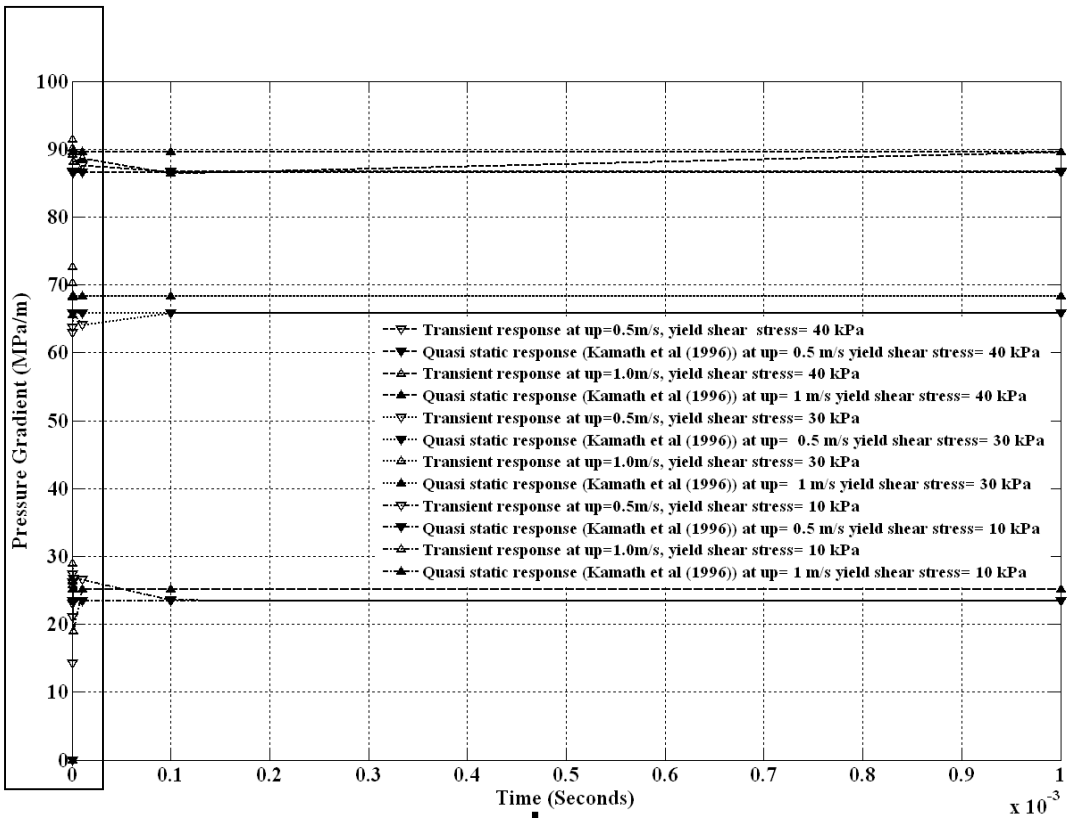

A

Fig 3.8 Variation of pressure gradient with time for piston velocities 0. 5-1m/s and yield shear stress 10-40 kPa.

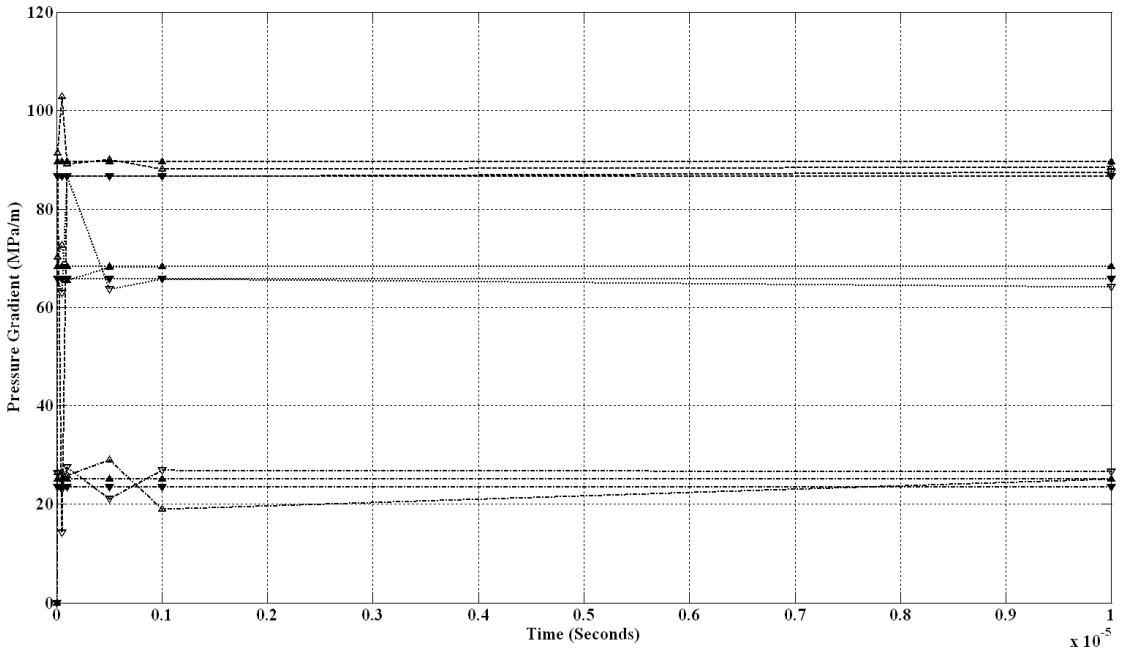

Fig 3.9 Enlarged view of box A showing transient effects at µ-seconds time scale.

The variation of plug thickness with the piston speed has been also shown in Fig 3.11 to facilitate the visualisation of change in velocity profile of MR fluid in the channel due the variation of piston speed and due to transient effect.

From Fig 3.10a it can be seen that the fluid transients also significantly contribute to the damper force. Since the fluid transients are non controllable component of damper force therefore they also tend to reduce the dynamic range of an MR damper. To further validate this observation the comparison of the damper force predicted by the transient model has been made with the results of quasi static model and experimental results given in Kamath et al (1996). The results are shown in Fig 3.10b. The transient model results agree very well with the experimental force of the damper. Based on the comparison of the results of transient model with the results of quasi static model it is concluded that the presence of fluid transients can be one of the contributors to such scatters. The error bars show the range of error which is likely to be introduced due to the neglecting of transient effect. The magnitude of error bar is in close agreement with the variation in the experimental and quasi static model results of Kamath et al (1996). The electrotrhological damper used in Kamath et al (1996) has a piston of 1" diameter, annular channel similar to Fig 3.1 with a gap size of 0.1" and the length of flow path is 4". The operating Reynolds number is much less than the critical Reynolds number and so the laminar flow assumption is valid. The comparison of damper force has been made in a velocity range of 0-0.2m/s. The fluid properties of VersaFLo ER fluid are given in the table 3.1.

Table 3.1 Fluid properties used for results of Fig 3.10b

Electric field strength(KV/mm)	Yield shear strength (kPa)	Post yield Viscosity (Pa s)
1	0.25	0.16
2	0.4	0.085
3	0.5	0.077

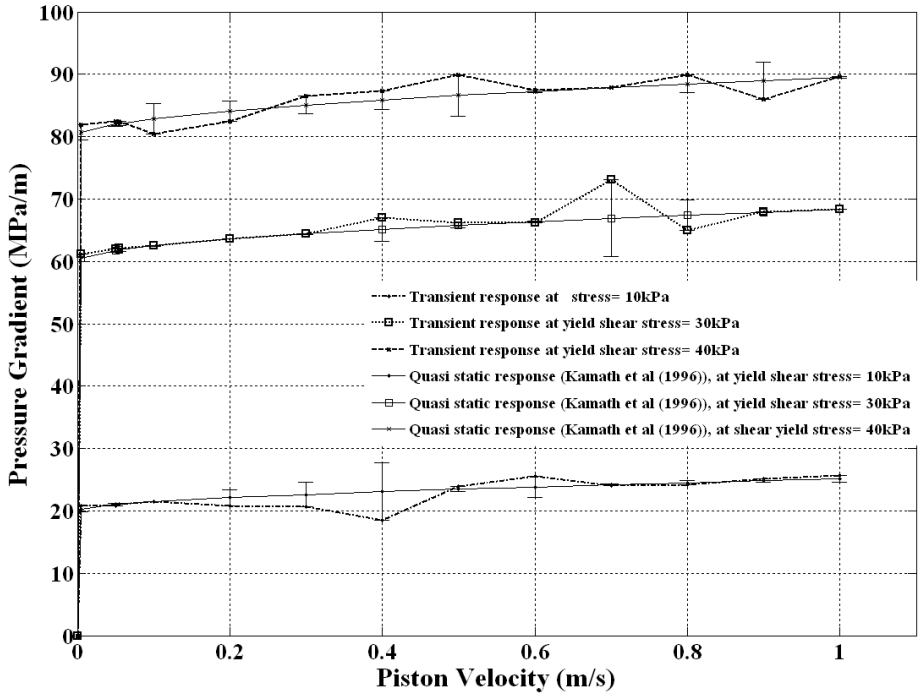

Fig 3.10a Variation of pressure gradient with piston velocity for yield shear stress values between 10 to 40 kPa using the sample rate of 10 kHz and quasi static solution.

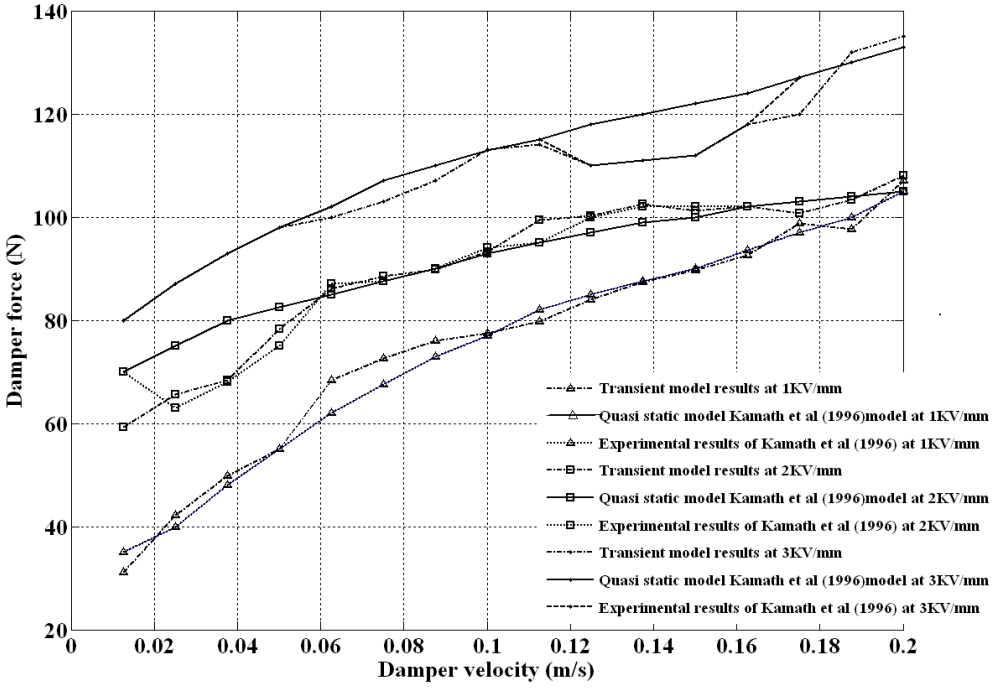

Fig 3.10 b Comparison of results of modelling and experiment given in Kamath et al (1996) with the transient model.

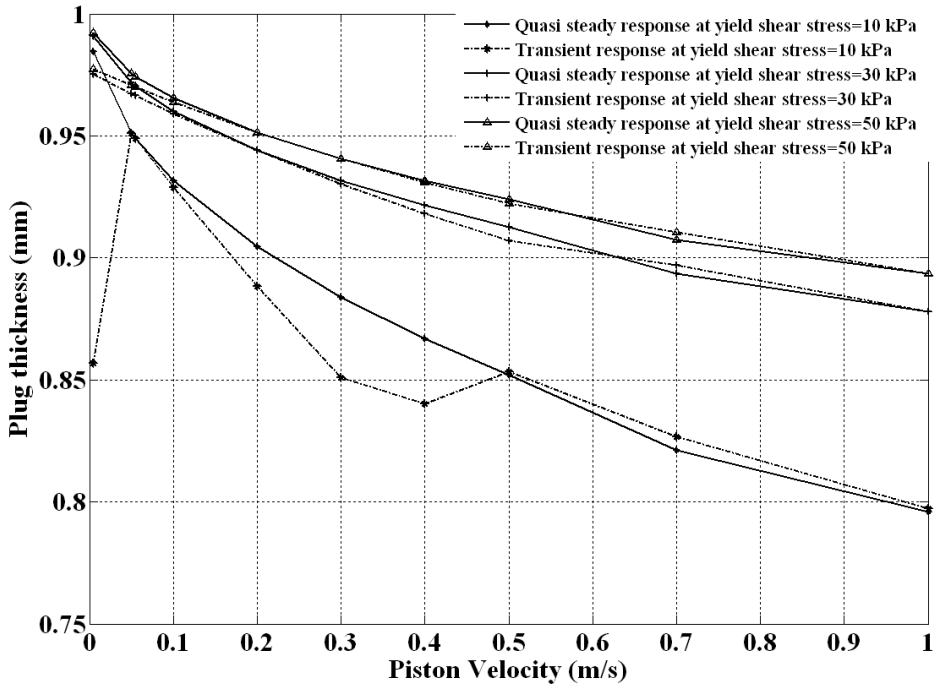

Fig 3.11 Variation of plug thickness with piston velocity for yield shear stress values between 10 to 40 kPa using sampling rate of 10 kHz and quasi static solution.

From the curves it is observed that the thickness of the plug for the MR fluid decreases with the increase in velocity of the piston. The variation of plug thickness for transient and quasi steady model is almost same for the values of yield stress between 30 kPa and 50 kPa. However, at the yield shear stress of 10 kPa the transient model predicts a fluctuation in the plug thickness. The transient solution predicts a lower value of plug thickness at low piston speed as compared to quasi static model. This can possibly because the acceleration or deceleration of plug results in an increase or decrease of plug thickness up to the limit at which the shear stress in the laminar region is equal to yield shear stress. Here it is mentioned that the curves in Fig 3.11 do not show the movement of the yield boundary for the annular channel of an MR damper which undergoes change in piston speed from 0 to 1m/s. This is because such a case has to be dealt with using Duhamel superposition principle for time varying wall velocity boundary condition.

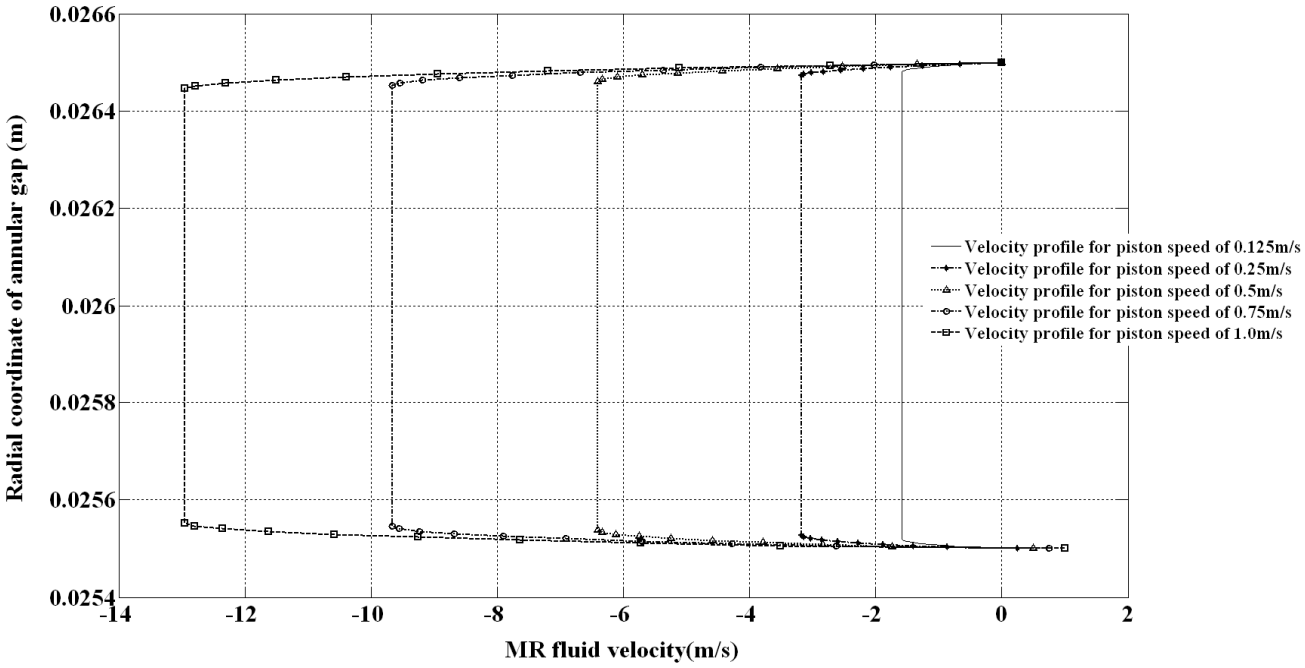

Fig 3.12 Velocity profile for different piston velocities representing quasi static and transient solution at yield shear stress of 40kPa.

Fig 3.12 shows the velocity profiles for the flow of MR fluid through the annular gap for piston velocities ranging from 0.125m/s to 1m/s. The velocity profile will not change significantly in its form for transient and quasi static solutions at the yield shear stress value of 40 kPa for MR fluid.

3.5 Comparison with the other models:

The comparative study of the results of transient model with other models has been done in three ways in this section. Firstly, the comparison of quasi static model is done with the transient model. For this comparison a sinusoidal velocity signal of 1m/s amplitude and 20Hz frequency has been used. Since the velocity varies with time therefore in this section the transient model has been used with Duhamel's superposition of boundary condition. The results of simulation using quasi static model (Kamath et al(1996)) and transient model are shown in Fig 3.13.

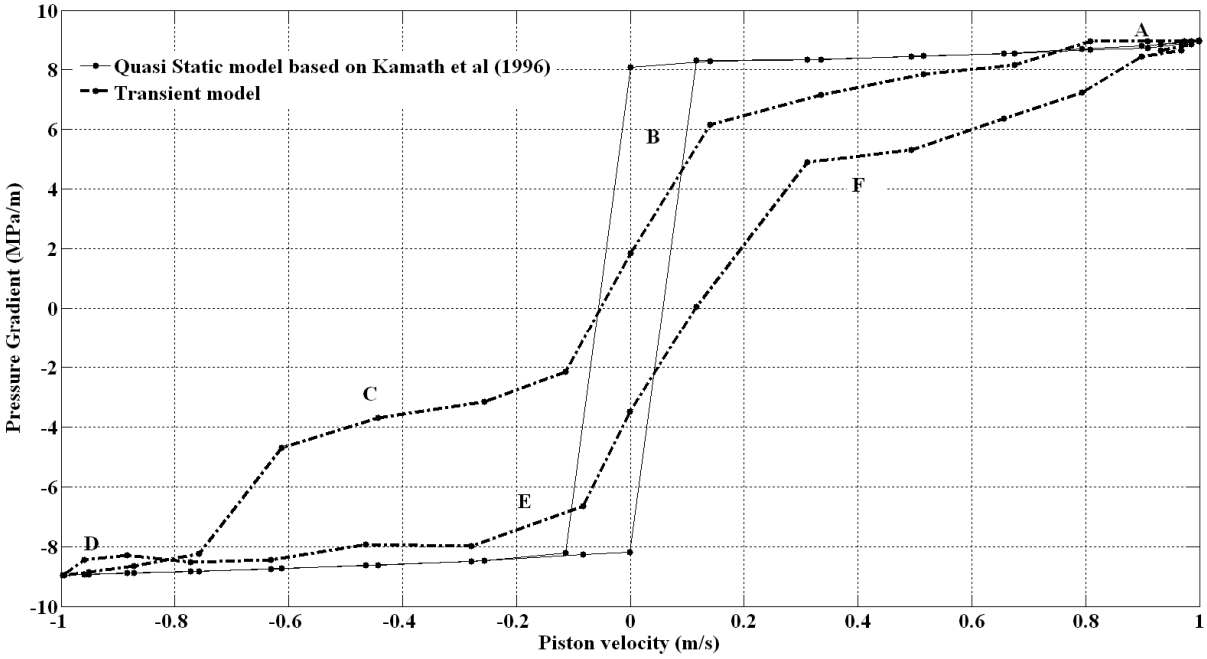

Fig 3.13 Variation of pressure gradient with speed for quasi static model and transient model for 40 kPa yield shear stress and 1m/s piston speed.

If the results for the quasi steady model in Fig 3.13 are compared with the results of Fig 3.10 a for 40 kPa yield shear stress it can be seen that the two curves are similar. This is because the initial condition and response to the velocity signal for each time step for the quasi static model lie on the same curve. In the case of the transient model the initial condition and the piston velocity are the function of the sine of angular frequency and time for each time step along the curve ABCD and DEFA. It is because of this reason that the two curves do not coincide and a hysteresis like curve is obtained. It can be shown that the shape of the curve for the variation of pressure gradient with the velocity for the transient model does not precisely match with the curve produced by a parametrically matched hysteresis equation. The model presented above is also required to be compared with the results of other published models to demonstrate its improved effectiveness in performance prediction over the existing models. Here it is mentioned that the effect of body force due the acceleration of the piston due to sinusoidal variation of velocity will also be included as it was done in the first case. The results of Wang and Gordaninejad (2007) and Wang and Liao (2011) have been used for comparison. The paper by Wang and Gordaninejad (2007), takes into account the compressibility of MR fluid and sealing friction in the

manner similar to the present work. The paper by Wang and Gordaninejad (2007) uses Herschel Bulkley model to take into account the shear thinning. The Herschel Bulkley model is able to take into account the nonlinear variation of the shear rate.

In Wang and Gordaninejad (2007), the experiment and modelling has been done using UNR damper MRD-001. The geometric properties of the MR damper are given as follows:

(1) Piston area = 1.9×10^{-3} m^2

(2) Length of channel = 57.0mm

(3) Diameter of channel = 6.35mm.

The MR fluid properties as given in the paper are taken as follows:

Post yield viscosity = 0.4 Pa-s

Density = 3000 kg/m^3 (assumed as not given)

Bulk modulus = $1.7GN/m^2$.

Yield shear stress (τ_0) : $\tau_0 = 2.7x104i_c^{1.5}$

The frequency of the velocity signal is 1Hz.

The study of paper does not elucidate how the effect of relative velocity of piston has been included in the volumetric flow rate. For comparison purpose the model with suitable boundary conditions for this geometry is described as follows:

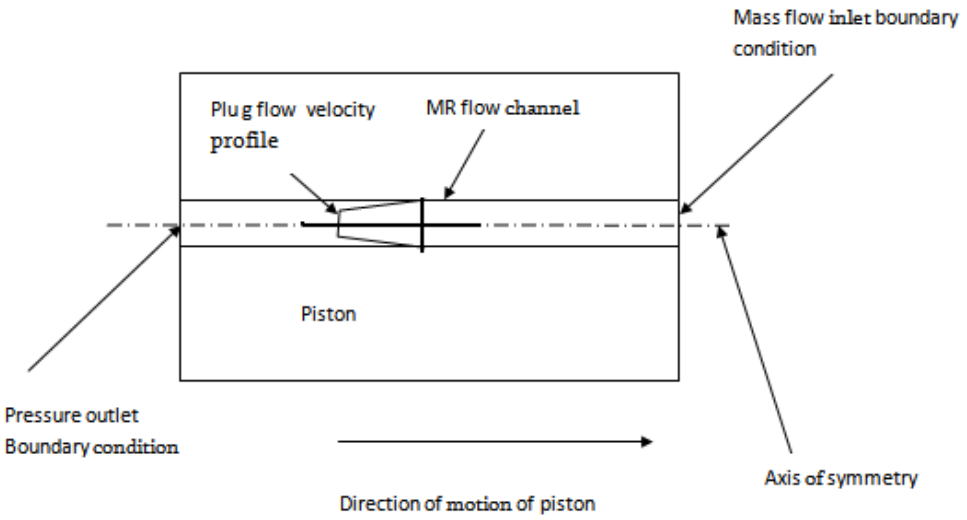

Fig 3.14 Computational domain of the UNR MRD-001 damper.

Since the domain is axi-symmetric therefore the equation for the velocity for one half of the domain will be sufficient to describe the complete model. Thus the equation for the condition of zero velocity gradient across the plug is not required because the plug flow has only one boundary. In this case we require the equations for the conservation of volumetric flow rate and the equilibrium of forces. The equations for the computational domain are given as follows:

$$u_x = \sum_{n=1}^{\infty} \left(\begin{array}{l} \dfrac{\pi\, u_p\, e^{-\nu\,\alpha_n^2\, t}}{\alpha_{n_i}} \cdot \dfrac{J_0^{'}(\alpha_{n_i} r_1) J_0(\alpha_{n_i} r_i)}{\left(J_0^2(\alpha_{n_i} r_i) - J_0^{'2}(\alpha_{n_i} r_1)\right)} \varphi_1 - \dfrac{\pi^2}{2} \left(\dfrac{\partial p}{\partial x} + a_p \rho\right) \dfrac{e^{-\nu\,\alpha_{n_0}^2\, t}}{\alpha_{n_i}\mu} \dfrac{J_0^2(\alpha_{n_i} r_{i)}}{\left(J_0^2(\alpha_{n_i} r_i) - J_o^{'2}(\alpha_{n_i} r_1)\right)} \varphi_1 \xi_1 \\ \\ + \dfrac{\pi^2}{2} \dfrac{\tau_{py}\, e^{-\nu\,\alpha_{n_i}^2\, t}}{\alpha_{n_i}\mu} \dfrac{J_0^2(\alpha_{n\,i} r_{i)}}{\left(J_0^2(\alpha_{n_i} r_i) - J_o^{'2}(\alpha_{n_i} r_1)\right)} \varphi_1 \chi_i \end{array} \right)$$
$$- \frac{\tau_{py}}{\mu}\left(r - r_i - r_1 \ln\left(\frac{r}{r_i}\right)\right) + \frac{1}{4\mu}\left(\frac{\partial p}{\partial x} + a_p \rho\right)\left(r^2 - r_i^2 - 2 r_1^2 \ln\left(\frac{r}{r_i}\right)\right)$$

(3.51)

Where,

$$\varphi_1 = \left(J_0(\alpha_{n_i} r) Y_0^{'}(\alpha_{n_i} r_1) - J_0^{'}(\alpha_{n_i} r_1) Y_0(\alpha_{n_i} r)\right) \tag{3.52}$$

$$\xi_1 = \left\{\left(r_1 J_1(\alpha_{n_i} r_1) - r_i J_1(r_i \alpha_{n_i})\right) Y_0'(\alpha_{n_i} r_1) - \left(r_1 Y_1(\alpha_{n_i} r_1) - r_i Y_1(r_i \alpha_{n_i}\right)\right) J_0'(\alpha_{n_i} r_1)\right\} \quad (3.53)$$

$$\chi_i = \left\{ \begin{array}{l} \left(r_1 \, {}_1F_2\left(\frac{1}{2}; 1, \frac{3}{2}; -\frac{1}{4}\alpha_{n_i}^2 r_1^2\right) - r_i \, {}_1F_2\left(\frac{1}{2}; 1, \frac{3}{2}; -\frac{1}{4}\alpha_{n_i}^2 r_i^2\right)\right) Y_0'(\alpha_{n_i} r_1) - \\ \left(\begin{array}{l} \frac{\pi}{2} r_1 \left(H_{-1}(\alpha_{n_i} r_1) Y_0(\alpha_{n_i} r_1) + H_0(\alpha_{n_i} r_1) Y_1(\alpha_{n_i} r_1)\right) \\ -\frac{\pi}{2} r_i \left(H_{-1}(\alpha_{n_i} r_i) Y_0(\alpha_{n_i} r_i) + H_0(\alpha_{n_i} r_i) Y_1(\alpha_{n_i} r_i)\right) \end{array} \right) J_0'(\alpha_0 r_1) \end{array} \right\} \quad (3.54)$$

In the above equation the variable a_p is the acceleration of the piston due to sinusoidal signal and the term containing this variable represents the body force acting on the fluid. This body force has also been accounted for, in a similar manner, in the model for hydraulic dampers in published works such as Bhatnagar et al (2009). For writing the equation for the conservation of volumetric flux, the velocity of the flow relative to the piston velocity needs to be calculated and as such the velocity of the piston is added to the equation of velocity. Here the velocity function for piston velocity has been taken as follows:

$$u_p = u_{p0} \sin \omega t \quad (3.55)$$

The velocity equation with Duhamel's superposition is given as follows:

$$u_x = \sum_{n_i=1}^{\infty} \gamma_i \left(\begin{array}{l} \frac{\pi \, u_p \, e^{-\nu \alpha_{n_i}^2 t}}{\alpha_{n_i}} \cdot \frac{J_0'(\alpha_{n_i} r_1) J_0(\alpha_{n_i} r_i)}{\left(J_0^2(\alpha_{n_i} r_i) - J_0'^2(\alpha_{n_i} r_1)\right)} \varphi_1 - \frac{\pi^2}{2} \left(\frac{\partial p}{\partial x} + a_p \rho\right) \frac{e^{-\nu \alpha_{n_i}^2 t}}{\alpha_{n_i} \mu} \frac{J_0^2(\alpha_{n_i} r_{i)}}{\left(J_0^2(\alpha_{n_i} r_i) - J_o'^2(\alpha_{n_i} r_1)\right)} \varphi_1 \xi_1 \\ + \frac{\pi^2}{2} \frac{\tau_{py} \, e^{-\nu \alpha_{n_i}^2 t}}{\alpha_{n_i} \mu} \frac{J_0^2(\alpha_{n i} r_{i)}}{\left(J_0^2(\alpha_{n_i} r_i) - J_o'^2(\alpha_{n_i} r_1)\right)} \varphi_1 \chi_i \end{array} \right)$$
$$+ \left(u_{p0} - \frac{\tau_{py}}{\mu} \left(r - r_i - r_1 \ln\left(\frac{r}{r_i}\right)\right) + \frac{1}{4\mu} \left(\frac{\partial p}{\partial x} + a_p \rho\right) \left(r^2 - r_i^2 - 2 r_1^2 \ln\left(\frac{r}{r_i}\right)\right)\right) \gamma_i' \quad (3.56)$$

where

$$\gamma_i = \left(\frac{\omega}{\left(\omega + \frac{\omega^2}{\left(\nu \alpha_{n_i}^2 \right)^2} \right) \left(\nu \alpha_{n_i}^2 \right)} \right) (-\cos(\omega t - \omega t_0) + \cos(\omega t_0)) + \left(\frac{\omega^2}{\omega + \left(\frac{\omega}{\nu \alpha_{n_i}^2} \right)^2} \right) \frac{1}{\left(\nu \alpha_{n_i}^2 \right)} (\sin(\omega t - \omega t_0) - \sin(\omega t_0))$$

$$\gamma_i^{'} = (\sin(\omega t + \omega t_0) - \sin(\omega t_0))$$

Now, Eq 3.51 and 3.56 can be used to obtain the equation for the conservation of volumetric flux in the following manner:

$$2\pi \int_{r_i}^{r_1} u_x r \, dr + \pi r^2 u_x \Big|_{r=r_1} - (u_p A_p - \dot{q}) = 0 \qquad (3.57)$$

In the above equation the symbol $\dot{q}$ stands for the rate of change of fluid volume due to the compressibility of the MR fluid and is given by Eq (3.42).

The equation of force equilibrium is given as follows:

$$f_3 = 2\tau_{py} - \left(\frac{\partial p}{\partial x} - \rho a_p \right) (r_1) + (r_1) \rho \frac{\partial u_z}{\partial t} \Big|_{r=r_1} = 0 \qquad (3.58)$$

The comparison of the experimental and modelling results of Wang and Gordaninejad (2007) with the transient model is shown in Fig 3.15. Since there were very few points for the experimental results in the region A-B and C-D therefore they were introduced by comparison with the results given in Fig 2 of Wang and Gordaninejad (2007). The experimental curve shown in Fig 3.15 is also similar shape to the curves given in Wang and Liao (2011).

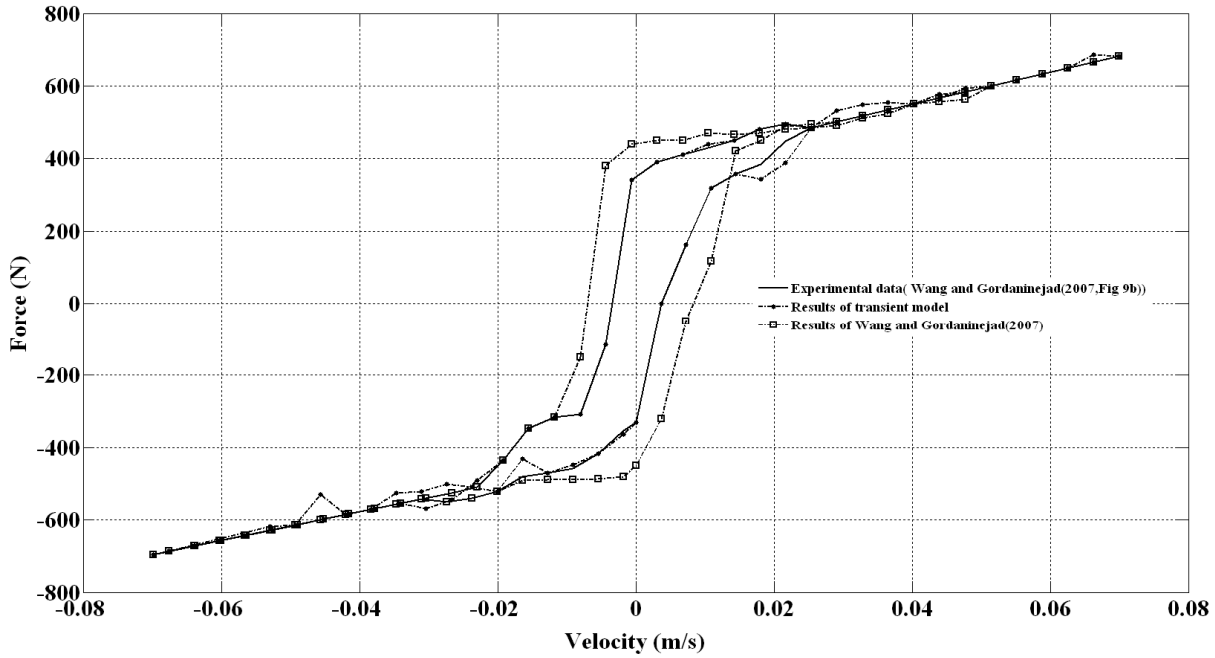

Fig 3.15 Comparison of MR fluid model due to Wang and Gordaninejad (2007) with Transient model and transient model (Duhamels' superposition of velcoity boundary conditions) for 1A current.

Similar results were also reported by Hong et al (2005) using their hydromechanical model which includes the effect of body force by the inclusion of inertance in the equation for the pressure drop. The hydromechanical model also includes the compressibility effects.

From the Fig 3.15 it can be seen that the transient model is in very good agreement with the experimental results and has a better accuracy as compared with Wang and Gordaninejad (2007) model. The transient model results were also compared with the results given in Spencer et al (1997) and Wang and Liao (2011) and is shown in Fig 3.16. These are the experimental results for 2.5Hz frequency velocity signal given in Spencer et al (1997, Fig 9a). Because the velocity function of this 2.5 Hz signal has a flatter shape in the peak velocity region therefore the variation of force with the velocity is almost

straight line in the velocity range of 0.045m/s to 0.12m/s. The trasient model results are in a good agreement with the results of Spencer et al (1997).

From the above comparison it is deduced that the transient model gives a more close agreement to the form of hysteresis curve obtained for a sinusoidal velocity signal. In the other published works such as Cesmeci and Tehsin (2010) which is the also a recent work, it is still reported that the quasi static model is unable to capture the hysteresis and so the paper resorts to the use of phenomenological model for predicting the predicting or modelling the force of MR damper. In Kamath et al (1996) and Wang and Gordaninejad (2008), the prediction of damper force by the calculation of pressure gradient using quasi static model has been discussed for different values of voltage and current excitation for ER and MR damper. In these papers also the piston has been assumed to be moving with a constant speed for the time step for which the pressure gradient and the coordinates of plug flow boundaries are calculated. In all the published works given in the introduction, the effect of piston force on the MR fluid channel has been neglected. In the published works on phenomenological models such as Wang and Liao (2011), Dominguez et al (2004) and Gavin et al (1996) there is a use of hyperbolic tangent or sine function to obtain the hysteresis shape which matches with the experimental data.

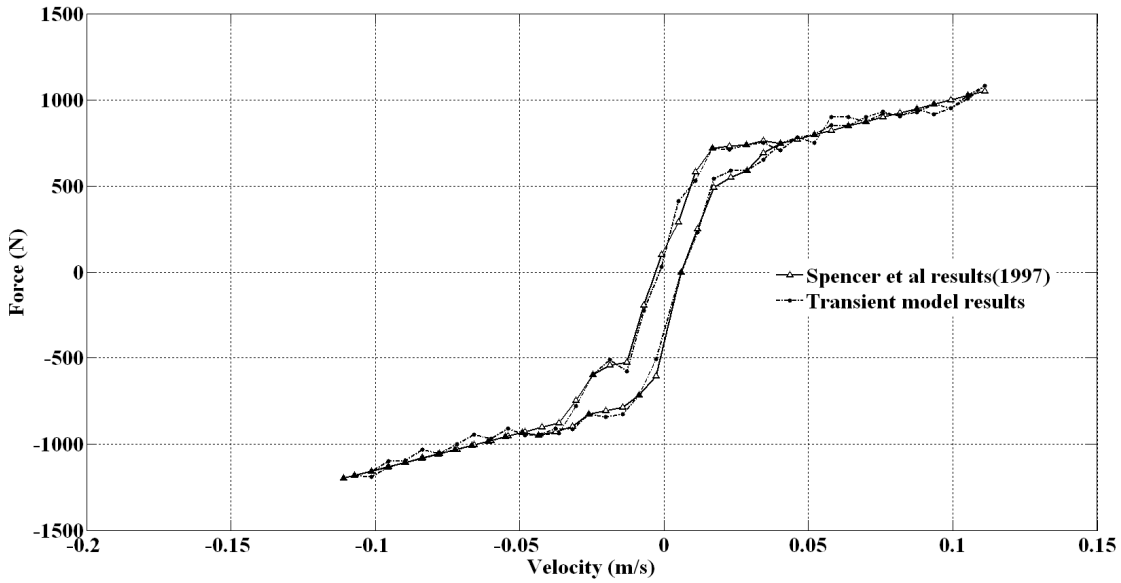

Fig 3.16 Comparison of MR fluid results given in Spencer et al (1997), Wang and Liao (2011) with transient model.

A comparison of these models with the transient model, leads to the conclusion that these are mathematically approximate form of the transient model**.** In the end, it will be interesting to note that the Fig 3.13 shows the transient response at high frequency and Fig 3.15 and 3.16 show low frequency response. For a low frequency signal the transient model, quasi static model, Wang and Gordaninejad (2007) model give almost straight line like force –velocity response when the piston velocity is close to the peak velocity. On the other hand for a high frequency velocity signal the transient model will give hysteresis like response even as the piston velocity is close to the peak velocity (see Fig 3.13). Lastly the question arises, as to how the transient model represents the correct physics. In this regards if the Fig 3.13 is restudied it will be noticed that in the regions BC and EF the curve cuts the x axis and these cases correspond to zero pressure gradient points at the corresponding piston velocities. The quasi static model is not able to capture this variation because in these part of the damper force velocity curve that transient effects due to transient velocity boundary condition, compressibility and fluid inertia effects are significant. These points correspond to the limiting cases of boundary driven flow. The region of boundary driven flow can get further enlarged if the presence of air bubbles in the damper fluid results in an increase in compressibility of the fluid. The curves have very small regions where the piston velocity and pressure gradient have opposite signs. These are the regions of flow reversal due to the change in the direction stroke. The experimental results of Spencer et al (1997) also confirm the same findings.

3.6 Conclusion:

The transient model proposed in this chapter is able to explain the response of magnetorheological damper on the basis of fully transient model. This has been demonstrated by comparison with the models presented in the other works. The proposed model has following advantages:

(1)The formulation is based on the fluid mechanics of the plug flow of MR fluid based on the Bingham Plastic model for the shear stress. As such the model has been found to accurately predict the damper force taking into account the transient effects. Here it is mentioned that the modified phenomenological model gives a mean error of 7%, however this can be only applicable to sinusoidal velocity signal. In Wang and Gordaninejad (2007) the results of constant velocity signal with time varying current signal have also been published. These results show that the force velocity relationship does not give a hysteresis curve and as such significant error in the prediction for force can be introduced if the effect of time varying boundary condition is neglected.

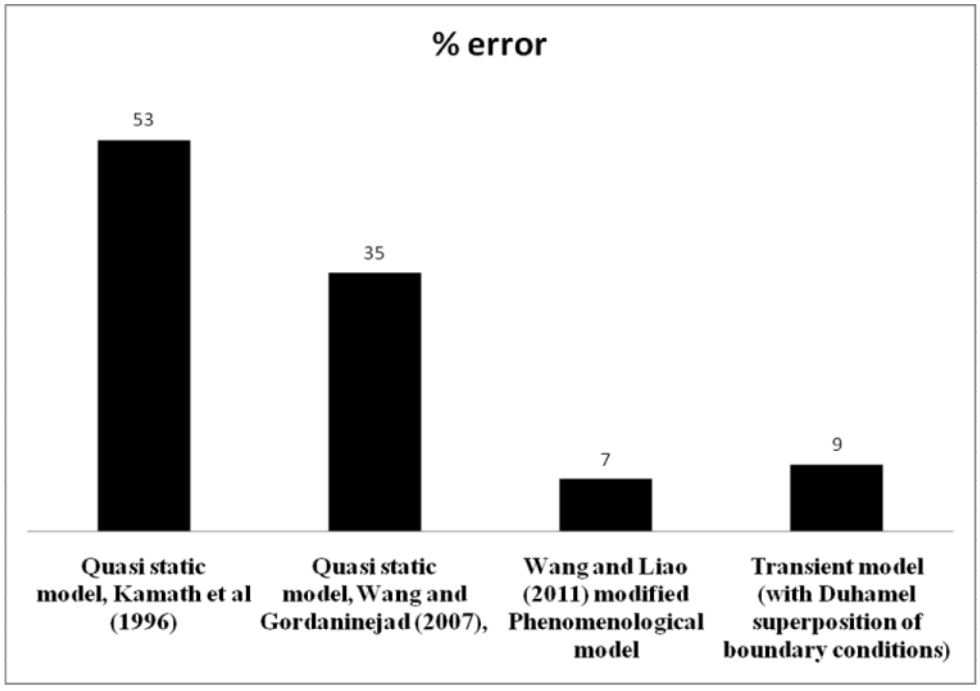

Fig 3.17 Error % comparison of different model for sinusoidal signal.

(2)The model is computationally efficient as the number of iterative steps are sufficiently low to predict the forces in the time of the order of hundredth of a millisecond for enabling practical implementation of control policies.

(3)The model is able to effectively capture the hysteresis in an MR damper and is able to explain that the hysteresis like variation of force versus velocity is due the effect of variation of velocity of the piston during the time step.

(4)The proposed model more accurately describes the physical phenomena of the flow of MR damper fluid.

(5) There is an explicit form of inverse model which is equally computationally efficient as the direct model. This enables the implementation of adaptive model reference control policies.

3.7 Summary:

This chapter presents a transient model for the flow of MR fluid in an annular channel of an MR damper. The annular channel is a gap between the piston and the cylinder. The flow through the annular channel can be considered as a pressure driven Poiseuille flow superposed with Couette flow. The Navier-Stokes equation for an axi-symmetric domain has been used with Bingham fluid constitutive model. The velocity profile of the flow of MR fluid through the channel has a plug flow with inner and outer layers of laminar flow. The validity of the assumption for laminar flow has been shown for the area ratios between 12.5 and 50 and for the pre yield shear values between 1-50 kPa. The solution of the Navier Stokes equation has been obtained by using a combination of Laplace and Weber transform. The results of the simulation of the model have been presented in the form of a parametric study for steady state moving wall boundary condition due to piston velocity. The results of the model with transient moving wall boundary condition have been presented as a comparison with the results of models of the other researchers such as Kamath et al (1996), Wang and Gordaninejad (2007) and Spencer et al (1997). The chapter presents following important findings:

(1) Based on the correlations of Nouar and Frigaard (2001) the cirtical Reynolds number for the flow MR fluid in the channel of an MR damper is significantly affected by the ratio of piston area to the flow area and the yield shear stress.

(2) The transient effects due to the inertia of MR fluid are significant even though the damper piston can be considered to move with constant velocity.

(3) Transient effects due to inertia of MR fluid, body forces, compressibility effects and transient velocity boundary condition are significant.

Chapter 4

Experimental validation of MR damper model at low speed

4.1 Introduction

In the previous chapter the results of simulation of transient model were compared with the results published by the other researchers. In this chapter the results of transient model will be validated by the experimental testing of a commercial damper followed the comparison of modelling results with the experimental results. The ability of the model to predict the damper force for different frequencies of velocity signals for the same parameter set leads to the system identification and validation of model. In this chapter the simulation will be done using transient model with Duhamel superposition of boundary conditions. This chapter deals with the description of experimental setup in the second section. The design of experiment for the testing the commercial damper on the rig has been described in the third section. The system identification and the validation of the model have been described in the fourth section.

4.2 Experimental setup

The experimental setup is intended to measure the force time response of MR damper for a given velocity time input signal. The MR damper used is of Lord Corporation make of following specifications:

MR Damper: Model no RD-8040-1(short stroke)

Maximum current -2 A (intermittent operation)

1 A sustained operation.

Force amplitude at 1A at 0.05m/s- 2447N

Off state 0.2m/s- 887N.

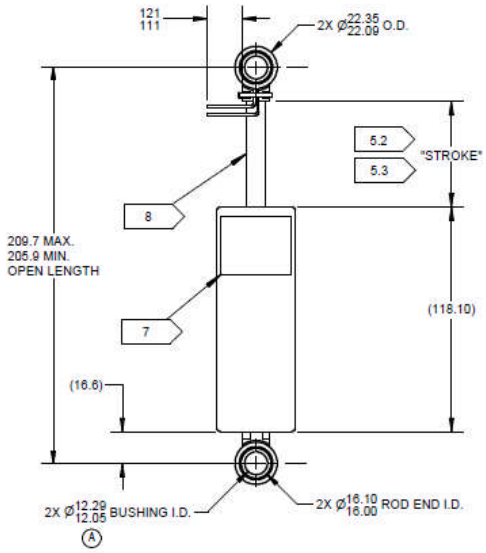

Fig 4.1 Drawing of Lord Corporation make RD-8040-1 short stroke MR damper.

The wonder box is controlling device for MR damper. It receives a voltage signal and feeds current to the MR damper as per voltage current characteristics given in Fig 4.2.

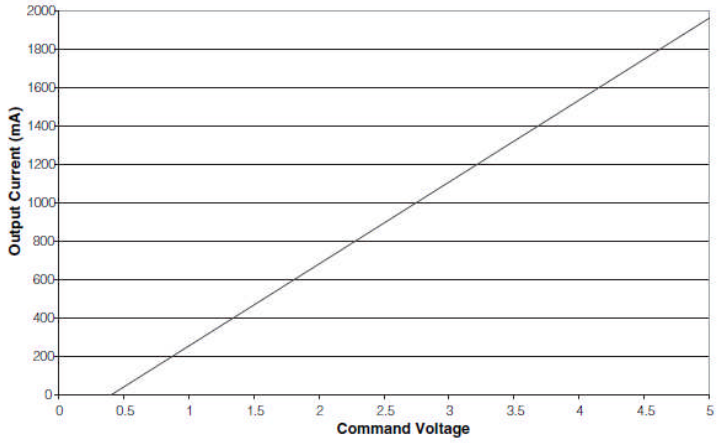

Fig 4.2 Current versus voltage characteristics for Wonder box (taken from Lord Corporation sheet).

In order to test the MR damper there are the following two pieces equipments required:

(1) A test rig for pulling the damper with a given velocity functions.

(2) A voltage signal generator with a data capturing device.

The variation of displacement of damper with time can be measured with a linearly variable differential transformer (LVDT) and the force can be measured by a ring type load cell. The specifications for the LVDT and the load cell are given in the table 4.1.

Table 4.1 Specifications of the instruments used.

Equipment	Specification	Make
Universal Load cell	**Load range 0-5000lb**	**RDP Electronic**
Linearly Variable Differential tranformer	**Stroke 200mm Voltage range 0-5V Current 0-20A**	**P3 America**
Kelsey digital servo-controller	**K-7500**	**Texas Instruments.**
Data acquisition V 4.08.06D	**Signal processing V 6.2.3**	**PROSIG**

The signal generation for the Hydraulic test rig is done by Kelsey controller. The brief specifications of the Kelsey controller are also give in table 4.1. For the signal generation of voltage signal a PROSIG DATS signal generator cum data capturing system was used (ref Table 4.1).

The PROSIG Digital to analog converter based signal generator generates signal in the range ±1V. For generating current signals in the range of 0.4 to 1 A the corresponding voltage range required was 1.25 to 2.75V. To convert the PROSIG voltage signal into voltage signal corresponding to the required current range for Wonder box requires 2.5 times amplification.

Now due to digital to analog conversion some aliasing error is introduced in the signal. This is due to the recovery of the original function from the corresponding under sampled digital signal by the application of inverse Fourier transforms. As such a low pass filter was used to minimise the noise in the signal. Since PROSIG instrument is a voltage based device so the measurement of current was done by using YOKOGAWA, DL-1520L, oscilloscope. The YOKOGAWA oscilloscope has the provision to store the data in a 3 1/4" floppy disc which can be processed using the MATLAB programming environment to cross check the current signal corresponding to the voltage signal.

The circuit diagram for test setup is given as follows:

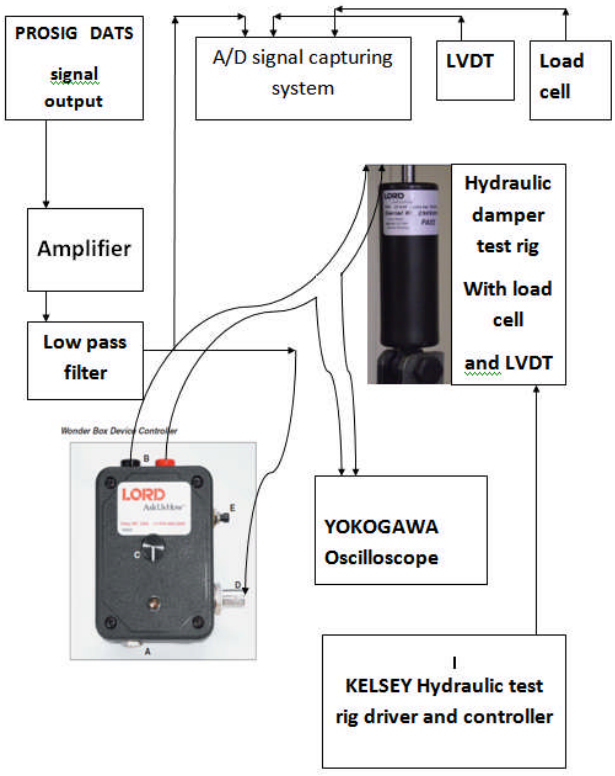

Fig 4.3 Circuit diagram showing wire connections of experimental setup.

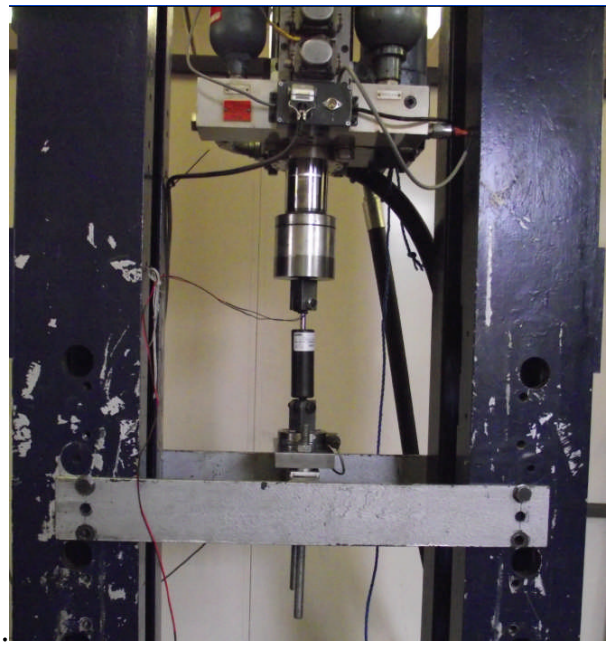

Fig 4.4 Snapshot of MR damper RD8040-1(LORD Corporation) mounted on damper test rig (7 kN/150mmstroke).

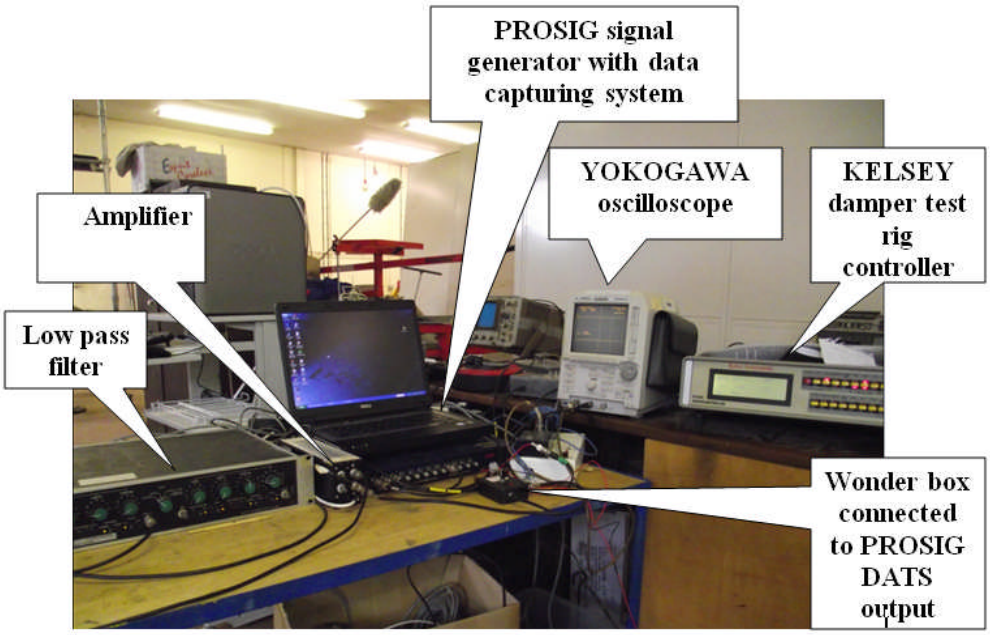

Fig 4.5 Snapshot of PROSIG setup with low pass filter, amplifier, Kelsey controller and Wonderbox.

The snapshot of the complete setup is shown in Fig 4.4 to 4.5.The DATS signal generator generates the signal at a sampling rate of 1 kHz. The DATS input captures signal at the rate of 5 kHz.

4.3 Design of Experiment

The MR damper was planned to be tested at 1A, 0.8A and 0.4 A and at speeds ranging from 0.05m/s to 0.2m/s. The voltages required corresponding to the excitation currents for MR damper are given in table 4.2. The speed and corresponding signal frequency are given in table 4.3. The MR damper was tested for constant current for constant velocity and sinusoidal signal. For the testing of MR damper for off and on state operation, the constant velocity signal was used for driving the rig.

Table 4.2 Voltage/ Current relation for wonderbox, DATS voltage and amplifier gain.

Current in A	Driving voltage for wonder box in V	DAC voltage	Amplifier gain
0.4	1.36	1	2.8
0.8	2.36	0.842	2.8
1.0	2.8	0.485	2.8

Table 4.3 Speed and damper test rig driving signal frequency.

Speed in m/s	Time period	Frequency in Hz
0.034	0.56	1.786
0.044	0.4	2.5
0.0125	1.91	0.523

Before starting the experiment the equipment needs to be calibrated to cross check the sensitivities for LVDT and load cell. The LVDT is calibrated by giving a measured voltage to the KELSEY controller and physically measuring the displacement of the jaws. The voltage output of LVDT can be seen on an oscilloscope to determine the voltage sensitivity. The sensitivity of the LVDT has been found to be 0.008m/V. Similarly the load cell can be calibrated by giving a measured load to the load cell and measuring the voltage on an oscilloscope to obtain the voltage sensitivity of the load cell. The voltage sensitivity has been found to be 2.5 kN/V. These voltage sensitivities are stored in record for the channel parameters for the DATS data capturing system of PROSIG.

To start the experiment the damper test rig is run with a specified velocity signal using the KELSEY controller. After a few number of strokes for allowing the warm up of the damper the data capture trigger is turned on. This trigger turns on the current signal through DATS output to the wonder box and the DATS input receives and stores the force, displacement and current signals through the input channels. The data capture takes place for 10 seconds. The damper run is stopped and after a pause of few minutes the next observation is recorded. The pause of few minutes is necessary to allow the damper to cool down. This will ensure that the density and viscosity of the MR fluid of the damper remain the same throughout the experiment. This is a standard procedure for conducting the experiment on the damper for allowing the damper to cool down although no measurements of temperature were done.

The stored data contains the displacement, force and current values for the sampling rate of 5000 kHz. The displacement time history can be used to determine the velocity time history using least square fit based Richardson's extrapolation. The least square fit based Richardson extrapolation minimises the noise in velocity time data, Bhatnagar (2006), Dahlquist (1974). The expression for the least square fit based Richardson's extrapolation is given as follows:

$$f_0' = \frac{2(f_2 - f_{-2}) + (f_1 - f_{-1})}{10h} \qquad (4.1)$$

In the above equation f_i is the function evaluated at i^{th} step in Richardson' extrapolation f'_i is the derivative of function evaluated at i^{th} step and h is the time step. In the above expression the derivative represents the velocity. This is followed by a further filtration of noise using an 8^{th} order Butterworth filter available in MATLAB R2010a with cut off frequency as 0.08Hz (MATLAB R2010a - help and lecture notes of Dr David Purdy).

4.4 Results and model validation

The model validation has been carried out using two sets of experiments. The first set of experiment will be used to identify the system and the last three sets of experiments will be used to validate the identified system. If the results of system identification for the first set agree with the results of the remaining sets of experiments then the model can be said to be validated. The system identification has been carried out in two steps. In the first step the quasi static model is used to predict the maximum force using different trial values of yield shear stress for the peak velocity of sinusoidal velocity function corresponding to the experimental results. The identified value of yield shear stress of MR fluid of the damper is the value at which the peak damper force predicted by the model, matches with the value of experimentally measured peak force. In this step the sealing force and gas spring force are also taken into account. The sealing force and the gas spring force are taken from the data sheet of RD-8040 MR damper and the off-state experimental measurements. In the second step the transient model results are superposed on the experimental results. If the simulation results are in good agreement with the experimental results the system identification can be considered to be correct.

Since the geometrical parameters of the damper were not available a priori because of being a commercial product, therefore the first step towards the validation of the model developed is to set some value of piston radius and cylinder radius such that there is a gap of 1mm. This procedure was resorted to as the supplier did not entertain the request for providing data for the flow path and fluid. The width of the piston is taken as 30 mm. These parameters are sensible because they seem to agree with the MR damper drawing of the LORD Corporation for RD8040-1 short stroke damper. Following this step the piston diameter was selected to be 30mm and the cylinder bore diameter was set at 32mm. Here it is mentioned that the MR damper may have a flow channel embedded in the piston (ref Fig 3.14) but the system identification is being carried out using the geometry of the MR damper given in Fig 3.1. In such a case also the boundary condition will not differ and this procedure can be called as equivalent system identification. This has been shown in section 3.5 of chapter 3. These values were arrived at using quasi static model to match maximum force for different values of piston and cylinder bore diameter with 1mm gap for flow of MR fluid. In this process the values of yield shear stress corresponding to the values of currents of 1A, 0.8A and 0.4 A for the above mentioned diameter of piston and cylinder bore, were found to be 16, 24 and 31 kPa respectively. The system identification was carried out using sinusoidal signal. The system identification should be done necessarily using a sinusoidal signal because a real life velocity signal is usually a continuously time varying signal and a sinusoidal signal is a close approximation to a real life signal. Using following parameters the simulation results of transient model were superposed on the experimental results for 0.34m/s amplitude and 1.786Hz sinusoidal signal. The results of the first step of system identification are given in table 4.4.

Table 4.4 Equivalent Parameters for MR damper RD8040-1

Parameter	Value
Piston diameter (mm)	**30**
Cylinder bore diameter (mm)	**32**
Shear stress (kPa) at 0.4 A current	**16**
Gas Spring pressure (bar) (Ref. Lord Corporation Data sheet)	**2.3**

The modelling results for the variation of damper force versus displacement given in Fig 4.6 show a very good agreement with the experimental results. This leads to the confirmation that the yield shear stress value of 16 kPa for 0.4 A current is correctly identified. The simulation results for the variation of damper force with velocity have been given in Fig 4.7. The modelling results and the experimental compare very well with each other. The mean error in the comparison of modelling results with the experimental results has been found to be 5.6 %. The peak damper force predicted by the model is in excellent agreement with the experimental results. Using the results of quasi static model and transient model the sealing friction force has been found to be 50N. The force due to gas spring has been found to be 30N. If the data for the gas spring pressure given in the table 4.4 is used the gas spring force is given as 28N. The difference in gas pressure obtained from the experimental measurements and manufacturer data differ by 7%. Since the major component of error is attributable to manufacturing tolerance in gas spring pressure as compared to the experimental error therefore the value of gas spring force is considered acceptable.

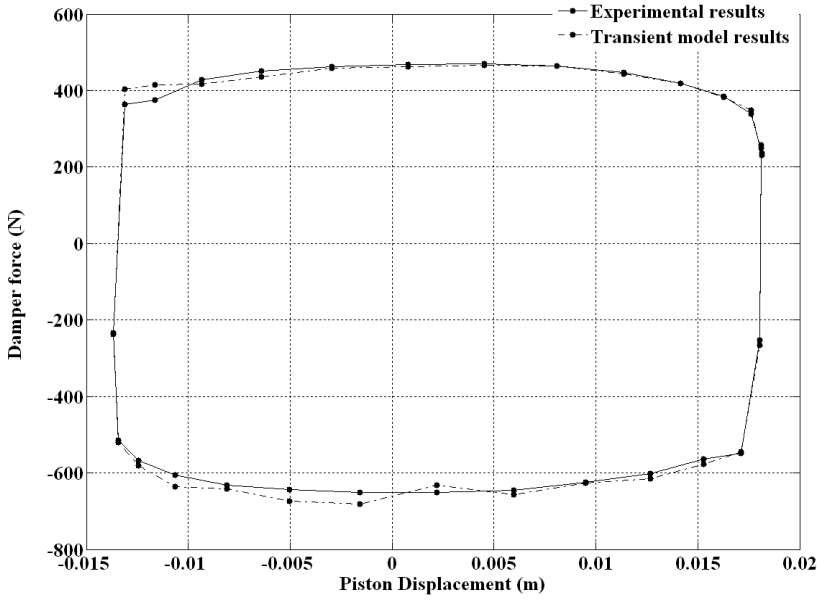

Fig 4.6 Variation of force versus displacement for 0.4A current (yield shear stress of 16kPa)and 1.786Hz sinusoidal velocity input for experimental measurement and model simulation.

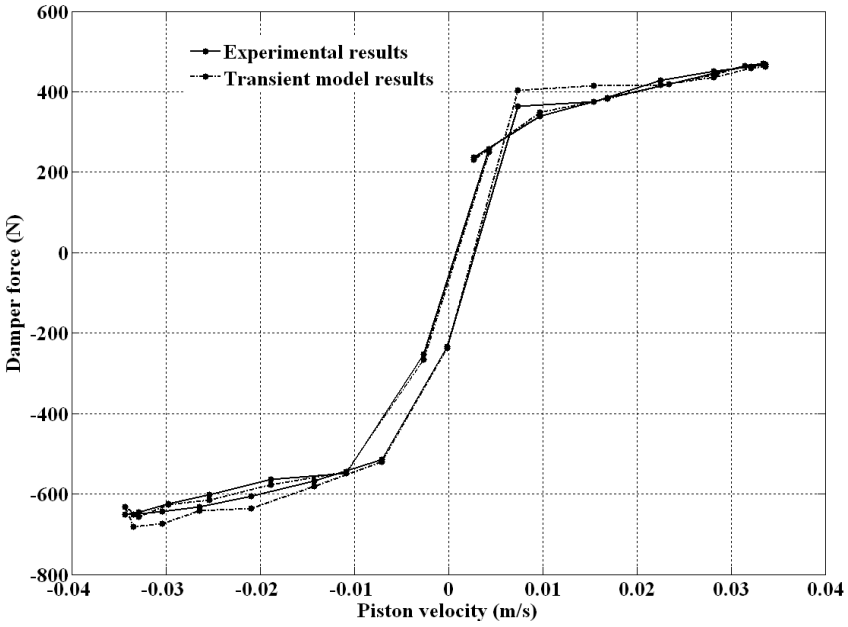

Fig 4.7 Variation of force versus velocity for 0.4A current (yield shear stress of 16kPa)and 1.786Hz sinusoidal velocity input for experimental measurement and model simulation.

The next experiment was performed at the 0.8A excitation current for the MR damper keeping all the other parameters given in the table 4.4 as same. The value of yield shear stress corresponding to 0.8A has been found to be 24 kPa. The damper rig was driven with 2.5Hz sinusoidal velocity signal. The results for the variation of damper force with dispalcement and damper force with velocity are given in Fig 4.8 and 4.9 respectively. In this case also the model results are in very good agreement with the experimental results. Therefore the shear stress value 24 kPa for the MR fluid of the damper has been correctly identified.

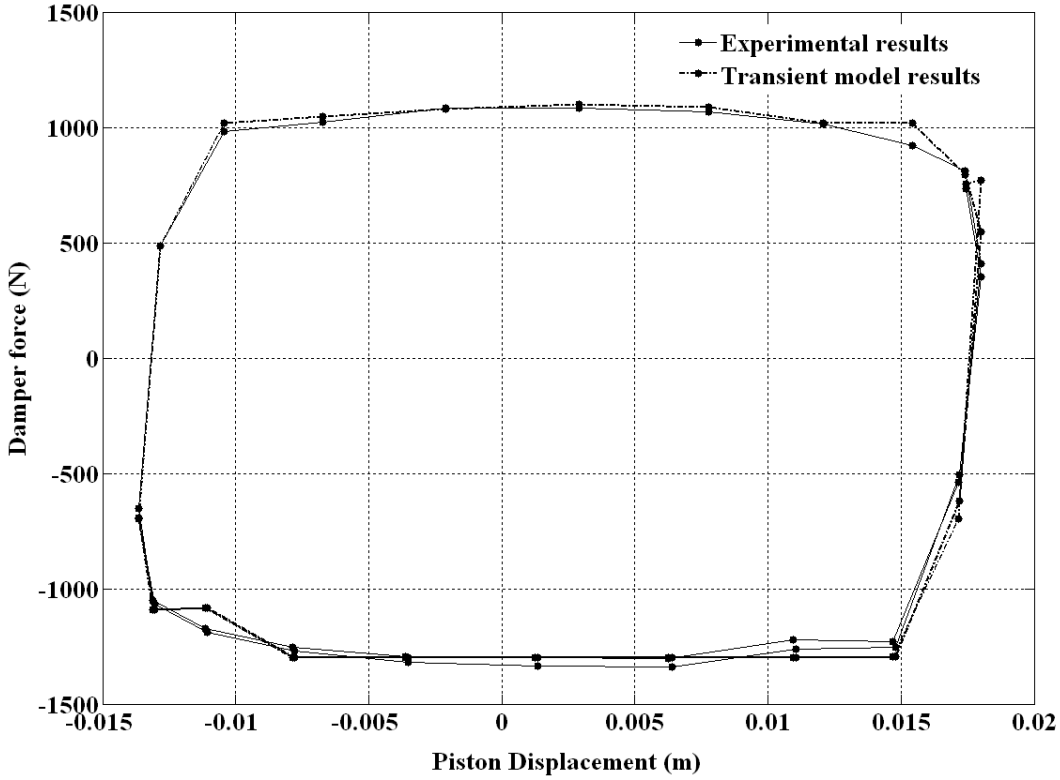

Fig 4.8 Variation of force versus displacement for 0.8A current (yield shear stress of 24 kPa)and 2.5 Hz sinusoidal velocity input for experimental measurement and model simulation.

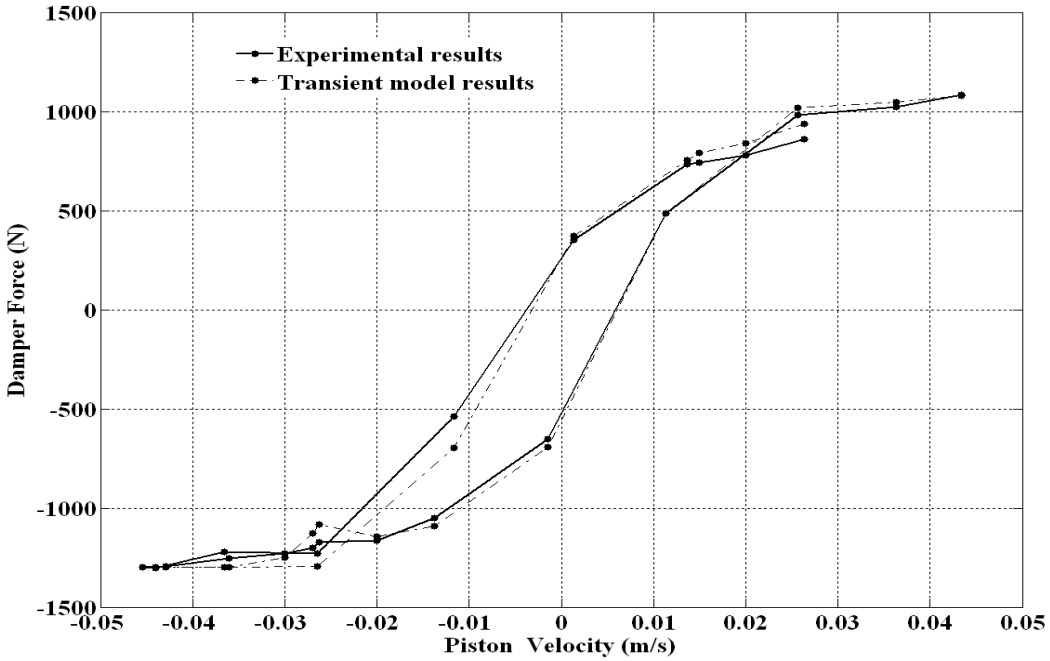

Fig 4.9 Variation of force versus velocity for 0.8A current (yield shear stress of 24 kPa)and 2.5 Hz sinusoidal velocity input for experimental measurement and model simulation.

The third experiment for 1A excitation current for MR damper, was carried out using a sinusoidal velocity signal of 0.523Hz frequency. The yield shear stress corresponding to 1A exciation current was found to be 31 kPa. The results for the variation of damper force with velocity and damper force with displacement are given in Fig 4.10 and 4.11. The experimental results and the results of transient modela are also in close agreement with each other. Since the modelling results and the experimental results are in close agreement with each other for all the three experiments therefore the model parameters can be said to be correctly identified. The system identfication also establishes the relationship between the excitation current and the

yield shear stress. The variation yield shear stress with applied current for the MR damper is given in Fig 4.12.

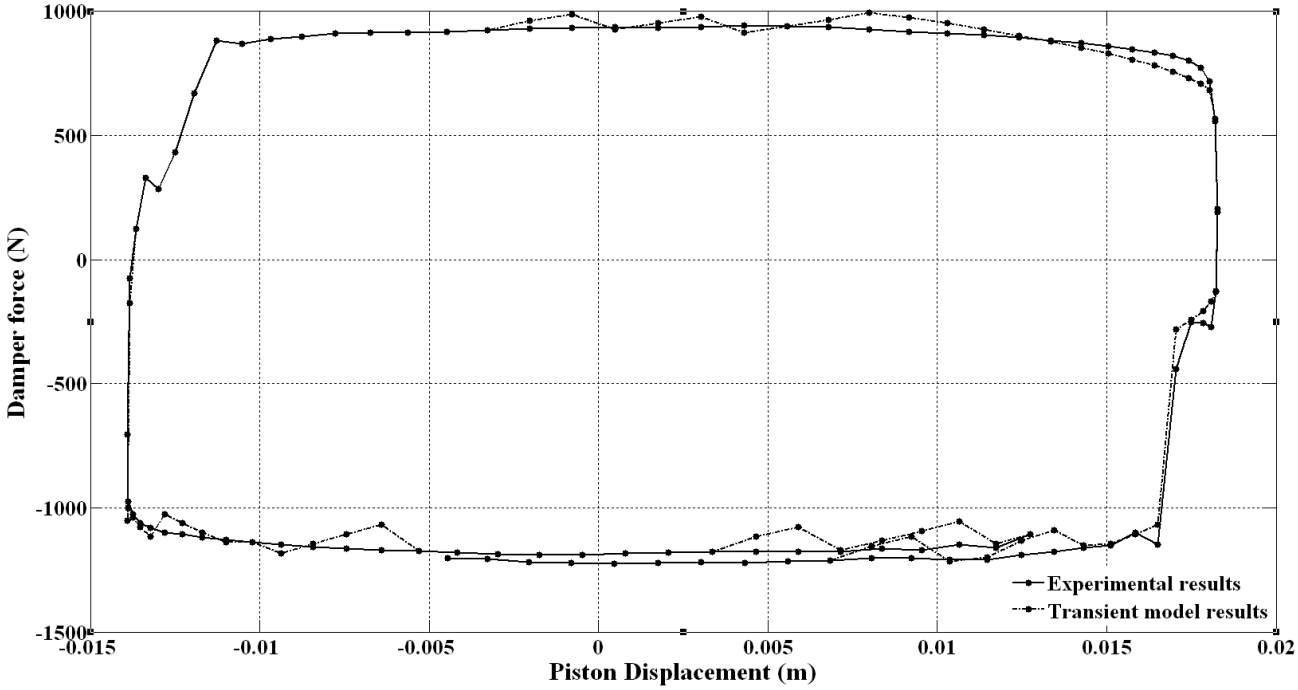

Fig 4.10 Variation of force versus displacement for 1A current (yield shear stress of 31 kPa)and 0.523 Hz sinusoidal velocity input for experimental measurement and model

simulation.

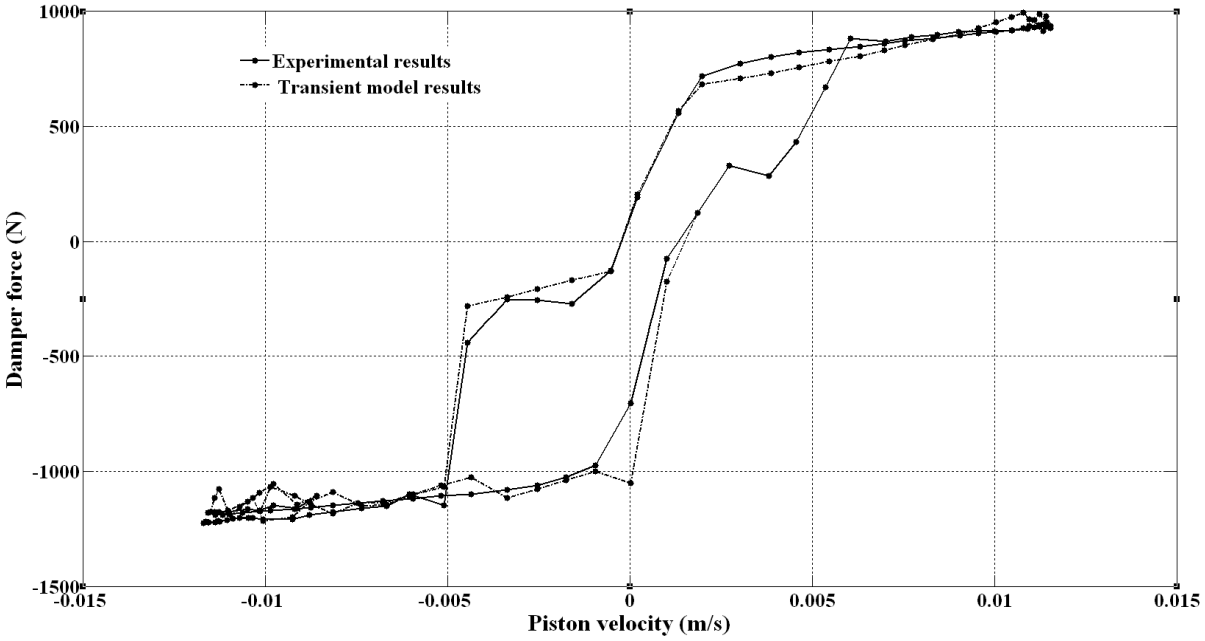

Fig 4.11 Variation of force versus velocity for 1A current (yield shear stress of 31 kPa) and 0.523 Hz sinusoidal velocity input for experimental measurement and model simulation.

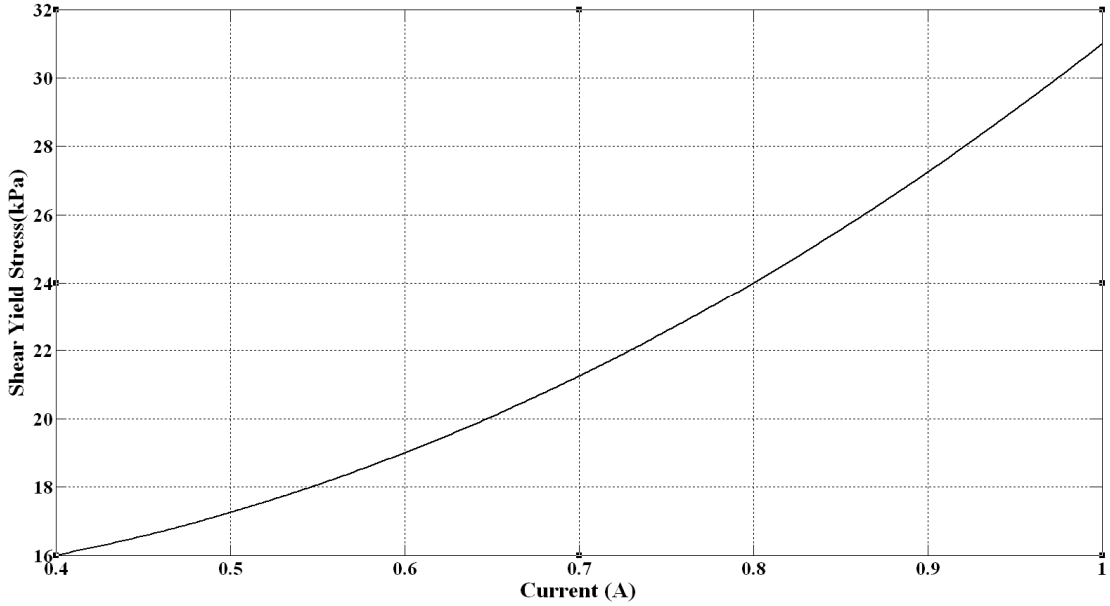

Fig 4.12 Vraiation of yield shear stress for the MR fluid of RD 8040-1 MR damper.

The equation for the yield shear stress as a function of excitation current is given as follows:

$$\tau_0 = 63541 i_c^3 - 104375 i_0^2 + 72833 i_c \qquad (4.2)$$

The second set of experiments were also performed using sinusoidal velocity signal. The first experiment of the second set was performed using 1.25Hz sinusoidal velocity signal.The results for the variation of damper force with dispalcement have been shown in Fig 4.13.

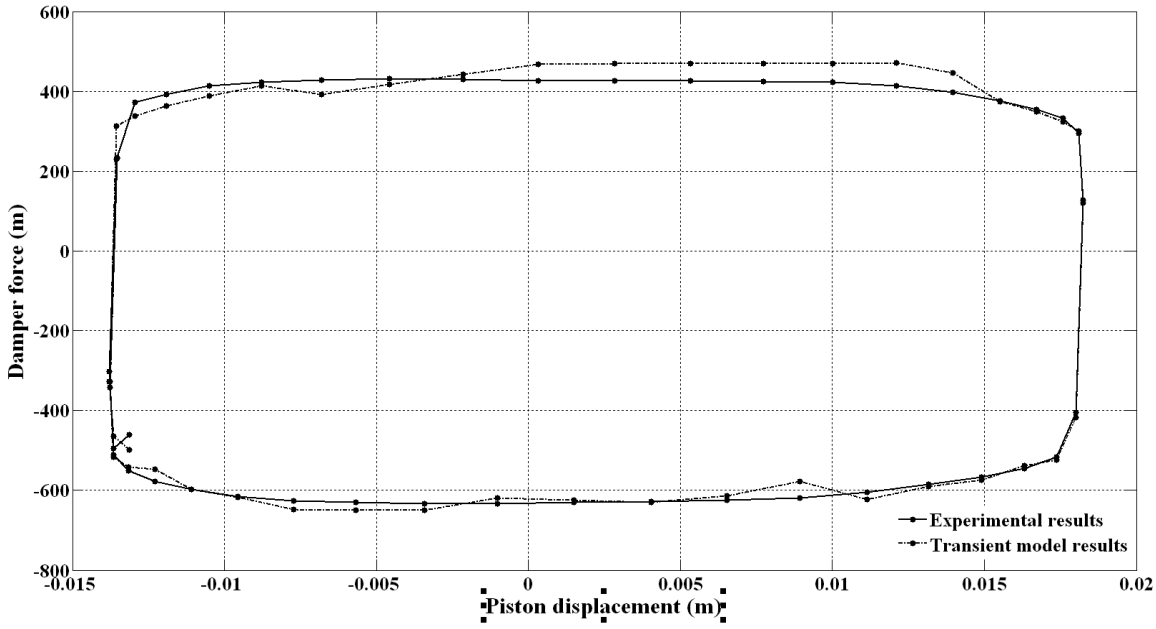

Fig 4.13 Variation of force versus displacement for 0.4A current (yield shear stress of 16 kPa)and 1.25Hz sinusoidal velocity signal.

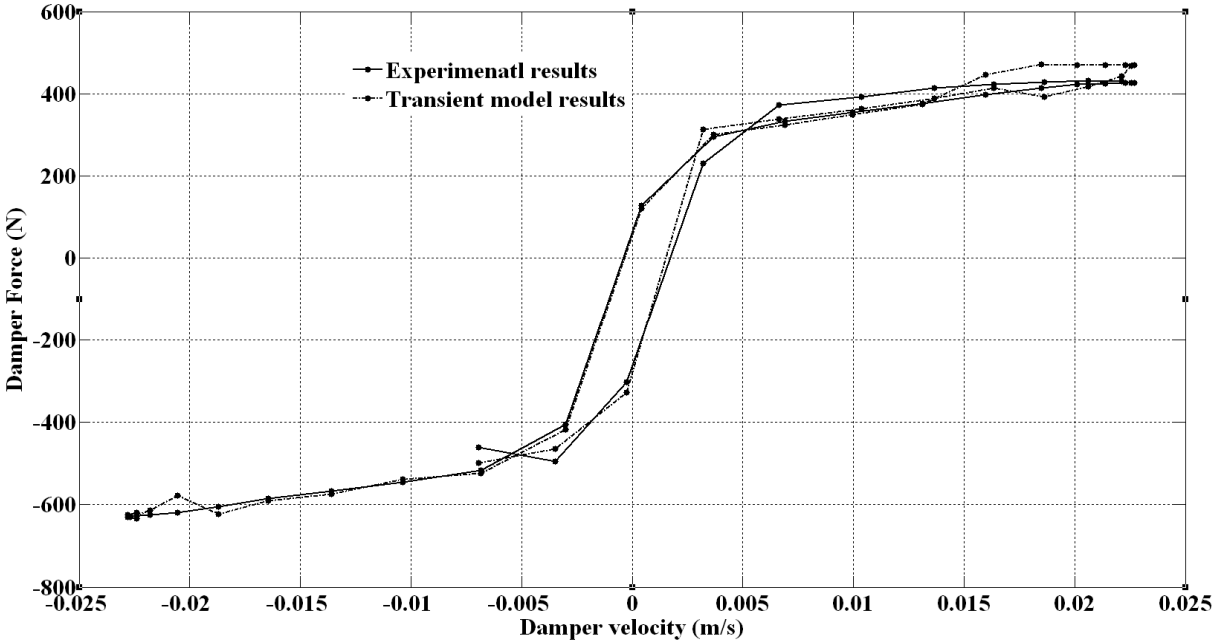

Fig 4.14 Variation of force versus velocity for 0.4A current (yield shear stress of 16 kPa) and 1.25Hz sinusoidal velocity signal.

The variation of damper force with velocity has been shown in Fig 4.14. These results also confirm that the transient model is able to predict the damper force within 5-7% mean error. The next experiment was performed using the vellocity signal of same frequency as the previous one. The damper current was changed to 0.8 A. If the Fig 4.14 and 4.16 are compared with each other it will be noticed that an increase in yield shear stress due to the increase in current leads to an increase in the area of the hysteresis loop. The shape of the hysteresis loop also changes. This is because an increase in yield shear stress results in an increase in plug thickness. Due to the increase in plug thickness the effect of body force is more significant. Similarly the effect of transient boundary condition also becomes significant and swelling of the hystresis loop is also because of transient effects listed in the previous chapter. Curve for the variation of force with displacement is, by and large, symmetric when the damper current was kept at 0.4A. In case of the second experiment with 0.8A current, the force versus dispalcement curve becomes unsymmetric.

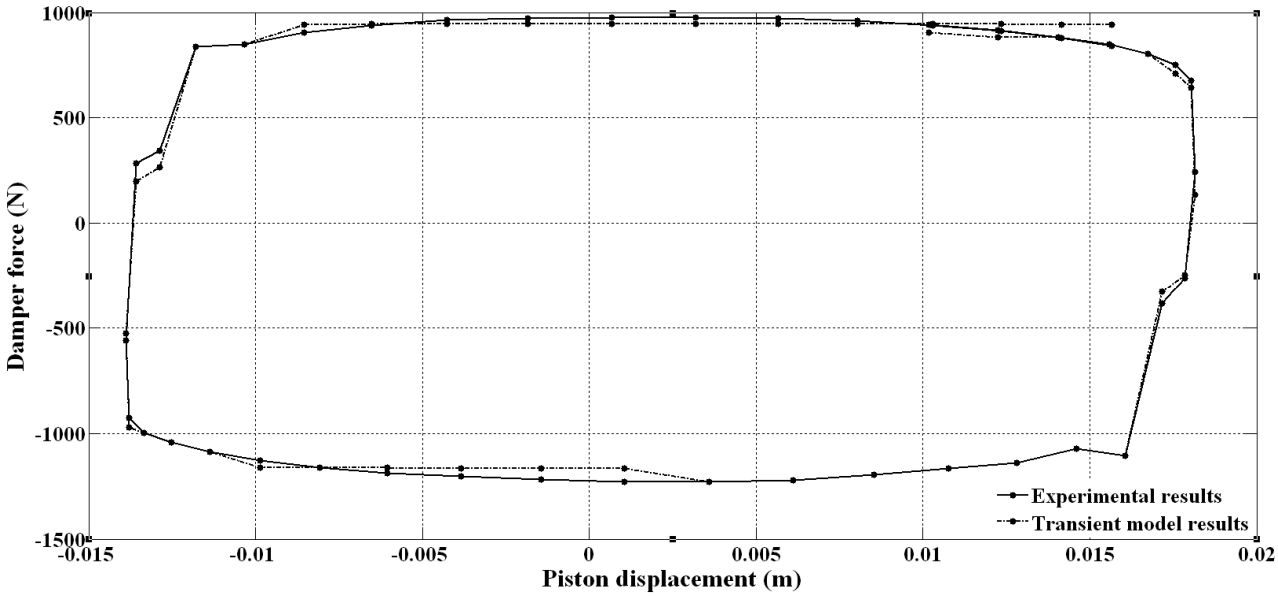

Fig 4.15 Variation of force versus displacement for 0.8A current(yield shear stress of 24 kPa) and 1.25Hz sinusoidal velocity signal.

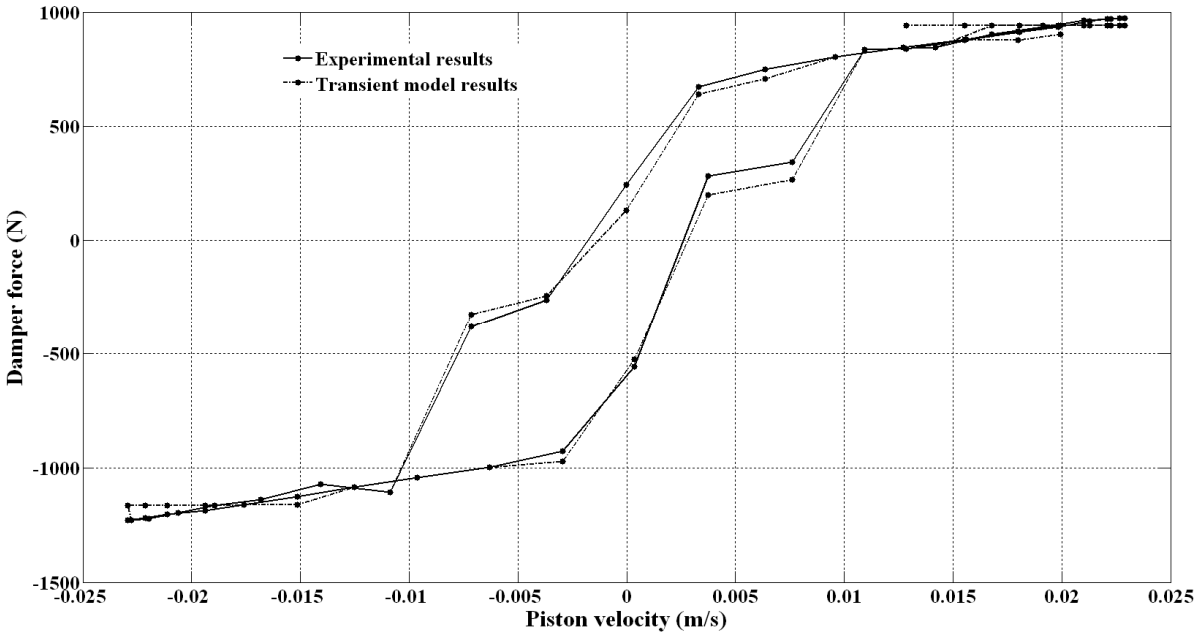

Fig 4.16 Variation of force versus displacement for 0.8A current(yield shear stress of 24 kPa) and 1.25Hz sinusoidal velocity signal.

There were two more experiments conducted with sinusoidal velocity signal of 2.5Hz and 0.56 Hz velocity signals. These experiments were performed for 0.8A and 1A excitation current respectively. The outcome of the comparison of modelling results with the experimental results remains the same as has been discussed previously. At this stage it will be interesting to reexamine all the force velocity curves and discuss the interpretation of the results. If the region of the force velocity curves corresponding to zero or negligible force are examined it will be noticed that for same values of damper velocities the damper force is zero during the up and down strokes of the MR damper. These regions correspond to the operational conditions when the pressure gradient across the flow path is negligibly small. In such a case the flow in the damper channel is purely piston driven flow or a Couette flow. When the piston velocity increases from zero value to the value corresponding to zero damper force, the damper force and damper velocity have opposite sign. In this velocity range the damper either tends to approach the end of the stroke or it just starts the reverse stroke. The pressure gardient in this region is governed by the body forces and the effect of fluid inertia. It can be seen that as the frequency of the velocity signal increases the velocity range for boundary driven flow increases. The combination of low frequency and high yield shear stress results in a significant reduction the range of velocities for which the damper force and damper velocity have opposite sign. If there are significant amount of air bubbles in the damper fluid, the fluid can become more compliant and the above mentioned velocity range can further increase. The results of Sims et al (2000), Batterbee et al (2007) and Wang and Gordaninejad (2007) point to some similar possibility. In Wang and Gordaninejad (2007) it has been mentioned that the presence of air bubbles can reduce the bulk modulus of an MR fluid by two orders of magnitude. This observation is important from the design and manufacturing point of view, because the presence of air bubbles in an MR damper can significantly affect the damper force. Therefore, a good design of MR damper must be least susceptible to the mixing of gas bubbles with the MR

fluid. Therefore the force velocity curves can give a good indication of the presence of gas bubbles in an MR damper fluid.

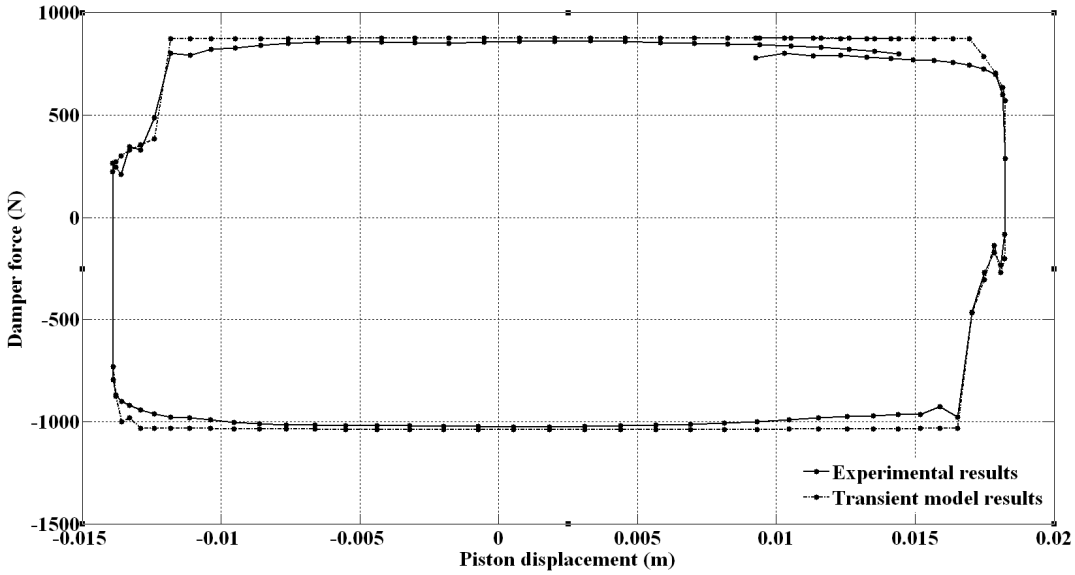

Fig 4.17 Variation of force versus displacement for 1A current(yield shear stress of 31 kPa) and 0.56 Hz sinusoidal velocity signal.

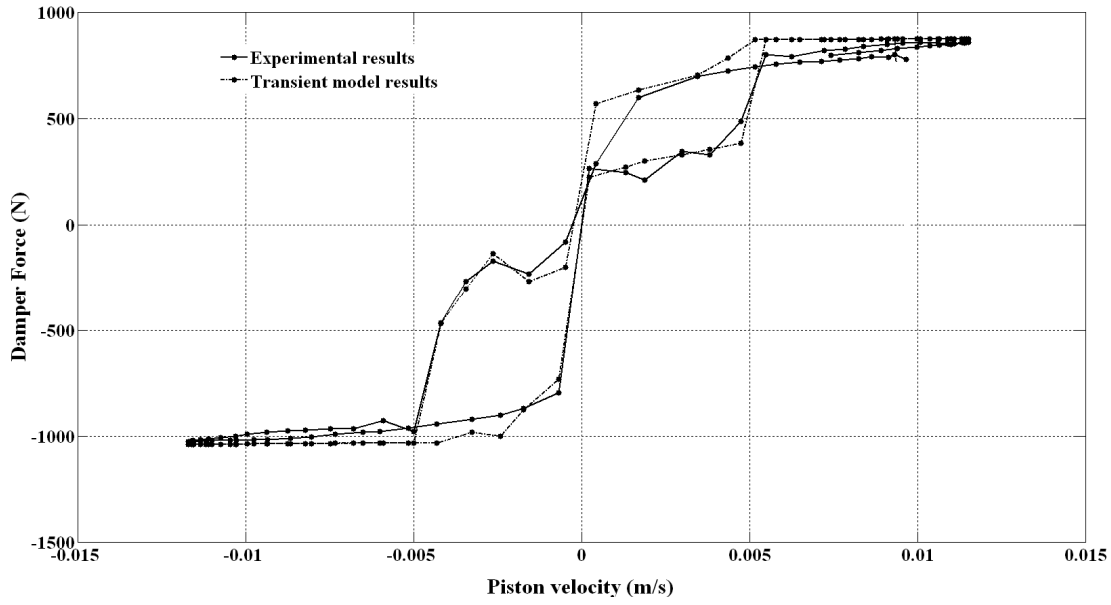

.

Fig 4.18 Variation of force versus velocity for 1A current(yield shear stress of 31 kPa) and 0.56 Hz sinusoidal velocity signal.

4.5 Sources of error in the experiment and modelling

Following the discussion on the experimental and modelling results and the comparison of model with other models it is important to discuss the sources of error for the refinement of the model in future. The major source of error in the modelling that can affect the value of damper force can be during the beginning of damper motion and at the reversal of motion from the extremities of upstroke and down stroke of the damper. The model presented in the present work includes body force with an assumption that the yield shear stress will remain constant even when the fluid is suddenly started from a state of rest or the direction of motion is reversed or it is stopped and restarted. In this regards it must be remembered that the density of the ferrite particles differs from the oil phase by one order of magnitude. As such due to the difference in inertia forces of the two phases there will be an additional interface shear stresses generated which may lead to fragmentation of plug flow. This phenomenon can only be detected by examining the flow of MR fluid through a glass tube and using laser stroboscopic technique. This investigation is presently out of the scope of this work. However it is mentioned that, if this is true then the governing differential equation needs to be modified by replacing or additionally including fractional time derivative for the velocity and the MR fluid will need to be modelled like Oldroyd fluid as has been similarly modelled in Fatecu et al, (2005-2009) and Hayat et al,2005. Another source of error can be due to approximation in dynamics of rig by using sine function for the displacement-time variation for a constant velocity function and numerical error in the solution due to reduced error tolerance for convergence. The other minor sources of error can be due to more number of experiments required to further refine the yield shear stress versus current relationship. The model can be further refined if the behaviour of the seals can be modelled by using suitable Mooney Rivlin model parameters.

4.6 Summary of chapter

This section presents the experimental validation of the model developed in the previous chapter. The comparison of transient model with the experimental data has been presented for sinusoidal velocity signals. The section finally discusses the other sources of errors and proposes further refinement using factional calculus based models.

Chapter 5

Modelling Of Magnetorheological Fluid Based Dampers At High Speed

5.1 Introduction

The modelling of an MR damper at low speed and its experimental validation has led to the conclusion that the compressibility effect, transient boundary condition and the configuration of MR damper play a very important role in the performance prediction of the MR damper. The neglecting of transient effects lead to inaccuracies in the model which have been observed by the previous researchers viz. Kamath et al (1996), Chooi and Oyadiji,(2008), Ikhuane et al (2007), Wang and Gordaninejad (2007), Cesmeci and Tehsin (2010), Dominiguez et al (2004), Gavin et al,(2001), and Norrsi and Ahmedian (2003). The error in the force predicted by the model is significantly higher at low velocities (up to 50%) as compared to peak velocities (2-5%) in the velocity range from 0-3m/s. It is because of this reason that the quasi static model is not able to predict slightly different form of hysteretic variation of force versus velocity than the experimental results. At higher piston speeds the flow in the laminar zones of the channel becomes turbulent. This is likely to erode the plug flow region and significantly reduce the controllability of an MR damper. Therefore there is a need to propose an innovative design in which the flow through the channel(s) remains laminar. This chapter deals with the investigation of an innovative design of an MR damper which can effectively attenuate transient effects and in which the flow of MR fluid remains laminar. The chapter has been organized into four sections. The first section deals with the underlying principle for the design of dampers in general and the need to attenuate the effect of transients in MR dampers. In the second section the design

modification for attenuating the effect of transients and the modelling of the modified design has been discussed. The parametric study of the dual channel has been presented in the third chapter. The fourth section concludes the findings of the design modification.

5.2 Dampers' Theorem

The design of damper plays a very important role in protection of a structure against the time varying loads such as seismic load, road shocks, time varying machinery shock loads etc. An ideal damper should transmit a sufficiently reduced force to the structure which should remain constant throughout the stroke of the damper. This is necessary because if the force transmitted by the damper is not constant then it will result in secondary vibrations of the structure. If the force of the damper is to be kept constant then there can be two situations for complying with this principle, such as a long stroke damper with a small constant force or a short stroke damper with a large constant damper force. In a seismic isolation application the stroke of a damper is limited by the amplitude of the seismic disturbance, the compliances of the structure to be protected from seismic loads and the spatial constraints. In an automobile the damper stroke is limited by the consideration of road clearance, passenger comfort, ease of handling and spatial constraints. In an artillery system design a long damper will results in bulky and heavy structure even if the damper force is reduced due to long stroke. On the other hand a short stroke damper will result in a high value of damper force leading to a heavy gun super structure. Some of the researchers such as Ahmedian and Poynor (2001), have reported that empirically the damper force remains constant throughout the stroke. In a spring mass damper system the functions of a restoring spring are twofold. In the forward stroke it stores about 70% of the energy input to the system and in the return stroke it uses the stored energy to restore the system to the initial position at a desired speed and the remain energy is dissipated with the help of a damper.

Considering that the damper force remains constant throughout the stroke of the damper, there can be more than one curve representing the variation of damper force with the stroke of a damper for a given value of work done by the damper. Therefore, there is a need to propose a suitable principle which leads to a simultaneous minimum of the damper force and the damper stroke. Since the damper stroke and damper force are functions of time, their dot product gives the energy dissipated by the damper together with its restoring spring. Since they obey the Minkowski's inequality and are Lipschitz functions therefore they form a 2D Hilbert space. The definitions of Minkowski's inequality and Lipschitz function are given as follows:

Minkowski's inequality:

Functions *f(x)* and *g(x)* that are well-behaved over an interval [a, b] (i.e. they don't become infinite at some point in the interval)

$$\left|\int_a^b |f(x)+g(x)|^p\,dx\right|^{\frac{1}{p}} \le \left\{\int_a^b |f(x)|^p\,dx\right\}^{\frac{1}{p}} + \left\{\int_a^b |g(x)|^p\,dx\right\}^{\frac{1}{p}} \quad (5.1)$$

where $p \ge 1$ and $f(x) \in \mathcal{H}$ and $g(x) \in \mathcal{H}$

In a metric space this inequality reduces to a triangular inequality.

Lipschitz function:

A function *f* such that

$$|f(x)-f(y)| \le C|(x-y)| \quad (5.2)$$

for all *x* and *y*, where *C* is a constant independent of *x* and *y*, is called a Lipschitz function. For example, any function with a bounded first derivative must be Lipschitz.

To facilitate the understanding of the Hilbert space the definition and properties of Hilbert space are produced below, Kreyszig, (2004):

For all scalars q_1,q_2,vectors **a**,**b**,**c** in $\mathcal{H}$

$$(q_1 \boldsymbol{a} + q_2 \boldsymbol{b},\boldsymbol{c}) = q_1 (\boldsymbol{a},\boldsymbol{c}) + q_2 (\boldsymbol{b},\boldsymbol{c}) \qquad \text{(linearity)}$$

For vectors **a**,**b** in $\mathcal{H}$

$$(\boldsymbol{a},\boldsymbol{b}) = (\boldsymbol{b},\boldsymbol{a}) \qquad \text{(symmetry)}$$

For every vector **a** in $\mathcal{H}$

$$(a,a) \geq 0$$

$$(\boldsymbol{a},\boldsymbol{a}) = 0 \quad \textbf{\textit{iff}}\ \boldsymbol{a} = 0 \qquad \text{(positive definitenesss)}$$

$$\|\boldsymbol{a}\| = \sqrt{(\boldsymbol{a},\boldsymbol{a})} \qquad (\geq 0) \qquad \text{(definition of norm)}$$

$$|(\boldsymbol{a},\boldsymbol{b})| \leq \|\boldsymbol{a}\|\ \|\boldsymbol{b}\| \qquad \text{(Schwartz inequality)}$$

$$\|\boldsymbol{a}+\boldsymbol{b}\| \leq \|\boldsymbol{a}\| + \|\boldsymbol{b}\| \qquad \text{(Triangle inequality)}$$

With the above definition of a Hilbert space the theorem for damper can be stated as follows (Bhatnagar, (2005)):

Theorem*: Simultaneous minimum of damper force and damper stroke can be achieved if the perimeter of the curve representing the variation of the damper force and damper stroke, in the Hilbert space ($\mathcal{H}$), is minimum.*

The proof of this theorem has been given in Bhatnagar, (2005). Based on the above theorem the generalised form of the curve representing the variation of damper force versus damper stroke is given in Fig 5.1

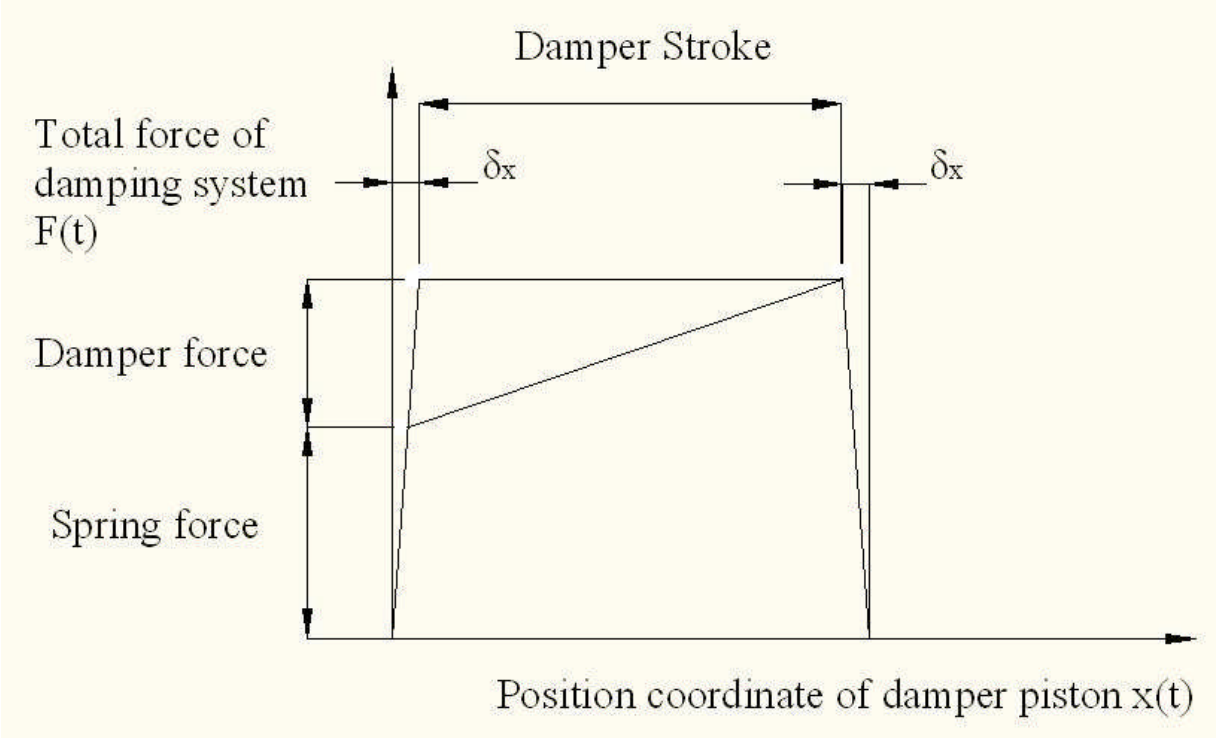

Fig 5.1 Generalised curve for the variation of damper force versus stroke.

The above theorem was developed for the gun recoil dampers, but it may be applicable to the dampers similar applications. In an automobile damper or a seismic damper or a vibration isolation damper for machine foundation the damping force varies as a function of velocity of sprung mass relative to the un-sprung mass. For instance in the automobile suspensions the minimisation of accelerations of sprung and un-sprung masses are the prime consideration for the suspension design and as such the application of the above principle may be detrimental to the suspension design. Such applications are more appropriately dealt using skyhook or ground hook or hybrid control strategies. The above applications are under-damped oscillating systems. An aircraft undercarriage damper or a gun damper is required to transmit reduced force to the structure without undergoing oscillations and as such these systems are over-damped systems.

Based on the above discussion it is concluded that the above theorem provides a reference model for the control of damper based on model reference control system for impact absorption applications.

5.3 Design and modelling of a high speed damper

The design, modelling and testing of MR dampers at high speed have been studied by Dug et al, (2002), Mao et al, (2007), Gordaninejad et al, (2004), Batterbee et al, (2007), Nguyen et al, (2009). In these papers the MR dampers either have flow paths as annular flow path between the piston and cylinder or flow path embedded in the piston. In the papers of Facey, et al,(2004), and Gordaninejad, et al,(2004) the MR damper designs the fluid displaced by the piston flows through the bypass annular duct. In case of MR damper design with flow paths embedded in the piston there are following fluid transients in the MR fluid flow:

Major components of transient effects:

(1) Transients due to the fluid inertia.

(2) Transients due to the transient velocity boundary condition, which is applied to the solution by Duhamel's superposition.

(3) Compressibility effects.

While the significance of compressibility effects have been pointed out by Sims et al (2000), Batterbee et al (2007) and Wang and Gordaninejad (2007), the possibility of the significance of transient effects due fluid inertia has been pointed out in Batterbee et al (2007,1&2), Sims(2000) and Peel and Bullough (1994).

Minor components of transient effects:

(1) Damper pressure dependent sealing friction.

(2) Transient electromagnetic response of the electromagnetic coils.

(3) The geometry of flow path is an idealized form of actual geometry (Batterbee et al (2007,1&2), Sims (2000)). This factor can contribute to the variation in steady state and transient response.

At high speed these transients have been observed to give force spike in the beginning of the damper stroke, Ahmedian and Poynor (2001), Gordaninejad et al (2004). The experimental results presented in chapter 4 for MR dampers, at low speeds, show force spike. In case of MR damper with bi-fold type geometry outlined in Facey et al, (2004) the variation of damper force due to transient velocity boundary condition will not be observed. This is for the obvious reason that there are no time varying wall velocity boundary conditions. In case of MR dampers with flow paths coupled to the piston geometry or embedded in the piston there is a limited scope of attenuation of fluid transients at high speed. At this stage it is also necessary to recall the definition of dynamic range of a MR damper. The dynamic range for a MR damper as defined in (Yang et al, (2002)) is given as follows:

$$D = \frac{F_{\eta} + F_f + F_{\tau}}{F_{\eta} + F_f} \tag{5.1}$$

In the above equation F_{η} is the force due to viscosity of the fluid, F_f is the friction force and F_{τ} is the force due to shear yield stress of MR fluid. This definition of dynamic range is good for a quasi static model. However, from the modelling and experimental results presented in the previous two chapters this definition of dynamic range may be required to be modified, as there can be an error of at least 10% in the estimate of dynamic range if the transient effects are not included. The sum of non controllable components in the above expression of dynamic range does not include the transient components. If the transient component is included in the expression for the dynamic range, the modified expression is given as follows, Fig 5.2:

$$D = \frac{F_{\eta} + F_f + F_{tr} + F_{\tau}}{F_{\eta} + F_f + F_{tr}} \tag{5.2}$$

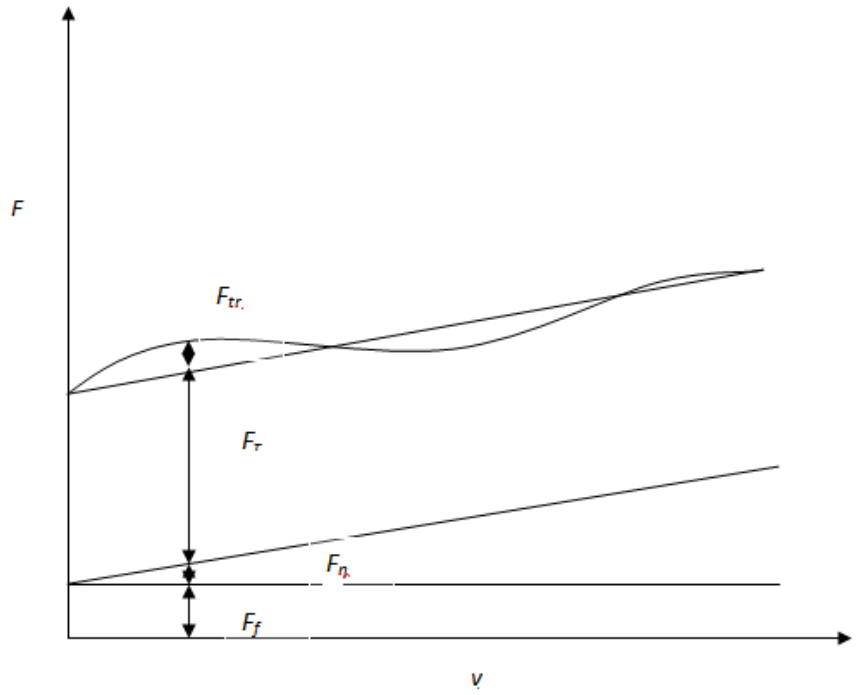

Fig 5.2 Illustration of components of damping force for an MR damper.

In the above expression F_{tr} is the transient force. In the figure above it can be seen that the transient force corresponding to the shear yield stress given value of has been considered. This is because the transient component of damper force will be different at different value of shear yield stress. It is for this reason that the transient component of damping force corresponding to the off state has not been shown. From the above expression it is clear that the dynamic range is significantly reduced due to transient effects. At the maximum value of yield shear stress and maximum piston velocity the transient effects are significant as seen from Fig 3.10a-b in chapter 3. The design of MR damper can be evaluated based on two important parameters viz. controllable force and the dynamic range. The controllable force can be

increased by reducing the gap of the annulus. This is because if the gap of the annulus is reduced the velocity of flow through the annulus will increase leading to an increase in the pressure drop and hence increase in the controllable force. If the gap is reduced the controllable force will increase leading to the increase in transient components and viscous force components. This will lead to the reduction in dynamic range. The controllable force and the dynamic range are significantly affected by the configuration of the MR damper. The MR dampers with flow path associated with the piston or flow path embedded with the piston as studied in Dug et al (2002), Mao et al (2007), Gordaninejad et al (2004), Batterbee et al,(2007), Nguyen et al (2009), have following characteristics:

(1) Large controllable force due to the increase in pressure drop. This is because the flow velocity has relative velocity component of the piston velocity for a given volume of MR fluid exposed to magnetic field.

(2) Low dynamic range because of transient forces due to fluid inertia, transient velocity boundary condition, sealing friction force variation and compressibility effects.

The MR dampers with piston driven flow through the annulus of the concentric cylinders such bi-fold design due to Facey et al (2004), have following advantages:

(1) Lower controllable force for the same volume of MR flow exposed to the magnetic field as in case of MR damper with piston with magnetized flow paths.

(2) Higher dynamic range because of components of transient forces is less in this case as compared to MR damper with piston with magnetized flow paths.

In all of the above works the validity of laminar flow assumption for high piston velocities has not been discussed. In chapter 3 the validity of laminar flow assumption was studied using the method of calculation of critical Reynolds number based on the correlations

given by Nouar and Frigaard (2001). In this section the same correlations have been used to show the variation of critical Reynolds number with piston velocity for an area ratio of 12.5 and 1mm annular flow gap. Here it is recalled, that the area ratio is defined as the ratio of piston area to the area of the channel for the flow of magnetised MR fluid. At higher area ratio the critical Reynolds number decreases rapidly and flow in the channel becomes turbulent. The annular gap has been taken as 1mm because the critical Reynolds number decreases with the decrease in the size of the gap. At higher value of the size of annular flow gap the condition of uniformity of magnetic flux may not be achievable and the assumption of constant shear yield stress across the depth of the annular flow channel may not hold good. If the above considerations are taken into account the variation of the critical Reynolds number with the piston velocities and shear yield stress is given as follows:

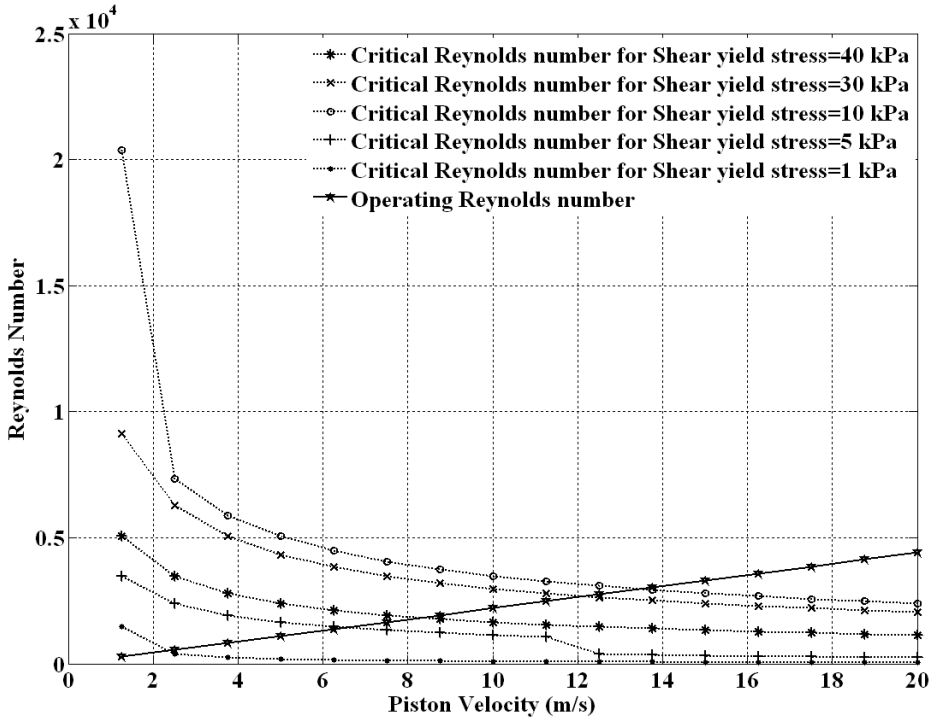

Fig 5.3 Variation of critical Reynolds number and operating Reynolds number for a damper with an annular flow gap of 1mm and area ratio of 12.5.

Considering the above results it is observed that the existing design of MR damper will have turbulent flow at high speed. There will also be a limitation of the piston diameter because the critical Reynolds number rapidly decreases with the increase in area ratio. Based on the above results a mono-channel type MR device is not suitable for high speed applications if the flow is required to be laminar. It is for this reason that the simulation results for the model derived in chapter 3 have not been presented for piston velocities beyond 1m/s. This is because of following reasons:

(1) The effect of magnetic field on turbulent flow vortices would require additional body force to be taken into account due to the presence of magnetic moments. This will also affect the shear stress of the MR fluid.

(2) The combination of fluid transients due to inertia effects and turbulent flow may result in an almost unpredictable change in plug flow thickness. The plug flow may or may not exist. In the turbulent flow regime the effect of pre yield shear stress is negligible (Hedstrom (1952)) and so the governing equation will not be valid.

(3) The dynamic range of the damper will also be affected by the effect of turbulence. This is because the turbulence will additionally contribute to the non controllable damper force.

(4) The development of correlations for the correction factor will require an elaborate experimentation for establishing the validity over wide range of area ratios and piston velocities.

(5) If the plug flow and turbulent flow exist at the same time in the channel then the turbulent flow will be bounded by two laminar sub layers. One of the laminar sub layers will be in vicinity of the wall and the other one will be in the vicinity of the plug. In such a case the governing differential equation will be non-linear in the sheared region.

In case of ER dampers the density of the ER fluid is around 1600 kg/m^3 and the values of the shear yield stress are in the range of 0.1 to 5 kPa and so the range of piston velocities will be almost same or slightly better than the range of piston velocities for the MR dampers. Since the damper force for an ER damper is lower than an MR damper of same area ratio therefore an ER damper may have turbulent flow for same damper force because the area ratio of an ER damper will be higher than comparable MR damper. Therefore a high speed damper design must have a high value of Bingham number and a low value of operating Reynolds number over wide range of shear yield stress. Another common drawback of the mono-channel design is that they have a single degree of freedom of control. Therefore there is a need to propose a design which can enable the reduction in transient effects by reducing the yield shear stress and at the same time achieve high dynamic range and controlling force. Based on the above discussion it can be gathered that this design problem involves the resolution of multiple conflicting requirements. All these objectives can be achieved if the design of damper uses a combination of piston embedded flow path and a piston driven annular flow path between two concentric cylinders. The splitting of the flow will result in an increase in Bingham number and also a reduction in the operating Reynolds number. The proposed design modification will additionally give an increase in the volume of MR fluid under the influence of magnetic field and an additional degree of freedom to change the yield shear stress of the outer channel to attenuate the pressure fluctuation due to transient effects. The proposed modification can be investigated in many different configurations for selecting the best design. However, the present work aims to outline the basic concept evolved by seeking the solution on the lines of the concept of compounding of hydraulic dampers for high speed applications (ref: Annexure-I, Section A.1.2.4). In a compounded damper there is

a bifurcation of the flow of damper fluid, displaced by the piston, to a variable area orifice and a pilot valve controlled orifice. The model of the proposed design of a dual channel is based on following assumptions:

(1) The pressure gradient is same in both the flow channels.

(2) The effect of the current transients is negligible as the response time of the electromagnetic coil can be reduced to less than 10 milliseconds and so the transient effect due to the time dependent shear yield stress can be made negligible.

(3) The pressure gradients in the un-magnetised region of fluid flowing ahead of the piston are negligible.

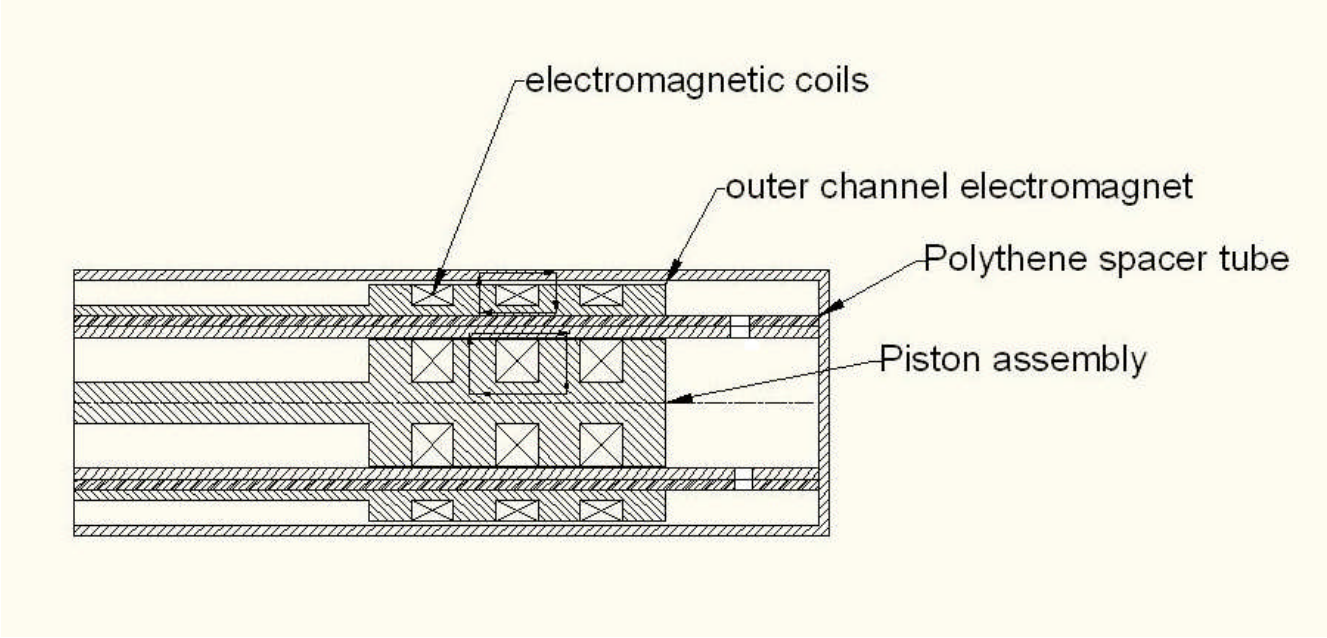

Fig 5.4 Proposed geometry of MR damper with dual passages.

The first assumption is valid if the flow path lengths are same for both the passages and this is actually done to simplify the solution. In an actual situation the flow path lengths should be one of the tuning parameters for such a design. In this work only the fundamental design is proposed with limited parametric study. The second assumption can be made valid if the response time of the electromagnetic coils can be limited to within 7 milliseconds. The third assumption is justified because the pressure drop due to the magnetised fluid flow is at least one order of magnitude greater than the pressure drop due to the flow of MR fluid through un-magnetised regions due to viscous effects. It is for this reason that if the transient effects are neglected it would result in an over prediction of dynamic range.

5.3.1 Solution algorithm

The computational domain for the above mentioned geometry of the MR damper is shown in Fig 5.5.

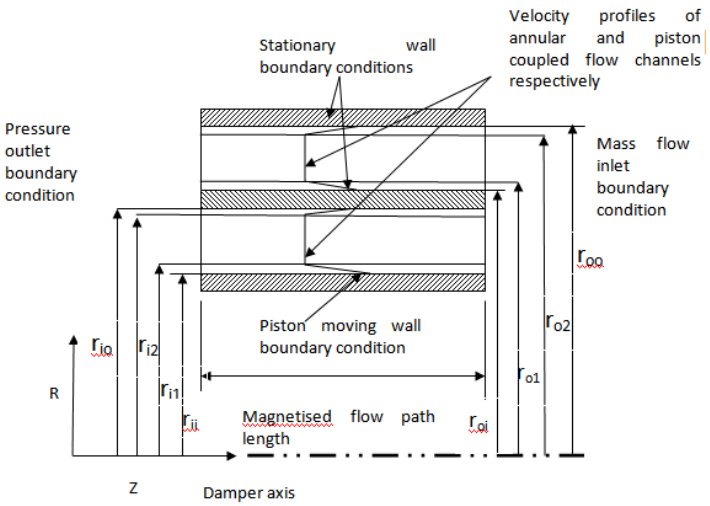

Fig 5.5 Computational domain of the dual flow MR damper showing velocity profiles, plug flow boundaries and boundary conditions for piston coupled flow channel (piston channel) and annular channel or bypass channel.

The equations for the velocity for the laminar sub-domains of the dual flow MR damper remain the same as outlined in Chapter 3. The algorithm can be simplified for improving the computational efficiency. However, in this work the code development has been minimised for the purpose of complying with the time constraints. Therefore in this section a split flow type Newton Raphson based solution scheme has been proposed. The velocity compatibility conditions for plug flow boundaries of inner and outer sub-domains of the MR damper computational domain are given by Eq 5.4. In the equation below the subscript *j* stands for inner (*i*) and outer sub-domains (*o*) indicated in Fig 5.5.

$$f_{1,j} = u_x\big|_{r=r_{1j}} - u_x\big|_{r=r_{oj}} = 0 \text{ For, } j = i, o \qquad (5.3)$$

The equation of mass flow balance is obtained by considering that the fluid displaced by the moving piston gets divided into inner and outer sub-domains by the fractions α_i and α_o respectively. The fraction α_i and α_o obey the following relationship:

$$f_{4,j} = \alpha_i + \alpha_o - 1 = 0 \qquad \text{for, } j = i, o \qquad (5.4)$$

The equations for mass flow balance for the two sub-domains are given as follows:

$$f_{2,j} = \int_{r_{ij}}^{r_{1j}} 2\pi r u_x dr + \pi(r_{2j}^2 - r_{1j}^2)u_x\big|_{r=r_{1j}} + \int_{r_{2j}}^{r_{oj}} 2\pi r u_x dr - \pi r_{ii}^2 u_p \alpha_j = 0$$

$$\text{For, } j = i, o \qquad (5.5)$$

The symbols in the above equation have been shown in Fig 5.5. The third equation is obtained by considering the equilibrium of forces in the plug flow region.

Since the model accounts for transient effects therefore there will be an additional inertia force acting in the plug flow region due to change in flow velocity. Therefore the equation of equilibrium of forces for the two sub-domains is given as follows:

$$f_{3,j} = 2\tau_{0,j} - (\left(\frac{dp}{dx}\right)_j + a_{p,j}\left(r_{2j} - r_{1j}\right)) + \left(r_{2j} - r_{1j}\right)\rho \frac{\partial u_x}{\partial t}\bigg|_{r=r_1,j} = 0$$

For, $j=i,o$ (5.6)

In the Eqs above $f_{1,j}$ is the velocity compatibility function for the j^{th} sub-domain (here ith subdomain is for the piston channel flow path and o^{th} subdomain is for the outer flow path or the bypass flow path), $f_{2,j}$ is the mass flow balance function for the j^{th} sub-domain, $f_{3,j}$ is the equilibrium of force function for the j^{th} sub-domain, $\tau_{py,j}$ is the shear yield stress for the j^{th} sub-domain, $(dp/dx)_j$ are the pressure gradients of the respective subdomains, ρ is the density of the MR fluid, r is the radial coordinate , $a_{p,j}$ is the acceleration of the piston or relative acceleration of the outer cylinder and u_x is the velocity of MR fluid in the x direction through the annular sub-domain concerned. At this stage it is mentioned that for the outer flow channel the term for the piston acceleration will not be applicable. However if the outer cylinder is attached to a moving support then the value of $a_{p,j}$ will be corresponding to the acceleration of the cylinder for the outer channel. The solution vectors for the above computational domain divided into inner and outer sub-domains are given as follows:

$$\mathbf{x}, _j = \begin{Bmatrix} r_{1,j} \\ r_{2,j} \\ \left(\frac{dp}{dx}\right)_{,j} \\ \alpha_j \end{Bmatrix} \quad \text{for } j=i,o \qquad (5.7)$$

The constraints for the solution vector are as follows:

$$
\begin{aligned}
& r_{i,j} < r_{1j,}, \\
& r_{i,j} \le r_{1,j} \le (r_{o,j} + r_{i,j})/2.0, \\
& (r_{o,j} + r_{i,j})/2.0 \le r_{2,j} \le r_{o,j} \qquad \text{for } j=i,o \qquad (5.8) \\
& \left(\frac{dp}{dx}\right)_i = \left(\frac{dp}{dx}\right)_o
\end{aligned}
$$

The Jacobean for each computational sub-domain is given as follows:

$$
\mathbf{J}_{,j} = \begin{bmatrix}
\frac{\partial f_{1,j}}{\partial r_{1j}} & \frac{\partial f_{1,j}}{\partial r_{2j}} & \frac{\partial f_{1,j}}{\partial\left(\frac{dp}{dx}\right)_j} & 0 \\
\frac{\partial f_{2,j}}{\partial r_{1j}} & \frac{\partial f_{2,j}}{\partial r_{2j}} & \frac{\partial f_{2,j}}{\partial\left(\frac{dp}{dx}\right)_j} & 0 \\
\frac{\partial f_{3,j}}{\partial r_{1j}} & \frac{\partial f_{3,j}}{\partial r_{2j}} & \frac{\partial f_{3,j}}{\partial\left(\frac{dp}{dx}\right)_j} & \frac{\partial f_{3,j}}{\partial \alpha_j} \\
0 & 0 & 0 & \frac{\partial f_{4,j}}{\partial \alpha_j}
\end{bmatrix} \qquad (5.9)
$$

$$
\mathbf{x}_{i+1,j} = \mathbf{x}_{i,j} + \mathbf{J}^{-1}\mathbf{f}_{,j} \qquad (5.10)
$$

for $j=i,o$

The algorithm for obtaining the solution vector is given as follows:

(1) for $j=i,o$ subdomains, set an initial value of $\boldsymbol{x}_{i,j}$ which is compliant with the constraints Eq 5.8.

(2) Calculate at least the first 20 roots of following characteristic equations:

$$
\varphi_1|_{r=r_{1,j}} = 0 \qquad (5.11)
$$

$$\varphi_2|_{r=r_2,i} = 0 \tag{5.12}$$

(3) Calculate $\mathbf{x_{i+1,j.}}$

(4) If all the elements of the function vector at $\boldsymbol{x}_{i+1}$ are less than the convergence criteria then $\boldsymbol{x}_{i+1}$ is the solution vector and the iterations are stopped.

(5) Else, set $\boldsymbol{x}_{i,j} = \boldsymbol{x}_{i+1,j}$ and repeat the steps 1-5 for each sub domain *i, o* till the convergence is achieved.

The convergence criterion is given as follows:

$$e = \sqrt{\sum_{j=i}^{o}\sum_{k=1}^{3} f_{k,j}^2} \le 1e-3 \tag{5.13}$$

Based on the above model the expressions for the Bingham number and the operating Reynolds number for the inner channel and outer channel are given as follows:

$$Bi = \frac{\tau_{0,j}\left(r_{2j} - r_{1j}\right)}{\mu_{py}\,\overline{A}_j u_p} \quad \text{(Mao et al (2005))} \tag{5.14}$$

$$\overline{A}_j = \frac{\alpha_j r_i^2}{(r_{2j}^2 - r_{1j}^2)} \tag{5.15}$$

$$\mathrm{Re}_{aj} = \frac{2\rho\overline{A}_j u_p \left(r_{2j} - r_{1j}\right)}{\mu_{py}} \tag{5.16}$$

The correlations for the critical Reynolds number are given in Chapter 3 Eq3.5. Although above proposed design has been developed based on the implementation of concept of compounding of hydraulic damper there are similar designs proposed by Gavin (2001) and Kuo et al (2006). The Gavin (2001) work describes a generalised design of an electrorheological damper with concentric ducts which are arranged in a series and parallel configuration. In Kuo et

al (2006) paper an ER damper with serially connected ducts has been discussed. The objective of both the designs is to increase the dynamic range by increasing the volume of field controlled fluid channel. In both the cases, the fluid that is displaced by the piston flows through the bypass ducts. On the other hand the proposed design attempts to achieve a compact design by combining the piston channel and a bypass channel. This is because the flow channel embedded in the piston or coupled to the piston as an annular flow path can give a higher pressure drop as compared to the bypass channel. This is because of higher wall shear stress due to the piston velocity. If the transient effects are considered for the cases of the above designs of dampers the multi duct and serial duct type dampers have transients due to fluid inertia and compressibility. But in the case of compounded type damper proposed in this work there will be additional transient due to transient wall boundary condition due to the variation of piston velocity with time. The effect of time varying boundary condition can also be there in multi-duct and serial duct designs of dampers as it depends upon the type of application. Based on the application there can be three cases of the combination of transient and steady wall boundary conditions. These are given as follows:

(1) Steady wall boundary condition: This can prevail in an application for a gun damper where the damper has a bypass channel and the fluid that is displaced by the piston flows through the channel.

(2) Transient and steady wall boundary condition: if the flow channel is an annulus between the cylinder and piston such that the cylinder is attached to the structure of the gun and piston is coupled to the recoiling gun, then the piston wall of the channel will have a transient wall velocity boundary condition and the cylinder will have a zero velocity boundary condition.

(3) Transient wall boundary condition: In case of dampers for an automobile suspension or an aircraft under carriage the piston and cylinder have independent degrees of freedom of linear motion. In such a case the piston and cylinder will have transient wall velocity boundary conditions for the case of a compounded damper design. In case of a multi-duct design or serial duct design there will be transient wall boundary conditions due to the velocity of the cylinder relative to the direction of the flow of fluid.

In all the above cases the body force will also be required to be taken into account. Considering the above three cases of boundary conditions a combination of ducts is required to attenuate the transient effects. The basis for the development of a compounded design is that if the combinations of flow path lengths and shear yield stresses for two channels can result in a minimum fluid transient then it can lead to the attenuation of transients. This design will require a suitable optimisation scheme for its implementation. This scheme will be proposed in the following chapter. Another more important consideration for the compounding is that at high piston velocity the flow of MR fluid, through the channel of a single channel MR damper, becomes turbulent (as shown in Fig 5.3). The laminar to transient flow transition in the channel of an MR damper can be prevented if the Bingham number is increased and the operating Reynolds number is decreased. This can be achieved by reducing the area ratio, increasing the shear yield stress and decreasing the density of an MR or ER fluid. Here it is once again mentioned that at high area ratio the velocity of fluid in the channel is high and so it results in an increase in operating Reynolds number in a single channel damper. Since the density of ER fluids is in the range of 1100 to 1600 kg/m^3 therefore if the area ratio of an ER is not more than 12.5 the operating Reynolds number will be lower than critical Reynolds number for low piston

velocities. But because the shear yield stress of ER fluids is one order of magnitude less than MR fluids therefore the flow in the channel of an ER damper can be turbulent if the area ratio is higher than 12.5. For the same damper force the area ratio of an ER damper will be more than the area ratio for an MR damper. Therefore the ER dampers will have turbulent flow at high speed. Based on these considerations the use of a multi duct design or compounded design can be an effective way of ensuring laminar flow regime in the flow channels over a wide range of piston velocities.

The volume of space occupied by the electromagnet coils in an MR damper is more than volume of space occupied by the electrode of an ER damper so a multi duct design is suitable for ER dampers for achieving high dynamic range and high damper force. The fluid velocity in the individual duct of an ER damper will be less than the fluid velocity in a single duct ER damper. As such a multi-duct design can be effective in preventing laminar to turbulent flow transition at high piston velocities. However, the addition of number of concentric also has a limitation. For the same size of annular gap and shear yield stress the flow areas of the outer ducts are more than the flow areas of the inner ducts. Therefore, the flow fractions, of the total fluid displaced by the piston, for the outer ducts are more than the flow fractions for the inner ducts. This may result in a situation in which the flow rates of ER fluid flowing through the inner ducts are much smaller as compared to the flow rates of ER fluid through the outer ducts. In such a case the inner ducts may not significantly contribute to the damper force. Thus the use of large number of ducts may follow a law of diminishing return. Since the MR fluid can achieve higher values of field controllable shear yield stress therefore the concept of compounding, as proposed in this work, will results in a compact design of damper with only one bypass duct and will permit laminar flow of MR fluid at higher piston velocities. The complexity of computation for predicting the

pressure gradient increases with the increase in the number of ducts and it also results in more number of degrees of freedom for the applied electrode voltages for controlling the shear yield stress.

5.4 Parametric study

The parametric study has been presented in this chapter with an objective to show that the use of an outer channel or a bypass channel, operating at a lower value of shear yield stress as compared to the piston channel, can operate at laminar flow condition at high speed and also attenuate the transient effect due to fluid inertia. In this section the curves for the transient response through the time range for 10^{-8} seconds to 10^{-1} seconds have not been presented as this does not reveal as significant information as the study of variation of pressure gradient with velocity at 10^{-1} seconds and 10^{-4} seconds. In this investigation the transient response has been studied at 10^{-4} seconds, because the experimental studies are usually done at the sampling rate of this order magnitude of time and this is adequate for the control system development. As the transient response time tends to increase towards values greater than or equal to 1sec., the response of MR fluid flow tends to become quasi static. This is because the roots of the Bessel's characteristic equation are significantly greater than 1. The transient response study at 10^{-4} seconds is further justified because the response time for MR fluid is around 10^{-4} seconds and for the electromagnetic coil it can be around 10^{-3} seconds, and so even if the response of MR fluid flow is considered at a time step lower than 10^{-5} seconds the system will be unable to respond to control input for attenuating the fluid transient by changing the shear yield stress. The verification of the effectiveness of the damper design to attenuate the fluid transient will require an elaborate experimental trial with the different designs of electromagnets for the piston channel and bypass channel. The parametric study in this section considers 4 x 4 levels of variation in

shear yield stress of the piston channel and the bypass flow channel i.e. 10 kPa, 20 kPa, 30 kPa and 40 kPa for transient model simulation at 10^{-4} seconds and quasi-static. The other input data is given as follows:

Diameter of the piston =55mm

Diameter of the piston housing cylinder =57mm.

Width of piston channel =1mm.

Outer diameter of the inner cylinder for bypass flow=68mm.

Inner diameter of the outer cylinder for bypass flow=70mm.

Width of outer bypass channel=1mm.

The flow path lengths for piston channel and outer-bypass channel have been taken as 40mm. In this study the variation of pressure gradient with piston velocity has been presented at fixed value of yield shear stress has been presented. The validity of laminar flow assumption has been shown by presenting the variation of critical and operating Reynolds number for each of the above mentioned results. Although the above set of parameters give a good performance in terms of attenuation of transient effect and a compact geometry of the damper the parameters can be further tuned if the flow path lengths of the channels are varied or if the diameter of the outer flow channel can be increased. These modifications can potentially ensure that the flow is laminar for piston velocities up to 20m/s. The design has been studied for variation of parameters at piston velocities greater than or equal to 1m/s per second to demonstrate the validity of laminar flow at higher piston velocities.

With the above background the stage is set to present the parametric study for the response of dual channel MR damper to the variation of shear yield stress at different piston velocities. If the shear yield stress of the MR fluid flowing through the outer bypass channel is

kept constant at 10 kPa and the yield shear stress of the MR fluid, flowing through the piston channel, is varied from the 10 to 40 kPa, the variation of pressure gradient with piston velocity given in Fig 5.6. From the Fig 5.6 it can be seen that the at low piston velocities in the range of 1-2.5 m/s the increase in pressure gradient with shear yield stress for MR fluid flowing through the piston channel, is not significant. This is because the two channels have same resistance to the fluid flow at low piston velocities. The transient effects are more significant when the shear yield stress of the piston channel is 10 kPa. The error bars show the expected variation of the pressure gradient due to transient effects. The curves for the variation of pressure gradient with velocity are not obtained as straight line as is the case for a mono channel damper. The curves for the variation of critical Reynolds number and operating Reynolds number with piston velocities (fig 5.7) show that the flow through the piston channel becomes turbulent as the piston velocity exceeds 14m/s if the values shear yield stress of MR fluid, in the piston channel, is in the range of 10 to 30 kPa. If the shear yield stress of MR fluid is 40 kPa the flow is laminar upto 18m/s (see Fig 5.7).

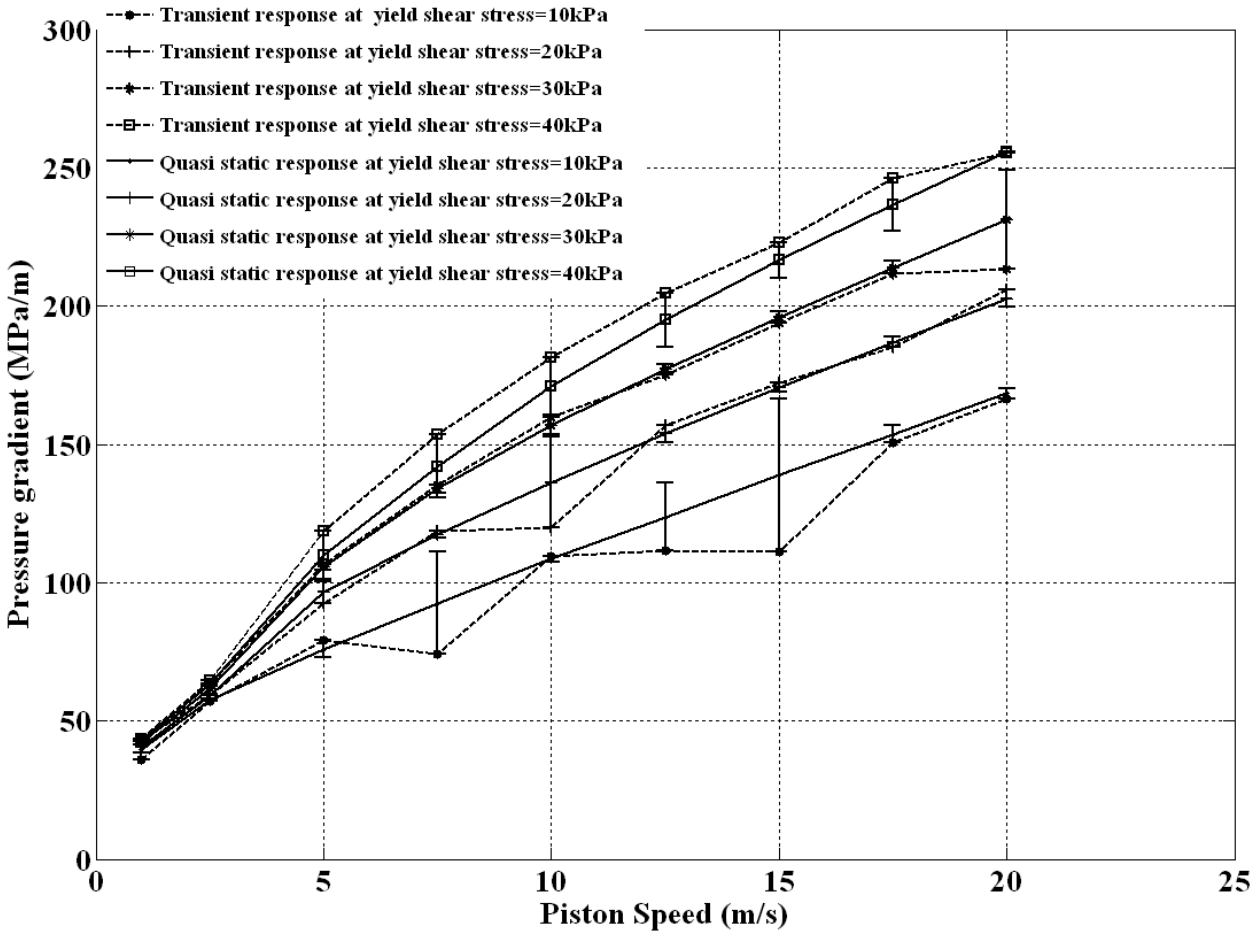

Fig 5.6 Variation of pressure gradient with piston velocity for different values of shear yield stress of MR fluid flowing through piston channel, and at shear yield stress of 10 kPa for MR fluid flowing through the outer bypass channel.

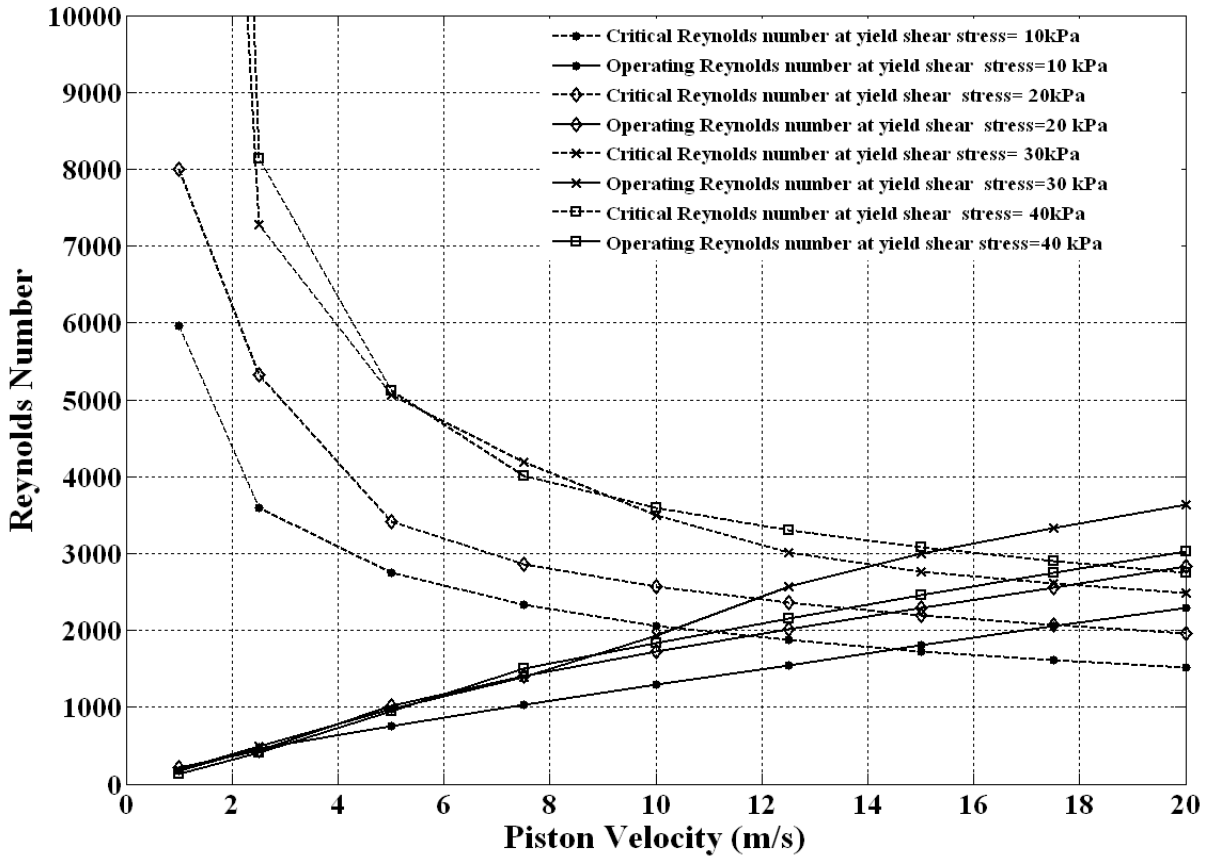

Fig 5.7 Variation of critical and operating Reynolds number with piston velocity for the different values of shear yield stress of MR fluid flowing through piston channel, and at shear yield stress of 10 kPa for MR fluid flowing through the outer bypass channel.

If the shear yield stress of the MR fluid flowing through the outer bypass channel is increased to 20 kPa the variation of pressure gradient with piston velocity is given by Fig 5.8. In this figure it can be seen that the pressure gradient gradually begins to show a significant increase with increase in the shear yield stress of MR fluid flowing through the piston channel if the piston velocity is in the range of 1 to 2.5 m/s seconds. This combination of shear yield stresses of MR fluid for the two channels gives a good attenuation in flow transient.

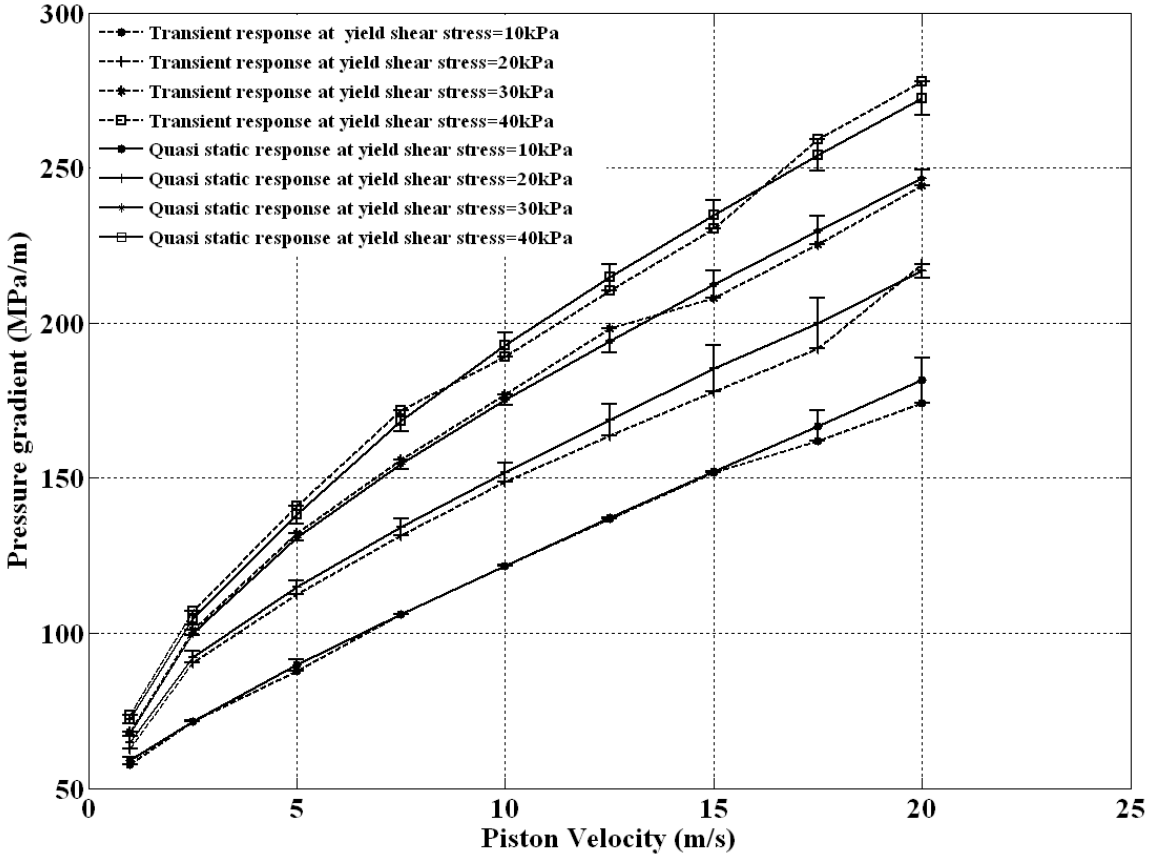

Fig 5.8 Variation of pressure gradient with piston velocity for different values of shear yield stress of MR fluid flowing through piston channel, and at shear yield stress of 20 kPa for MR fluid flowing through the outer bypass channel.

For the above set of results the transition from laminar flow to turbulent flow takes place at piston velocity of 16 m/s second. This is because of the increase in the Bingham number for the piston channel. Since the value of Bingham number is also dependent upon the fraction of the total flow that flows through the piston channel, the trend for the variation of the critical and operating Reynolds number, as shown in Fig 5.9, is the similar to the previous case.

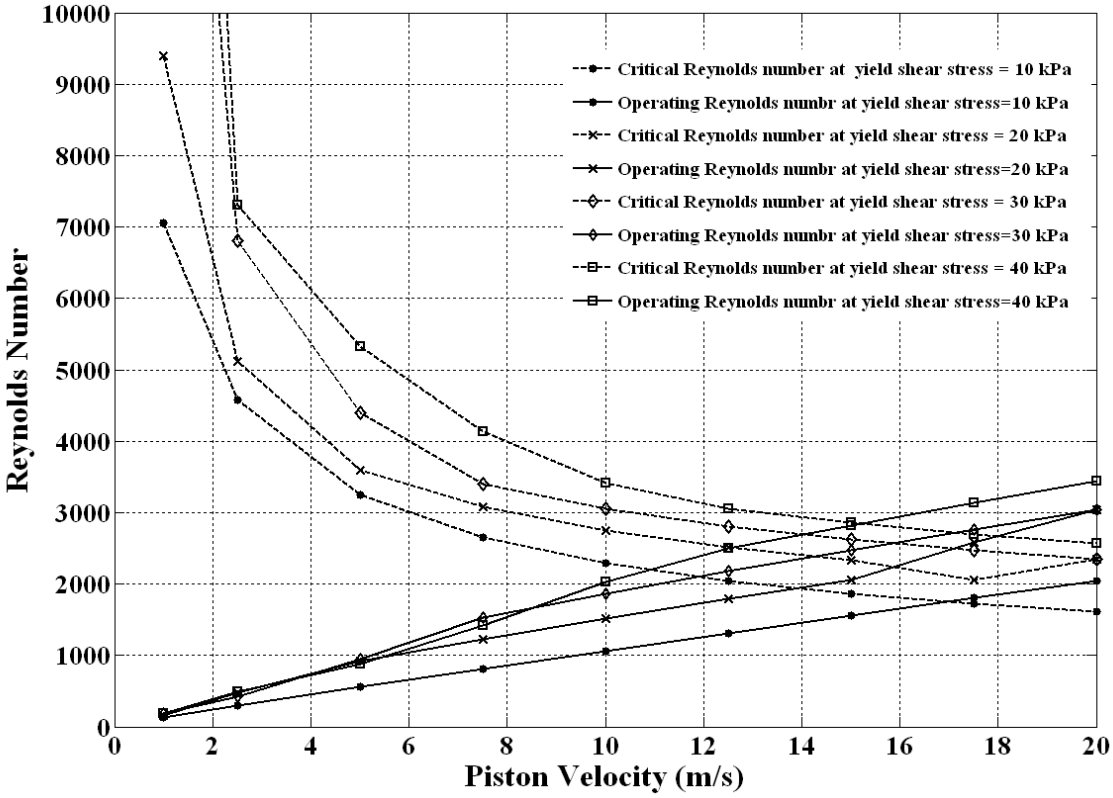

Fig 5.9 Variation of critical and operating Reynolds number with piston velocity for the different values of shear yield stress of MR fluid flowing through piston channel, and at shear yield stress of 20 kPa for MR fluid flowing through the outer bypass channel.

The variation of pressure gradient with piston velocity for the shear yield stress of 30 kPa for MR fluid flowing through the outer bypass channel is shown as Fig 5.10, for different values of shear yield stress for MR fluid flowing through the piston channel. The curves shown in Fig 5.10 can be seen to separate at low piston velocities as the shear yield stress of the MR fluid flowing through the outer bypass channel is increased. There is also an overall increase in the value of pressure gradient as the shear yield stress of the MR fluid flowing through the outer bypass channel is increased. This indicates that the dual channel can give higher damper force

for the same size of the mono channel damper. The transient effects can also be seen to be attenuated. This indicates that the design can give an improvement in the dynamic range due to transient attenuation. The variation of critical and operating Reynolds number with piston velocity show that this combination for shear yield stress for the MR fluids, flowing through the two channels, can permit laminar flow in the piston channel up to 20m/s. Here it is mentioned that the curve for the variation of critical and operating Reynolds number have not been presented for the outer bypass channel because the flow operating Reynolds number remains well within the critical value for all piston velocities and for all the combination of shear yield stresses for the MR fluid flowing the inner and outer channels. This is because the flow through the piston channel is a pressure driven Poisieulle flow superposed with Couette flow. Due to this reason the fluid flow rate in the piston channel is always higher than the flow rate in the outer bypass channel.

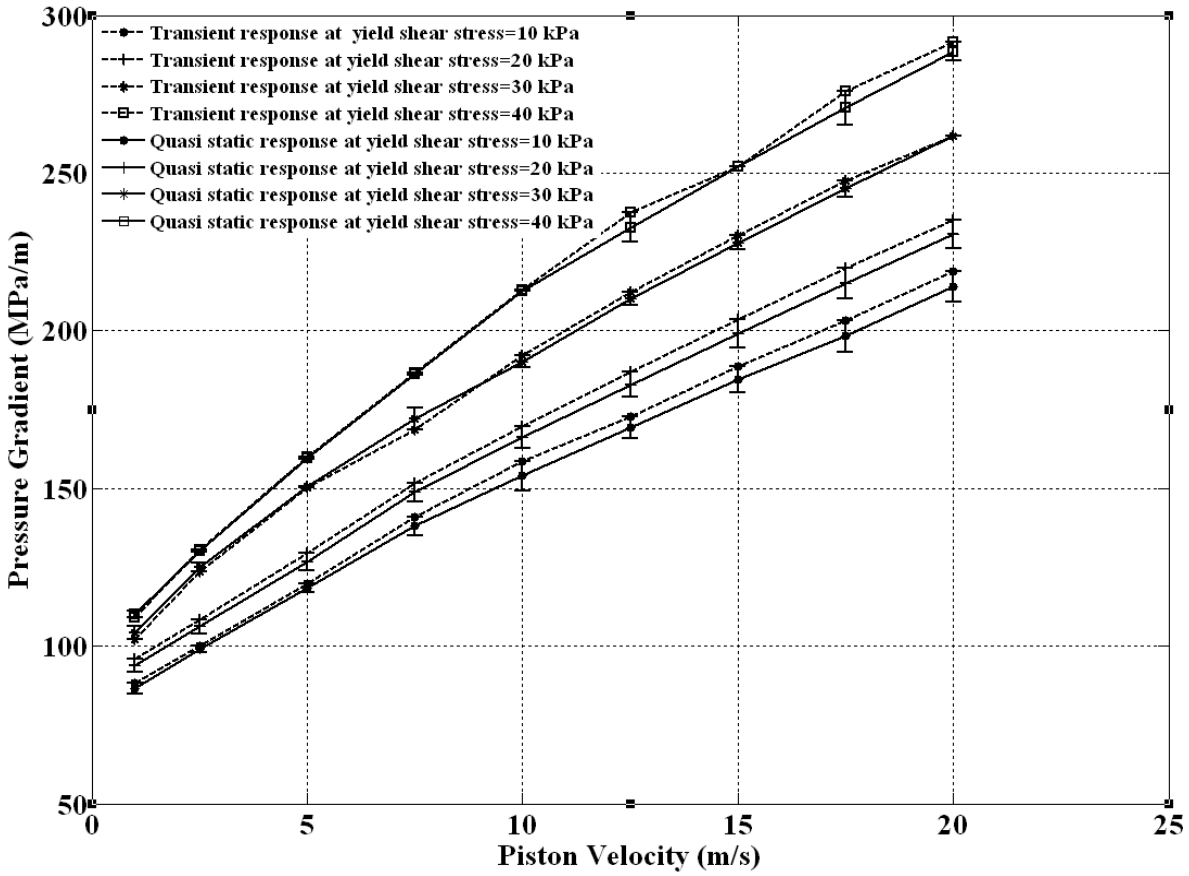

Fig 5.10 Variation of pressure gradient with piston velocity for different values of shear yield stress of MR fluid flowing through piston channel, and at shear yield stress of 30 kPa for MR fluid flowing through the outer bypass channel.

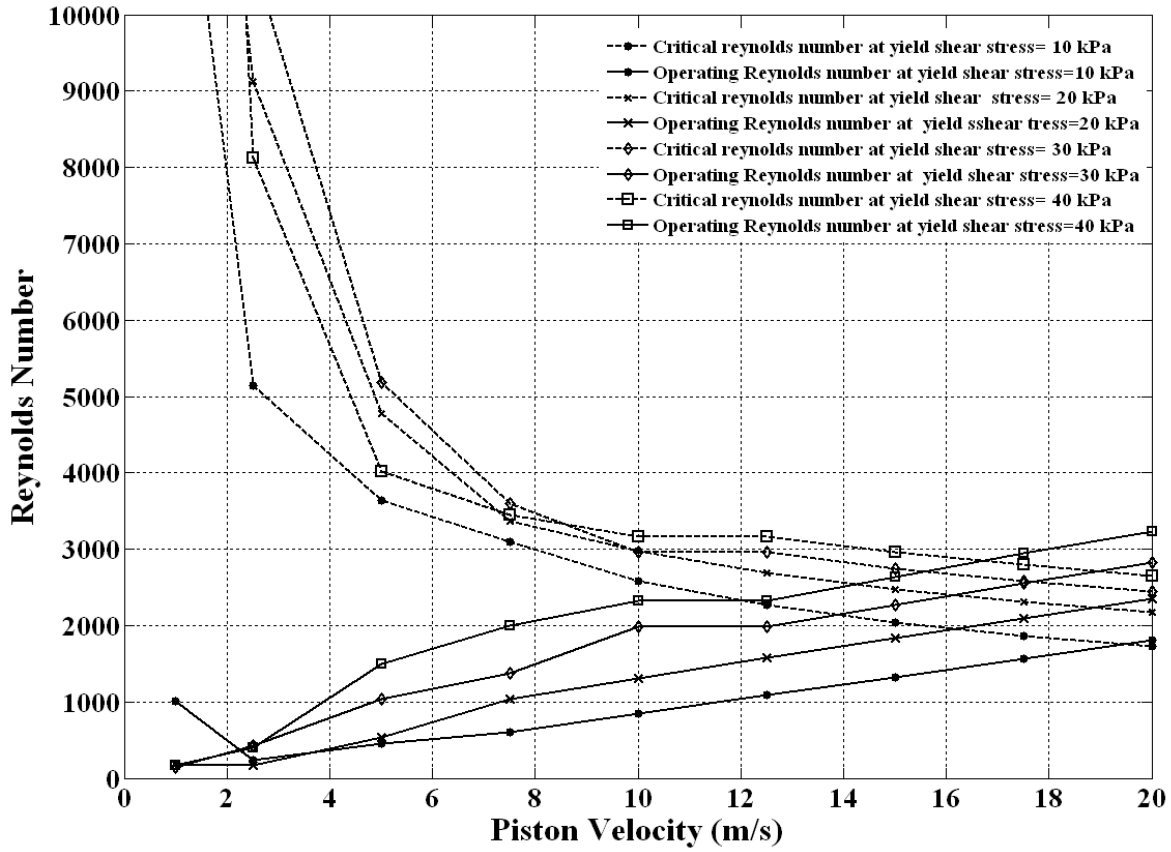

Fig 5.11 Variation of critical and operating Reynolds number with piston velocity for the different values of shear yield stress of MR fluid flowing through piston channel, and at shear yield stress of 30 kPa for MR fluid flowing through the outer bypass channel.

When the shear yields stress for the MR fluid flowing through the outer bypass channel is increased to 40 kPa the variation of pressure gradient for different piston velocities at different values of shear yield stress for MR fluid flowing through the piston channel is given in Fig 5.12. It can be seen that the pressure gradient curve have completely separated out at piston velocity of 1m/s. The effect of fluid inertia transient is significant. This is because the flow rate of MR fluid flowing through the piston channel is higher than the flow rate of MR fluid through the outer bypass channel when the yield shear stress of MR fluid flowing through the piston channel

is lower than yield shear stress of MR fluid flowing through the outer bypass channel. As a result of this the outer channel is not able to effectively dampen the fluid transients developed by the piston channel. The Fig 5.13 shows that flow in the piston channel remains laminar up to the piston velocity of 20 m/s.

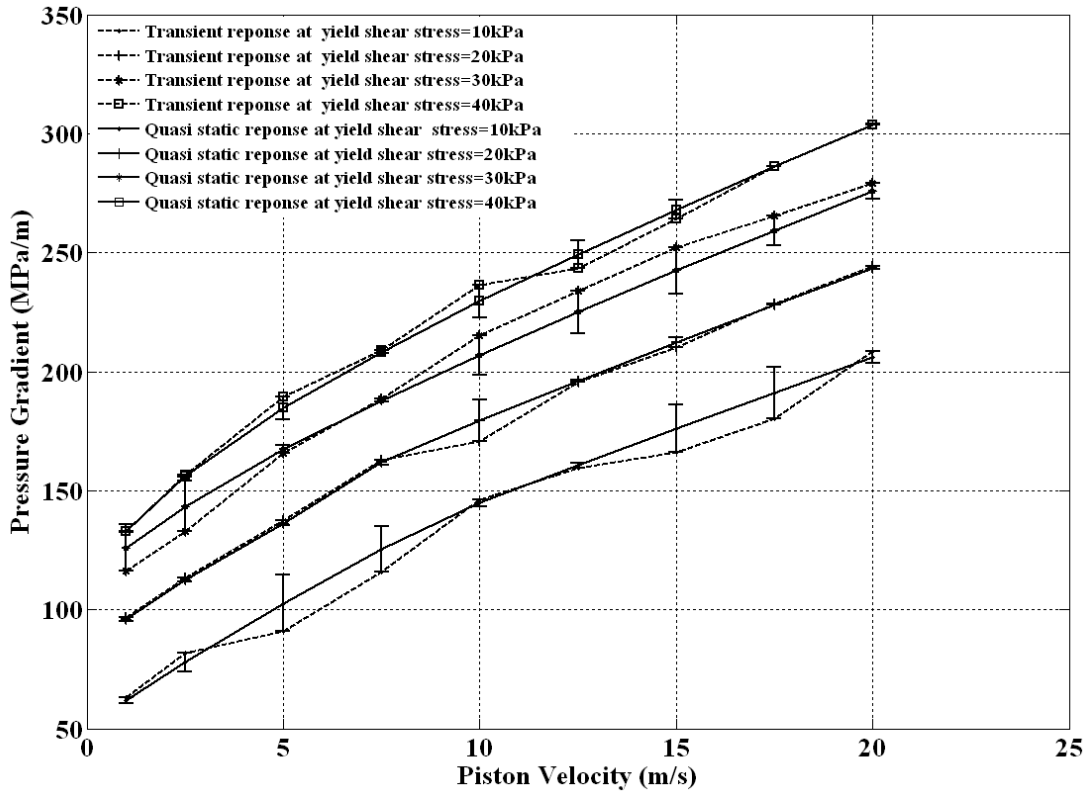

Fig 5.12 Variation of pressure gradient with piston velocity for different values of shear yield stress of MR fluid flowing through piston channel, and at shear yield stress of 40 kPa for MR fluid flowing through the outer bypass channel.

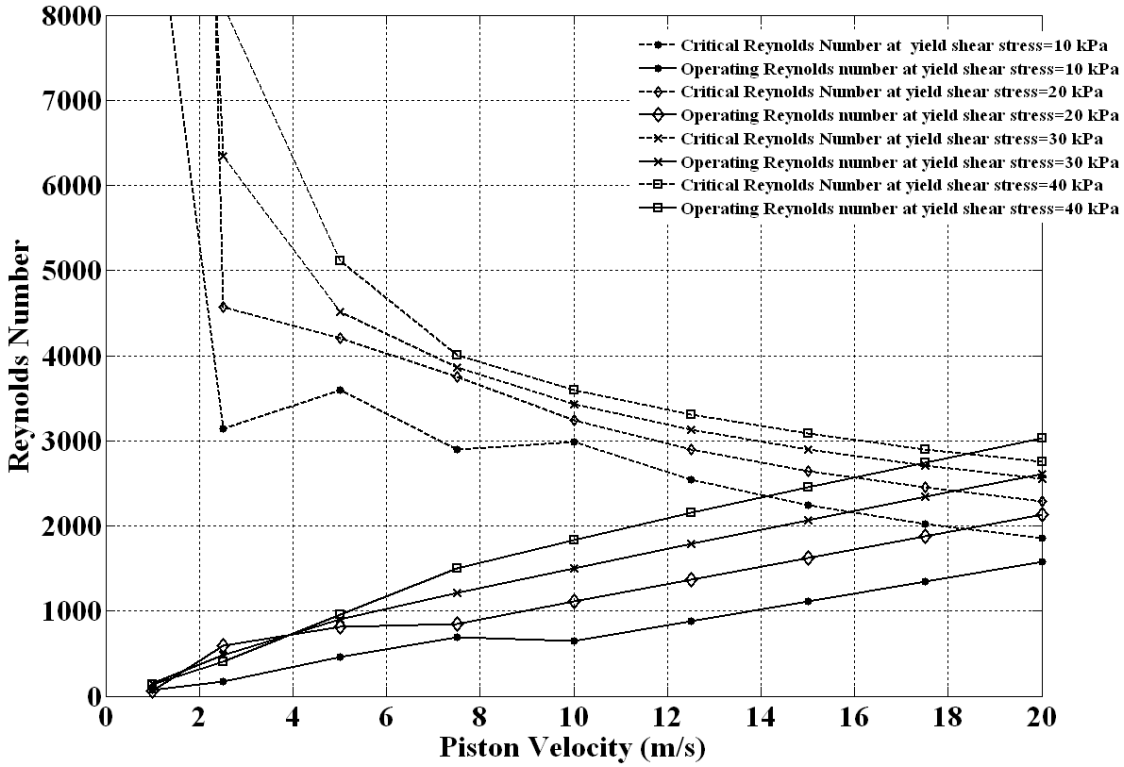

Fig 5.13 Variation of critical and operating Reynolds number with piston velocity for the different values of shear yield stress of MR fluid flowing through piston channel, and at shear yield stress of 40 kPa for MR fluid flowing through the outer bypass channel.

From the above parametric study it is concluded that compounded or the dual channel damper is able to effectively attenuate the transients and has good controllability as it permits laminar flow at piston velocities up to 20 m/s.

5.4 Summary

The chapter begins with the statement of damper's theorem to emphasise the need for attenuation of damper force fluctuation or spikes due to transient effects. This chapter presents the modelling

and parametric study for a dual channel flow MR damper. The parametric study establishes following features of MR damper design:

(1) The damper is able to attenuate the transient effects.

(2) The new design is an effective solution in resisting the onset of turbulent flow in the mR flow channel up to the piston velocity of 20m/s.

(3) The new design is capable of developing higher damper force than a MR damper with single channel flow of same diameter.

(4) The new design has significantly improved dynamic range by at least 30%.

Chapter 6

Proposed design of a dual channel flow MR damper

6.1 Introduction

This chapter deals with the design of dual channel flow damper. The model for this damper has been presented in the previous chapter. In this chapter the design of damper in respect of optimisation of actuators and the design of piston and outer bypass channels have been presented. The first section deals with the introduction to the problem of optimisation of dual channel flow damper and the classification of the optimisation problem. The second section deals with the design of flow paths for maintaining equal pressure gradient, the optimisation of the actuator for the damper. In the third section the electromagnetic modelling of the actuators based on finite element model has been presented. The proposed embodiment of the solution has been described in the fourth section. The last section presents the conclusion of finding followed by the summary of the chapter.

6.2 Proposed design of a dual channel flow damper

The design of damper can be split into two problems viz. calculation of damper parameters for the flow path and actuators and the mechanical design of damper. The second problem involves the structural design of the damper. However the important aspect to be considered in the mechanical design of damper is the design of seals. Since the MR fluid is a suspension of ferrite particles in hydrocarbon oils therefore the rubber based seal materials deteriorate due to their contact with MR fluids. This chapter will not deal with the structural design of damper, but will briefly describe the selection of seals for the MR damper. The objectives of the first problem of the design of MR damper is to minimize the force transmitted to the structure, to which the

damper is attached, minimise the weight and volume of the damper and finally to minimise the weight of the structure to which it is attached. This set of design objectives envisages the fluid mechanical design of an MR damper and electromagnetic design of the actuator coils. The ultimate objective of the fluid mechanical design of MR damper is to achieve simultaneous minimum of damper force and damper stroke as given by damper's theorem. The dual channel damper design has been proposed in this work to achieve attenuation of fluid mechanics transients by suitable design of magnetised lengths of outer bypass channel and piston flow channel. The application of currents to the actuator coils for the optimised flow lengths corresponding to the combination of yield shear stress for the inner and outer channel is a control system problem. Apart from this if the response time of the coils is high it will result in additional transients due to the change in the yield shear stress due to current transients of the electromagnetic coils. Therefore the design of actuator coils is the second part of the design of dual channel flow damper. This section will deal with the brief description of optimisation strategy for the flow paths design of damper followed by the electromagnetic design of actuator coils. The following block diagram illustrates the listing of the problem set for the design of MR damper:

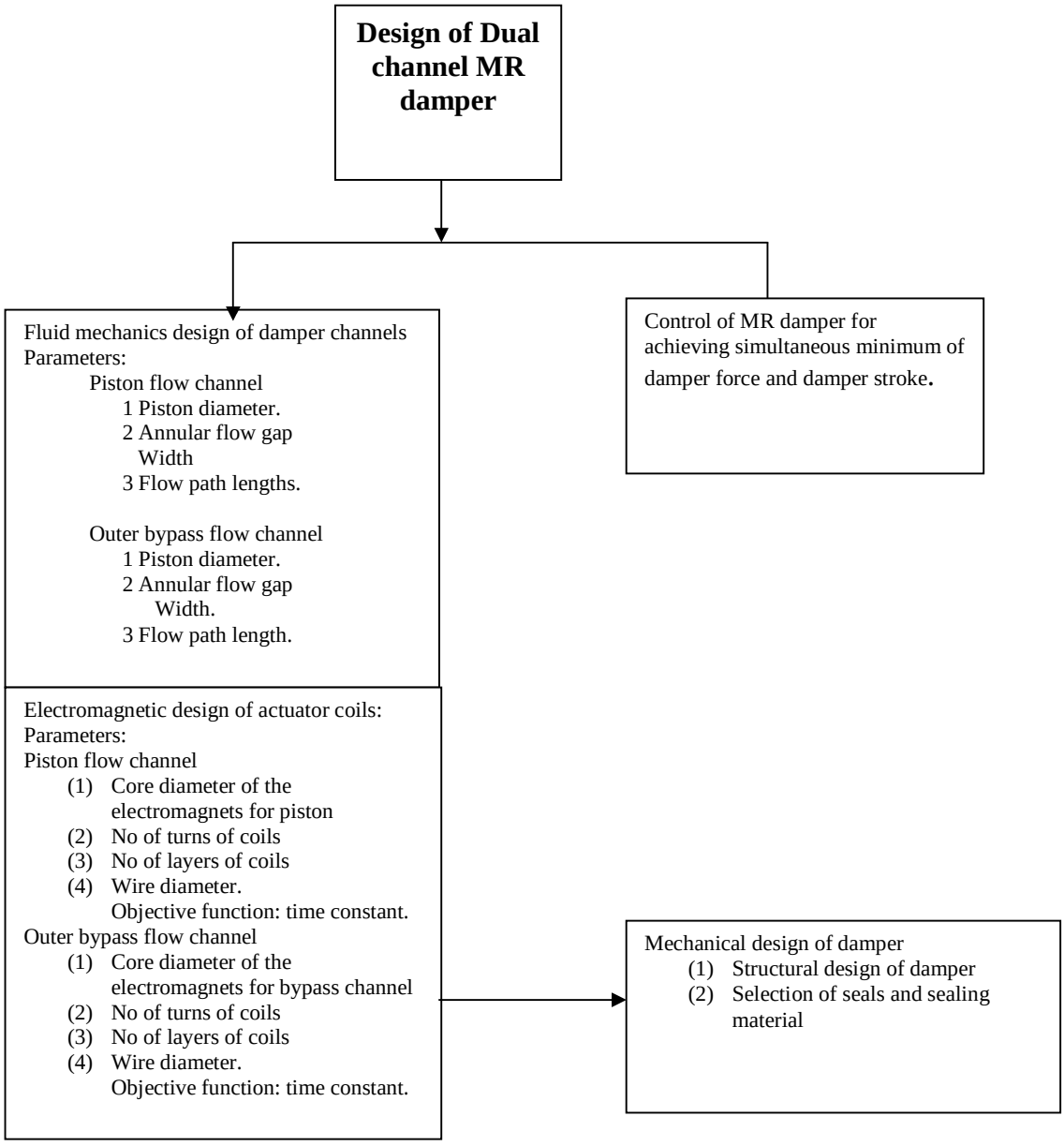

Fig 6.1 Block diagram representation of the problem set for the design of dual channel flow MR damper.

In the Fig 6.1 above, the set of problems of optimisation of damper flow paths and the electromagnetic design of the damper have been listed in one block because these problems are coupled to each other as there may be different pressure gradients across the two flow paths. The maximum diameter of the piston is governed by the diameter of the electromagnetic core of the

piston. This parameter is independent of the geometry of the flow path associated with the piston. This relationship is more explicit when the flow path is between the piston and the cylinder. In such a case the core of the electromagnetic coil is coaxial with the piston. For the design of flow path of the damper the following factors have to be taken into account:

(1) The width of the plug, of the MR fluid flow through the channel, should not be very thin and it should not so thick so as to be close to the walls of the channel. The optimum width of plug is required because the shear stress in the regions between the wall of the channel and the plug boundary is higher than the yield shear stress within the plug flow and as such the dissipation of the energy input to the system can be maximized leading to the development of optimal pressure gradient across the length of the flow path. This will lead to minimum force transmitted to the structure and minimisation of the stroke of the damper. On the other hand if the plug width is thin then the transient effects in the laminar flow region will dominate and this will result in reduction of dynamic range. The reduction in dynamic range will result in reduction in the controllability of the damper. Here it is pertinent to mention that in a dual channel damper the width of MR plug, at high piston velocity, is less for the flow through the piston channel as compared to the thickness of the plug for the flow of MR fluid through the outer bypass channel. The combination of these two effects results in an increase in dissipation of energy input to the damper system and the attenuation of transients leading to improved dynamic range of the damper. However for normal high speed damping application where the weight saving of the structure is an important consideration the design of flow gap for both the channels are quite

important for optimisation for obtaining the best performance of the dual channel flow damper.

(2) Similarly the lengths of the flow paths of both the channel are another pair of parameters which can be used to change the plug widths and the attenuation of fluid transients. The two flow paths together contribute to the total volume of the magnetised MR fluid. A long piston flow path may unduly increase the length of the damper and may have higher transient effects. On the other hand a short piston channel flow path can have reduced transient effects but the outer bypass flow channel can get blocked at lower values of yield shear stress for MR fluid flow through the outer-bypass channel because of higher resistance offered by the outer by-pass channel. This is because the transients in the MR channel are due to inertia effects. Therefore if the flow path length of the channel is long the volume of field controlled fluid is larger and so the inertia effects also increase with the increase in flow path length. Therefore an optimal combination of lengths of the flow paths of the two channels will give the best results in terms of optimal damper force and improved dynamic range due to reduction in transient effects.

Presently the optimisation of the lengths of flow paths of damper and channel widths has not been included in this work. However this is an important problem for the design of a high performance MR damper and will be dealt with in future work. Here the optimisation problem for the flow paths and channel width has been described with the equations to lay the foundation of the problem solving technique to be used for solving such a problem in future. In an optimal design of MR damper flow channel the objective function has been taken as the sum of the difference between the force due transient effects and the force due to quasi static solution for a

given velocity range, flow path lengths, flow path widths, value of yield shear stress for the MR fluid flowing through the piston flow channel and the yield shear stress for the MR fluid flowing through the outer by-pass channel.

$$\mathscr{R} = \sum_{k=1}^{l}\sum_{j=1}^{m}\sum_{i=1}^{n}(f_{trans} - f_{qs})^2{}_{i,j,k} \tag{6.1}$$

Subject to constraints:

$$\begin{aligned}
&0.5 \le g_p \le 2.0\ mm \\
&0.5 \le g_o \le 2.0\ mm \\
&10 \le l_i \le 50\ mm \\
&10 \le l_o \le 100\ mm \\
&d_{piston\ \min} \le d_{piston} \le d_{piston\ \max} \\
&d_{inner\ \min} \le d_{inner} \le d_{inner\ \max} \\
&10000 \le \tau_{piston\ flow} \le 40000\ N/m^2 \\
&10000 \le \tau_{outer\ bypass} \le 40000\ N/m^2
\end{aligned} \tag{6.2}$$

$$\mathrm{Re_a} \le \mathrm{Re_c} \tag{6.3}$$

where $\mathscr{R}$ is the square of the residual of the difference between the force (f_{trans}) due to transient effects and force (f_{qs}) due to quasi static flow condition and the subscripts i ,j and k stand for the summation over n levels of velocities, m number of levels of yield shear stress for MR fluid flowing through the piston flow channel and l number of levels for the yield shear for the MR fluid flowing through the outer bypass channel respectively. The symbol g_p is the annular flow gap for the piston flow channel, g_o is the annular flow gap for the bypass flow channel, l_i is the flow length for piston flow channel, l_o is the flow length for the outer-bypass flow channel, d_{piston} is the diameter of the piston, The max. and min. subscripts associated with this symbol represent maximum and minimum values respectively which need to be fixed depending upon the

application, d_{inner} is the inner diameter of the outer bypass channel, The max. and min. subscripts associated with this symbol represent maximum and minimum values which need to be fixed depending upon the application, $\tau_{piston\ flow}$ is the yield shear stress for the MR fluid flowing through the piston flow channel and $\tau_{outer\ bypass}$ is the yield shear stress for the MR fluid flowing through the outer-bypass channel. The objective function described above will be further improved in course of future work on the optimal design of dual flow damper. In this work the above mentioned objective function serves the purpose of identifying the computational complexity of the problem and select suitable optimisation technique to be used for the optimisation of the electromagnetic actuator. Since the two problems are coupled so these problems will share a common optimisation tool. The residual can be evaluated based on solution of nonlinear set of equation for the dual flow MR damper using Newton Raphson based algorithm described in Ch 3, and 5. Since the Newton Raphson method has quadratic convergence therefore the optimisation problem can be solved by an algorithm in polynomial time. The set of nonlinear equation have roots which either satisfy the above constraints or do not satisfy the above constraints therefore the optimisation problem additionally involves selecting the roots which satisfy the constraints. Therefore by definition of the NP-hard problem the above problem is also a NP-hard problem of optimisation. The rigorous proof of this statement is presently kept out of the scope of this work. Considering above classification of the optimisation problem and the type of objective function the optimisation technique that is most suitable will be genetic algorithm based technique. In the future work the problem may be solved by suitable evolutionary algorithm.

6.3.1 Introduction to genetic algorithm

A large number of techniques used for optimisation are gradient based techniques. These techniques require the function to be smooth or at least piecewise smooth. The well known techniques amongst them are path following based methods and the integral based methods and the integral based procedures Goldberg, (1985), Fakhreddine et al, (2009). The drawback of these methods is that whether the solution is at the local maxima or the global maxima the gradient is zero and therefore the algorithm terminates without giving the indication about local or global maxima. In the case of the present problem the evaluation of gradient is difficult and the objective function is in the discrete form. Therefore based on above consideration and the class of complexity of the problem the use of genetic algorithm based technique should give the desired results. In this work the optimisation of electromagnetic actuator will be done using this technique.

The genetic algorithm was formulated by Holland (1975) based on the biological evolution and the survival of the fittest principle. These are derivative free techniques and have been found to be quite effective in solving the problem of global optimisation and are applicable to smooth, piecewise smooth and discrete functions. They are based on the evaluation of objective function at a set of points in the variable space which are chosen randomly in the initial steps and subsequently through the processes of genetic evolution such that the set of points comply with the constraints. As the iterations of the genetic algorithm proceed the solution set converges to the global optima by the principle of survival of the fittest through the process of genetic evolution. To further elucidate this technique of genetic algorithm the steps of genetic algorithm are listed below:

(1) Choose the random process in the range of optimisation with a fixed size such that the population satisfies the constraints.

(2) The population of initial solution set is converted into set binary strings which represent the genomes. This leads to a population of elements represented by *p* rows, of number of possible initial solutions, by *q* columns of number of variables of the objective function.

(3) The process of evolution is implemented by means of Selection, Crossover and Mutation to create a new population for which the objective function progressively gives maximum or minimum value depending upon the whether the objective function is to be maximised or minimised respectively.

The genetic algorithm operators are explained as follows:

(1) Selection: This process is applied to select the fittest individuals, and remove the bad ones, that are required to participate in the reproduction process to give birth to the next generation, Fakhreddine et al, (2009). The selection of the individual can be viewed as two separate processes, MATLAB, Genetic algorithm Toolbox:

   (a) The determination of the number of permissible trials for each individual.

   (b) Conversion of expected trials into discrete number of offspring.

The first step deals with the evaluation of fitness values and which can be implemented by suitable heuristics, including elitist model or for instance by Roulette wheel type selection. In this process the total fitness values for all the individuals are summed up followed by the comparison of individual fitness value relative to the sum of the fitness values. The specified number of individuals with highest fitness value is selected for reproduction and the rest of them are discarded.

(2) Cross over: This is based on the principle of genetic recombination. In this two genotype called the parents are selected and their sites of crossover are selected at random such that the new offspring satisfies the constraints. The site of cross over here means the randomly selected sub-lengths of each of the pair of binary strings representing the element of the solution set.

(3) Mutation: This process introduces completely new alleles into the population. Thus the process of selection and cross over reproduces new fit individuals, the mutation process introduces replaces the discarded elements of the solution set with the new individuals.

In this work the dimensions of the cylinders, cylinders and flow path length have been taken as follows:

(1) Piston diameter = 53mm

(Considering optimal dimension of the core to be around 15 to 20mm and the width and height of the coil to be 10mm.)

(2) Number of poles of the piston = 4 coaxial with piston.

(3) Width of the pole = 10mm.

(4) Length of the annular piston flow channel is = 40mm (considering pressure drop across the fluid between the poles to be negligible as it is not magnetized and the flow gap is more than 5mm.)

(5) Annular flow gap for the piston flow channel= 1mm.

The thickness of the inner cylinder which houses piston has been taken as 10mm so that the magnetic field due to the coils for the bypass channel does not interfere with the flow through the annulus between the piston and inner cylinder when the piston position within the width of the bypass channel electromagnetic coils. The dimensions of bypass channel are given as follows:

(1) Inner diameter of the bypass flow channel = 68mm

(2) Outer diameter of the bypass flow channel = 70mm

(3) Bypass flow channel length = 40mm

(4) Annular flow gap for the bypass channel = 1mm

The above mentioned values for the dual channel flow damper are expected to be close to the optimum values as they have been derived by trial and error to be close to optimum values. In future these values will be refined by the above mentioned optimisation strategy.

6.3.2 The design of electromagnetic actuators

With the above brief introduction to the selection optimisation technique for the optimisation for the dual channel flow damper and genetic algorithm the design of electromagnetic actuator and the optimisation of parameters can be discussed. The optimal design of electromagnetic actuators for a MR damper has been studied by a number of authors such as, Quoc et al, (2009), Batterbee et al (2007), Likang et al (2008), Gavin et al (2001). The publications after 2001 use some of the principles of core optimisation based on Rosenfield et al (2004).

Batterbee et al (2007), suggest an optimisation strategy for the design of damper for the landing gear of an aircraft. In this work similar strategy has been mentioned, with a modification to take into account the transient effects. The transient effects have been shown to significantly reduce the dynamic range of a MR damper. The optimisation strategy in the above paper is also based on the quasi steady response of a single channel damper therefore the optimal solution may not be satisfactory for the high speed applications such as aircraft landing gear. The design and the optimisation approach for damper mentioned in this work is more generalized and is based on accurate solution for the response of the damper. The operating speed for the aircraft landing gear is around 6-7 m/s and so the transient effects need to be taken into account for the design of

aircraft landing gear. In the papers described above the objective function for the fluid mechanics of the damper have not been explicitly defined. As a result of this the optimal design strategies described in these works are partially empirical in approach or are partially based on trial and error approach. In Gavin et al (2001), Likang et al (2008) the objective function for optimisation of actuator either consider a combination of power consumption of the coil and time constant or power consumption of the coil. A simple consideration of the fact that the time constant of the actuator is the ratio inductance to the resistance, leads to the concept that if inductance and resistance are simultaneously minimised then the objective of limited minimisation of power consumption can be achieved. For minimising the time constant the inductance needs to be minimised at a higher rate than the resistance. Therefore it is proposed that the objective function for the optimisation of the electromagnetic actuator should be the time constant of the coils. In this work only one actuator coil is optimised. The other coils are included in the circuit depending upon the flow path length. The number of coils to be wound is calculated by dividing the flow path length by the width of the pole and subtracting 1 from the nearest integer so obtained. Based on the work of Schechter (1982) and Lord Corporation engineering note the design objectives for the design of actuator can be listed as follows:

(1) The reluctance of the flux conduit should be low. In this work steel to specifications BS6004IEC227 has been used.

(2) Maximise the magnetic field energy in the fluid gap while minimizing the energy lost in the steel flux conduit and regions of non working MR fluid and other areas. This objective can be best met when the flow path and the magnetic coils are embedded in the piston itself. This may result in design complexities if the flow path length is long.

(3) Maintain sufficient cross section of steel to keep field strength *H* in the steel very low so that the core does not saturate and its ability to control the yield shear stress by magnetising the MR fluid is greatly reduced.

(4) The response time for the electromagnet is minimised. This is because the implementation of model reference bases system would require a good computational power and ability of the actuator to respond in less than 10 milliseconds. This objective requires the coils to be organized in spools of parallel and series coils, Schechter, 1982.

The design of electromagnetic actuator is based on nonlinear magnetostatics. Based on the geometry of the piston and the cylinder assembly for the piston flow channel given in Fig 6.2 the magnetic circuit can be analysed using magnetic Kirchhoff law. In the Fig 6.2 the arrows indicate the magnetic circuit for each coil. The magnetic Kirchhoff law in generalized form is given as :

$$\sum H_k l_k = N i \qquad 6.3$$

where, H_k is the field strength l_k is the effective length of k^{th} element in the magnetic circuit.

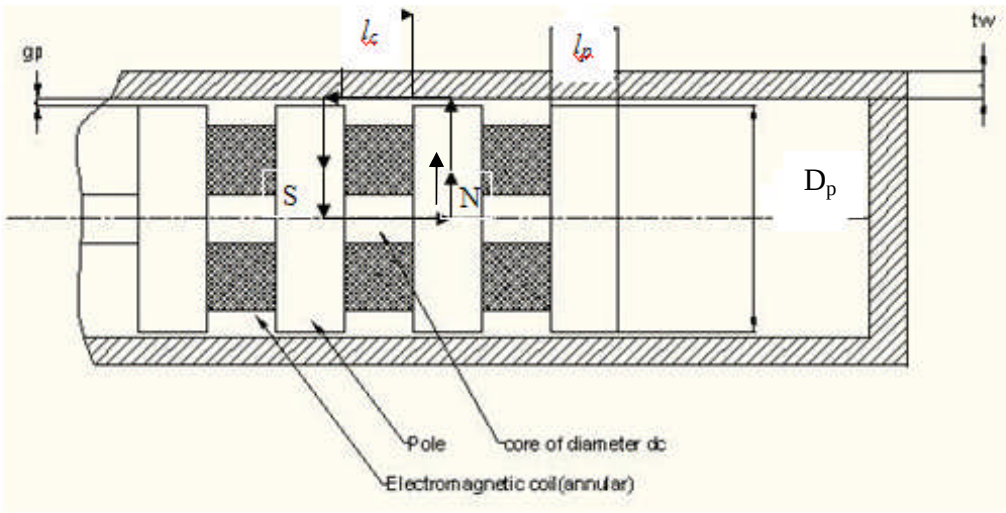

Fig 6.2 Schematic of the piston and the electromagnetic coil configuration.

For the magnetic circuit of one of the coils of the piston design being considered in this work the expression for the current using Kirchhoff law is given as follows:

$$i_{ac} = \frac{1}{n_p n_l n_s}\left(2H_g g_p + H_c(l_c + 2l_p/2) + 2H_p(D_p + t_w) + H_w(l_c + 2l_c/2)\right) \quad (6.4)$$

In the above equation i_{ac} is current, H_g is the magnetic field intensity through the gap,g_p is the width of the gap, H_c is the magnetic field intensity through the core of the piston, l_c is the length of the core between the poles, l_p is the width of the pole, H_p is the magnetic field intensity through the pole, D_p is the diameter of the pole, t_w is the thickness of the cylinder wall, H_w is the magnetic field intensity through the cylinder wall, n_p is the number turns per layer in the coil, n_s is the number of spools in the coil and n_l is the number of layers of windings in one spool. The resistance of one spool (R_{spool}) of the coil is given by the following equation:

$$R_{spool} = \frac{4\pi\left(n_l d_c + (n_l - 1)d_w\right)n_p k_r}{d_w^2} \quad (6.5)$$

If the spools are connected in parallel the resistance of coil is given as:

$$R_w = \frac{R_{spool}}{n_s} \quad (6.6)$$

$$R_w = \frac{4\pi\left(n_l d_c + (n_l - 1)d_w\right)n_p k_r}{d_w^2 n_s} \quad (6.7)$$

The inductance of the spool is given as :

$$L_{spool} = \frac{n_p n_l \phi_B}{i_c n_s} \tag{6.8}$$

If the spools are connected in parallel inductance of the coil is given as:

$$L_w = \frac{n_p n_l \phi_B}{i_c n_s^2} \tag{6.9}$$

In the above equations R_{spool} is the resistance of the one spool of the coil. In this scheme of the coil circuit, a coil consists of a number multilayer layer coils, called as spools, which are connected in parallel to achieve minimisation of time constant. The symbol R_w stands for the resistance of coil, L_{spool} stands for the inductance of spool and L_w stands for inductance of coil. For calculating the flux through each of the elements of the magnetic circuit the flux density corresponding to the operating points is fixed and the flux densities for the other elements are expressed in terms of the maximum flux density of the MR fluid. The maximum flux density is obtained from the B-H curve of the MR fluid. In this case the MR fluid used is Lord Corporation make MR132DG, Fig, 6.3

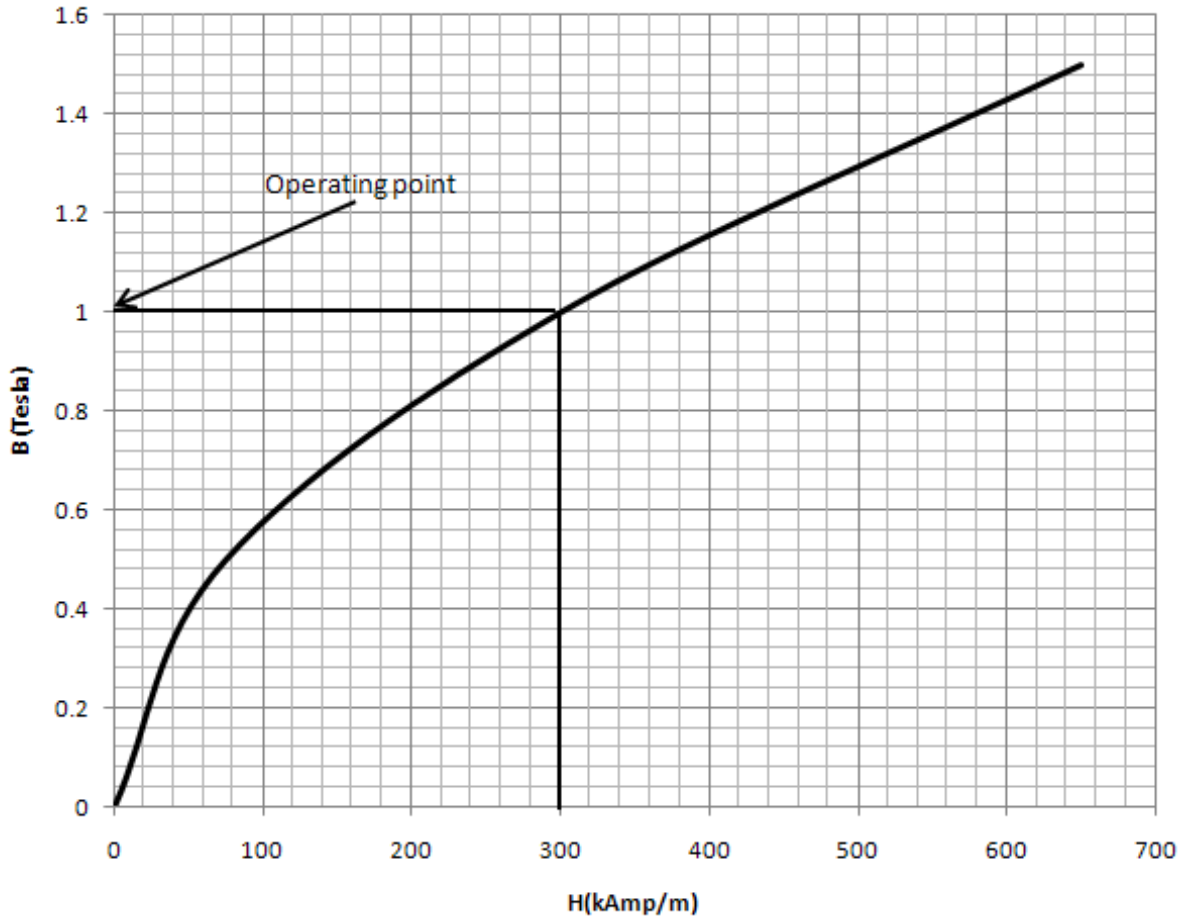

Fig 6.3 B-H curve of MR132DG MR fluid(Lord Corporation).

The expression for the flux density of MR fluid flowing thorugh the gap is given as :

$$B_g = \frac{4\phi_B}{\pi\left((D_p + 2t_w + 2g_p)^2 - \left(D_p + 2g_p\right)^2\right)} \tag{6.10}$$

If B_g =1T then the Expression for ϕ_B is given as follows:

$$\phi_B = \frac{\pi\left(\left(D_p + 2t_w + 2g_p\right)^2 - \left(D_p + 2g_p\right)^2\right)}{4} \tag{6.11}$$

The expression for the flux densities through core (B_c), pole (B_p), cylinder wall (B_w) are given as follows:

$$B_p = \frac{\phi_B}{\pi D_p l_p} \tag{6.12}$$

$$B_c = \frac{4\phi_B}{\pi\ d_c^2} \tag{6.13}$$

$$B_w = \frac{4\phi_B}{\pi\left(\left(D_p + 2g_w\right)^2 - \left(D_p + 2g_w + 2t_w\right)^2\right)} \tag{6.14}$$

With the above set of equations the objective function is defined as:

$$\chi = \frac{L_w}{R_w} \tag{6.15}$$

Subject to following equality constraints:

$$d_c = \frac{1}{2}\left[-\left(n_s n_l d_w + g_p\right) + \sqrt{D_p^2 - \left(n_s\ n_l d_w + g_p\right)^2}\ \right]$$

And the inequality constraints are given as follows:

$$\begin{aligned}
&n_p > 1 \\
&n_s > 1 \\
&n_l > 1 \\
&d_{c\min} \le d_c \le d_{c\max} \\
&0.5 \le g_p \le 2.0mm \\
&d_{w\min} \le d_w \le d_{w\max} \\
&l_{c\min} \le l_c \le l_{c\max} \\
&l_{p\min} \le l_p \le l_{p\max}
\end{aligned} \tag{6.16}$$

In the constraints equations given above the min and max symbols associated with the subscript stand for minimum and maximum respectively. The value of H for the pole, cores and wall are calculated by using the B-H curve given in the Fig 6.4.

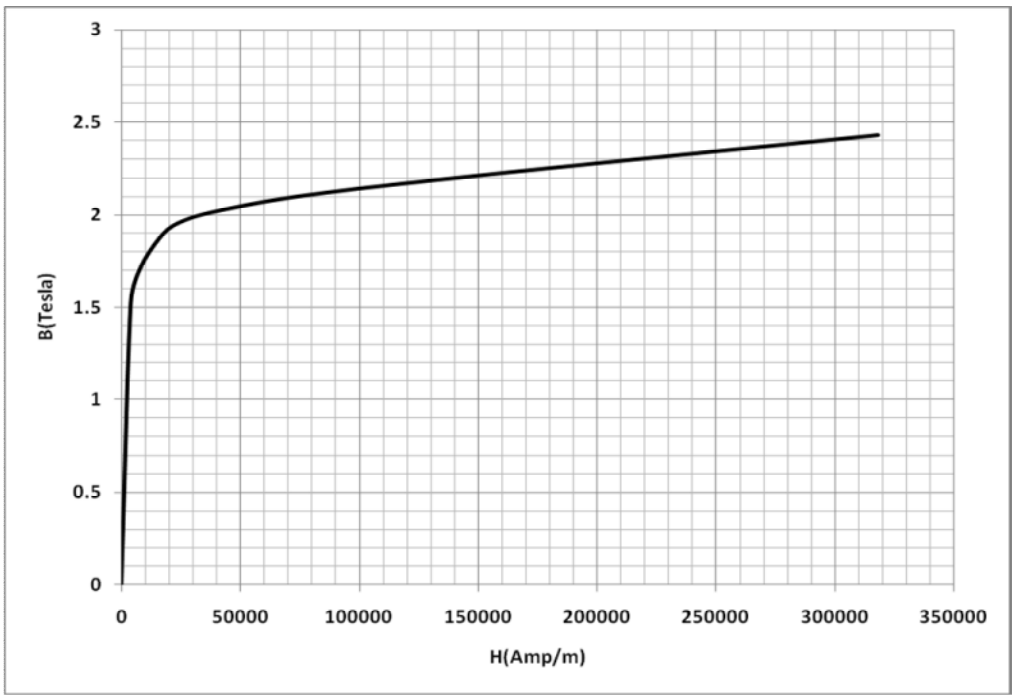

Fig 6.4 Variation of flux density versus magnetic filed intensity for BS60004,IEC227.

With above set of equations for the objective function following observation can be made:

(1) The gradient based methods can lead to computational complexities.

(2) With the above scheme of connecting coils in the form of shunted spools of coils the problem is a routing type of problem. A travelling salesman problem can be transformed into its equivalent form. Thus, this problem is also a NP hard problem of optimisation.

Based on above observations the optimisation technique that has been selected is genetic algorithm. The above optimisation program has been implemented using MATLAB genetic algorithm toolbox. In using the above code the maximum and minimum limits of the piston core diameter was taken to be 10mm and 20mm respectively. This is based on the diameter of the

tube used for housing the cylinder, which has been taken as 55mm. Further considering that the current capacity of the wire to be at least 1 A, the maximum and minimum limits of the wire diameter were taken as 2mm and 0.9 mm respectively. The limits of the width of the pole have been taken as 5mm to 20mm. The length of the coil was constrained to lie within the limits of 5mm to 20mm. With the above constraints the effects of variation of core diameter on time constant was studied and the results are shown in Fig 6.5.

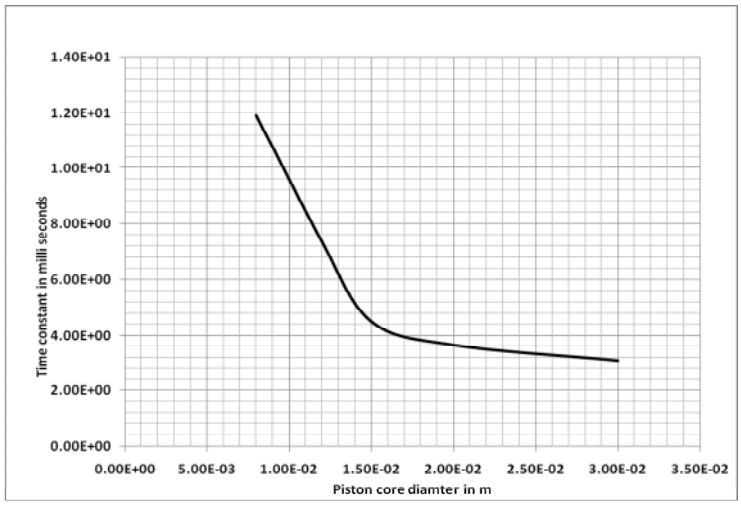

Fig 6.5 Variation of time constant with piston core diameter.

From the above figure it is clear that the time constant of the coil increases with the decrease in the core diameter. Considering the spatial constraints due to the diameter of the cylinder which houses the piston the the diameter of the core has been taken as 20mm. Similarly the time constant is reduced with the reduction in diameter of the wire but considering the current carrying capacity of the wire a time constant of 3 milli seconds is an acceptable solution, Fig 6.6.

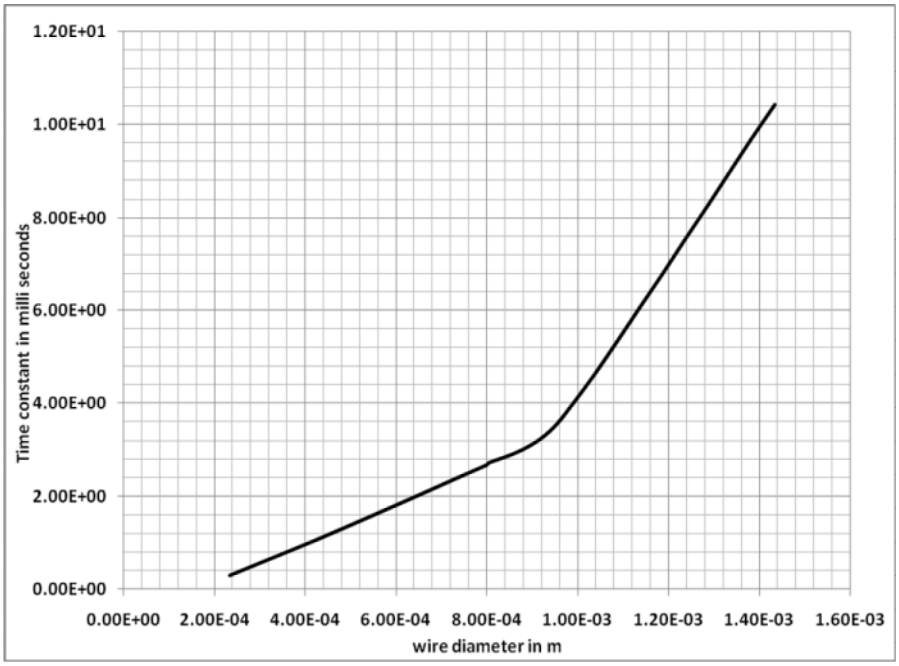

Fig 6.6 Variation of the time constant with wire diameter.

Considering the above constraints the optimal solution is given as follows:

No of layers in one spool = 1

No of no of turns one layer = 10

Core diameter = 20mm

No of spools = 10

Wire diameter = 0.9mm (20SWG).

Pole widths = 10mm

Time constant =3.113650e+000 in milliseconds.

In the above solution the electromagnetic coils have been obtained as an assembly of parallel connected layers. As such for same current density this configuration requires an increase in input current by a factor equal to the number of coils connected in parallel as compared to a single coil. This will result in an increase in power consumption. However the response of the actuator will be within the response time required controlling the damper force. The

above solution has been applied for all the three coils. The validation of the solution has been done by static finite element simulation on ANSYS. For the coils of outer by pass channel a similar optimisation solution can be made. However in this work the scheme of the coil connectivity has been kept identical. Since the thickness of the outermost cylinder is the core of the external coils therefore the depth of the coils has been taken as 10mm. The wire diameter has been kept as 20SWG. For the design of damper apparatus the implementation of above scheme of winding requires the design of insulated bus architecture. This presently could not be achieved due to time constraints. As such in the present design of apparatus 3 coils of 100 turns each has been used. A similar solution has been applied for the external coils as well. The configuration of the external coils has been shown in Fig 6.7.

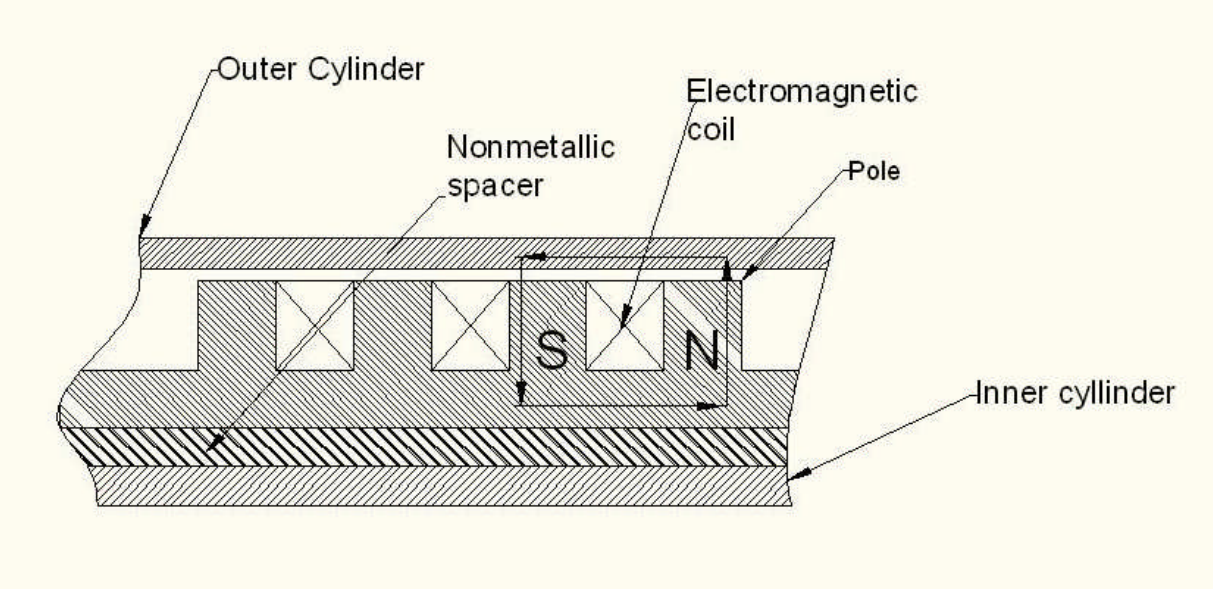

Fig 6.7 Configuration of the electromagnetic coils for the outer bypass channel.

6.3.3 Finite element simulation of an electromagnet

The finite element simulation of the electromagnetic coils is required to verify that the cores of the electromagnets are not saturated at the maximum current density. This is necessary because if the core is saturated then further increase in current in the coil will not result in the change in the flux density of the electromagnet and as such the MR fluid will not be controllable if the current exceeds the value of magnetic flux density corresponding to the saturation of the core. The finite element simulation has been done using ANSYS V12. Here a brief description of the formulation is being made. The governing differential equations are given as follows:

The Maxwell equations are:

$$\nabla \mathrm{X}\mathbf{H} = \mathbf{J} + \frac{\partial \mathbf{D}}{\partial t} \tag{6.17}$$

$$\nabla \mathrm{X}\mathbf{E} = \frac{\partial \mathbf{B}}{\partial t} \tag{6.18}$$

$$\nabla.\mathbf{B} = \mathbf{0} \tag{6.19}$$

$$\nabla.\mathbf{D} = q_e \tag{6.20}$$

Since the magnetic field is solenoidal therefore it can be shown to be a curl of magnetic potential **A**.

$$\mathbf{B} = \nabla \mathrm{X}\mathbf{A} \tag{6.21}$$

In the above equation **B** is the magnetic flux density, **J** is current density, **E** is the electric field intensity, **D** is the electric flux density, **H** is the magnetic field intensity and q_e is the electric space charge density. Combining Eq 6.21 and 6.18 following equation is obtained, which is a mathematical expression for Faraday's law:

$$\nabla X\left(\mathbf{E}-\frac{\partial \mathbf{B}}{\partial t}\right)=0 \qquad (6.22)$$

From the above equation and E = -∂A/∂t the following curl-curl problem is obtained:

$$\nabla X\frac{1}{\mu}\nabla \mathbf{A}=\mathbf{J}_i-\gamma\frac{\partial \mathbf{A}}{\partial t}+\gamma\left(v\,X\nabla\, X\mathbf{A}\right) \qquad (6.23)$$

where, γ is the electrical conductivity. For a static 2D problem v=0 , Ji is expressed as current θ direction and the above equation can be reduced to following form:

$$-\nabla.\frac{1}{\mu}\nabla A_\theta=J_\theta \qquad (6.24)$$

The residual functional for the above equation is obtained by multiplying the above equation by a weighted function Ψ and integrating the equation over the whole domain. This is called as the weak formulation. Thus the statement of finite element problem is given as follows:

Given:

$$\mathbf{A}:\Omega\rightarrow\mathbf{R}^2$$

$$\mu:\Omega\rightarrow\mathbf{R}$$

Find

$$\mathbf{A}(t):\overline{\Omega}X\left[0,T\right]\rightarrow\mathbf{R}^{2\prime}$$

$$-\nabla.\frac{1}{\mu}\nabla\mathbf{A}_\theta=\mathbf{J}_\theta$$

+ Boundary, interface and initial conditions.

By using the Green first integral theorem the following weak formulation is obtained:

$$\int_{\Omega} (\nabla \Psi) \frac{1}{\mu} (\nabla \mathbf{A}) d\Omega = \int_{\Omega} \Psi \, \mathbf{J}_{\theta} \, d\Omega \qquad \forall \Psi \in H_0^1 \qquad (6.25)$$

Following using shape functions corresponding to PLANE 13 quadrilateral elements of ANSYS 12 the following system of linear equation is obtained:

$$K\mathbf{A} = f$$
$$where,$$
$$K_{ij} = \int_{\Omega} (\nabla N_i)^T \frac{1}{\mu} (\nabla N_j) \, d\Omega, \qquad (6.26)$$
$$\mathbf{f_i} = \int_{\Omega} N_i J_i d\Omega$$

The above formulation is applied to the computational domain of the coils and piston flow path (Fig 6.2) and is shown as Fig 6.8.

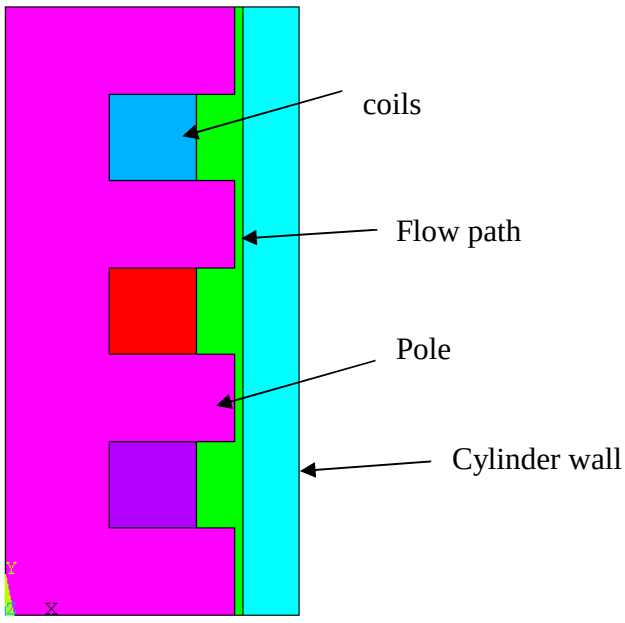

Fig 6.8 Computational domain of piston flow path, piston and coil assembly

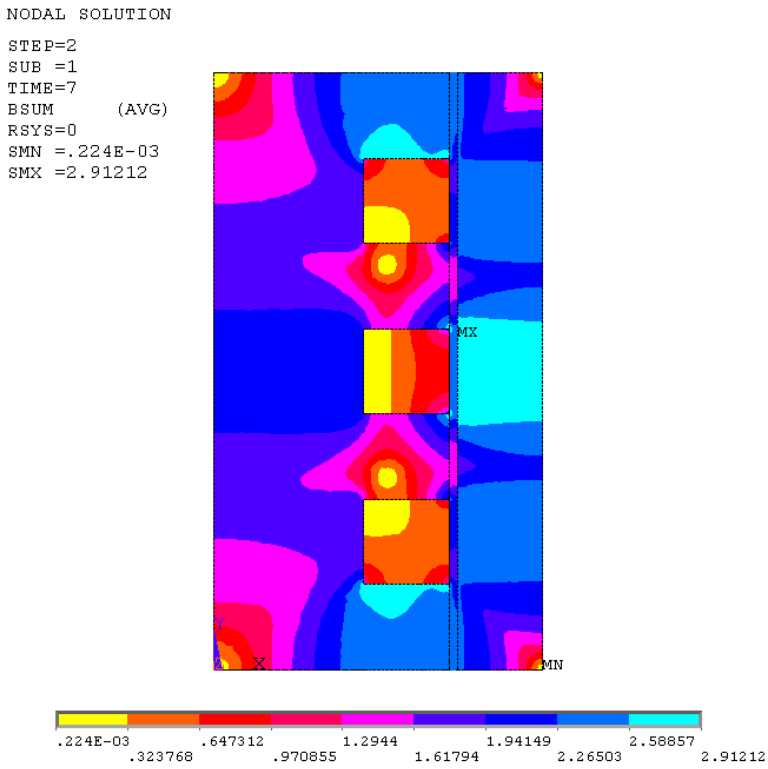

Fig 6.9 Contour plot of the resultant magnetic flux at 1 MA/m^2 current density.

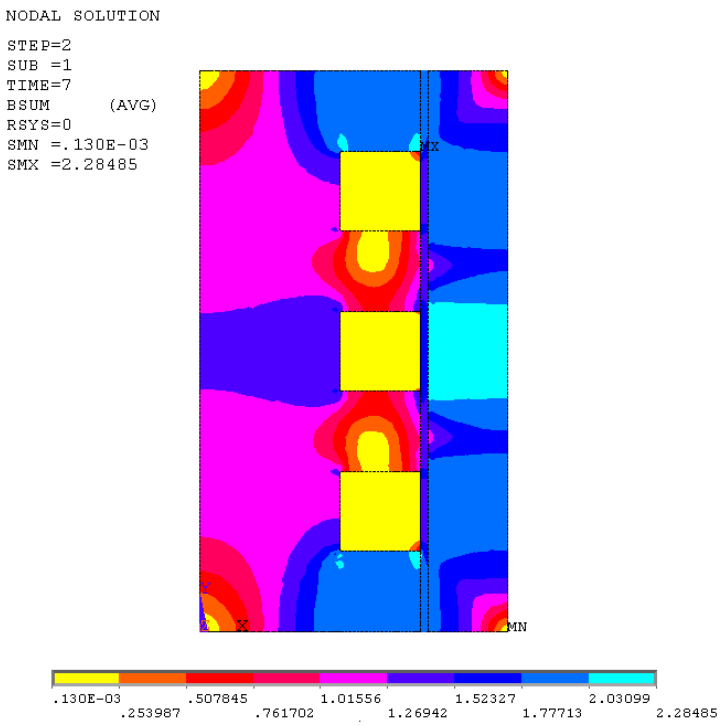

Fig 6.10 Contour plot of the resultant magnetic flux at 10kA/m^2 current density.

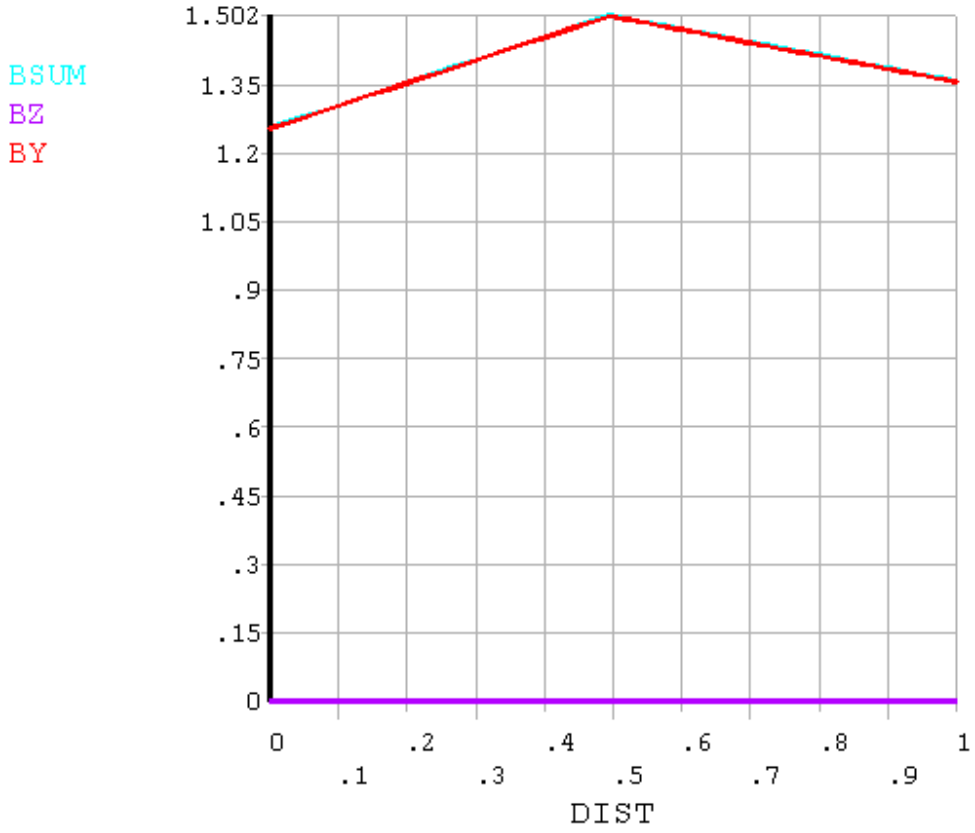

Fig 6.11 Variation of magnetic flux through the gap for 1kA/m^2 current density.

From Fig 6.4, BH curve and the contour plot for simulation of piston electromagnet at 10kA/m^2 current density it is seen that the core does not saturate (Fig 6.10) and the MR fluid crosses the operating point, Fig 6.11. This is an indication that the coils with shunt connection as given by the optimisation scheme can be used to magnetise the MR fluid at the operating point. This is because for the same input current, the current density for the shunted coils gets reduced by the factor equal to the number of shunted coils. Alternately a single coil can operate at lower input

current leading to the saving the power. The advantage of the shunted coils is that their time constant is low and so the response time of the actuator is low. This will require some trial and error simulation, which has not been presented in this work. The contour plot for simulation for 10MA/m^2 current density in Fig 6.9 shows that the piston core is still controllable up to 100 times the current density. The plot of variation of magnetic flux through the gap shows that the flux is nearly constant in the gap except for the last 0.2mm part towards the cylinder wall. Therefore the calculations for the fluid flow under a given value of yield shear stress will be valid with some correction applied to it. The flux line plot for the piston electromagnet is shown in Fig 6.12. The flux lines obey the flux parallel boundary condition and as such they bend inwards at the boundary of the piston. The pattern of magnetic field is, by and large, symmetrical.

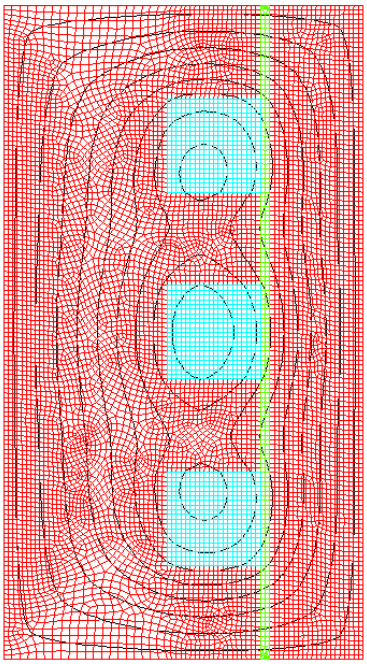

Fig 6.12 Contour plot of the resultant magnetic flux line 10kA/m^2 current density.

The electromagnetic simulation for the outer bypass channel has been done in the similar manner with 10kA/m^2 current density. The computational domain is shown in Fig 6.13.

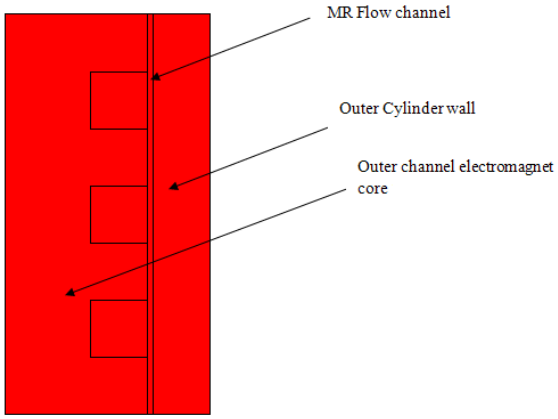

Fig 6.13 The computational domain for the electromagnetic simulation for outer by pass channel.

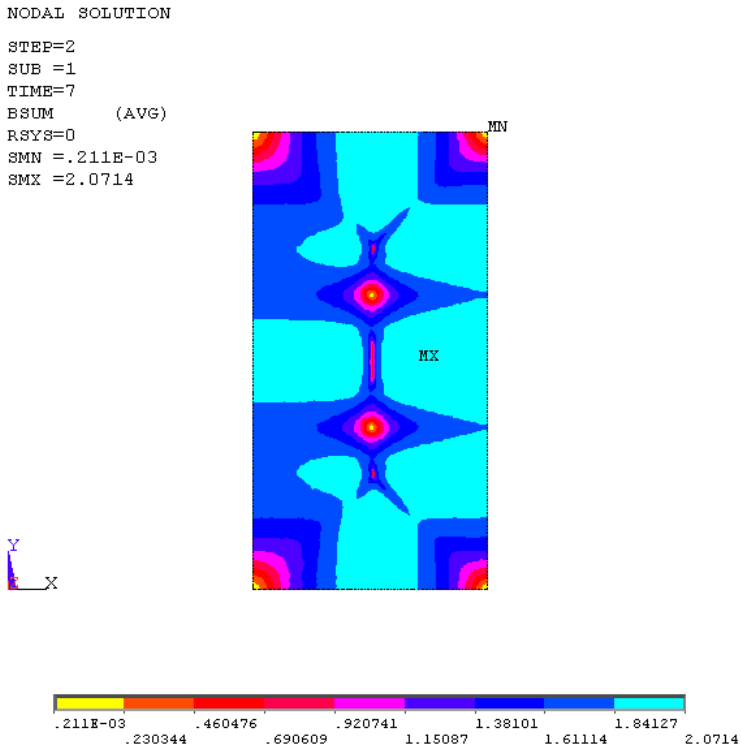

Fig 6.14 The contour plot for the electromagnetic simulation of outer-bypass channel electromagnet showing flux variation for 10kA/m^2 current density.

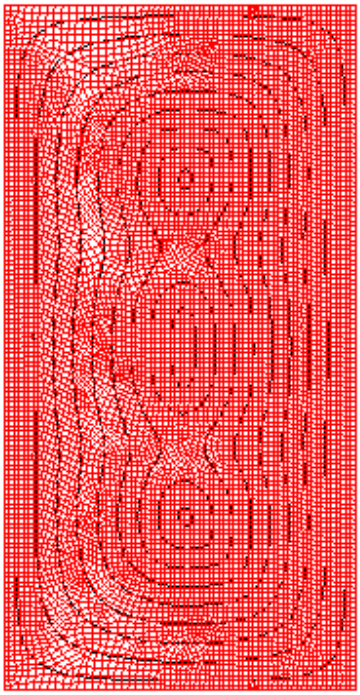

Fig 6.15 The contour plot for the electromagnetic simulation of outer bypass channel electromagnet showing flux lines for 10kA/m^2 current density.

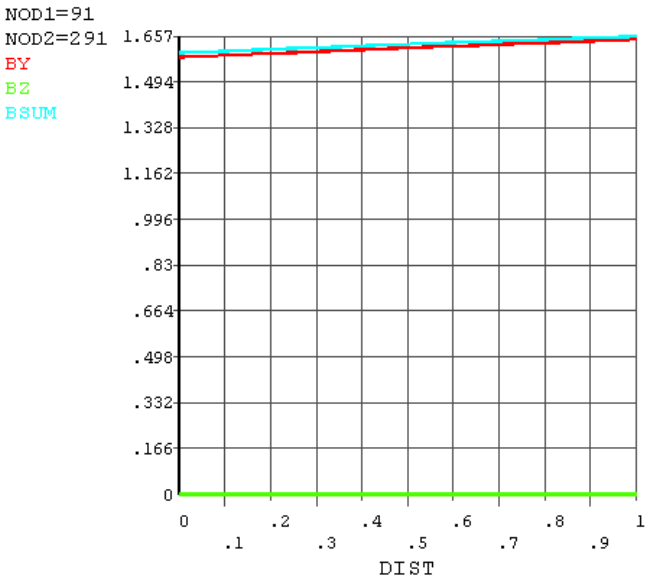

Fig 6.16 Variation of magnetic flux through the outer-bypass channel gap for 10kA/m^2 current density.

From Fig 6.16 it is gathered that at 10kA/m^2 current density the MR fluid will reach the saturation value and so the lower values of current will be applied for attaining yield shear strength of 40kPa. This solution is acceptable as it ensures that the fluid reaches the maximum value of yield shear stress for the above current density. The yield shear stress is almost constant throughout the gap except for the outer 0.2mm part of the channel. Therefore in the experimental setup some deviation in pressure gradient will be observed and so a correction factor for such a variation can be developed.

6.4 Proposed Mechanical design of MR damper

The proposed implementation of mechanical design for dual channel flow MR damper has two coaxial tubes of following dimension:

(1) Piston housing tube : Inner diameter of 55mm

Outer diameter of 68mm.

The piston housing tube has two rows of perforations on the top and on the bottom end. The top end perforations connect the tube to the accumulator through the top cylinder head. The bottom end rows of perforations connect to the outer bypass channel formed by the gap between the coaxial assembly of the inner and outer cylinder. The outer cylinder has following dimensions:

(2) Outer cylinder: Inner diameter of 70mm

Outer diameter of 80mm.

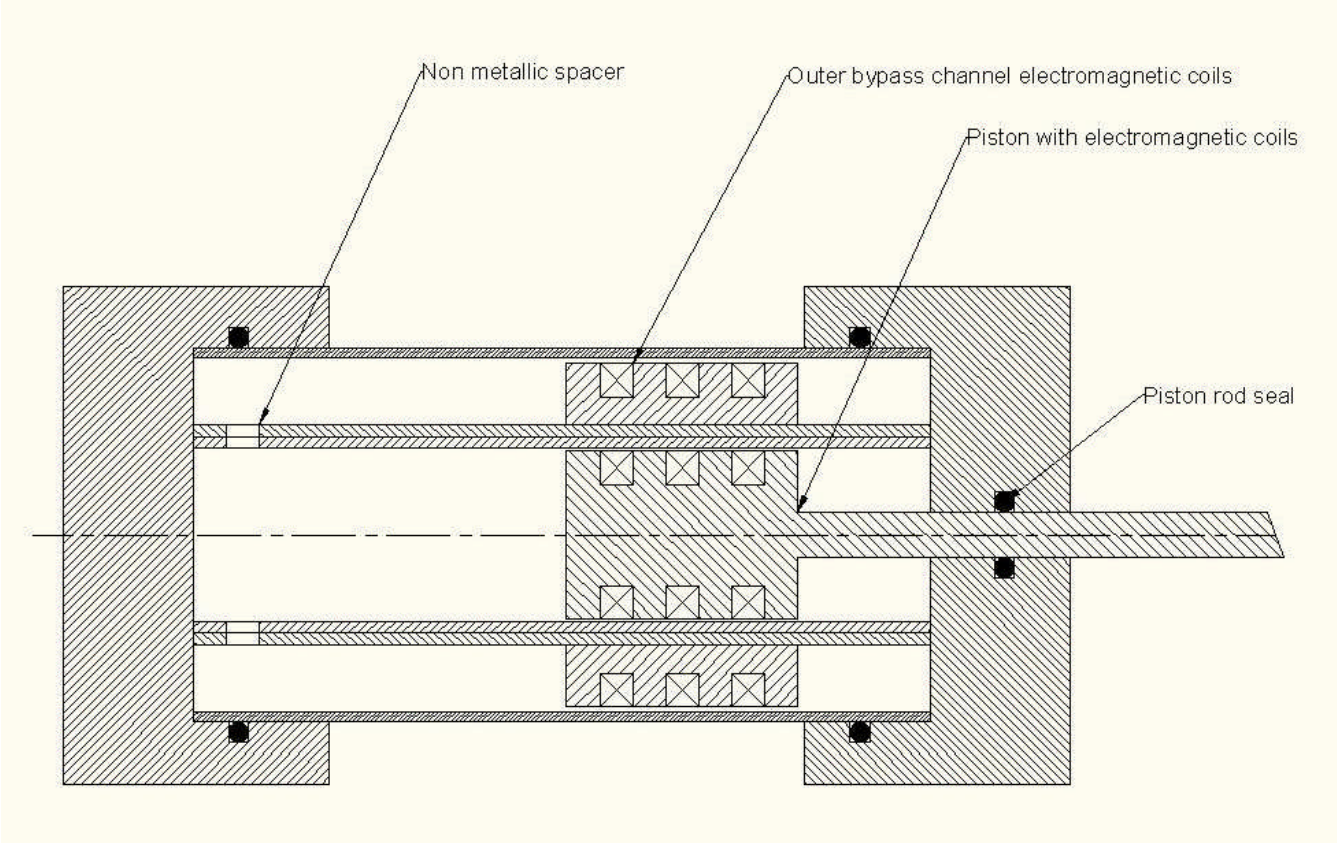

Fig 6.17 Proposed conceptual design of dual channel flow MR damper apparatus.

The structural design of the apparatus is based on standard procedure of pressure vessel design and as such the description has been excluded from the thesis. However, the design of seals is an important point of consideration in the design of MR dampers and so the same has been described in this work.

The design of seals is important from the point of view of the life of seals. The sealing materials rapidly deteriorate in contact with the suspension of fluid of the MR fluid. Commercial MR fluids are suspensions of ferrite materials in hydrocarbon oils. Study of paper by Jolly et al, (1998) leads to the conclusion that PTFE materials and neoprene materials have good resistance to degrading effect of hydrocarbon oils. Therefore all the seals such as O-ring were used of Viton

material (PTFE).The selection of rod seal is extremely important as it should be able to seal the fluid and resist wear at 20 m/s.

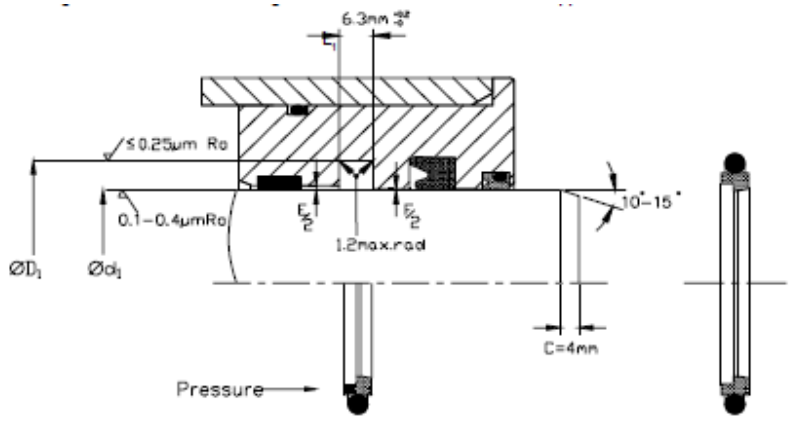

Fig 6.18 Claron^{TM} make seal HBT035

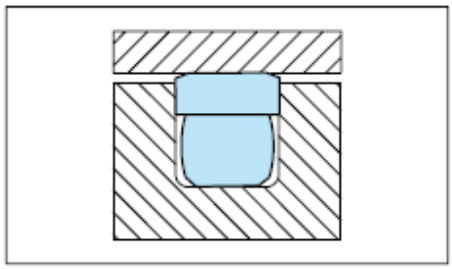

Fig 6.19 Turcon Glydring Trelleborg^{TM} make.

From the study of product catalogues of Claron^{TM} and Trelleborg^{TM} it was found that the seals such as HBT035 (Fig 6.18) and Trelleborg^{TM} Glydring (Fig 6.19) were found to be most suitable. The Claron^{TM} make seal shown in Fig 6.18 is available in Viton material. The Trelleborg^{TM} seals seem to be the best solution because the sealing material is Turcite^{TM} which has low friction and good wear resistance. This material is almost immune to lubricating oils and is used in lining the guide ways of machine tools. This seal is expensive to procure in small quantities and so the choice can be exercised in favour of Claron^{TM} make seal. If the results of the chapter 5 are

studied it leads to the conclusion that, ideally, there is no need for the design of seal installation such as above. The entire assembly can be considered to be a three channel type damper. From the previous chapter it is seen that when the yield shear stress for the MR fluid in the outer channel exceeds the yield shear stress of MR fluid flowing through the inner channel then the fluid flow gets blocked in the outer channel. Thus the MR fluid itself can be used to seal the damper by use of a permanent magnet ring at the sealing location. This aspect requires further investigation by experimentation.

6.5 Summary

Chapter discusses a new optimisation scheme for the design of MR damper. The scheme is based on the genetic algorithm. The chapter discusses the electromagnetic design of actuator for the piston flow channel and outer bypass channel. In the last section the mechanical design of a dual flow channel damper has been proposed.

CHAPTER 7

CONCLUSION

7.1 Primary outcomes

The work presents a transient model for predicting the response of an MR damper. The proposed model has been derived using the combination of Laplace and Weber transform to the Navier Stokes equation. The important underlying assumptions such as laminar flow and inclusion of body force due to the acceleration of piston have been justified. The assumption of laminar flow has been validated by comparison of operating Reynolds number with the critical Reynolds number. It has been shown that for single channel damper the flow remains Laminar for low piston velocities, but the flow becomes turbulent if the piston velocities exceed 2m/s. This is based on the correlation for the critical Reynolds number given in Nouar and Frigaard (2001). The computational domain of the MR damper has been considered to be an annulus between the piston and cylinder this because the solution for this type of domain can be applied to any other design of MR damper such as bypass duct damper with the modification of boundary conditions. The flow through the annulus can be considered to be a pressure driven Poiseuille flow superposed with the Couette flow. The variation of the piston velocity has been considered by applying Duhamel superposition principle for transient wall velocity boundary condition. The results of the model have been compared with the quasi static model given by Kamath et al (1996). The results show that the transient effect is significant even in the case of steady state piston velocity boundary condition. This is because the density of MR fluid is quite high and so the transient effects due to the inertia of the MR fluid become significant. This is a major

contribution of this work. The model presented in this work was validated by comparison of the predicted results with the experimental results for the Lord Corporation make RD8040 damper. The proposed model is able to predict the hysteresis like variation of the damper force with the velocity. The model also explains the effect of transient velocity boundary condition is particularly significant when the change in damper stroke is about to take place. This is because the effect of body forces and the change of damper velocity with time was found to be significant. Therefore the consideration of body forces and transient wall velocity boundary condition becomes important. The proposed model follows and identical algorithm for the direct and inverse model. The inverse model can be used to determine the yield shear stress required to generate the targeted damper force. Since the yield shear stress is function of applied magnetic field therefore current input required for the producing the applied magnetic field can be calculated. Therefore the inverse model can be used design a model reference based control system to determine the current input for a given value of damper force. The inverse model can also be used for the estimation of current compensation for the electromagnetic actuator based on the feedback for the measured damper force.

It has been shown in this work that the flow through the channel of an MR damper becomes turbulent as the piston velocity exceeds 2 m/s. Therefore a need was felt to propose a novel concept of compounded MR damper in which the laminar flow conditions can be maintained at higher piston velocities. The concept of compounding has been inspired by concept of compounding applied to hydraulic dampers. The compounded MR damper has two channels such as piston flow channel and an outer by pass channel. The bifurcation of MR fluid displaced by the piston into piston flow channel and outer bypass channel results in an increase

in Bingham number and a reduction in the operating Reynolds number for each of the channels of the MR fluid. Based on this assessment of laminar flow consideration the compounded or a dual channel type MR damper is able to maintain laminar flow condition up to 20 m/s. This is another major contribution of this work. The design has been compared with the multi-duct type (Gavin (2001)) damper and it has been shown that the proposed design can give higher damper force than the multi-duct damper due to two reasons:

(1) Multi-duct damper (Gavin (2001)) is based on electrorheological fluids.

(2) The multi-duct design consists of a bypass ducts. Since the dual channel design has one of the duct as a piston flow channel therefore due to the combination of pressure driven Poiseuille flow and Couette flow the pressure gradient will be higher than the corresponding multi-duct damper with the same piston diameter, same fluid properties and the same flow path length.

7.2 Secondary outcomes

The work introduces a new split flow scheme for predicting the force for the dual channel damper. The scheme can also be applied to the multi-duct damper developed by Gavin (2001). For high speed dampers the control of spike and response time for the electromagnetic actuator is an important consideration for the design of MR damper for high speed applications. Therefore a new optimisation scheme has been proposed for the optimisation of flow path length and response time of the electromagnetic actuators. It has been shown that the optimisation for the dual channel flow damper is an np-hard problem, therefore genetic algorithm has been found to be an effective technique for the optimisation for dual channel damper design. The application of

genetic algorithm for the optimisation of the electromagnetic actuators has given acceptable results which have been validated by finite element based static electromagnetic analysis.

7.3 Contribution to knowledge

The important contribution to the knowledge in the field of MR damper is the significance of transient effects due to fluid inertia, body force due to the acceleration of the piston and the effect of transient wall velocity boundary condition due to the change in the piston velocity. The work also introduces the application of critical Reynolds number correlations (Nouar and Frigaard (2001)) for validating the laminar flow assumption for MR fluid flow. These correlations have been used to demonstrate the effectiveness of dual channel damper in maintaining laminar flow conditions at high piston velocities.

7.4 Future work

In future the investigation on dual channel damper will aim at following:

(1) Development of fractional calculus based model for modeling fragmentation of plug of MR flow due sudden starting and stopping of MR fluid and it experimental validation.
(2) Improving the convergence of the Newton Raphson method based on the globally convergent algorithm outlined in Press et al, (2009).
(3) Development of robust technique to impose Piston velocity Boundary condition by Duhamel's superposition for estimating velocity function for a generalise spring mass damper system.
(4) Complete solution for the optimisation problem of damper described in chapter 6 to minimise the transients in MR damper.

(5) Development of model reference control based control policy to achieve constant damper force throughout the stroke as given by the damper's theorem for high speed damper applications.

APPENDIX-I

A.1. INTRODUCTION:

A.1.1 Background:

The design of hydraulic shock absorbers for reduction of load transmitted to the structure, has dominated all the applications for almost a century. Over the period of hundred years the design of hydraulic dampers has evolved into different variants to suit the applications ranging from a door closure to the recoil system of an artillery gun. A hydraulic damper is passive device and it dissipates the energy input to it by forcing the fluid through a narrow orifice. The fluid emerging out of the orifice is in the form of submerged free jet, which mixes with the stagnation fluid, and the kinetic energy of the free jet is dissipated as heat energy. The pressure drop due to the change in kinetic energy of the fluid across the orifice gives rise to an increase in pressure acting on the damper piston on which the external load acts. Thus, the net effect is that a damper transmits a very small force to the structure. The magnitude of the force transmitted to the structure is generally the difference between the external load and the force corresponding the pressure acting on the damper piston.

If the velocity of the damper is constant the orifice area is to be kept constant for keeping the damper force constant. However, as the damper stroke progresses the damper decelerates the system and the velocity gets reduced to zero at the end of the stroke. Due to the reduction in the velocity of the damper piston the braking force of the damper reduces and so in order to maintain the constant braking force the orifice area is progressively reduced with the stroke to a very small value at the end of the stroke. Whenever the load transmitted by the

damper to the structure is a major contributor, the design of a structure is dependent upon the simultaneous minimization of transmitted force and the stroke of a damper. A very long damper stroke will result in reduction in transmitted force but will also result in an increase in the size of linkages and components for the supporting or fixing system of the damper. A damper with a long stroke will itself be required to be sufficiently rigid to resist buckling. Thus, a long stroke damper will indirectly lead to an increase in the weight of the structure. In the case of dampers for seismic application, the amplitude of seismic force is not large and so the simultaneous minimization of transmitted force and damper stroke is required for compatibility with the load amplitude and its magnitude. In the case of automobile dampers, the compatibility with the vibration amplitude, force magnitude, and structural weight along with terrain and mission are important considerations (Hajihosseinloo (1989), Brown (1946) and Bhatnagar et al (2009)). In the majority of dampers, the damping force is designed to vary with the stroke by variation of area using a taper rod. Thus a hydraulic damper is an open loop control system in which the control law for varying the orifice area is implemented by means of a taper control rod type arrangement (see Fig A.1).

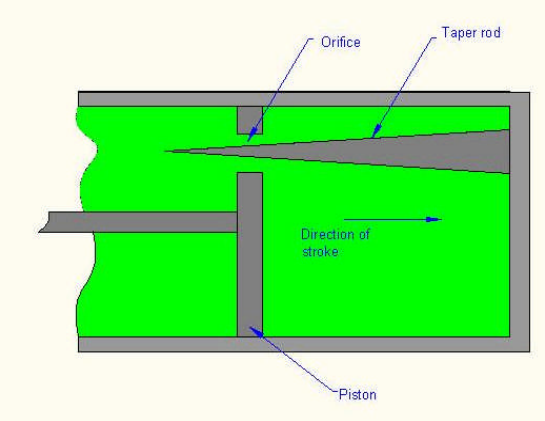

Fig A.1 Schematic of taper rod type damper.

However, the results of computational models (Hajihosseinloo (1989), Brown (1946) and Bhatnagar et al (2009)) and experiments show that the variation of damping force with the damping stroke is not constant as is the aim of this design approach. The approximate behavior of such a damper can be attributed to the non-linearities of the governing differential equation and lack of adaptability inherent in the system-design. The control law for the variation of orifice area is based on inviscid flow analysis and as such in actual case an appearance of spike in curve for the variation of damper force versus stroke is observed. In a manufactured product the geometric errors due to manufacturing tolerances and variation of coefficient of discharge due to inherent and environmental reasons contribute to the variation in the response. The presence of spike leads to secondary vibrations in the structure or fatigue failure of the structure at the joints due to stress concentration. In case of applications requiring vibration isolation such as engine mounts, suspension and driver seat mountings of an automobile the damper force is required to be adjusted with the frequency of vibration such that the damping coefficient is high at low frequencies and low at high frequencies. These are mutually conflicting requirements which cannot be met by a hydraulic damper which is reactive in nature. Here the term reactive means that the damper develops the damper force as a result of force input to the damper.

Since the hydraulic dampers have been used in wide range of application from low speed upto high speed and heavy loads therefore it was considered relevant to present a survey of the hydraulic damper designs. The survey presented in this thesis is considered to be helpful in evolving some of the concepts of magneto-rheological dampers from hydraulic dampers.

A.1.2 Survey of Hydraulic damper designs:

The designs of a hydraulic damper can be categorized based on the magnitude and the speed of application of the load in the following manner with exemplified applications:

	Range of Speed (m/s) and load (N)	Design of Hydraulic damper
(1)	Low speed 0-2	Taper rod type with short stroke(0-100mm)
	Light load 0-1000	

Applications: Door closures, vibration isolators, shock absorbers for passenger cars.

(2)	Medium speed 3-6	Taper rod type with medium stroke(100-500mm)
	Medium load 1000-10000	Valve type, bleeding hole and shim valve type

Applications: Passenger cars, Racing cars, Aircraft landing gears, armored fighting vehicles, rotary dampers used in armored fighting vehicles, seismic dampers.

(3)	High speed 7-30	Taper rod type with long stroke(1100-1500mm)
	Medium load 0-10000	Throttle valve type, compounded type

Applications: recoil systems of artillery guns.

A.1.2.1 Taper rod type dampers

At low speeds, which are less than 1m/s, the orifice area is not required to be varied for maintaining constant force along the stroke of the damper. Such dampers are suitable for door closures, bicycle shock absorbers and very low amplitude vibration isolators. However, if the speed is more than 1m/s, the loads are heavy and the amplitude of vibration or load amplitude is large then the force transmitted to the structure and the stroke of the damper is required to optimised simultaneously. This is because if the stroke is too long the damper will be required to be sufficiently rigid to resist buckling or the structure is required to provide long guide ways to for supporting the damper. On the other hand if the damper stroke is too small the force transmitted to the structure will be large. Thus, in both the cases the structure will become heavy and the advantage of using shock absorber will be offset and hence there is a need to control the variation of orifice for maintaining a constant damper force along the stroke for achieving simultaneous minimum of damper force and stroke. This is achieved by varying the orifice area by means of taper rod (see FigA.1). The other variations of implementing the variation of orifice such as tapered groove type and perforated tube are shown in Fig A.2.

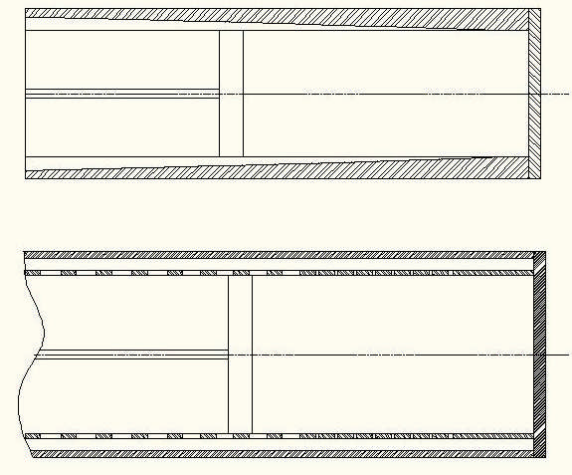

Fig A.2 Taper groove type and perforated tube type dampers.

The variation of orifice area is given by parabolic law (Eq1) as outlined in [2, 3].

$$A = -\frac{A_0 - A_e}{l^2} x^2 + A_0 \qquad \text{(Eq1)}$$

Where, 'A' is the orifice area at the instant 'x' of the stroke, 'A_0' is the area of orifice at the beginning of the stroke, 'A_e' is the area at the end of the stroke and 'l ' is length of the stroke of the damper.

A.1.2.1 A. Modeling of the taper rod type damper

There are two techniques to simulate the model of a taper rod type damper viz.

(1) Lumped mass parameter model.

(2) Computational fluid dynamics based semi lumped mass parameter model.

A.1.2.1 A (1) Lumped Mass parameter model

The structure and the damper with restoring spring are represented by one dimensional equation of functions of mass, spring stiffness, damper velocity, density of fluid, stroke of the damper and acceleration. The lumped mass parameter model is given by the following equation with reference to Fig A.3:

$$M_s \ddot{x} = F(t) - k\,x - f_d - \mu M_s\, g\cos\theta - M_s\, g\sin\theta \qquad (2)$$

$$f_d = C_d \frac{\left(1-\left(\frac{q}{Q}\right)\right)^2}{\xi}\left(\frac{\rho Q^3}{2q^2}\right)v_r^2 \quad \text{(Rhienmetall)} \qquad (3)$$

Where, '$\ddot{X}$' is the acceleration of the sprung mass, 'x' is the displacement of the system , 'M_s' is the sprung mass, '$F(t)$' is the time varying input load, 'k' is the spring constant of restoring spring, 'μ ' is the coefficient of friction, 'g' is the acceleration due to gravity, 'q ' is the orifice area, 'Q' is the effective area of the damper piston, 'ξ' is correction factor for viscosity, 'ρ' is the density of damper fluid, 'C_d' is the coefficient of discharge of the orifice, 'f_d' is the damper force 't' is time and 'v_r' is relative velocity of the damper fluid relative to piston.

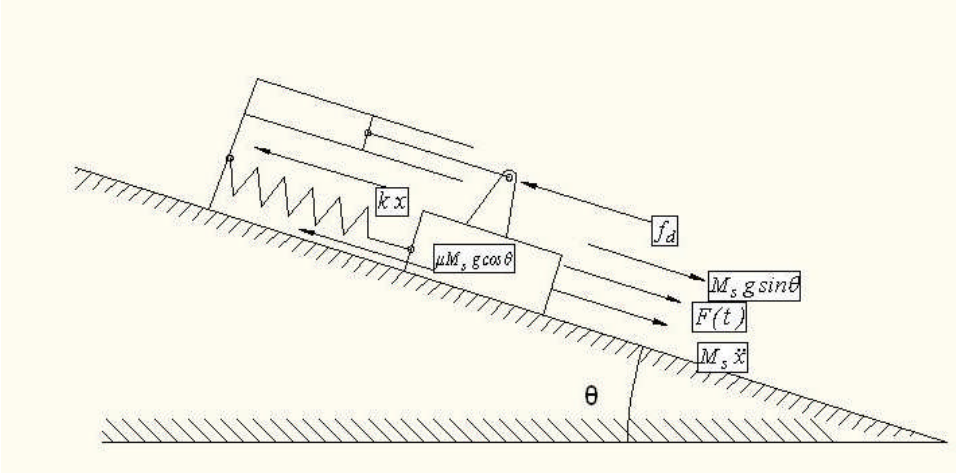

Fig A.3 Lumped mass parameter model of a structure with restoring spring and damper.

The lumped mass parameter is sufficiently accurate if for modeling a taper rod type damper. The only major limitation of the model is that the coefficient of discharge for the submerged orifice is required to be determined accurately. The solution of the above differential equation is obtained by standard numerical integration methods. The validity of the model has been established and results presented in (Hajihosseinloo (1989), Brown (1946) and Bhatnagar et al (2009)). In this survey the simulation results for taper groove type damper for an artillery gun have been presented. The variation of pressure acting at the base of the gun barrel with time is given in Fig A.4. In the FigA.4 the negative force denotes the equivalent force due the reduction of recoil momentum by the muzzle device. The input load to the damper is product of area of cross section at the base of the gun barrel and the pressure acting at the base of the barrel.

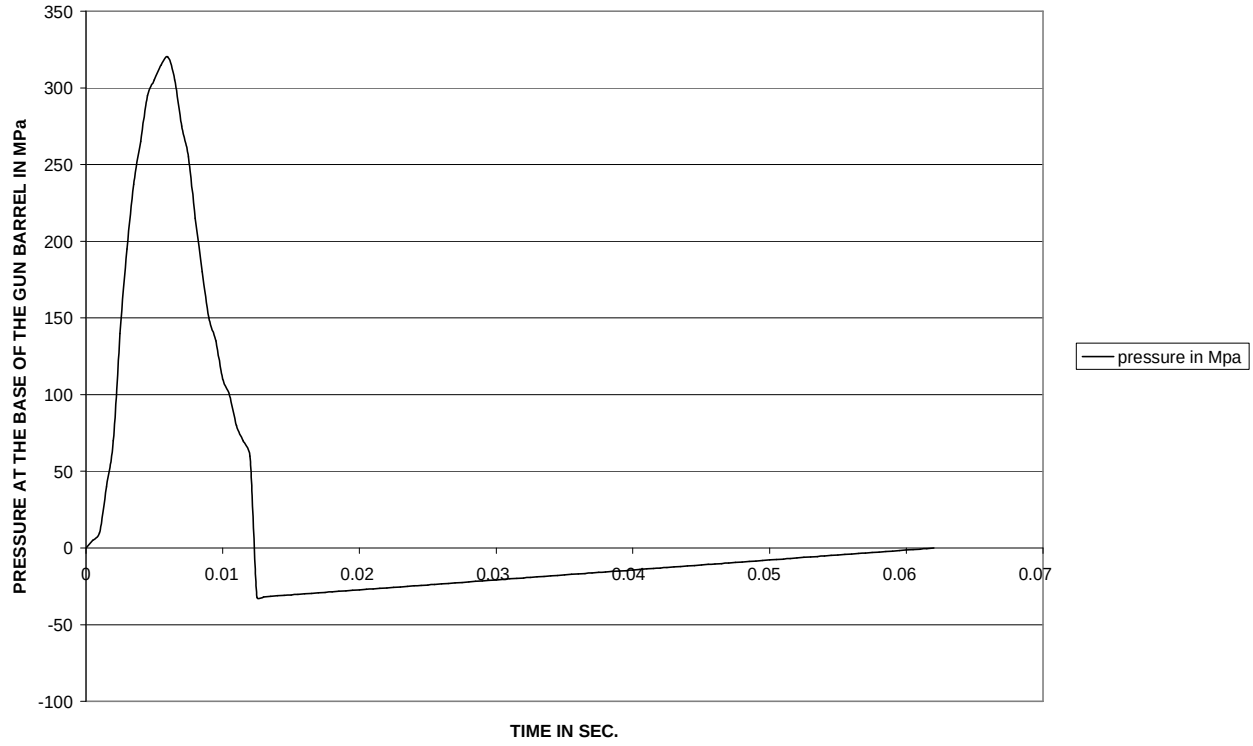

Fig A.4 Variation of propellant firing pressure acting at the base of the gun barrel with time

The profile of the taper grooves is approximately parabolic (see fig A.5) for the following reasons:

(1) During the gun fire of projectile form an artillery gun the damper should offer minimum resistance so as to prevent violent oscillation of the gun structure. This explains the presence of step at 0.1m in the initial part of recoil stroke as shown n Fig A.4.

(2) For manufacturing convenience the parabolic profile is approximated as a series of tapers.

(3) The grooves are rapidly closed during the end part of the stroke to prevent the damper piston hitting the damper cylinder head as a safety measureas shown in FigA.4 between 1.4 and 1.6m recoil stroke.

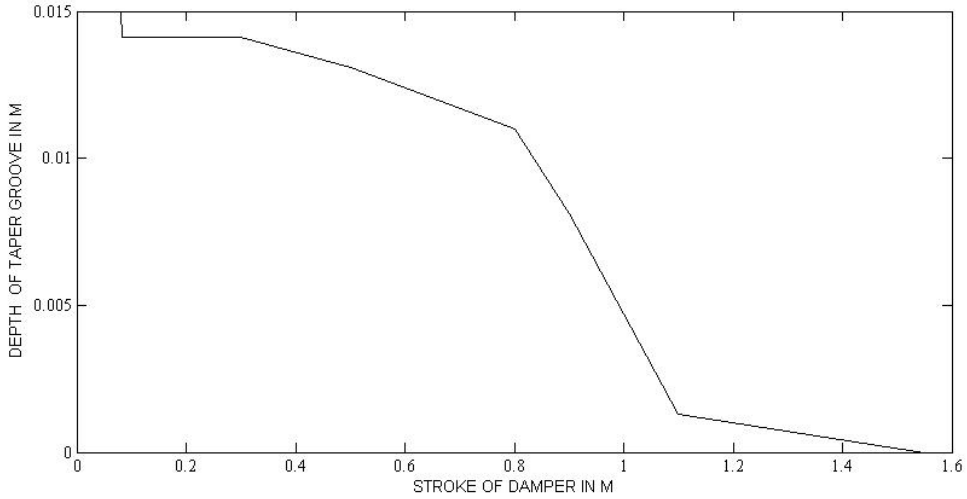

Fig A.5 Variation of depth of grooves with stroke for a taper groove type damper.

The total damper force versus stroke obtained from the numerical simulations, for different densities of fluid (see Fig A.6) shows that the spike of the damper force increases with the decrease in density of the fluid. On the other hand at fluid density equal to 1090Kg/m^3 the peak value of damper force in the initial part of the stroke is almost same as the value of total force at the spike for the density of fluid equal to 800k/m^3. The simulation explains why the density of damper fluids is kept near 800Kg/m^3. From the simulation it is also concluded that the presence of total damper force spike or peak in damper force cannot be minimized beyond a limit by changing the density of damper fluid. If the density of the damper fluid is increased to 1090kg/m^3 the stroke length required to bring the recoiling gun to stop can be reduced but the peak force increases to a value corresponding to the damper force at the spike for damper fluid

with density equal to 800Kg/m^3. Here the total damper force is the sum of force developed in damper due to pressure drop across the orifice, the force due to the restoring spring and the force of friction due to seals and slideways friction.

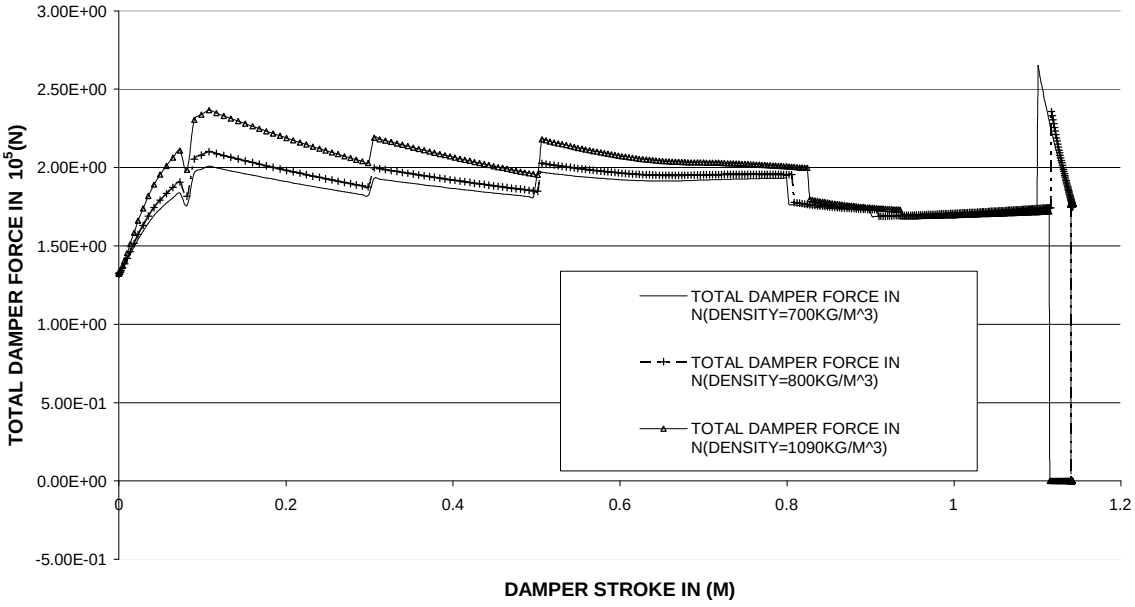

Fig A.6 Variation of total damper force versus stroke for taper rod type damper for different density of fluids.

A.1.2.1 A(2) Computational fluid dynamics based semi lumped mass parameter model:

In this approach the entire spring mass damper system is divided into trivial and non trivial domains. The trivial domains are the domains which can be represented by lumped mass parameter models with an acceptable accuracy. The region of orifice within the bounds of piston with taper rod is considered as the computational domain with inlet, wall and outlet boundary conditions. For each iteration step the pressure field is calculated to get the pressure at the inlet

and the lumped mass parameter equation is integrated to obtain the inlet velocity boundary condition. The inlet velocity boundary condition is the product of ratio of effective piston area to the orifice area and the velocity of the piston. The outlet boundary conditions are the outlet pressure and the mass flow rate which is equal to rate of fluid displacement by the effective piston area. If the solution converges the groove depth is calculated and the position of the wall representing the groove is changed by the value equal to the displacement corresponding to the change in depth of the groove and the mesh is updated. The iteration is carried for next time step followed by the updation of mesh and the solution continues to march till the piston speed is very near to zero value. The computational domain representing the piston and groove surfaces bounding the orifice is shown in Fig A.7.

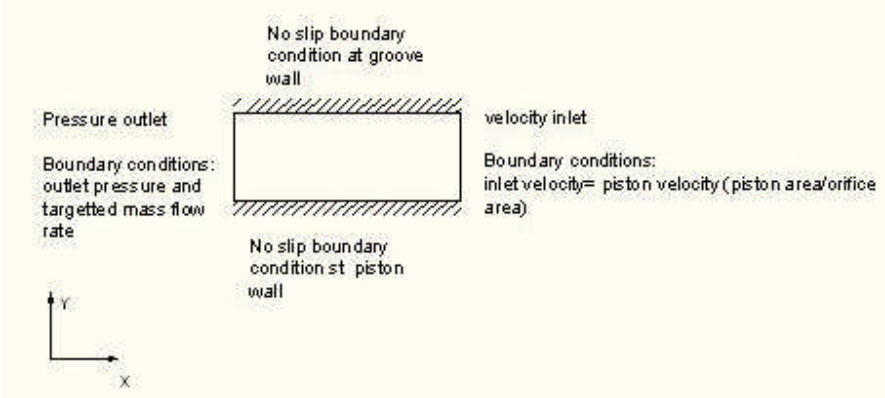

Fig A.7 Computational domain of the damper representing the piston and groove walls and the orifice of a taper groove damper.

The computational fluid dynamical model can be used to study the dissipation mechanism in the damper by simulating the transient free jet flow. It eliminates the use of Eq (3) in the lumped

mass parameter model and is also an effective tool for proof or damper design before the field trials. The model is able to account for the changes in flow due to the moving wall effect of the changing groove depth which results in dynamic changes in the discharge coefficient of the orifice. The only drawback of this technique is that it is computationally expensive. Since the lumped mass parameter is computationally inexpensive and has reasonable accuracy therefore taper rod type damper can be design using lumped mass parameter approach. However for diaphragm spring valve or valve type dampers or compounded type the computational fluid dynamics approach is more productive in rendering the effective design of dampers by reducing the experimental and testing efforts. It is for this reason that the results for computational fluid dynamical model for taper groove type dampers have been kept out of the purview of this survey.

A.1.2.2 Shim valve type dampers:

These dampers are essentially valve type dampers in which there is a bleeding hole for generating pressure gradient for damper force at low pressure and low velocity. However, as the velocity of the input load increases the damper pressure also increases up to a value at which the damper springs start deflecting resulting in an increase in orifice area and the damper force remains approximately constant for the rest of the damper stroke. The schematic of shim valve type damper is shown in Fig A.8. The schematic only show the single acting type damper. In case of double acting type damper the holes covered by the shim on the either side of the piston are staggered and the shims have rosette geometry to permit the opening of the holes on the opposite side of the piston.

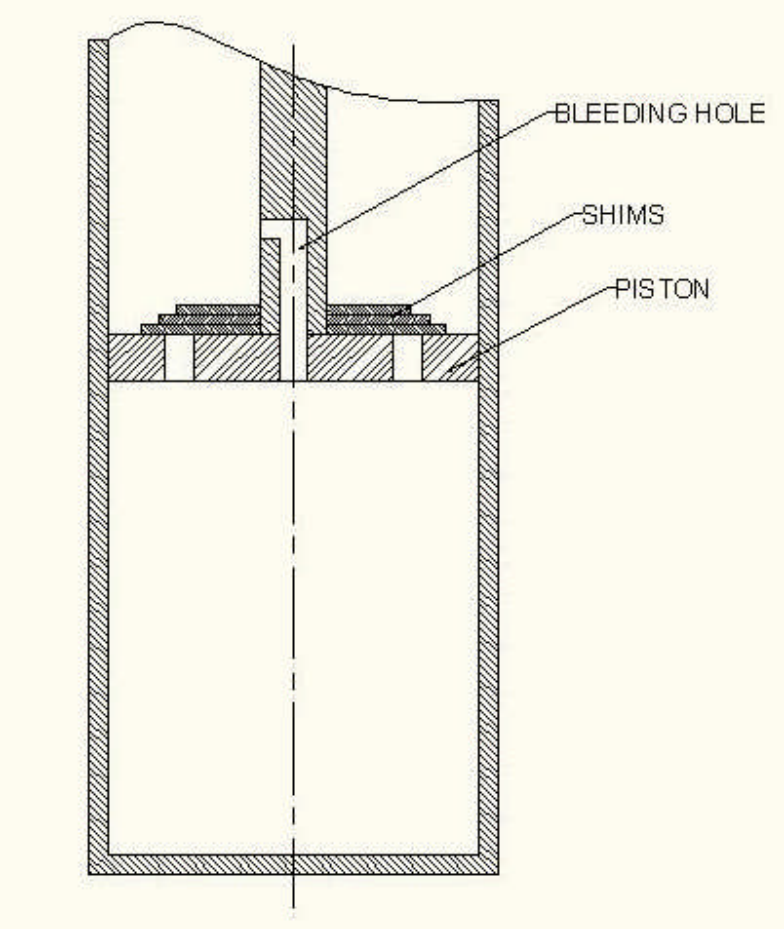

Fig A.8 Schematic of a shim valve type damper.

A.1.2.2 A Modeling of Shim valve type damper

A. 1.2.2 A (1) Lumped mass parameter model:

The lumped parameter model and Computational fluid dynamics model can also be used to simulate the diaphragm valve type damper. The Computational fluid dynamics approach is more accurate and can simulate the flow and pressure acting on the shims. The lumped mass parameter

model for shim valve type damper requires modifications in the calculations for the damper force. The expression for 'q' in Eq 3 for shim valve damper is given as follows:

$$q = \pi \frac{d_b^{\,2}}{4} + n\pi\, d_s\, w \qquad (4)$$

Where, 'd_b' is the diameter of bleed hole, 'd_s' is the diameter of holes covered by the shims,'w' is the deflection of shim and 'n' is the number of holes covered by the shim. The value of 'w' can be calculated by solving the equations for equilibrium of forces, moments and compatibility of deflection for the set of shim based on Roark (1975) The data for the simulation of shim valve type damper is given as follows:

(1) Damper diameter 50mm

(2) Bleeding hole diameter 4mm

(3) Number of shims 3

(4) Shim outer diameter 34mm

(5) Shim inner diameter 20mm

(6) Piston rod diameter 20mm

(7) Retracting spring type Pneumatic type integral with damper.

(8) Initial of gas volume of spring 1.96e-3m^3

(9) Retracting spring pressure 10 bar.

The response of the damper has been simulated for the sine wave velocity function given as follows:

$$F(T) = 100\sin(40\pi t) \qquad (5)$$

The dynamics of the shim valve is given by following equation:

$$m_{shim}\ddot{x}_{shim} = \Delta P_d A_{holes} - k_{shim}x_{shim} - \frac{1}{2}\rho C_{dshim}\dot{x}^2 A_{shim} \qquad (6)$$

In the above equation 'm_{shim}' is the mass of shim,' $\ddot{x}_{shim}$ ' is the acceleration of the shim, 'ΔP_d', is the pressure drop across the orifice, 'k_{shim}' is the stiffness of shim, 'A_{holes}' is the holes covered by the shim valve,'x_{shim}' is the deflection of the shim, 'C_{dshim}' is the coefficient of drag on the shim,' $\dot{x}$ ' is the velocity of shim,'A_{shim}' is the surface area of the shim.

The symbols used in the above expression have already been defined in the previous section. The variation of curve for variation of total damper force versus stroke is a smooth curve for square sine function (ref Fig A.8).Because of the low velocity (2.2m/s) of damper the model does not show the presence of spike. However in actual situation there is a presence of spike at the pressure at which there is a significant deflection of shim.

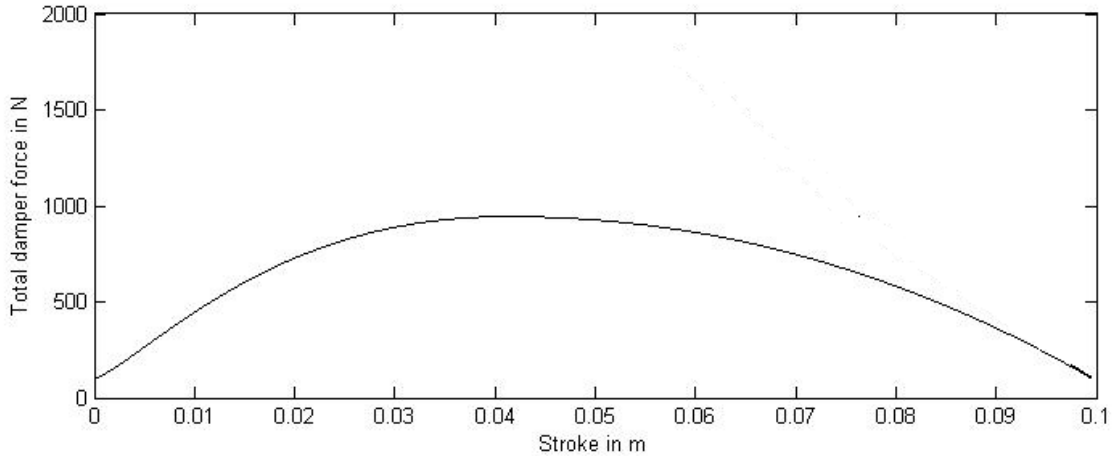

Fig A.8. Variation of total damper force versus stroke for the shim valve type damper.

The detailed design procedure has been outlined in Dixon (1999). The analytical and computational fluid dynamics models have been also reported in (Dixon (1999), Guzzoni et al (2007), Talbot and Starkey (2002)). In Talbot and Starkey (2002) the experimental validation of the model shows a very good agreement of the results with the results of the model.

A.1.2.2 A (II) Computational Fluid Dynamics Model

The modeling technique for the shim valve type damper is identical to the modeling technique for taper groove type damper. However the computational domain has some different boundary conditions due to shim. The computational domain for the shim valve damper is shown in Fig 11. In this work the computational fluid dynamics model for damper is 2D axi-symmetric. However for more accurate results a 3D model should used because the mechanism of dissipation is essentially turbulent in nature and so a 3D model is more appropriate. In this work 2D axi-symmetric realisable k-ε turbulent model (Lumley (1978)) has been used to demonstrate the technique and to present the reasonably accurate survey. In the computational domain there are two inlet boundary conditions for bleeding holes and shim valve. The valve area for shim valve

has been transformed to an equivalent axi-symmetric inlet with a shim of diameter weighted average thickness. The shim is considered to be a moving wall with mesh displacement corresponding to the deflection of shim using the formulas outlined in Roark (1975). For calculating the outlet boundary conditions the following equations are used:

$$\dot{m} = \pi\, d_p^2\, \dot{x}\rho \qquad (7)$$

Where, '$\dot{m}$' is the rate of fluid displacement by the damper piston, 'd_p' is the diameter of the piston, '$\dot{x}$' is the velocity of the piston, 'ρ' is the density of the fluid. The pressure of the restoring gas spring is given by following equation:

$$p_x = p_i\left(\frac{V_i - \pi d_r^2 x}{V_i}\right)^{1.31} \qquad (8)$$

In the above equation 'p_x' is the gas pressure of the restoring spring at 'x' position of the damper piston, 'p_i' is the initial gas pressure of the restoring spring, 'V_i' is the initial volume of gas of the restoring spring, 'd_r' is the diameter of the damper rod. The Eq (7) is used to apply the targeted mass flow rate and Eq(8) is used to calculate the outlet pressure boundary condition. The velocity inlet boundary condition is given as follows:

$$v_{inlet} = \frac{Q\,\dot{x}}{q} \qquad (9)$$

The pressure inlet pressure for each time step and at each iteration is used to calculate the damper for 'f_d' and is substituted in lumped mass parameter model of the system given by Eq(2) to calculate the refined value of acceleration. The integration of acceleration with initial value of

velocity and displacement of the damper piston is used to obtain the refined guess of boundary conditions for the computational domain shown in Fig A.9 till the convergence is obtained. The solution marches through the subsequent time steps till the damper velocity becomes zero.

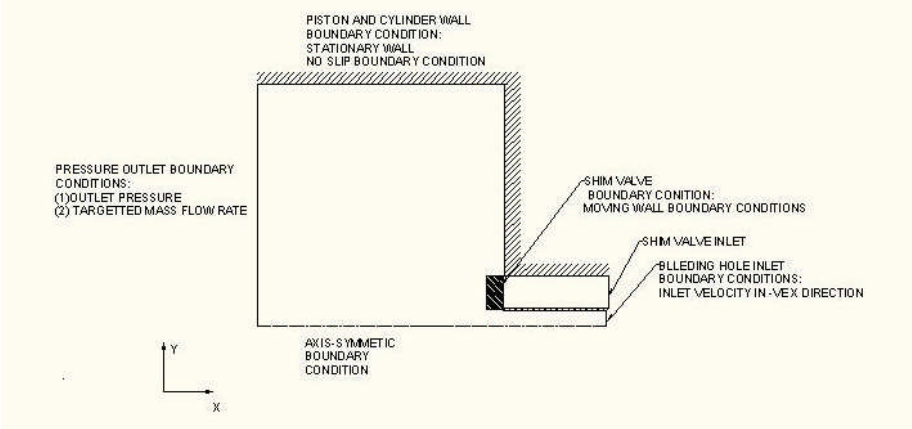

Fig A.9 The computational domain of shim valve type damper.

The finite volume mesh is shown in Fig A.10.

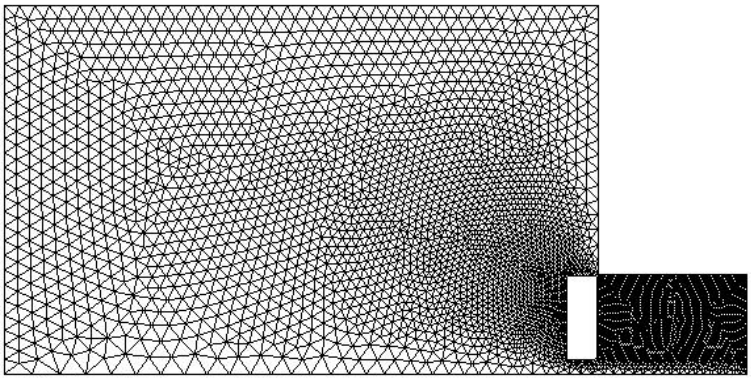

Fig A.10 The Finite volume meshes of shim valve type damper.

The simulated pressure and velocity fields are as shown in Fig 14,15.

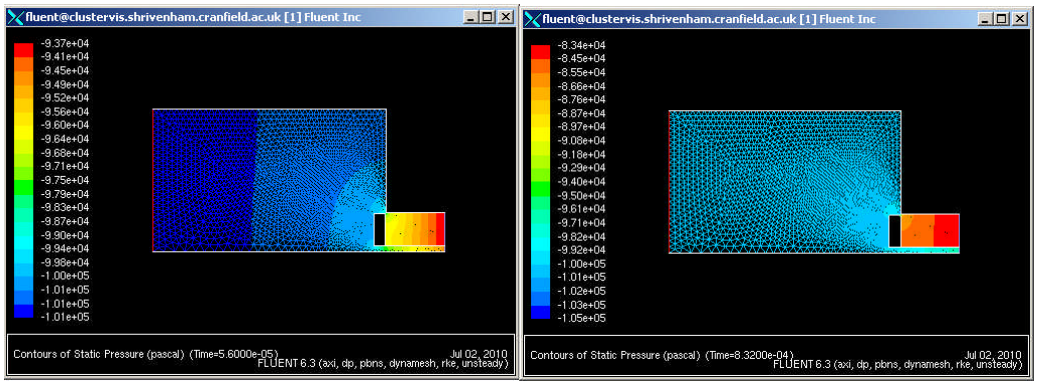

Fig A.11 Plot of pressure field simulated by k-ε CFD model of shim valve damper

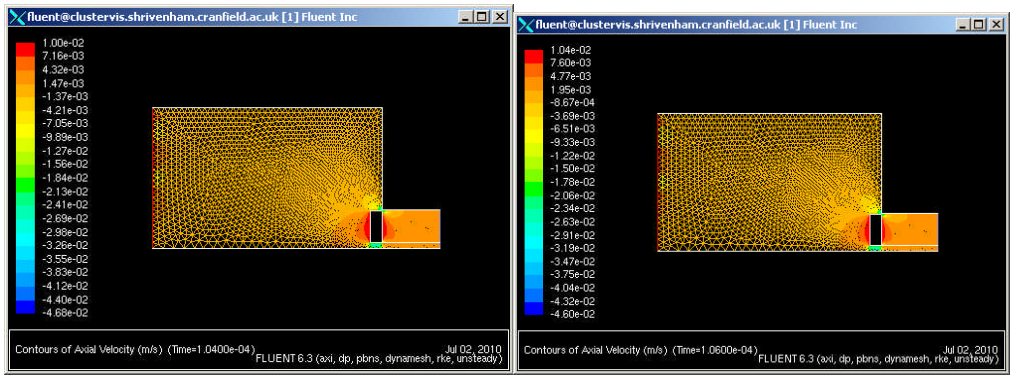

Fig A.12 Plot of axial velocity field simulated by k-ε CFD model of shim valve damper

A.1.2.3 Throttle valve type damper

The working of this type of damper is much similar to shim valve type damper except that the shim valve is replace by a spring loaded valve (see Fig A.13).

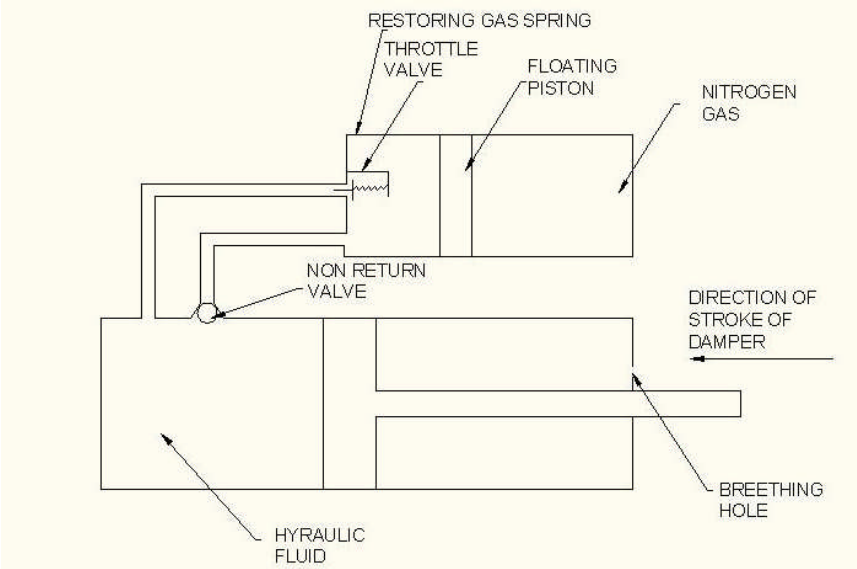

Fig A.13 Schematic of a throttle valve type damper.

The variants of a throttle valve type damper are used in racing cars shock absorbers, aircraft landing gear shock absorbers and artillery system recoil dampers. In case of artillery recoil dampers most widely used design is called as the Schneider type recoil damper (Ordnance Department Document No 2035 (1921)). The modeling of the throttle valve type damper is similar to modeling of shim valve type damper with a variation that the throttle valve has longer lift and higher flow rate as compared to the shim type damper. Since the damper characteristics of this type of damper has close resemblance with shim valve type damper and compounded type damper therefore the survey presents the investigation on compounded damper in more details. The findings based on results of the simulations the compounded damper are generally applicable to all other designs of dampers. The total damper force characteristics for valve type dampers differ from the similar characteristics of taper rod type dampers in respect of occurrence

of pressure spike. In case of valve type dampers the occurrence of spike takes place at the instant the throttle valve lifts up or pilot valve lifts up in case of a compounded damper.

A.1.2.4 Taper rod and pilot valve type compounded damper

The taper rod and pilot vale compounded type damper is a combination of taper rod and throttle valve type damper as shown in Fig 18.

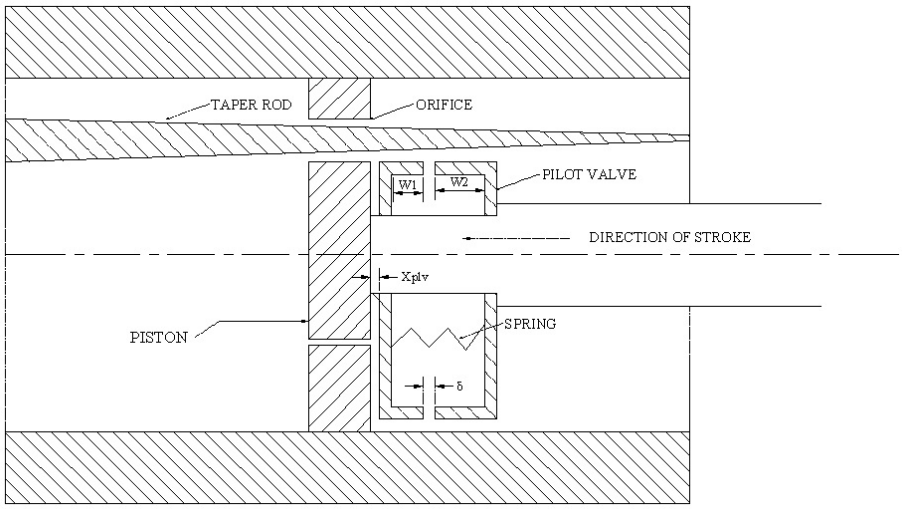

Fig A.14 Schematic of a damper with taper rod and pilot valve [3].

The taper rod and pilot valve damper is a compounding device used in high speed and high loading applications such as heavy artillery guns. In this type of damper the pilot valve open as the damper reaches the maximum velocity which is in the range of 12-25m/s. From the study of total damper force versus the stroke and velocity versus stroke characteristics it is observed that there is an occurrence of spike at a velocity of 12m/s and at this instant the pilot valve starts opening and is fully open at maximum velocity. The total damper force becomes almost constant once the spike dies down.

A.1.2.4 A Modeling of taper rod and pilot valve type compounded type damper[3]

1.2.4 A (1) Lumped Mass Parameter model:

The lumped mass parameter model of the taper groove and pilot valve type damper is described by two differential equations viz. Eq (2) and the equation of motion for the lift of the pilot valve. The flow area of the taper grooves and flow area due to the lift of the pilot valve is the total orifice area, across which the pressure gradient due to damper piston velocity. The schematic of the lumped mass parameter model for the damper is shown in Fig A.14.

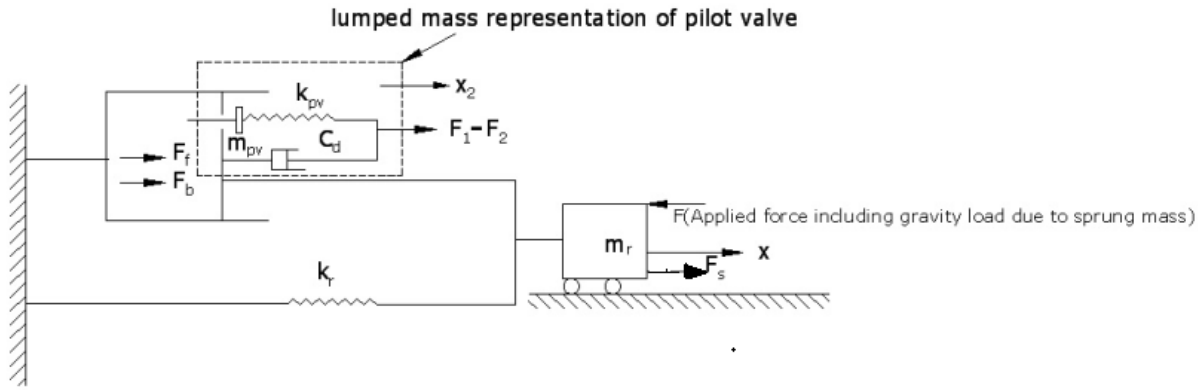

Fig A.14 Lumped mass parameter model of taper rod type damper.

The modeling forces acting on the pilot valve is base on inviscid flow theory and the assumption to this model are as follows:

(1) Inertia forces are significantly larger than the viscous forces and so the viscous force can be neglected. The braking force is a stronger function of

density than viscosity of the fluid.

(2) The compressibility effects are negligible. This assumption is particularly valid if the damping fluid is water-glycerin or water-ethylene glycol mixture.

(3) Properties of the fluid remain constant as the change in temperature remains negligible for a single stroke of damper. The algorithm used in this paper can also take into account for the change in density but the same has not been accounted for, in this paper.

(4) The piston of the damper and pilot valve act like rigid bodies. The expression for braking force ' f_d ' as mentioned in Bhatnagar et al (2009) is given as follows:

$$f_d = \rho v_r^2 \frac{\left((A_p - a_h) - \frac{(A_p - a_h)^3}{(n_2 C_{dgrv} a_{grv} - C_{dpv} \pi d_o x_{lpv})^2} \right)}{2} \quad (10)$$

Where, 'f_d' is the damper force, 'A_p' is the area of the damper piston, 'a_h' is the area of the jet holes shown in Fig 20, 'a_{grv}' is the area of the taper grove, 'n_2' is the number of taper grooves, 'C_{dgrv}' is the coefficient of discharge for the , 'C_{dpv}' is the coefficient of discharge of the orifice due to the lift of the pilot valve,' d_o' is the outer pilot valve diameter, 'v_r' is the velocity of the piston and 'x_{lpv}' is the lift of the pilot valve. For calculating the lift of the pilot

vale the fluid domain surrounding the rear of the piston and the pilot valve is divided into sub-domains (see Fig 20) for solving the Euler's momentum equations.

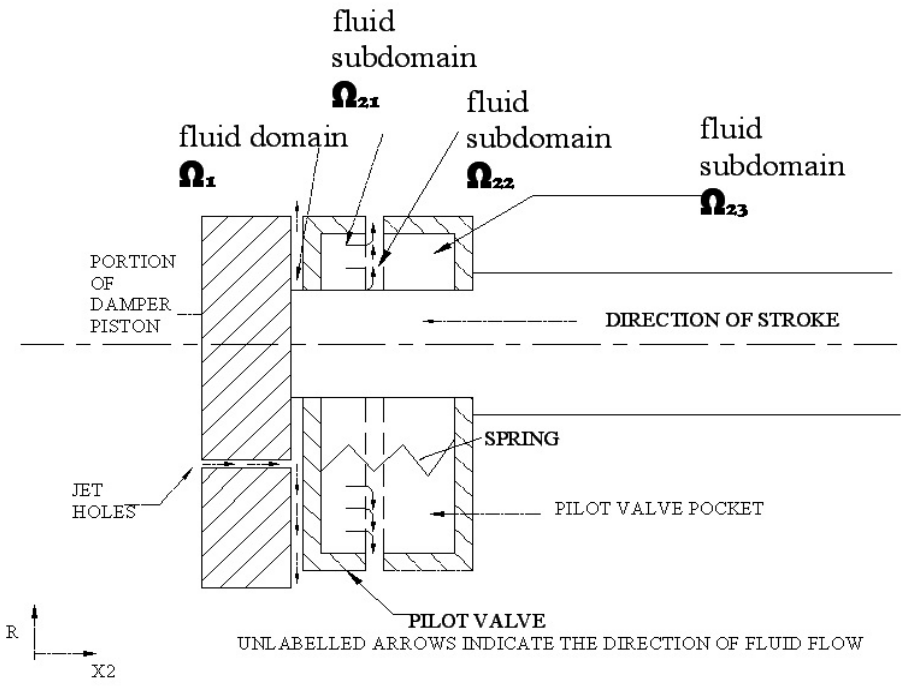

Fig A.15 Enlarged view of schematic of damper piston with pilot valve showing fluid flow through the gap due to the lift of valve through the valve pocket

The additional assumptions are as follows:

(1) The fluid domain Ω_1 is subjected to body force due to the acceleration of damper piston.

(2) The fluid sub-domain Ω_{21} is subjected to the body force due to acceleration of piston and relative acceleration due to lift of pilot valve. The entire fluid sub-domain has velocity equal to the velocity of the lift of the valve.

(3) The fluid sub-domain Ω_{22} is subjected to body force due to acceleration of piston.

(4) The fluid sub-domain Ω_{23} is subjected to body force due to acceleration of piston of damper.

The above assumptions are justified as the governing differential equations such as Euler equations, potential flow equations and the continuity equations for sub-domains are compatible. The detailed derivation for the expression of forces developed due to pressure gradients in each of the above fluid sub-domains have been outlined in Bhatnagar et al (2009). Here the final expression will be presented for the sake of brevity.

The expression for pressure force developed in the fluid domain $\Omega_1$is given as follows:

$$F_1 = F_{11} + F_{12} + F_{13} + F_{14} + F_{15} \tag{11}$$

$$F_{11} = 2\pi\rho\left(\frac{(A_p - a_h)\dot{v}_r}{a_o} - \frac{(A_p - a_h)v_r\dot{a}_o}{a_o^2}\right) r_o\, r_i^2\left(\frac{R^2\, ln(R)}{2} - \frac{R^2}{4} - \frac{1}{4}\right) \tag{12a}$$

Where,

F_{11} is the pressure force due to the inertia effect of variation of radial velocity of flow with respect to time. The symbols with superscripted dots represent the time derivatives of the variables represented by the symbols.

$$F_{12} = \pi\rho\left(\frac{(A_p - a_h)v_r}{a_o}\right)^2 r_o^2\left(ln(R) - \frac{(r_o^2 - r_i^2)}{2r_i^2}\right) \quad (12b)$$

and

$$R = \frac{r_o}{r_i}$$

Where, F_{12} is the pressure force due to radial variation of the radial velocity and 'a_o' is the total area of the orifice at the instant x of damper stroke and x_{plv} of pilot valve lift..

$$F_{13=}\rho a_h v_r^2\left(\frac{(A_h - a_h)\pi d_o x_{plv}}{a_o} - \frac{v_{rel}}{v_r}\right)^2 \quad (12c)$$

Where, F_{13} is the pressure force due to impact of jets from the jet-holes on pilot valve.

$$F_{14} = \rho x_{plv}\left(\frac{\pi \dot{v}_r(A_p - a_h)d_o x_{plv}}{a_o} + \frac{\pi v_r(A_p - a_h)d_o v_{rel}}{a_o} - \frac{\pi v_r(A_p - a_h)d_o v_{rel}\dot{a}}{a^2}\right) \quad (12d)$$

Where, F_{14} and, F_{15} are the pressure forces due to time derivative of the velocity through the jet holes.

$$F_{15} = -\rho \dot{v}_{rel} a_h x_{plv} - \rho \dot{v}_r x_{plv}\pi(r_o^2 - r_i^2) \quad (12e)$$

In the above expressions v_{rel} is the velocity of the pilot valve relative the velocity of the damper piston, r_o and r_i are outer and the inner radii of the pilot valve. The above expressions have been

derived by considering the jet holes at the inner radius. The final expression of the force on the inner surface of the pilot valve is given as follows:

$$F_2 = F_{21} + F_{22} + F_{23} + F_{24} + F_{25} \tag{13}$$

The pressure force due to the axial velocity of the pilot valve is given as:

$$F_{21} = \frac{\rho\pi(r_o^2 - r_i^2)(-v_r + v_{rel})^2}{2} \tag{13a}$$

The pressure force due spatial and time derivatives of the axial velocity of the fluid is given as:

$$F_{22} = -\rho\pi \left(\begin{array}{l} -\frac{(-\dot{v}_r + \dot{v}_{rel})(\delta - x_{plv})}{2} - (-v_r + v_{rel})\left(-\frac{(v_r + v_{rel})}{2} + (v_r + v_{rel}) \right) \\ +\frac{(-v_r + v_{rel})v_{rel}}{2} + (-\dot{v}_r + \dot{v}_{rel})(\delta - x_{plv}) \end{array} \right) (r_o^2 - r_i^2) \tag{13b}$$

The pressure force due spatial and time derivatives of the radial velocity of the fluid is given as:

$$F_{23} = F_{231} + F_{232} \tag{13c}$$

Where the terms F_{231} and F_{232} are given by

$$F_{231} = -\frac{\rho\pi}{2}\left(-\frac{(-\dot{v}_r + \dot{v}_{rel})}{(\delta - x_{plv})} - \frac{(-v_r + v_{rel})}{(\delta - x_{plv})^2} v_{rel} \right) \left(\frac{(r_o^4 - r_i^4)}{4} - \frac{r_i^2(r_o^2 - r_i^2)}{2} \right)$$

and

$$F_{232} = -\rho\pi r_i^4 \left(\frac{(-\dot{v}_r + \dot{v}_{rel})}{(\delta - x_{plv})} + \frac{(-v_r + v_{rel})}{(\delta - x_{plv})^2} v_{rel} \right) \left(\frac{R^2}{2} \ln(R) - \frac{R^2}{4} - \frac{1}{4} \right)$$

The pressure force due to the radial variation of kinetic energy due to radial velocity is given as:

$$F_{24} = -\rho\pi \frac{(-v_r + v_{rel})^2}{(\delta - x_{plv})^2} \left(\frac{(r_o^4 - r_i^4)}{4} + r_i^4 \ln(R) - r_i^2 (r_o^2 - r_i^2) \right) \quad (13d)$$

The pressure force due to body forces acting on the sub-domains of fluid domain Ω_2 is given as follows:

$$F_{25} = \rho\pi (r_o^2 - r_i^2)(w_1(-\dot{v}_r + \dot{v}_{rel}) + (\delta - x_{xplv})\dot{v}_r + w_2 \dot{v}_r) \quad (13e)$$

The equation of motion of pilot valve can now be written as:

$$m_{pv} \frac{d^2 x_2}{dt^2} = F_1 - F_2 - k_{pv}(x_1 + x_{plv}) - C_{vdamp}\ \rho\ \pi(r_o^2 - r_i^2) sgn(-v_r + v_{rel})(-v_r + v_{rel})^2 / 2.0 \quad (14)$$

In the equation above, 'm_{pv}'is the mass of pilot valve; the third term represents the spring force due to lift of pilot valve and preload deflection and the last term represents the damping due to the viscosity effects of the fluid used for the damper. The symbols 'C_{vdamp}' represents the damping coefficient to account for viscosity effects in the equation. The initial and boundary conditions for the model are given as follows:

Initial conditions:

(damper stroke) $x=0$, (damper piston velocity) v_r=0, (pilot valve lift)

x_{plv}= 0.0001mm,

(Pilot valve velocity relative to the piston) v_{rel}=0 at t=0.

In the initial conditions, it may be noted that some small value of pilot valve lift must be prescribed for obtaining the finite values of pressure forces.

Boundary conditions:

For $t>0$

$v_r=0$ at $x_{plv}=x_{pmax}$ (Maximum pilot vale lift)

when

x_{plv}=0.0001 mm $v_{rel}=0$

x_{plv}=δ-0.0001 mm $v_{rel}=0$

The last two boundary conditions on the pilot valve lift indicate that the pilot valve comes to rest as it reaches the mechanical limits of the maximum and minimum lift. The solution procedure is based on Newmark-β Predictor method (Subbaraj and Dobainish (1989)) and has been described in details with stability criteria in Bhatnagar et al (2009)). The simulation for two loading cases (Fig A.16) was experimentally validated and it was simulation results were found to be in good agreement with the experimental measurements (see FigA.16& FigA.17).

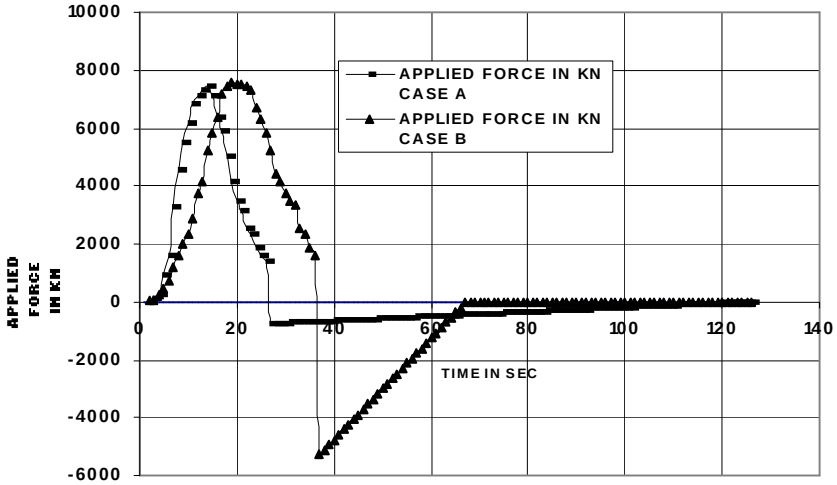

Fig A.16 Variation of load versus time for the load acting on the taper groove and pilot valve compounded damper Bhatnagar et al (2009)).

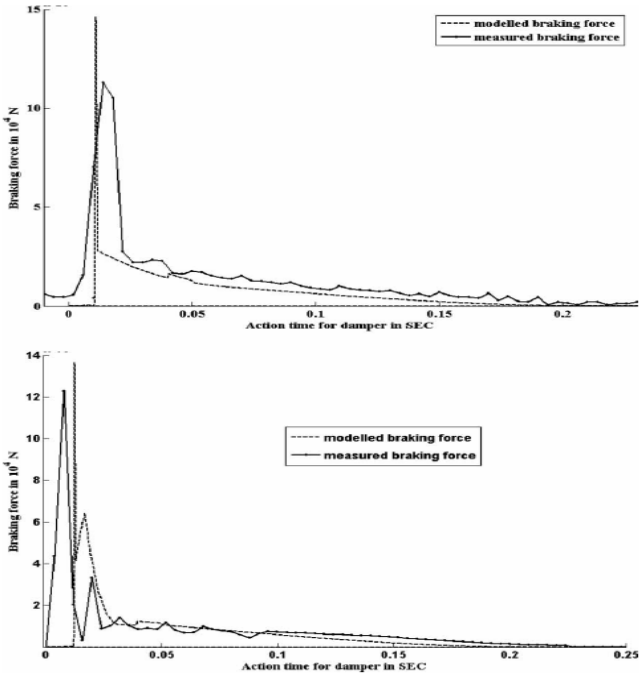

Fig A.17 Variation of experimentally measured and predicted braking force with time for loading case A and (b) case B Bhatnagar et al (2009)).

The variation of total damping force for load case A for different density of fluid shows that the taper groove and pilot valve type compounded damper gives the best performance for high density fluid. At less than 1050 kg/m^3 density the model gives fictitious oscillation but is able to show that the peak damper force rapidly increases with the decrease in the density of the fluid (see Fig A.18). This leads to the conclusion that the taper groove and pilot valve compounded damper is suitable for high density damper fluids.

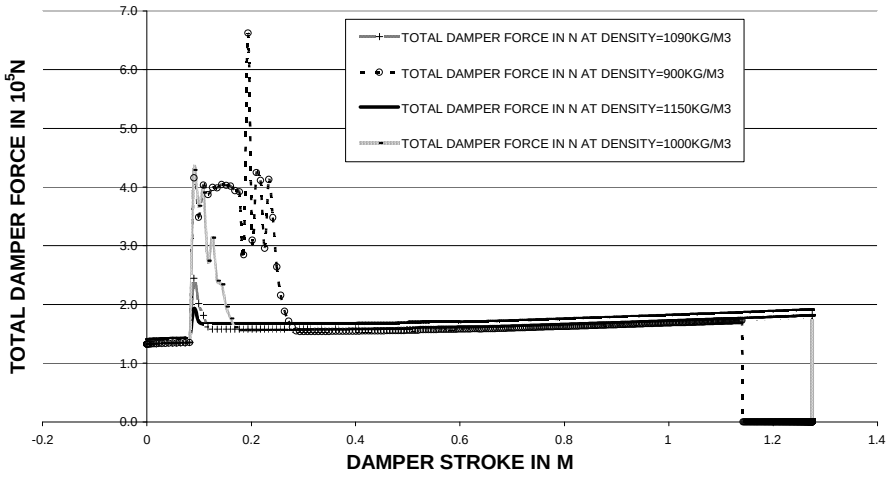

Fig A.18 Variation of total damper force versus stroke for different densities of damper fluid.

The parameter study for the effects of variation of sprung mass, damper fluid density, maximum pilot valve lift will be presented in the following section which deals with the computational fluid dynamics modeling of taper grooves and pilot valve compounded damper.

A.1.2.4 A (II) Computational fluid dynamics model

The computational fluid dynamics modeling of the taper groove and pilot valve compounded damper is achieved by stepwise division of entire computational domain into trivial and non trivial sub-domain. This is necessary for achieving computational economy with reasobale accuracy of the solution. The solution of entire computational domain including piston and restoring spring is definitely most accurate but it is extremely computationally expensive and may result in formidable debugging difficulties. In view of this the computational domain is divided into trivial and non trivial domains in following steps (see also FigA.19):

(1) The pressure of the restoring spring can be computed in the manner similar to the procedure given in section 1.2.2 A (II) for calculating the pressure outlet boundary condition. The force acting of the piston as product of pressure of restoring spring at a given time step and the damper piston area for using in Eq (2). Thus, the restoring spring is treated as a lumped mass parameter sub-model.

(2) The taper grooves in this model are not modeled with the computational domain. The effect of variation in depth is used to compute the orifice area and added to the orifice area due to the lift of the pilot valve as obtained from the computational fluid dynamics model for calculating the inlet velocity to the jet holes shown in Fig A.15 using Eq (8). This simplification results in the neglecting of the effect of moving wall boundary condition due to the change of the depth of grooves. Since this velocity component is small as compared to the maximum velocity of the damper, which is in the range of 18-19m/s for loading cases similar to case A or B, therefore this simplification will not induce significant error in the solution.

(3) The net effect of drag force and pressure force acting on the pilot valve is obtained by integrating the pressure and wall shear stress acting on the surface area of the pilot valve for each iteration of a given time step using the CFD solution and the lumped parameter equation of motion is integrated to obtain the lift and velocity of pilot valve to obtain the moving wall boundary condition for the pilot valve and the mesh displacement for the adjacent meshes. The equation of motion pilot valve is similar to Eq(13) with a variation that the first two terms on the left hand side and the four the term are replaced by the net force as above the calculation of restoring of the spring of pilot valve is calculated using pilot valve lift in the second term.

(4) The piston walls and stationary pilot valve walls have no slip stationary wall boundary conditions.

(5) The computational domain showing the pilot valve and rear side of the piston (see figure A.15) is given in Fig A.20. is the non trivial computational domain for which the finite volume mesh is laid out (see Fig A.21).

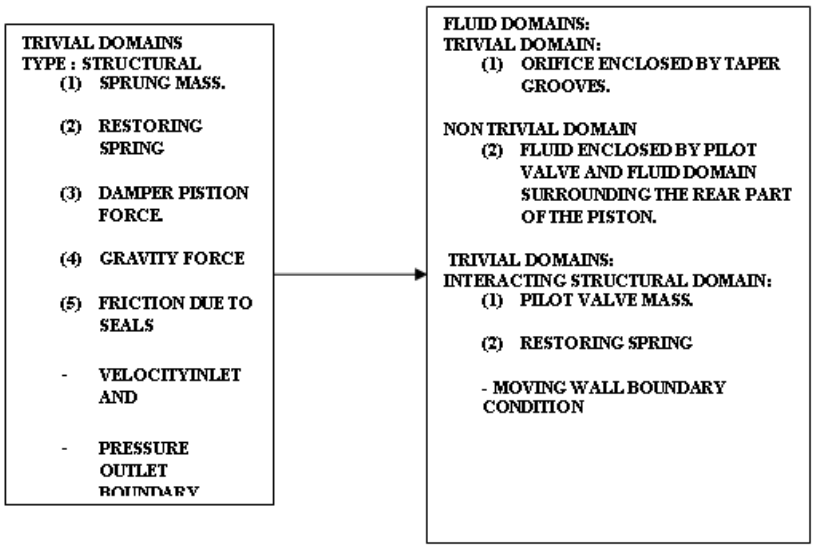

Fig A.19 Subdivision of computational domain for taper rod and pilot valve compounded damper.

For the modeling of dampers the software package found to be most suitable for the implementation was FLUENT Ver 12.x. This is because the user defined routine programming is more straightforward in FLUENT. The modeling of dampers with valves will require moving mesh finite volume method based on Ferziger and Peric (2002).

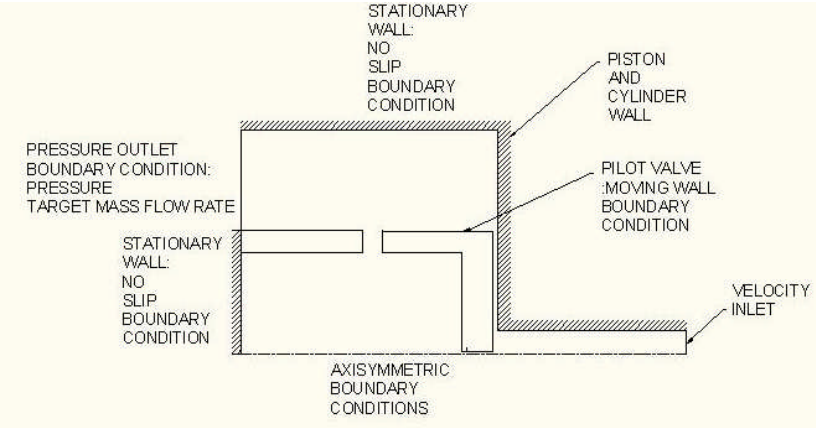

Fig A.20 Computational domain of taper groove and pilot valve compounded damper.

The subdivision of the computational domain is given in Fig 24 below:

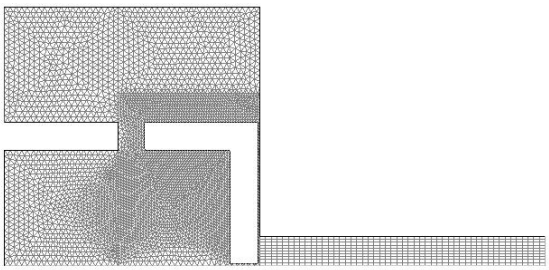

Fig A.21 Finite volume mesh of the computational domain of taper valve and pilot valve compounded damper.

The pressure and velocity fields computed by the model at various instants of time are shown in Fig A.22a and b respectively. The pressure filed plot shows that at low piston velocity there are small pressure gradients in the region between the cylinder wall and pilot valve. However as the piston speed reaches maximum velocity the pressure pike appears and during this time duration there is formation and oscillation of vortex. As the pressure spike subsides there is formation of larger vortex which oscillates with low velocities. The pressure gradients in the pilot valve pocket do not change significantly.

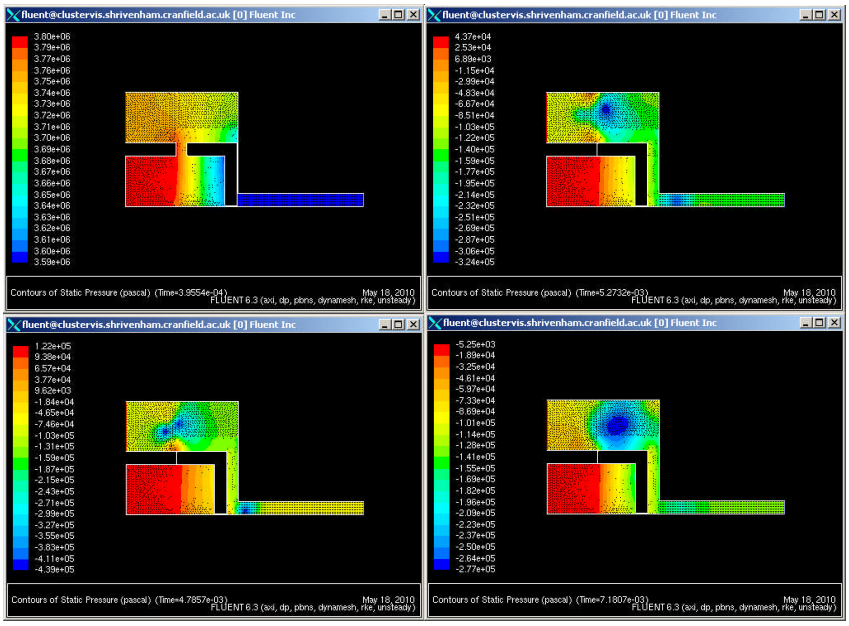

Fig A.22a Pressure field plot of simulation of taper groove and pilot valve compounded damper.

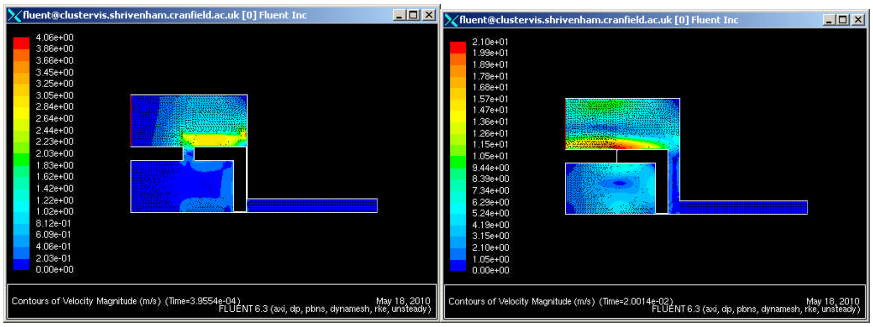

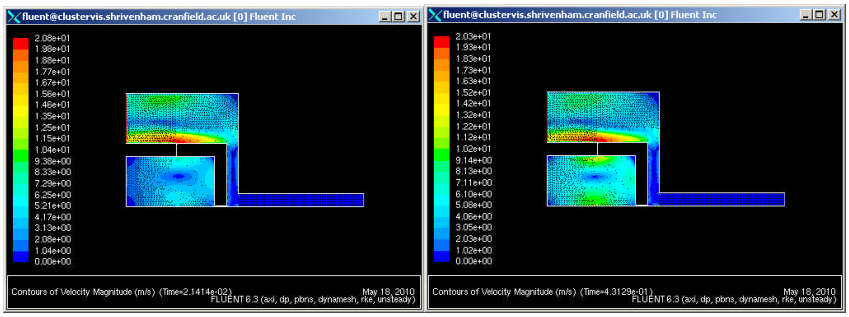

Fig22b Velocity field plot of simulation of taper groove and pilot valve compounded damper.

The comparison of variation of damper force using computational fluid dynamics model and experimentally measured damper for load case A is shown in Fig A.23.

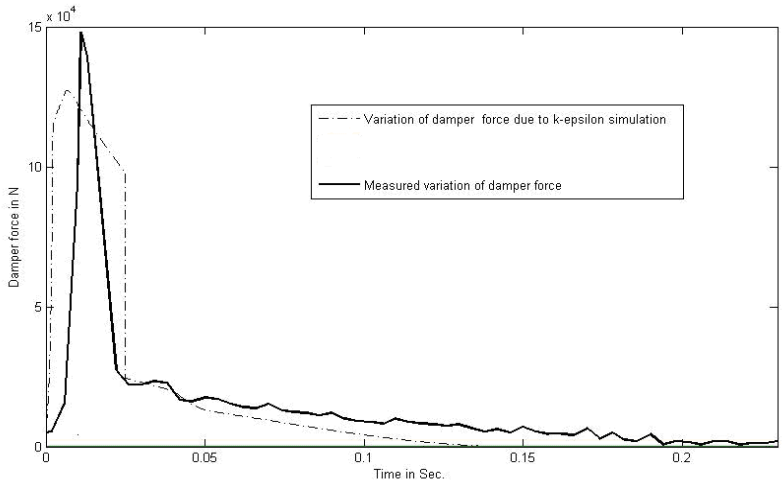

Fig A.23 Comparison of damper force versus time variation predicted by k-ε turbulent flow CFD model with experimental results for load case A.

The comparison of CFD model with experimental measurements show that the CFD model under predicts the damper force spike. The inviscid flow model over predicts the damper force spike. This leads to the conclusion that the laminar flow model or inviscid CFD model may give better results. Such investigations have been kept out of the purview of the survey in as much as such investigations are beyond the scope of thesis work. Since the design of damper is required to be safe and reliable therefore inviscid model can be considered to give an acceptably conservative design. It also pertinent to mention that inviscid flow model is computationally

inexpensive. Based on above conclusion the parametric study based on inviscid flow model is presented below (Bhatnagar et al (2009))).

The performance characteristics of the damper have been studied for variation of peak damper force with density of the damping fluid, sprung mass and maximum permissible pilot valve lift. The peak braking force has been studied because the damper force remains fairly constant in the rest of the damper stroke. The peak damper force has been non-dimensionalised with reference to density of fluid, maximum permissible pilot valve lift and peak velocity of the damper. The expression for non –dimensional damper force is given as:

$$F_{bnd} = \frac{F_b}{\rho x_{plv}^2 v_{r\max}^2} \tag{14}$$

The variation of peak braking force with density is shown in Fig. A.24.

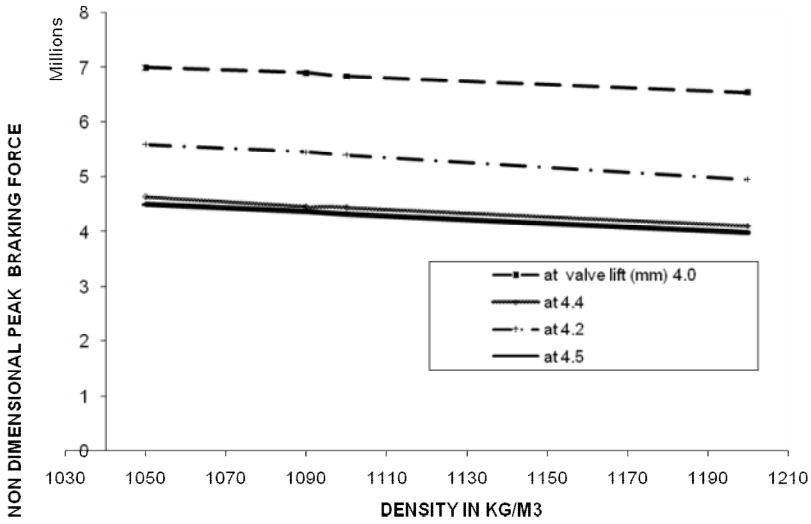

Fig A.24 Variation of non-dimensionalised peak damper force at constant valve lift in mm with the change in density

The curves for the variation of peak braking force after non dimensionalisation show similarity in form. The peak braking force in non-dimensionalised form is a measure of specific rate of dissipation of momentum which is similar to specific impulse used to define the performance in jet engines. The peak braking force increases with the decrease in the density of the damping fluid because the specific rate of change of momentum of damping fluid at the combined effective area of orifice of the damper is higher.

The peak braking force has been found to increase with the increase in sprung mass. This observation is also in agreement with Brown (1947). The damper stroke and the peak velocity of a damper decrease with the increase in the sprung mass if the kinetic energy imparted to the damper by the dynamic load is kept constant. Since the damper is designed for maintaining constant braking force therefore for same dissipation of kinetic energy the mean and peak braking force should increase with the reduction in damper stroke due to increase in sprung mass. The variation of braking force with the increase in the sprung mass is shown in Fig. A.24.

The peak braking force decreases with the increase in the maximum lift of pilot valve due to increase in the orifice area and also because the braking force is inversely proportional to the orifice area. The curves shown in Fig A.25 for sprung mass 2565 kg and 2765 kg are approximately same.

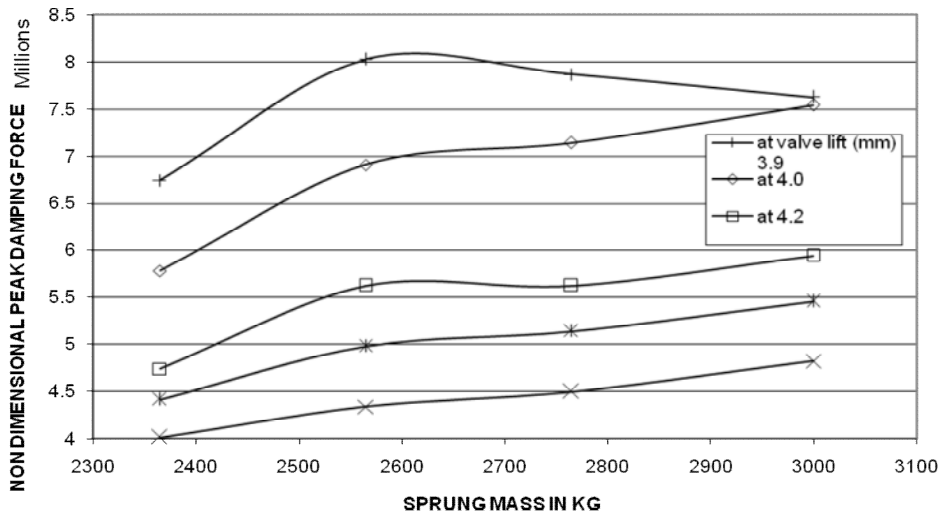

Fig A.24 Variation of non-dimensional peak braking force at constant valve lift in mm with the change in sprung mass.

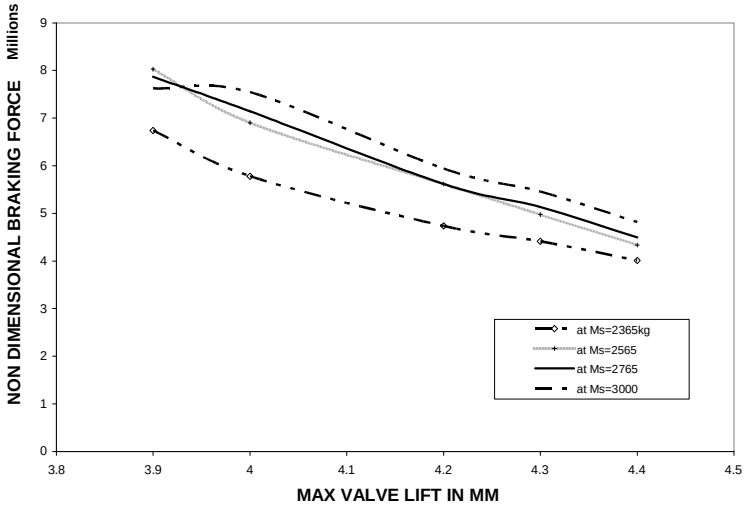

Fig A.25 Variation of non dimensional peak braking force at constant sprung mass with the change in pilot valve lift.

A.2 Overview of Magnetorheological (MR) Dampers

The basic objective of this section is to present an overview and to derive the problem definition of this work. The MR fluids/damper from this section onwards will now be referred to as MR fluids/dampers. The findings led to explore the solution in terms of smart fluid based dampers. Since the MR dampers operate at low power current source therefore they have started finding application in areas such as vibration proof tables, mountain bike, seismic protection systems for civil structures and automobiles. The development of MR dampers started in early nineties by the manufacturers such as Lord Corporation and the early model series from the same manufacturer was named as “Motion Master”. These dampers were used in truck seat suspension and prosthetic legs. General Motors introduced these dampers for an exclusive model of Cadillac in 2003. All of the above applications are low speed applications as maximum speed of the damper piston is not more than 2 m/s. However there is a recent interest in exploring the possibility of using MR dampers for high speed applications such as aircraft landing gears and artillery dampers.

A.2.1 Magnetorheological fluids

MR fluids are the slurry of hydrocarbon oils or silicone oils and micron size ferrite particles. The ferrite particles are coated with anticoagulant for preventing them to for lumps due to coagulation. When un-activated by the magnetic field they behave like an ordinary Newtonian fluid. However, when a magnetic field applied in the direction of perpendicular to the flow the ferrite particles align along the magnetic field to form columnar structures which offer resistance to the parent fluid as it flows over them. The shear stress developed due to the flow of parent fluid over them results in the breaking and reformation of ferrite particles chains. This results in

an increase in apparent viscosity of fluids. The magnetic fluids can be divided into following three types:

(1) Magnetorheological fluid.

(2) Ferro fluids.

(3) Bi –disperse fluids.

Out of the above magnetic fluids the behaviour of magneto-rheological fluids has be already described above. The Ferro-fluids are the suspensions of nano-ferrite particles in hydrocarbon oil. These fluids exhibit increase in viscosity under steady magnetic field in the manner similar to MR fluids, with the difference that the increase in apparent viscosity is limited to twice the viscosity of parent fluids. In case of MR fluids the increase in viscosity is 5-7 times that of parent fluid. The ferro-fluids have many other interesting properties such as they show a reduction in apparent viscosity as compared to the parent fluid when subjected to oscillatory magnetic field.

The bi-disperse fluids are the mixture of MR and Ferro fluids and they have faster response to magnetic field as compared to MR fluids and they have a longer sedimentation time for ferrite particles as compared to MR fluids. The behavior of all of the above types of fluids under the influence of steady magnetic field is same. The formation of columnar structures of ferrite particles in magnetic fluids is as shown in Fig A.26.

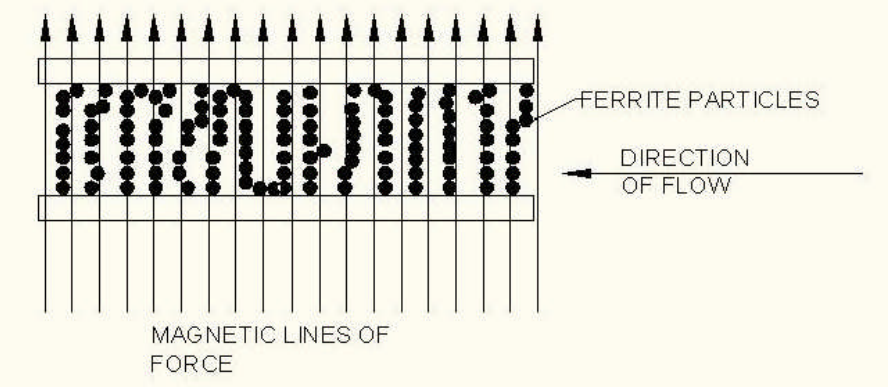

Fig A.26 Behavior of ferrite particles under the influence of magnetic field as the MR fluid flows between the two parallel plates.

The MR fluids can be used in three modes of flow. In the valve mode the fluid flow is like a Poisueille flow. In this mode the resistance of the fluid flow can be varied as the fluid flows between two stationary plates or an annular gap. This is called as the valve mode (see Fig 32).

In the shear mode one of the plate or cylinder is moving in the direction opposite to the flow. The MR fluid can be stationary or moving with some value of velocity. In latter case it is more appropriately called as the mixed mode operation of MR device (ref Fig A.27).

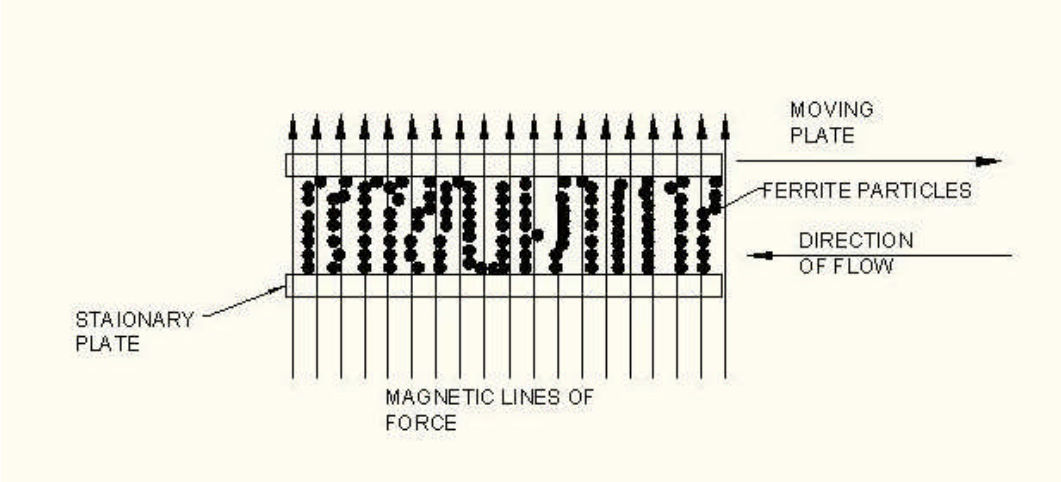

Fig A.27 Shear mode operation of MR device.

In the rotatry devices such as clutches and brakes pure shear mode type operation of MR fluid takes place. the In the squeeze mode operation of the MR device one of the parallel plate moves perpendicular to the direction of flow as shown in Fig A.27.

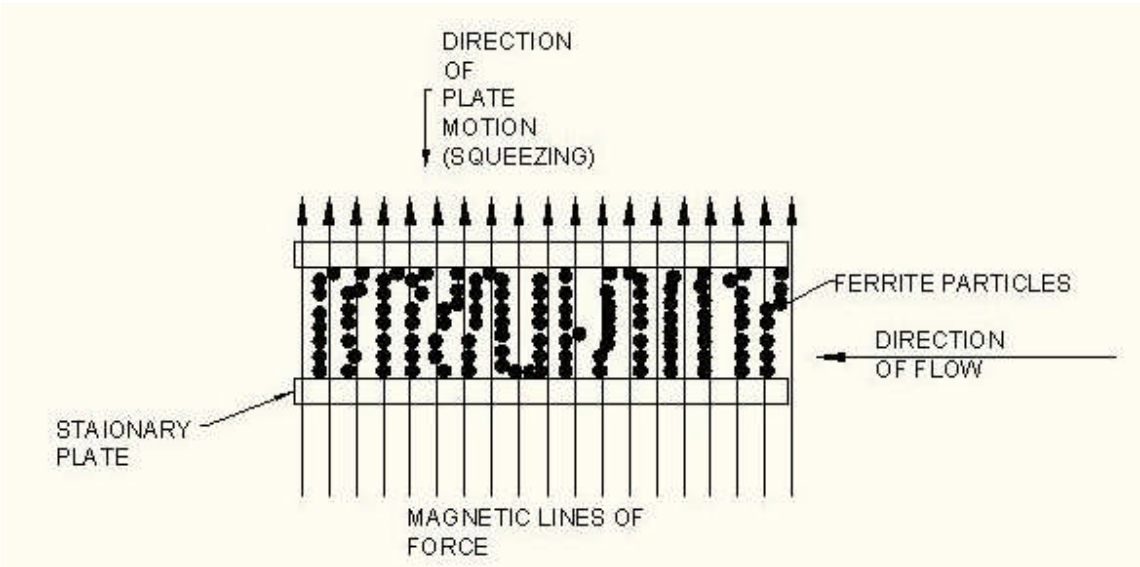

Fig A.28 Squeeze mode operation of MR device.

A.2.3 MR Devices

The MR fluids can be used in various applications such as dampers, clutches, seals, bearing etc. In this work the application of MR devices shall be confined to the dampers as it is the theme of this investigation. Out of the application of above three modes the dampers use valve mode or shear mode operations. The simplest design of MR damper has a piston which has magnetic coils provided with suitable wiring arrangement for energisation. The damper is usually provided with an integral or separate gas type restoring spring. If the damper has an integral restoring spring then it is called as twin tube damper. On the other hand if the restoring gas spring is separate then the MR dampers are usually mono-tube type construction (See Fig A.29(Dixon (1999), (2001), Boelter et al (1997), Gregory et al (2007), Liao et al (2007), Poynor (2001)). In this design the Mr fluid flows between the cylindrical surface of the piston and the wall of the cylinder

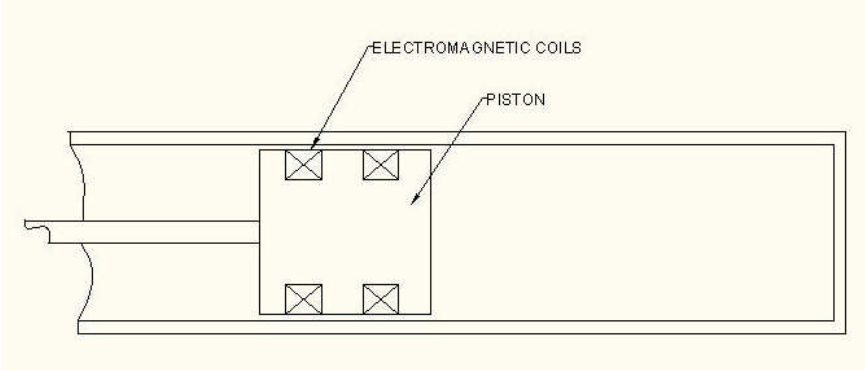

Fig A.29 Schematic of a mono-tube damper

Thus, it is a flow and shear mode type damper or mixed mode type damper. In valve mode type dampers the MR fluids either flows through a hole in the piston which is surrounded by the coils

or the piston forces the fluids through an annular gap which is surrounded by the coil as shown in Fig A.30,A.31 (Dixon (1999), Kawashima et al (2001), Boelter et al (1997), Gregory et al (2007), Liao et al (2007), Poynor (2001))..

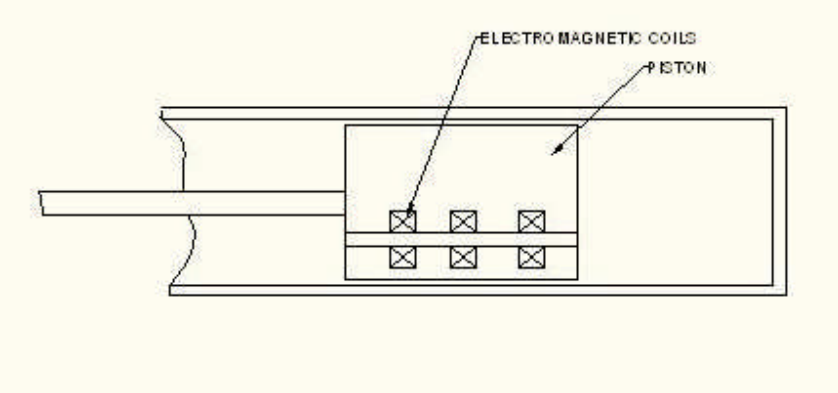

Fig A.30 Schematic of a mono-tube valve mode type damper with flow passage embedded in the piston.

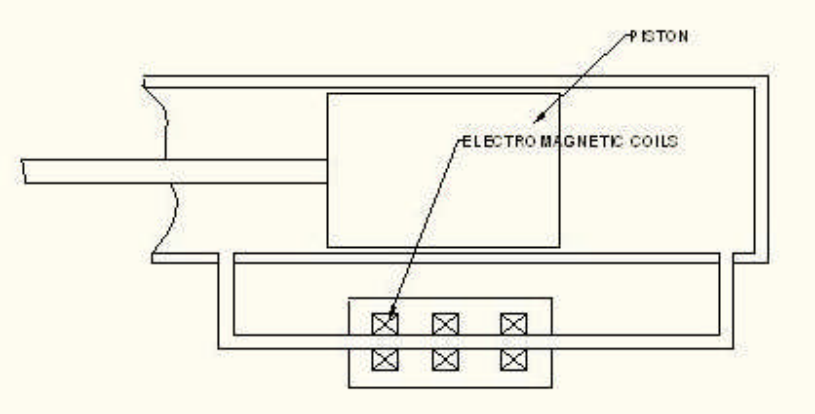

Fig A.31 Schematic of a mono-tube valve mode type damper with bypass type flow passage.

The principle of valve mode type damper can also be used for valve application as described in Ai (2006). For enhancing the effectiveness of the valve the coils can be designed to be positioned in the annular gap so that the flow of MR fluid under the influence of magnetic field can be radial and annular. This design results in an increase in the fluid volume affected by the magnetic field. The MR fluids based valve can be modified into a more compact form and used to control the valve lift of the valve type damper described in the survey of conventional hydraulic type dampers to control the damper force spike. The schematic of such a design which has be also referred to in Poynor (2001) is shown in Fig A.32.

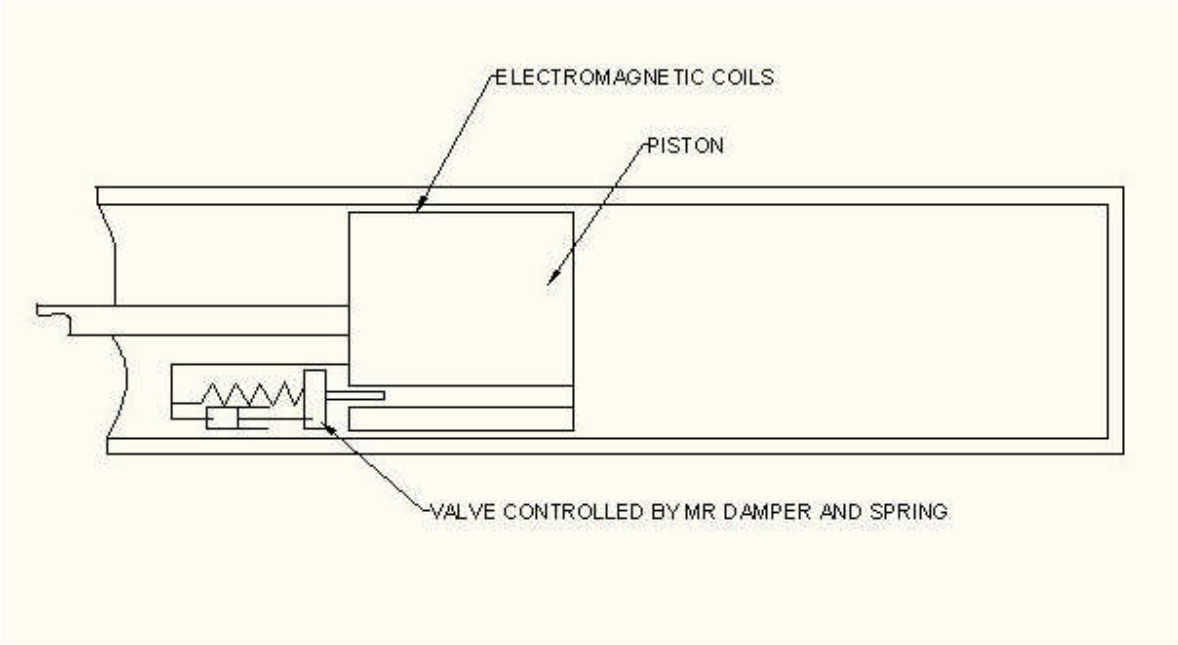

Fig A.32 Schematic of a MR damper or valve controlled conventional valve type damper Poynor (2001).

A brief survey of the all the dampers designs based on study of literature such as (Dixon (1999), Boelter et al, (1997), Gregory et al (2007), Liao et al (2007), Poynor (2001)) shows that the MR

dampers have so far been subjected to speed in the range [0-2m/s]. However towards the later part of the decade 2000 the work on MR dampers subjected to impact loading has started appearing (Wang and Li (2006), Lee and Wereley (1999), Norrsi and Ahmedian (2003), Facey et al (2005)). The study of these findings on the MR dampers subjected to speeds in the range of 5-7 m/s show the presence of damping force spike (Wang et al (2006)). There are very few publications describing the performance of the damper behavior at speeds above 8m/s second. This can be possibly because a large number of real life applications which require dampers to operate in the speed upto 2m/s. The applications of dampers for aircraft landing gears operate at heavy loads and in the speed range of 5-7m/s. The other reason for use of MR dampers for low speed application is due to the need for development of a satisfactory and stable fluid dynamic model. So far the behavior of the MR dampers have been described by the fluid dynamics model based on Herschel Bulkley model of Bingham plastic type non-Newtonian fluids (Kamath et al (1996)). Due to the formation and breakage of the chain ferrite particles in the MR fluids subjected to the magnetic field, MR fluids behave like Bingham fluids(nature of flow is similar to toothpaste). A generalized plot showing the variation of shear stress with the shear rate is shown in Fig A.33. The fig A.33 shows that the Bingham plastic remains stationary until the shear stress corresponding to the shear stress in the fluid is less than the initial shear stress. If the shear stress corresponding to the pressure gradient across the fluid channel exceed the initial shear stress then the fluids flow in such a way that the increase in shear stress is linearly proportional to the shear rate.

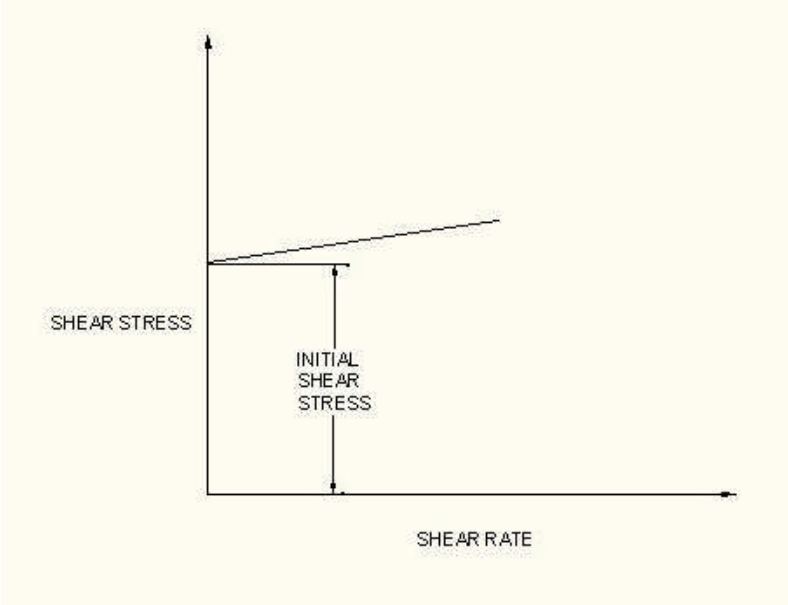

Fig A.33 Herschel Bulkley model for Bingham plastics.

The model has been used in [26-27] to calculate the pressure gradient across the fluid channel of MR damper to get the value of damper force. The second category of MR damper models describe the damper force versus stroke variation by an experiment based phenomenological model Wereley et al (1999), Butz and Von Stryk (2002), Mohammad et al (2007) and Wang and Liao (2011). In this model the transient response fluid dependent upon the transient response of the electromagnetic coil and the constant force versus stroke behavior is described by limit cycle curve obtained as a solution to differential equation for hysteretic systems. The constants of the solutions are determined by experimental methods.

A.3 Conclusion

Based on the survey of the dampers following conclusions are drawn:

(1) The taper grooves dampers can be used for applications at all speeds. The damper fluid to be used for taper grooves type dampers, gives the best performance if the density is kept around 800kg/m^3.

(2) For speeds in the range of 3- 6m/s shim vale type damper and valve type dampers are suitable. These designs generally give pressure spike at the instance the valve starts opening. The valve type dampers can also be used for high speed applications like artillery guns.

(3) For high speed and heavy loads the taper groove and pilot valve compounded dampers are suitable. Just as in case of a shim vale type damper there is a bleeding hole, in the same way the compounded type dampers are provided with taper grooves as variable orifice. The compounded type dampers give best performance in terms for lowest vale of spike, minimum mean damper force and minimum stroke if the density of the damper fluid is in around 1090kg/m^3.

(4) The survey also shows that the inviscid flow model gives the upper limit of the damper force spike and the CFD simulation based k-ε turbulent flow model gives the lower limit of the pressure spike. The selection of suitable flow model for CFD simulation can be further investigated. However, the survey also brings out the fact that the inviscid flow models are computationally inexpensive and give a conservative design.

(5) The pressure spike in the damper can be minimized based on the appropriate choice of the damper depending upon the application; however the spike cannot be eliminated by tuning the system parameters. This is because the control of orifice in a damper is an open loop system. In case of valve type dampers it is quite possible to design a feedback control system to control the lift of the valve. The development of such a system had so far been constrained by the overall response time of the systems which include the electromagnetic coil and the dynamics of the spring mass damping system associated with valve itself. As such elimination of pressure spike continues to be a challenge in the field of the design of hydraulic dampers.

(6) Over and above this, applications which operate in wide range of speed require that the damping force should correspond to high damping ratio at low frequencies and low damping force at high frequencies. Since the hydraulic dampers are controlled by open loop control laws (in the form of taper rod, shim valve, compounded vale etc.) therefore they cannot meet such mutually conflicting requirements. Hence there is a need to evolve the design of dampers which can meet such requirements.

(7) It is pertinent to reiterate that the requirement in point (6) can only be met in the best way if the spike minimized to a value as close to the constant damping force, otherwise the system will be subjected to secondary vibrations. The dampers of the car suspension have damping ratio corresponding to under damped system, whereas an artillery system has a damper which provides over damping.

APPENDIX-II

Table A.1 for Fig 4.6 and 4.7

Velocity in m/s	Displacement in m	Experimetally measured force in N	force due to Duhamel superposition model in N
0	-0.01369	-164.1225586	-170.6874609
0.005269	-0.01333	5.09829092	5.302222557
0.01391	-0.01207	29.91553116	31.1121524
0.020963	-0.00996	52.62701035	54.73209076
0.027146	-0.00713	71.81760406	74.69030823
0.0314	-0.00377	173.2462921	180.1761438
0.033348	-0.00011	331.7265625	344.995625
0.033624	0.003637	425.516571	442.5372339
0.032036	0.007266	419.7636719	436.5542188
0.029369	0.010636	414.0394592	430.6010376
0.02494	0.013577	386.1195679	401.5643506
0.018577	0.015862	356.4514465	345.7579031
0.011447	0.017383	321.3700256	311.7289249
0.00433	0.0181	257.2425842	249.5253067
-0.00261	0.018053	-253.1562805	-245.5615921
-0.01085	0.017133	-548.4633179	-532.0094183
-0.01887	0.015299	-563.713562	-546.8021552
-0.02535	0.012676	-602.2567139	-584.1890125
-0.02974	0.009516	-625.2366943	-606.4795935
-0.03288	0.005968	-645.3695068	-626.0084216
-0.03435	0.002195	-651.3868408	-631.8452356
-0.03341	-0.00156	-651.4395142	-631.8963287
-0.03034	-0.00505	-644.0988159	-624.7758514
-0.02642	-0.00811	-631.3317871	-612.3918335
-0.02095	-0.01063	-604.987915	-586.8382776
-0.01423	-0.01243	-568.2130127	-551.1666223
-0.00709	-0.01344	-515.1734009	-499.7181989
-0.00011	-0.01368	-233.9036255	-226.8865167
0.007341	-0.01311	363.706543	352.7953467
0.015444	-0.01165	375.4630737	364.1991815
0.022567	-0.00935	428.9964905	416.1265958
0.028189	-0.0064	450.3093872	436.8001056
0.03212	-0.00294	463.3418274	449.4415726
0.033692	0.000786	467.6229553	453.5942667
0.033443	0.004531	469.6450195	455.5556689
0.031496	0.008107	464.0280762	450.1072339

Velocity in m/s	Displacement in m	Experimetally measured force in N	force due to Duhamel superposition model in N
0.028456	0.011382872	447.4996338	434.0746448
0.023447	0.014177024	419.5187683	406.9332053
0.016879	0.016288172	384.9803772	373.4309659
0.009714	0.017612617	338.5162659	328.3607779
0.002681	0.018151337	237.5289307	230.4030627
-0.00439	0.017917218	-368.3213806	-357.2717392
-0.0128	0.016785773	-557.2355347	-540.5184686
-0.02071	0.014749534	-589.59021	-571.9025037
-0.02653	0.011971569	-623.4527588	-604.749176
-0.03056	0.008702214	-645.2404175	-625.883205
-0.03344	0.005078713	-660.4921265	-640.6773627
-0.03416	0.001301507	-664.8288574	-644.8839917
-0.03302	-0.002414664	-662.6759033	-642.7956262
-0.02954	-0.005815799	-653.0280762	-633.4372339
-0.02514	-0.008760951	-637.7532349	-618.6206378
-0.01966	-0.011126544	-611.0457153	-592.7143439
-0.01254	-0.012742948	-566.260498	-549.2726831
-0.00532	-0.013577851	-497.9233398	-482.9856396
0.001556	-0.013627957	-61.87593842	-60.01966026
0.009342	-0.012858869	385.9193726	374.3417914
0.017529	-0.011168205	389.9460754	378.2476932
0.023929	-0.008706665	439.8912048	426.6944687
0.029337	-0.00560133	459.0175781	445.2470508
0.032457	-0.002086108	471.0367126	456.9056113
0.033823	0.001657322	477.1019897	462.7889301
0.032938	0.005369441	478.5027771	464.1476938
0.031024	0.008893976	468.4570618	454.4033499
0.02749	0.012085949	450.6754456	437.1551822
0.022026	0.014737736	419.8209839	407.2263544
0.015333	0.016679021	377.2737122	365.9555008
0.007901	0.017810132	323.0715637	313.3794168
0.001199	0.018162267	147.5253906	143.0996289

Table A.2 for Fig 4.8 and 4.9

Velocity in m/s	Displacement in m	Experimentally measured force in N	Damper force due to Duhamel superposition model in N
0	-0.006629077	79.64711761	0
0.043243	-0.002004	97.1207962	663.9127798
0.045485	0.003032937	102.2569199	389.1992454
0.042412	0.00787801	92.73053741	446.7055708
0.036819	0.01218887	503.0501404	504.7521988
0.026391	0.015496922	859.5554199	936.0080228
0.01371	0.017447487	731.742981	753.3533823
0.001313	0.017997487	350.1419067	771.6819287
-0.01166	0.017157892	-536.7483521	-696.4409437
-0.02647	0.014699568	-1230.061157	-1294.134794
-0.0365	0.010947299	-1219.578979	-1297.46241
-0.04398	0.006270586	-1300.869141	-1299.879769
-0.04537	0.001250402	-1300.807251	-1300.326488
-0.04286	-0.003630775	-1292.863892	-1299.522201
-0.036	-0.007870092	-1255.161011	-1297.300228
-0.02629	-0.011148608	-1173.266846	-1085.000078
-0.01375	-0.01309662	-1050.918213	-1091.512666
-0.00143	-0.01365048	-650.4717407	-692.6987627
0.011338	-0.012845876	487.087677	487.1773327
0.025665	-0.010442896	980.4146729	1016.305585
0.036294	-0.006732928	1023.997375	1017.436039
0.04338	-0.002119952	1082.36377	1018.149869
0.045563	0.002918341	1084.110718	1018.365438
0.042544	0.007767482	1067.208618	1018.06683

Velocity in m/s	Displacement in m	Experimentally measured force in N	Damper force due to Duhamel superposition model in N
0.0425445	0.007767482	1067.208618	1018.06683
0.0370088	0.012093444	1012.721313	1017.509197
0.026656	0.015426799	921.0614014	1016.41534
0.0141503	0.017412962	809.9043579	792.9275161
0.001673	0.01799882	409.4971619	546.5938337
-0.011266	0.017200124	-505.2940979	-618.8175045
-0.026023	0.014787403	-1254.125488	-1293.984231
-0.036335	0.01105096	-1261.341309	-1297.408315
-0.043811	0.006404459	-1340.738525	-1299.826823
-0.045603	0.001366489	-1337.209473	-1300.400892
-0.042953	-0.003527751	-1317.091187	-1299.551022
-0.036042	-0.007776403	-1268.534424	-1297.312697
-0.026526	-0.011068329	-1188.412354	-1085.067768
-0.014009	-0.013055049	-1065.908569	-1091.596743
-0.001741	-0.013649226	-696.3122559	-692.8530963

Table A.3 for Fig 4.10 and 4.11

Velocity in m/s	Displacement in m	Experimentally measured force in N	Model force due to with Duhamel superposition in N
0	0.017158402	-194.4437103	0
-0.00476	0.016639808	-196.568161	-166.370692
-0.00583	0.016027823	-199.4237213	-204.2755244
-0.00655	0.015322166	-208.4920959	-242.1745137
-0.00715	0.014540406	-762.9533081	-280.0802741
-0.00796	0.01367825	-1104.695435	-1068.753276
-0.00858	0.01273196	-1108.177856	-1107.643961
-0.00912	0.011727012	-1160.522339	-1146.636139
-0.00976	0.010659242	-1148.48938	-1053.972327
-0.01015	0.009535287	-1170.602051	-1092.743019
-0.01046	0.00836309	-1164.600586	-1131.608661
-0.01102	0.007157171	-1176.805664	-1170.693932
-0.01127	0.005909595	-1175.92688	-1077.661989
-0.01137	0.004644446	-1178.407593	-1116.416668
-0.0115	0.003360698	-1178.935181	-1155.299336
-0.01156	0.00207345	-1179.828979	-1194.294124
-0.01137	0.000794845	-1185.426025	-1100.914132
-0.01135	-0.000482088	-1188.901367	-1139.697086
-0.01115	-0.001734194	-1189.714111	-1178.536463
-0.01097	-0.002961912	-1188.455566	-1085.294297
-0.01062	-0.004158724	-1180.026978	-1123.905301
-0.01013	-0.005301961	-1174.975708	-1162.573787
-0.00985	-0.006398918	-1171.450439	-1069.444806
-0.00918	-0.007444349	-1164.694458	-1107.873678
-0.00875	-0.008431775	-1158.425659	-1146.489354
-0.00814	-0.009364164	-1149.465698	-1185.144612
-0.00744	-0.010211149	-1140.330566	-1177.956842
-0.00677	-0.010997752	-1129.043823	-1139.81838
-0.00595	-0.011683739	-1118.165039	-1101.620501
-0.00517	-0.012290329	-1107.203735	-1063.44731
-0.00435	-0.012800515	-1099.654785	-1025.250524

Velocity in m/s	Displacement in m	Experimentally measured force in N	Model force due to with Duhamel superposition in N
-0.00595	-0.011683739	-1118.165039	-1101.620501
-0.00517	-0.012290329	-1107.203735	-1063.44731
-0.00435	-0.012800515	-1099.654785	-1025.250524
-0.00336	-0.013219448	-1081.913452	-1115.434579
-0.00254	-0.013526328	-1060.7771	-1077.15649
-0.00175	-0.013751229	-1028.150024	-1038.858527
-0.00093	-0.01388411	-974.7607422	-1000.480441
3.07E-05	-0.013910036	-704.194397	-1052.122376
0.001026	-0.013824832	-72.0686264	-172.2071906
0.00187	-0.013647825	123.9560928	254.0551117
0.00273	-0.013374221	331.1929626	278.3427838
0.003825	-0.012985656	285.0030212	302.6619655
0.004561	-0.012495923	433.5426331	683.5611598
0.005377	-0.011929561	671.7174072	708.4346475
0.006059	-0.011264661	882.8078003	733.3597798
0.00703	-0.010521705	870.6826782	758.4199171
0.007728	-0.009677073	889.3515625	783.5259123
0.008429	-0.008761198	899.7466431	808.735268
0.009017	-0.007776952	912.0770264	834.0387428
0.009578	-0.006727129	915.3312378	859.4607793
0.010002	-0.005625582	914.8013306	884.993949
0.010501	-0.00446404	919.2504883	910.6856232
0.010908	-0.003268171	925.4579468	936.5194051
0.011103	-0.002036816	931.6987915	962.4862556
0.011237	-0.000789516	933.9373779	988.6253008
0.011538	0.00048166	937.0224609	926.3009434
0.011434	0.001762868	935.7693481	952.1495508
0.011419	0.003036076	938.4251099	978.1888942
0.011338	0.004308003	942.3510132	915.9673682
0.01121	0.005558648	941.1767578	941.7443365
0.010961	0.006791872	937.2044678	967.6690107

Velocity in m/s	Displacement in m	Experimentally measured force in N	Model force due to with Duhamel superposition in N
0.010792	0.008001186	926.3847046	993.7899031
0.010469	0.009174482	919.2169189	976.6388965
0.010052	0.010307143	913.274231	952.3162147
0.009573	0.011390786	904.609375	927.9851302
0.009072	0.01241454	895.7136841	903.6528194
0.008309	0.013366882	883.5418701	879.2754103
0.007542	0.01423747	873.7749634	854.8992296
0.006993	0.01504081	861.4448853	830.565798
0.006319	0.015763031	849.1486816	806.2110034
0.005468	0.01640722	834.7681274	781.8232175
0.00465	0.016957229	822.6129761	757.4412962
0.003877	0.01741823	802.2116089	733.0677613
0.003036	0.017772697	772.8515625	708.6770446
0.001978	0.018034883	718.7365112	684.2292744
0.001336	0.018200601	559.9385986	659.8743126
0.000218	0.0182603	192.5799866	635.3801171
-0.00052	0.018225431	-125.7751389	-128.2198745
-0.00159	0.018087741	-269.1176453	-166.0785975
-0.00253	0.017836031	-252.8595428	-203.949579
-0.00335	0.017485093	-251.1887207	-241.8308515
-0.00444	0.017038481	-443.7146606	-279.7684598
-0.00509	0.016498277	-1149.348633	-1067.558699
-0.00604	0.015858021	-1100.585449	-1106.605396
-0.00667	0.015128274	-1151.299194	-1145.625201
-0.00735	0.014323979	-1161.834106	-1053.090024
-0.00813	0.013441763	-1177.385498	-1091.996207
-0.00879	0.012484252	-1191.432007	-1130.979208
-0.00924	0.011467217	-1209.832642	-1170.014933
-0.01004	0.010376654	-1210.057617	-1077.238487
-0.01032	0.009235402	-1202.097168	-1116.042605

Velocity in m/s	Displacement in m	Experimentally measured force in N	Model force due to with Duhamel superposition in N
-0.01071	0.008053659	-1204.286133	-1155.009097
-0.01104	0.00684148	-1212.533569	-1194.096822
-0.01129	0.005594432	-1217.337402	-1100.885886
-0.01154	0.004327181	-1221.203491	-1139.765103
-0.01163	0.003037592	-1220.62207	-1178.71474
-0.01156	0.001755384	-1222.648438	-1085.494769
-0.01169	0.000464114	-1225.833618	-1124.284986
-0.01135	-0.000804822	-1223.76001	-1163.029379
-0.01124	-0.002056042	-1217.873291	-1069.924087
-0.01088	-0.003268669	-1207.713379	-1108.489923
-0.01045	-0.004446536	-1201.54187	-1147.139336
-0.01018	-0.005577167	-1194.45459	-1185.966718
-0.0096	-0.006656247	-1187.170532	-1178.844211
-0.00928	-0.007696205	-1178.494385	-1140.838955
-0.00869	-0.008674767	-1165.819702	-1102.74321
-0.00803	-0.009582917	-1152.908813	-1064.626374
-0.00731	-0.010422028	-1140.317993	-1026.495509
-0.00645	-0.011171068	-1125.487061	-1116.975716
-0.00594	-0.011840417	-1115.52478	-1078.920554
-0.00499	-0.012416802	-1103.374634	-1040.674311
-0.00427	-0.012912468	-1086.255127	-1002.529382
-0.0033	-0.013307087	-1065.531494	-1067.038477
-0.00242	-0.0136004	-1041.309814	-1028.735341
-0.00151	-0.013798806	-1009.770691	-990.3656219
-0.00071	-0.013905249	-931.1515503	-952.0013874
0.00039	-0.013895786	-507.5906067	-643.2155124

Table A.4 for Fig 4.13 and 4.14

Velocity in m/s	Displacement in m	Experimentally measured force in N	Model force due to Duhamel superposition in N
0	-0.003310351	-250.5461731	0
-0.01965	-0.005572338	-254.1684265	-280.9403246
-0.01792	-0.007637172	-256.0968628	-314.8990797
-0.01584	-0.00947144	-254.1969757	-348.7671957
-0.01316	-0.01102316	-254.8069611	-382.4832616
-0.01005	-0.012249485	-350.3986206	-416.0517151
-0.00694	-0.013131941	-460.861969	-499.2317867
-0.00349	-0.013636876	-495.2926025	-464.2376245
-0.00027	-0.013778604	-303.303009	-428.8470266
0.003207	-0.013548139	230.6412659	313.3049524
0.006628	-0.012936401	372.8485107	338.5188424
0.010377	-0.011906195	391.8568115	363.8149704
0.013646	-0.010506022	413.2306824	389.1731884
0.016331	-0.008789423	422.3583069	414.6197223
0.018618	-0.006799195	428.7138672	392.1246152
0.020616	-0.004574447	431.7062683	417.5383274
0.022142	-0.0021554	429.5416565	443.0774327
0.02257	0.000334857	425.7673645	468.7030933
0.022689	0.002848194	425.8077087	469.1734832
0.02228	0.005329089	426.6517029	469.133177
0.021372	0.007729223	425.2041321	469.043228
0.02012	0.010007983	423.6563721	468.9180927
0.018484	0.012113131	414.0014648	471.4661258
0.015965	0.013968093	397.6633301	446.5460445
0.013131	0.015522923	377.0718384	374.7936762
0.009969	0.016727785	355.5700989	349.8776196
0.006899	0.017587382	332.7150574	324.9755789
0.003694	0.018095883	295.5377502	300.0392854
0.000416	0.018240904	127.3865814	274.9708891
-0.003	0.018014751	-405.4958801	-418.6566757
-0.00682	0.017370442	-516.510498	-453.9666567

Velocity in m/s	Displacement in m	Experimentally measured force in N	Model force due to Duhamel superposition in N
-0.003	0.018014751	-405.4958801	-418.6566757
-0.00682	0.017370442	-516.510498	-453.9666567
-0.01035	0.016329322	-545.3163452	-489.2797741
-0.01358	0.014917546	-566.5169067	-524.713458
-0.01644	0.013168219	-586.0153198	-560.2889864
-0.01871	0.011153206	-605.4094849	-542.7917557
-0.02054	0.00892395	-619.3908081	-578.2494401
-0.02178	0.006540729	-625.4989624	-613.7985196
-0.02269	0.004039854	-628.1972656	-649.531136
-0.02279	0.001503662	-630.3266602	-685.3150248
-0.02239	-0.001013747	-633.6859131	-650.070469
-0.0214	-0.003424047	-633.7078247	-649.7530886
-0.01961	-0.00567646	-630.5980225	-649.17509
-0.01782	-0.007725582	-625.8583984	-648.5907043
-0.01562	-0.009544274	-614.9550781	-647.8663654
-0.01296	-0.011078706	-598.6951904	-646.9753586
-0.00994	-0.012288715	-577.9613647	-547.6796724
-0.00684	-0.013154178	-550.380249	-512.7764251
-0.0034	-0.013644215	-511.4543762	-477.75217
-0.00019	-0.013775311	-327.948822	-442.2842227
0.003276	-0.013530857	234.1187134	313.3138748
0.006947	-0.012897764	369.1399536	338.5509459
0.010529	-0.011842711	390.5693054	363.8289916
0.01378	-0.010427651	415.3550415	389.1853419
0.016473	-0.008693076	428.7046814	414.6329069
0.018679	-0.006694489	436.8439636	392.129747
0.020646	-0.004462107	441.9160767	417.5409601
0.022072	-0.002051221	442.6753845	443.070885
0.022679	0.000442831	440.9316406	468.7137939
0.02274	0.002966437	440.8877869	469.1734832

Velocity in m/s	Displacement in m	Experimentally measured force in N	Model force due to Duhamel superposition in N
0.022089	0.005445623	442.1492004	469.133177
0.021283	0.007835508	442.8896484	469.043228
0.0201	0.010112929	435.7674866	468.9180927
0.018264	0.012207191	421.4771729	424.5705466
0.015857	0.014040545	403.1083374	399.6869355
0.013008	0.015580885	383.0870972	374.7827696
0.009844	0.016776236	362.4646912	349.8663272
0.006782	0.01761961	339.387146	324.9642258
0.003556	0.01811826	299.4841003	300.0229961
0.000253	0.018244911	119.9337845	274.93673
-0.00325	0.017996108	-413.5569763	-451.1818199
-0.0071	0.017328719	-518.8592529	-486.6643415
-0.01056	0.016263075	-549.6282959	-522.1420567
-0.01374	0.014829753	-572.1288452	-557.7680054
-0.01646	0.013072317	-594.9464111	-593.5335094
-0.01886	0.01105262	-614.5176392	-542.832026
-0.02058	0.008822979	-623.5392456	-578.2613291
-0.02193	0.006428057	-628.5577393	-613.8428757
-0.02265	0.00392423	-633.0916748	-649.5160086
-0.02288	0.001367167	-636.6022339	-685.3444228
-0.02236	-0.001141228	-636.5722046	-650.070469
-0.02128	-0.003542671	-635.1405029	-649.7530886
-0.01966	-0.005783243	-631.6390381	-649.17509
-0.01762	-0.007814751	-626.4315186	-648.5907043
-0.01554	-0.009620314	-615.6993408	-647.8663654
-0.01288	-0.011141058	-598.7266235	-646.9753586
-0.00983	-0.012338058	-578.0453491	-547.6466692
-0.0067	-0.013191092	-554.4240723	-512.7335303
-0.00329	-0.013667514	-511.3687134	-477.7109834
0.000119	-0.013775952	-288.0732117	-265.5745713

Velocity in m/s	Displacement in m	Experimentally measured force in N	Model force due to Duhamel superposition in N
0.003414	-0.013513496	250.0748596	389.1853524
0.007297	-0.012844801	361.87146	414.6367642
0.010729	-0.011775993	385.0799866	440.2253326
0.01378	-0.010347905	410.320282	465.9583509
0.016515	-0.008601774	423.0389404	443.0722947
0.018909	-0.006589928	435.329071	469.1734832
0.020772	-0.004351016	441.9724121	443.0722947
0.022087	-0.001930716	443.7956238	469.1734832
0.022837	0.000568724	443.252594	469.1734832
0.022746	0.003094223	444.0126038	469.133177
0.021987	0.005567878	448.724884	469.043228
0.021282	0.0079584	446.562561	468.9180927
0.019986	0.010216171	434.0139771	496.2984988
0.018118	0.012294441	421.0714722	424.5569141
0.015791	0.014122627	404.3694763	399.6809601
0.012949	0.015652604	383.8356323	374.7774759
0.009741	0.01682926	363.6542358	349.8569692
0.006561	0.017660059	339.2228088	324.9427763
0.003397	0.018136764	299.2769775	300.0039374
0.000127	0.018248212	89.59132385	274.9089557
-0.00358	0.017969934	-429.2356567	-451.2956121
-0.00716	0.017280223	-521.454834	-486.6820108
-0.01064	0.016205616	-552.2199707	-522.1650931
-0.01378	0.01475274	-577.0558472	-557.7823271
-0.01654	0.012988737	-598.9830322	-593.5573378
-0.01891	0.010954173	-613.7316895	-542.8476861
-0.0208	0.008702481	-621.5969849	-578.3248834
-0.02198	0.006293984	-628.4096069	-613.8595585
-0.02263	0.003789441	-632.4646606	-649.510714
-0.02279	0.001247909	-634.6575928	-685.313881
-0.02226	-0.001257496	-635.4281616	-650.070469

Table A.5 for Fig 4.15 and 4.16

Velocity in m/s	Displacement in m	Experimentally measured force in N	Damper force due to Duhamel superposition model in N
0	-0.0043746	0	0
0.021934	-0.00195797	983.6624756	944.3159766
0.022819	0.000545149	987.489624	947.9900391
0.022639	0.003064725	979.4627686	940.2842578
0.022066	0.005536465	974.5167236	935.5360547
0.021171	0.007924858	964.1929932	925.6252734
0.01994	0.01018684	942.3361206	904.6426758
0.018008	0.012257541	917.1647949	880.4782031
0.015601	0.01407195	882.2235107	882.2235107
0.012712	0.015585911	847.9944458	847.9944458
0.00958	0.016751066	804.5449829	804.5449829
0.006376	0.017566206	752.6019897	710.8459473
0.003317	0.018034859	675.2150879	643.0713459
-1.6E-05	0.018142361	242.834137	133.4737072
-0.0037	0.017847596	-263.0570679	-244.5589594
-0.00713	0.017159309	-383.0418701	-327.7004307
-0.01089	0.016066981	-1106.887695	-1106.887695
-0.01407	0.014599923	-1070.899048	-1070.899048
-0.01683	0.01281293	-1140.207153	-1140.207153
-0.01895	0.010770921	-1164.010132	-1164.010132
-0.0206	0.00852876	-1196.755859	-1196.755859
-0.02195	0.006118106	-1221.386475	-1221.386475
-0.02276	0.003599937	-1230.238037	-1230.238037
-0.02294	0.001054682	-1229.142944	-1164.42232
-0.02214	-0.00144653	-1219.577759	-1164.14947

Velocity in m/s	Displacement in m	Experimentally measured force in N	Damper force due to Duhamel superposition model in N
-0.01251	-0.0113567	-1085.461304	-1085.461304
-0.00961	-0.01252267	-1042.838623	-1042.838623
-0.00631	-0.013338011	-997.4239502	-997.4239502
-0.00296	-0.013790265	-925.6080322	-971.2070434
0.000353	-0.013881848	-558.2980957	-526.9000316
0.003762	-0.013582715	283.7832642	199.1434514
0.007606	-0.012878436	342.7577515	266.6460778
0.010924	-0.011782438	838.5613403	838.5613403
0.014184	-0.010324937	847.3214722	847.3214722
0.016786	-0.008551358	903.8077393	943.9391814
0.019125	-0.006521101	938.7865601	944.2206723
0.021022	-0.004262883	964.9400635	944.4406989
0.022269	-0.001839329	972.5430298	944.5821412
0.022903	0.000666296	974.8847656	944.6531977
0.022672	0.003186681	975.4602051	944.6273517
0.022099	0.005658127	971.1404419	944.5629728
0.021301	0.008041845	961.8928223	944.4726395
0.019855	0.010286132	938.7717896	944.3061584
0.018064	0.012345273	913.3657227	944.094444
0.015542	0.014148218	879.3493042	943.7840196
0.012841	0.015651425	840.0698853	943.4298866
0.00958	0.01680797	797.8287354	942.9583421
0.006266	0.017600358	751.6296387	942.3982944
0.003106	0.018049702	668.5351563	941.721184
-0.00013	0.018134549	181.1732025	1153.540542

Table A.6 for Fig 4.17 and 4.18

Velocity in m/s	Displacement in m	Experimentally measured damper Force in N	Force predicted by Duhamel superposition model in N
0	0.002794296	17.95718765	0
0.007682	0.014124746	777.6766968	874.1484188
0.007142	0.014941829	771.7510376	873.8387422
0.006496	0.01569012	767.3946533	873.4674189
0.005788	0.016359128	757.9074707	873.0594445
0.005163	0.016957687	745.2353516	872.6986907
0.004358	0.01747648	726.8430176	785.4288216
0.003456	0.017890697	698.6914673	706.8859395
0.001714	0.018149229	600.8239136	636.1973455
0.000439	0.018248122	287.811615	572.577611
-0.00047	0.018222803	-80.5763092	-197.6213328
-0.00156	0.018089736	-229.86586	-265.770882
-0.00264	0.017849896	-169.2612457	-132.9454385
-0.00344	0.017496573	-267.6330261	-300.0222365
-0.00419	0.017056862	-463.5889893	-467.0588108
-0.005	0.016536873	-977.8692017	-1031.766871
-0.0059	0.0159014	-927.2484131	-1032.84352
-0.00678	0.015182982	-965.1329346	-1033.893391
-0.00747	0.014379201	-966.7216797	-1034.7143
-0.00821	0.013490544	-971.9904785	-1035.527055
-0.00873	0.012548186	-974.4886475	-1036.209975
-0.00937	0.011525704	-980.4298096	-1036.96207
-0.00996	0.010452542	-990.5818481	-1037.651677
-0.0103	0.009319791	-1000.976746	-1038.051092
-0.01074	0.008141641	-1007.447571	-1038.569004
-0.01111	0.006921581	-1013.966858	-1039.002124
-0.01134	0.005675129	-1018.100769	-1039.280333
-0.01156	0.004399689	-1020.714294	-1039.535422

Velocity in m/s	Displacement in m	Experimentally measured damper Force in N	Force predicted by Duhamel superposition model in N
-0.0116	0.003109784	-1023.424744	-1039.581841
-0.01155	0.001826493	-1027.174438	-1039.521668
-0.0117	0.000538397	-1026.467163	-1039.695549
-0.01135	-0.00072826	-1024.780396	-1039.288787
-0.01118	-0.001976962	-1022.392517	-1039.095031
-0.011	-0.003195172	-1020.133728	-1038.878082
-0.01046	-0.004370379	-1019.616455	-1038.241963
-0.01027	-0.005515463	-1019.727112	-1038.026508
-0.00975	-0.006609958	-1018.225342	-1037.410714
-0.00934	-0.007649612	-1015.606079	-1036.928377
-0.00865	-0.008624144	-1010.720764	-1036.117507
-0.00803	-0.009536157	-1003.297913	-1035.374011
-0.00733	-0.010372995	-992.3458862	-1034.545422
-0.00515	-0.0123926	-962.1398315	-1031.946389
-0.0043	-0.012890317	-943.5213623	-1031.946389
-0.00326	-0.013287945	-921.2411499	-980.3490692
-0.00241	-0.013574756	-901.8682861	-1000.987997
-0.00173	-0.013783396	-868.8716431	-877.1544303
-0.00068	-0.013894405	-796.3024902	-732.0269741
0.000226	-0.013896026	265.5778198	223.5303459
0.001316	-0.013792876	247.7327499	273.3392578
0.001892	-0.01359925	212.1833801	301.3273603
0.002989	-0.013302392	347.2420349	329.4577855
0.003818	-0.012897427	330.1000366	357.5703312
0.004745	-0.012391025	489.3109436	385.7484358
0.0055	-0.011801114	803.4400024	872.893357
0.006261	-0.01111828	793.3079224	873.3323536
0.007219	-0.010350083	822.5409546	873.8828855

Velocity in m/s	Displacement in m	Experimentally measured damper Force in N	Force predicted by Duhamel superposition model in N
0.007852	-0.009492913	828.5744629	874.24559
0.0084	-0.008563862	841.3186646	874.5593639
0.009097	-0.007567454	851.7003784	874.8367071
0.009576	-0.00651098	858.1802368	875.2313322
0.010091	-0.005392363	858.9711914	875.5246285
0.010624	-0.004224536	857.3307495	875.8276345
0.010907	-0.003019382	852.4978027	875.9885836
0.01102	-0.00178784	851.2507324	876.0529087
0.011411	-0.00053041	856.2057495	876.2746519
0.011514	0.000746024	859.0791016	876.3333595
0.011459	0.002029543	861.3707886	876.3023916
0.011462	0.003308238	862.8345947	876.3039485
0.011315	0.004567769	858.9383545	876.2203199
0.01109	0.005817262	855.15271	876.0929166
0.010979	0.007044278	851.8765259	876.0293644
0.010657	0.008245207	847.821167	875.8464478
0.010368	0.00941014	843.5518799	875.6823789
0.01	0.010529721	839.1735229	875.4725839
0.009408	0.011605359	830.1657715	875.1351717
0.008929	0.012617062	821.9984131	874.861768
0.008263	0.013552008	811.5940552	874.4809757
0.007424	0.014413548	798.4235229	874.0004358
0.006889	0.015199834	789.9356079	873.693277
0.006119	0.015903207	781.8046265	873.2502022
0.005392	0.016531877	769.5627441	872.8305671

REFERENCES

Ahmedian M., Poynor J. C., 2001, An evaluation of magneto rheological dampers for controlling gun recoil dynamics, *Shock and Vibration*, 8 (3-4), 147-155.

Ai, H. X., Wang, D. H., Liao, W. H., 2006, Design andmodeling of a magnetorheological valve with bothannular and radial flow paths. *J. Intell. Mater. Syst.and Struct*., 17, 327–334.

Alanoly J and Sankar S, 1987, A New Concept In Semi-Active Vibration Isolation, *Trans. ASME J. Mech. Transmissions*, Automation Design, 109,242-247.

Bagley R.L., 1983, A Theoretical Basis for The Application of Fractional Calculus to Viscoelasticity, *J. Rheol*., 27, 201–210.

Bhatnagar R.M., Bhattacharya B. And Biswas G., 2009, Analysis of Pilot Valve and Taper Groove Based Damper, *Proc. Of IMechE London Part C, J. Mech. Engg Sci.*, Vol. 223 (C4), 859-871, DOI: 10.1243/09544062JMES1299.

Butz, T.,Von Stryk, O., 2002, Modelling and Simulation of Electro- and Magnetorheological Fluid Dampers, *ZAMM _ Z. Ang. Math. Mech.,* 82, 3—20.

Batterbee, D. C., Sims N. D., Stanway, R., Rennison M., 2007, Magnetorheological Landing Gear 1: A Design Methodology, *Smart Mater. Struct*., 16, 2429-2440.

Batterbee, D. C., Sims N. D., Stanway, R., Rennison M., 2007, Magnetorheological Landing Gear 2: Validation using Experimental Data, *Smart Mater. Struct*., 16, 2441-2452.

Boelter, R. and Janocha, H., 1997, Design Rules for MR Fluid Actuators in Different Working Modes, *Proc. SPIE*, Vol. 2.1645, 148-159.

Bossis G., Lacis S., Meunier A., Volkova O.,2002,Magnetorheological fluids, Journal of Magnetism and Magnetic Materials, 252, 224–228.

Brown J., 1946, Hydraulic Shock Absorbers, Orifice Designs and Equations, *Product. Eng*, 19, 92–95.

Carlson J.D., Catanzarite D.M.,St Claire Ka, 1996,Commercial Magnetorhelogical Devices, *Intl J. of Mod Phy B*, 10(23-24), 2857-2865.

Carlson J.D., Jolly M.R., 2000, MR Fluid, Foam and Elastomer Devices, Mechatronics,10,555-69.

Cesmeci S., Tehsin E., 2010,Modelling And Testing of Field Controllable Magnetorheological Fluid Damper, *Intl. J. of Mech Sci* ,52, 1036-1040.

Chang C.C., Roschke P., 1998, Neural Network Modelling of a Magnetorheological Damper, *J. of Intgnt Mater. Sys & Struct*,9(9), 755-764.

Chase G.W., Dachavijit P., 2008, An Experimental Study Of ER Fluid Flow Through a Packed Bed of Glass Beads, *Trans Porous Med*., 72, 25-35.

Choi Y .T., Wereley N. M., Jeon Y.S., 2002, Semi-Activevibration Isolation Using Magnetorheological Isolators, *Proc. SPIE Smart Structures And Materials 2002*: Damping And Isolation, 4697, 284–91.

Crosby M.J., Karnopp D.C, (1973), The Active Damper: A New Concept for Shock and Vibration Control, *Shock and Vibration Bulletin*, 43, pp119–133.

Crolla, D. A., 1988, Theoretical Comparisons of Various Active Suspension Systems in Terms of Performance and Power Requirements', *Inst.Mech.Eng*. C420/88.

Dahlquist G,Björk Å, 1974,Numerical Methods, *Dover Publication*, Ch.6-12.

Das D., Arkeri J, 1998,Transition of Unsteady Velocity Profiles with Unsteady Flow,*J. Fluid Mech.*, 374,252-283.

David E Goldberg, 1985, Genetic algorithm in search optimization and machine learning, Pearson's publication, 1-Ed,1-100.

Dixon J C., 1999, The Shock Absorber Handbook, SAE International; 1st edition, Ch-6-7.

Dominguez A, Sedaghati R And Stiharu I, 2004,Modelling The Hysteresis Phenomenon of Magnetorheological Dampers, *Smart Mater. Struct*., 13, 1351–1361,

Dug YL, Young T.C., Wereley N.M., 2002, Performance Analysis Of ER/MR Impact Damper System Using Herschel Bulkley Model, Journal *Of Intelligent Material Systems and Structures*,13:525, 525-531.

Dyke S. J., Spencer B. F. Jr., Sain M. K., Carlson J. D.,1997, An Experimental Study of Mr Dampers for Seismic Protection, *Smart Mater. Struct*.,7,693–703

Ehrgott R.C., Masri S.F., 1992,Modelling The Oscillatory Dynamic Behavior of ER Materials, *Smart Mater. Struct*,8(5),602-615.

Falk F, Konopka P, 1990, Three-dimensional Landau Theory Describing the Martensitic Phase Transformation of Shape Memory Alloys, *J. Phys.: Condens. Matter*, 2, 61–77.

Facey W. B., Rosenfeld N. C., Choi Y. T.,Wereley N. M., 2005, Design and Testing of a Compact Magnetorheological Damper for High Impulsive Loads, *Intl J. of Mod Phy B*, Vol,19, Nos 7,8 &9, 1549-1555.

Fakhreddine O.K., Clarence D.S., 2009, Soft computing and intelligent systems design-Theory, Tools and Applications, Pearson's publications, 370-390.

Fetecau C, 2004, Analytical Solutions for Non-Newtonian Fluid Flows in Pipe Like Domains, Internat. *J. Non-Linear Mech*.,39, 225-231.

Fetecau C, Fetecau C., 2005, Starting Solutions for Some Unsteady Unidirectional Flows of a Second Grade Fluid, *Intl.. J. Engrg. Sci.* 43,781–789.

Fetecau C, Fetecau C., 2006, Starting Solutions For Motion of a Second Grade Fluid Due To Longitudinal and Torsional Oscillations of a Circular Cylinder, *Internat. J. Engrg. Sci*. 44, 788–796.

Fetecau C., Fetecau C., 2007,Vieru D., On Some Helical Flows of Oldroyd-B Fluids, *Acta Mech*. 189,53–63.

Freziger, JH, Peri´c M, 2002, Computational Methods for Fluid Dynamics, 3rd Ed.(rev),*Springer*,373-381.

Friedrich C., 1991, Relaxation and Retardation Functions of The Maxwell Model with Fractional Derivatives, *Rheol. Acta* 30, 151–158.

Frigaard A, Howison S.D., Sobey I.J., 1994, On the Stability of Poiseuille flow of a Bingham fluid, *J. of Fluid Mechanics*,263,133-150.

Chooi W.W., Oyadiji S.O., 2008, Design, Modelling And Testing of Magnetorheological (MR) Dampers Using Analytical Flow Solutions, *Comp. & Struct.*,Volume 86 , 473-482.

Gavin H., Hoagg J., Dobossy M., 2001, Optimal Design of MR Dampers, *Proc. US Japan Workshop on Smart Structures for Improved Seismic Performance in Urban Regions* (Seattle,WA, Aug. 2001), 225–36.

Gandhi F, Wang K W, Xia L, 2001, Magnetorheological Fluid Damper Feedback Linearization Control for Helicopter Rotor Application, *Smart Mater. Struct.*,10, 96–103.

Garg V.K., Rouleau W.T., 1972, Linear Spatial Stability of Pipe Poiseuille Flow,*J. Fluid Mechanics*, 54(1),113-127.

Gavin H.P., Hanson R.D.,Filisko F.E., 1996, Electrorheological Damper 2. Testing And Modeling, *ASME J. of Appl. Mech.*,63(3),676-682.

Gavin H.P., 2001, Multi –Duct ER Dampers, *J. Intel. Mater and Struct.*,12,353-366.

Gavin H., Hoagg J., Dobossy M., 2001, Proc. U.S.-Japan Workshop On Smart Structures For Improved Seismic Performance In Urban Regions, Seattle, WA, 225-236.

Gordaninejad F. And Kelso S.P., 2000, Failsafe Magneto-Rhelogical Fluid Dampers for Off Highway, High Payload Vehicles, *J. intell. Mater. Syst. Struct.*, 11,395-406.

Gordaninejad, F. , Fuchs, A. , Dogrour, U. , Karakas, S. , Liu, Y., 2004, A New Generation of Magneto-Rheological Fluid Dampers, *Defense Technical Information Center*, report no. ADA426496.

Gregory H. H., Wang X., Gordaninejad F. , 2007,A New Bypass Magnetorheological Fluid Damper, *Vib. Acoust.* , Volume 129, Issue 5, 641 (7 pages),doi:10.1115/1.2775514.

Guzzomi F.G., O'Neill P.L., Tavner A.C.R., 2007, Investigation of Damper Valve Dynamics Using Parametric Numerical Methods, *16th Australasian Fluid Mechanics Conference*,Crown Plaza, Gold Coast, Australia,1123-1130.

Hajihosseinloo, M. A., Hooke, C. J., and Walton, D., 1989, Gun recoil system performance measurement and prediction. Proc. Instn Mech. Engrs, Part C: J. Mechanical Engineering Science, 203, 85–88. DOI: 10.1243/PIME_PROC_1989_203_091_02.

Hayat T., Khan M., Ayub M., 2006, Some Analytical Solutions for Second Grade Fluid Flows for Cylindrical Geometries, Math. Comput. Modelling,43,pp 16–29.

Hayat T., Khan M., A.M. Siddiqui, Asghar S.,2004, Transient Flows of a Second Grade Fluid, *Internat. J. Non-Linear Mech*.,39, 1621–1631.

Hayatt., Khan M., Ayub M., Siddiqui A.M., 2005, The Unsteady Couette Flow of a Second Grade Fluid in A Layer of Porous Medium, *Arch. Mech*. 57,404–416.

Hedström B.O.A., 1952, Flow of plastic materials in pipes, Ind. Eng. Chem., 44 (3), 652–656.

Hiemenz G., Choi Y. T., Wereley N. M., 2003, Seismic Control of Civil Structures Utilizing Semi-Active MR Braces, *J. Comput. Aided Civil Infrastruct. Eng.*, 18, 31–44.

Hogg, I.V., 1971, The Guns 1914-1918, *Ballantine Books*, Inc., New York, New York.

Holland J, 1975, Adaptation in Natural and artificial systems, University of Michigan press, Ann Arbor.

Hong S.R., Choi S.B., Choi Y.T., Wereley N.M., 2005, A Hydro-Mechanical Model for Hysteretic Damping Force Prediction of ER Damper: Experimental Verification, J. of Sound and Vibration, 285, 1180-1188.

Jiang J., Tian Y., Ren D., Meng Y., 2011, An Experimental Study on the Normal Stress of Magnetorheological Fluids, Smart Mater. Struct., 20, 085012-085022.

Jolly M.R., Jonathan W.B, Carlson J.D., 1998, Properties and application of commercial magnetorheological fluids, *Smart Structures and Materials - Passive Damping and Isolation* Volume: 3327, Issue: 1, Publisher: SPIE, 262-275.

Kamath G. M., Wereley N. M., Jolly M. R., 1999, Characterization of Magnetorheological Helicopter Lag Dampers, *J. Am. Helicopter Soc.*, 44, 234–48

Kamath G. M. , Hurt K. M. , Wereley N. M. , 1996,Analysis and Testing of Bingham Plastic Behavior in Semi-Active Electrorheological Fluid Dampers, *Smart Mater. Struct*, Volume 5, Number 5, 576-590.

Karnopp D.C., Crosby M.J., Harwood R.A., 1974, Vibration Control Using Semi-Active Force Generators, American Society of Mechanical Engineers, Journal of Engineering for Industry, 96 (2), 619–626.

Kleinstreuer C., 1997, Engineering Fluid Dynamics – An Interdisciplinary Systems Approach, Cambridge University Press.

Kreyszig E.,2004, Advanced Engineering Mathematics, 8Th Edition, John Wiley and Sons Inc., New York, Ch 5, 10,17-20.

Kuo W.H., Wu T.N., Guo J. Chiang M.H., Chen Y.N., 2006, *Design and Performance Evaluation of a Serial Multi Electrode Electrorheological Damper*, J. of Sound and Vibration, Vol 292(3-5), 674-709.

Lookman T., Shenoy S.R., Rasmussen K., Saxena A., Bishop A.R 2003, Ferroelastic Dynamics and Strain Compatibility, *Phys. Rev. B*, 67, 024114.

Leitmann G., Reithmeier E., 1993, Semi-Active Control of a Vibrating System by Means of Electrorheological Fluids Dynamics Control 3 7-33 Damper (An Application Of Electro-Rheological Fluid), *Trans. ASME J. Wb. Acoust*., 114 , 354-357.

Liao C. R., Yu M., Huang S. L., Zhang H.H., 2007, A Study Of An Inner Bypass Magneto-Rheological Damper With Magnetic Bias**,** *Smart Mater. Struct*., 16, N40–N46.

Lipscomb G. G., Denn M. M., 1984, Flow Of Bingham Fluids in Complex Geometries, *J. of Non Newtonian Fluid Mechanics*, 14, 337-346.

Lee D.Y., Wereley N. M. , 1999, Quasi Steady Herschel –Bulkley Analysis of Electro- and Magneto-Rheological Flow Mode Dampers, *J. of Intlgt Mater. Sys & Struct*,Vol. 10, 761-769.

Li W. H., 2000, Rheology of MR Fluids And MR Damper Dynamic Response: Experimental And Modelling Approaches, *Phd Dissertation,School Of Mechanical And Production Engineering*, The Nanyang Technological University, Singapore.

Lumley JL, 1978, Computational modeling of turbulent flows, *Adv. Appl. Mechanics* , Vol 118,123-176

Mao M., Choi Y.T., Wereley N.M., 2005, Effective Design Strategy for a Magnetorheological Damper Using a Nonlinear Flow Model, *Proc. of SPIE*, 5760, 446-455.

Mao M., Hu W., Choi Y.-T., Wereley N.M. , 2007, A magnetorheological damper with bifold valves for shock and vibration mitigation, *Journal of Intelligent Material Systems and Structures*, 18 (12), 1227-1232.

Mohammed I., Fayçal I. , Rodellar J, 2007,The Hysteresis Bouc-Wen Model, A Survey ,*Achves of Comptl. Mthds in Engg* , Publisher Springer Netherlands ISSN1134-3060 (Print) Issue Volume 16, Number 2, 1886-1784 .

Mishra P., Tripathi G., 1971, Transition from laminar to turbulent flow of purely viscous non-Newtonian fluids in tubes, Chem. Eng. Sci., 26 , 915–921.

Nguyen Q.H., Choi S.B., 2009, Optimal Design Of A Vehicle Magnetorheological Damper Considering The Damper Force And Dynamic Range, *Smart Mater. Struct*., 18, 1-10.

Norrsi J. A., Ahmedian M, 2003, Behaviour Of Magnetorheological Fluids Subject to Impact and Shock Loading, *Proceedings of IMECE'03-2003, ASME International Mechanical Engineering Congress*, Washington DC, USA,pp1-5.

Norrsi J. A., Ahmedian M. , 2005, Behaviour of Magnetorheological Fluids Subject to Impact And Shock Loading, *Proceedings Of IMECE'03-2003, ASME Itl. Mech. Engg Cong.* USA, 1-5, Washington DC.

Nouar C., Frigaard I.A., 2001, Nonlinear Stability of Poiseuille Flow of a Bingham Fluid: Theoretical Results and Comparison with Phenomenological Criteria, *J. of Non-Newtonian Fluid Mechanics*, 100(1-3),127-149.

Novak Z, Gajdeczko B, 1983, Laminar Entrance Region Flow of the Bingham Fluid, *Acta Mechanica*, 49, 191-200.

Ngatu G.T., Wereley N.M., 2007,Viscometric and Sedimentation Characterisation of Bi-disperse Magnetorheological Fluids, *IEEE Trans. on Magnetics*, Vol 43, No. 6, 2474-2476.

Ordnance Department Document No.2035, 1921, Theory and Design of Recoil Systems and Gun Carriages, Chapter XI.

Oh H. U., Onoda J., 2002, An Experimental Study of a Semiactive Magneto-Rheological Fluid Variable Damper for Vibration Suppression of Truss Structures, *Smart Mater. Struct*., 11, 156–62.

Özisik M.N., 1980, Heat Conduction, Wiley, New York.

Park D W, Choi S B, Suh M S And Shin M J, 2001, ER Suspension Units for Vibration Control of a Tracked Vehicle,*Proc. SPIE* , 4327,159–64.

Peel D. J., Bullough W. A., 1994, Prediction of electro-rheological valve performance in steady flow, *Proc.Inst. Mech. Eng.,* 208**,** 253–266.

Philips R.W., 1969, Engineering Application of Fluids With a Variable Yield Stress. Phd Thesis, University Of California Berkley, CA.

Poole R.J., Chhabra R.P., 2010, Development length requirement for fully developed Laminar pipe flow of Yield stress fluids, *J of Fluid Eng*.,132(3),034501-034505.

Poynor J. C., 2001, Innovative Designs for Magneto-Rheological Dampers Master Dissertation Virginia Polytechnic Institute and State University.

Press W.P., Teukolsky S.A., Vetterling W.T., Flannery B.P., 2009, Numerical recipes in C, Cambridge university Press, 2nd edition,389-389.

Quoc H.N.,Seung B.C., 2009, Optimal design of a vehicle magnetorheological damper considering the damping force and dynamic range, *Smart Materials and Structures*,18, 015013,1-10.

Rhienmetall Handbook on weaponary,1982, Rhienmetall,Dusseldorf.

Roark R J, Young W C, 1975, Formulas for Stress and Strain, 5th ed.,*McGraw-Hill Inc.,* 37-340.

Rosenfeld N, Wereley N.M., 2004, Volume Constrained Optimization of Magnetorheological and Electrorheological Valves and Dampers, *Smart Mater. Struct*. , 23, 1303-1313.

Schechter M.M., 1982, Fast Response Multipole Solenoids, *SAE technical paper series*, 820203, 27-38.

Stanway R., Sproston J.L., Stevens N G., 1987, Non-Linear Modelling of an Electro-Rheological Vibration Damper, *J. Electrostat.,* 20,167-184.

Sims N.D., Peel D.J., Stanway R., Johnson A.R., Bullough W.A.,1999, Controllable Viscous Damping: An experimental Study of an Electrorheological Long Stroke Damper Under Proportinal Feedback Control, Smart Mater. Struct., 8(5),601-615.

Sims N.D., Peel D.J., Stanway R., Johnson A.R., Bullough W.A., 2000, The Electrorheological Long-Stroke Damper: A New Modelling Technique with Experimental Validation, *J. of sound and Vibrations*,229(2), 207-227.

Spencer B.F. Jr., Dyke S.J., Sain M.K., Carlson J. D., 1997, Phenomenological Model for Magnetorheological Dampers, *J. Eng. Mech. ASCE*, 123, 230-238.

Stanway R., Sproston J.L., EI-Wahed A.K., 1996, Application of Electro-Rheological Fluids in Vibration Control: A Survey. *Smart Mater. and Struct.*, **5** 4,. 464–482.

Subbaraj, K., Dobainish, M. A., 1989, Survey of direct time integration methods in computational structural dynamics– II, implicit methods, *Comput. Struct*., 32(6),1387–1401.

Symans M.D., Constantinou M.C., 1999, Semiactive Control Systems For Seismic Protection of Structures: A State of the Art Review, *Engg. Struct*,21(6), 469-487.

Talbott M. S. , Starkey J. , 2002, An Experimentally Validated Physical Model of a High-Performance Mono-Tube Damper, *SAE Technical paper series,2002-01-3337, Proceedings of the 2002 SAE Motorsports*, Engineering Conference and Exhibition,2002,pp382-402.

Tan Wenchang, Pan Wenxiao, Xu Mingyu, 2003, A Note On Unsteady Flows Of A Viscoelastic Fluid With The Fractional Maxwell Model Between Two Parallel Plates, *Intl. J. Non-Linear Mech.*, 38, 645–650.

Vuchkov, I.N. and Boyadjieva, 2001, L.N. Quality Improvement with Design of Experiments: A Response Surface Approach, Kluwer Academic Publishers. Dordrecht.

Walter J., Weiss K.,Carlson J. D., 1992, Electroreheological Materials And Their Usage In Intelligent Material Systems And Structures, Part II: Applications, *Recent Advances In Sensory And Adaptive Materials And Their Applications*, Ed. C A Rogers (Lancaster, PA: Technomic).

Wang E.R., Ma X.Q., Rakhela S., Su C. Y., 2003, Modelling The Hysteretic Characteristics of a Magnetorheological Fluid Damper, *Proc. Inst. Mech. Eng. D*, 217, 537–550.

Wang D.H., Liao W.H., 2011, Magnetorheological Fluid Dampers: A Review of Parametric Modeling, *Smart materials and structures*, 20, 1-34.

Wang J., Li Y., 2006,Dynamic Simulation and Test Verification of MR Shock Absorber Under Impact Load, *Journal of intelligent materials systems and structures*, Vol. 17,309, 309-313.

Wang S., Xu M., 2009, Couette Flow of Two Kinds of Fractional Viscolelastic Fluids in An Annulus, Nonlinear Analysis: *Real World Applications* 10, 1087-1096.

Wang X., Gordaninijad F., 2007, Flow Analysis And Modeling of Filed Controllable, Electro- And Magneto-Rheological Fluid Dampers, *J of Appl Mech*, Vol 74, 13-22.

Wereley N.M., Kamath G.M., Madhavan V., 1999, Hysteresis Modeling of Semi-Active Magnetorheological Helicopter Lag Dampers, *Journal of Intelligent Material Systems and Structures*, Vol. 10(8) , 624–633.

Wereley N.M. , Li P., 1998, Nondimensional Analysis of Semi Active Electrorheological and Magnetorheological Dampers using Approximate Parallel Plate Model, *Smart Mater Struct.*, 7,732-743.

Xu Mingyu, Tan Wenchang, 2001, Theoretical Analysis Of The Velocity Field, Stress Field And Vortex Sheet of Generalized Second Order Fluid with Fractional Anomalous Diffusions, *Sci. China Ser. A,* 44, 1387–1399.

Zhang H.H., Liao C.R., Yu M., Huang S.R., 2007, A Study of an Inner Bypass MR Damper With Magnetic Bias, *Smart Mater. Struct*., 16, 40-46.

Zhao Y., Choi Y.T.,Wereley N.M., 2004, Semi-active Damping of Ground Resonance in Helicopters Using Magnetorheological Dampers, *J. Am. Helicopter Soc.*, Vol. 49, No. 4, 468-482.